



Development of Ynamines as Next- Generation Bio-orthogonal Tagging Reagents

Frederik Peschke

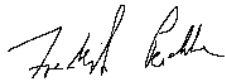
Thesis submitted to the University of Strathclyde in fulfilment of the
requirements for the degree of Doctor of Philosophy

6th September 2021

Academic Supervisor: Prof. Glenn. A. Burley

Declaration of Authenticity

This thesis is the result of the author's original research. It has been composed by the author and has not been previously submitted for examination which has led to the award of a degree. The copyright of this thesis belongs to the author under the terms of the United Kingdom Copyright Acts as qualified by University of Strathclyde Regulation 3.50. Due acknowledgement must always be made of the use of any material contained in, or derived from, this thesis.

Signed: 

(Frederik Peschke)

Date 6th September 2021

Contents

Declaration of Authenticity.....	ii
Contents.....	iii
Acknowledgements.....	viii
Abstract.....	ix
Abbreviations.....	xi
Chapter 1.....	1
1.1 Native Enzymatic and Chemical Ligation	2
1.1.1 Green Fluorescent Protein.....	2
1.1.2 Native Enzymatic Ligation	3
1.1.3 Bioconjugation using NHS Esters.....	6
1.1.4 Bioconjugation using Maleimides and Bromomaleimides	8
1.2 Bio-orthogonal Methods and Strategies.....	12
1.2.1 Staudinger Ligation for Bioconjugation.....	12
1.2.2 Copper Catalysed Azide Alkyne Cycloaddition (CuAAC).....	15
1.2.3 Strain-Promoted Azide-Alkyne Cycloaddition (SPAAC)	28
1.2.4 Inverse Electron Demand Diels Alder Reaction	33
1.3 Incorporation of Unnatural Moieties.....	43
1.3.1 Incorporation of Unnatural Moieties by Native Enzymes	43
1.3.2 Genetic Code Expansion for the Incorporation of Bio-orthogonal Reagents	45
1.4 Aromatic Ynamines as Unique Bio-orthogonal Reagents	47
1.4.1 Sequential Bio-orthogonal Labelling using Ynamines	48
1.4.2 Mechanistic Investigations of the Ynamine-CuAAC.....	51
1.1 Glutathione.....	52
1.1.1 Glutathione and Copper Redox Chemistry	53
1.1.2 GSH as a Nucleophile to Deactivate Bio-orthogonal Reagents.....	56
1.2 Hypothesis.....	58

1.3	Thesis Aims	59
Chapter 2.....		61
2.1	Introduction.....	62
2.1.1	Requirements of Bio-orthogonal Reagents	62
2.1.2	Glutathione as a Source of Side-reactivity with Bio-orthogonal Reagents	63
2.2	Hypothesis to be tested in this Chapter	64
2.3	Aims of Chapter 2	65
2.4	Results & Discussion	66
2.4.1	Synthesis of Aromatic Ynamines.....	66
2.4.2	Synthesis of Alkynes and Bio-orthogonal Reagents	67
2.4.3	Development and Optimisation of a HPLC Assay to Determine the Stability of Bio-orthogonal Reagents.....	72
2.4.4	Ynamine Stability in the Presence of Glutathione	75
2.4.5	Susceptibility of Common Bio-orthogonal Reagents to Reactivity with Glutathione.....	84
2.4.6	Influence of Glutathione on the CuAAC Reaction	86
2.4.7	Influence of Glutathione on SPAAC/IEDDA Cycloadditions	93
2.5	Summary of Chapter 2	96
2.6	Experimental	97
2.6.1	General Experimental Techniques and Procedures.....	97
2.6.2	Liquid Chromatography-Mass Spectrometry (LC-MS) and Ultra-Performance-Mass-Spectrometry (UPLC-MS)	98
2.6.3	Synthetic Procedures.....	98
2.6.4	HPLC Assay.....	115
Chapter 3.....		120
3.1	Introduction.....	121
3.1.1	The Glutathione and Copper Interplay.....	121
3.2	Hypothesis to be tested in this Chapter	122

3.3	Aims of Chapter 3	123
3.4	Results & Discussion	124
3.4.1	Influence of Increasing Glutathione Concentrations on the Ynamine-CuAAC Reaction	124
3.4.2	Comparison of the Ynamine-CuAAC in the Presence and Absence of Glutathione.....	126
3.4.3	Influence of Sodium Ascorbate on the Ynamine-CuAAC.....	127
3.4.4	Influence of Ligand THPTA on the Ynamine-CuAAC	129
3.4.5	The Ynamine-CuAAC Reaction in the Presence and Absence of Glutathione in Water.....	130
3.4.6	Design of Experiment on the Ynamine-CuAAC Reaction in the Presence of Glutathione.....	131
3.4.7	Hypothesis of the Ynamine-CuAAC in the Presence of Glutathione	136
3.4.8	Kinetic Analysis of the Ynamine-CuAAC using Visual Time-Normalised Analysis.....	138
3.4.9	Conventional Alkyne using the Optimal Reaction Conditions	140
3.4.10	Solvent Screen for the Ynamine-CuAAC using the Optimal Conditions	143
3.5	Summary & Future Work	147
3.6	Experimental Procedures	148
3.6.1	HPLC Assay Procedures.....	148
3.6.2	Instruments and Methods	148
3.6.3	VTNA Analysis.....	149
Chapter 4.....		150
4.1	Introduction.....	151
4.1.1	CuAAC for Bio-orthogonal Conjugation of Peptides and Oligonucleotides	151
4.2	Hypothesis to be tested in this Chapter	153
4.3	Aims of Chapter 4.....	154
4.4	Results & Discussion	155

4.4.1	Synthesis of Reagents	155
4.4.2	Optimization of the Solvent System used in the Ynamine-CuAAC Conjugation.....	157
4.4.3	The Ynamine-CuAAC Ligation is Modulated by Glutathione Addition	159
4.4.4	Chemoselective Ynamine Click Labelling of Azido Peptides	160
4.4.5	Sequential Click Labelling of Dual Azide-Modified Peptides.....	164
4.4.6	Synthesis of Ynamine-modified Oligonucleotides	170
4.5	Conclusion & Future Work.....	175
4.6	Experimental.....	177
4.6.1	General Experimental Techniques and Procedures.....	177
4.6.2	Liquid Chromatography-Mass Spectrometry (LC-MS) and Ultra-Performance-Mass-Spectrometry (UPLC-MS)	178
4.6.3	Synthetic Procedures.....	178
4.6.4	General Peptide Synthesis Protocol	184
4.6.5	General Protocol for DNA Synthesis.....	186
4.6.6	HPLC Assay Procedure for Peptide Conjugation	188
Chapter 5	190
5.1	Introduction.....	191
5.1.1	The Utility of the CuAAC Reaction for Live Cell Labelling.....	191
5.2	Hypothesis to be tested in this Chapter	193
5.3	Aims of Chapter 5	193
5.4	Results & Discussion	194
5.4.1	Synthesis of “Turn-on” Azide and Testing of Fluorescent Assay	194
5.4.2	Synthesis of further “Turn-on” Azides and Modified Ynamines.....	195
5.4.3	Testing the Solubility of Modified Ynamine Triazoles	199
5.4.4	Optimization of the Ynamine-CuAAC Ligation in Buffer	200
5.4.5	Exploration of Ynamine-CuAAC Ligations in Cell Lysate	206
5.5	Summary & Future Directions	210

5.6	Experimental Procedures	213
5.6.1	General Experimental Techniques and Procedures.....	213
5.6.2	Liquid Chromatography-Mass Spectrometry (LC-MS) and Ultra-Performance-Mass-Spectrometry (UPLC-MS)	214
5.6.3	Synthetic Procedures.....	214
5.6.4	Fluorescent Plate Assay	224
5.6.5	Coumarin Azide Solubility Data.....	225
5.6.6	DoE 1 Additional Data.....	225
5.6.7	DoE 2 Additional Data.....	227
Chapter 6	228
6.1	Conclusions and Future Directions	229
List of References	232
Appendix	247

Acknowledgements

I would like to thank Prof. Glenn Burley for giving me the opportunity to carry out a PhD in his research group and his continued support throughout the PhD. I would also like to thank Louise Young for giving me the opportunity to carry out biological work in her laboratory and Dr. Inga Kruse for teaching me and guiding me in all things cell culture and biology.

I would like to thank all the members of the Burley group at the University of Strathclyde for their guidance and support throughout the duration of my project.

Specifically, I would like to thank Andrea Taladriz-Sender and Emma Campbell for their incredible patience when dealing with all things related to finance and ordering. I would like to thank Jack Robertson for keeping the lab a “paradise” and Iain McKean for sharing the joys of HPLC. I would like to thank Steven Pauff for his peachy outlook on life and Fergus McWhinnie for fixing things whenever they needed fixing. In addition, I would like to thank “Team Ynamine” for understanding and appreciating the consistency of ynamines and Roderick Peterjan Bunschoten for always driving me to the Highlands.

Finally, I would like to thank my wife and my family for their help and support through the past four years.

Abstract

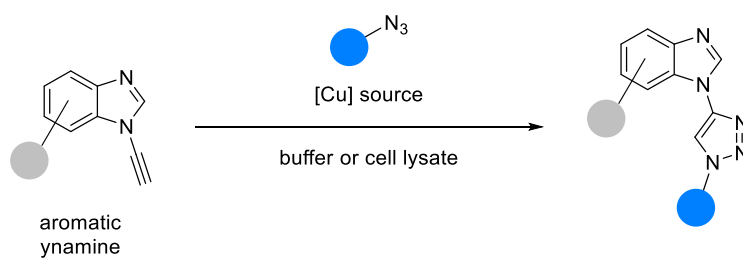
The copper-catalysed alkyne azide cycloaddition (CuAAC) or “click” reaction is a powerful bio-orthogonal tool used throughout chemical biology. However, its use *in vivo* is hindered by an abundance of biological functionalities and small molecules such as glutathione (GSH) which bind copper. This results in the need for super-stoichiometric amounts of the copper catalyst, which in turn exacerbates copper toxicity. Several mitigation strategies such as chelating ligands and azides have been developed to reduce copper loading and increase reactivity. In contrast, little progress has been made to improve reaction efficiency and lower the copper loading by exploring novel alkyne reagents. Aromatic ynamines have previously outcompeted traditional alkynes under standard organic synthesis CuAAC reaction conditions. The enhanced chemical reactivity of ynamines promises superior reactivity in bioconjugation, making it a potential reagent for bio-orthogonal chemistry.

Glutathione, the major antioxidant and nucleophile in cells, reduces the efficiency of the CuAAC reaction by sequestering copper and causing side-reactions with alkynes. The impact of GSH on the CuAAC reaction at physiologically-relevant concentrations (0.1 – 10 mM) has not been explored. This thesis aims to investigate the use of aromatic ynamines as bio-orthogonal reagents, first by comparing the influence of GSH – both stability and reactivity – on CuAAC and bio-orthogonal reactions and then moving into investigating aromatic ynamine reactivity in cell lysate.

Common bio-orthogonal reagents, alkynes and ynamines displayed good stability (> 80%) in the presence of GSH (10 mM) after 24 h and the reactivity of SPAAC and IEDDA reagents remained unaffected. In contrast, GSH dominated CuAAC reactivity and the Cu:GSH ratio could be used to tune the reaction from full conversion to complete inhibition over 24 h. Uniquely, GSH could be used to accelerate the ynamine-CuAAC reaction and in combination with fluorinated solvents (HFIP or TFE) optimised to reach full conversion within 10 min. These conditions were successfully applied to the labelling of cell-penetrating peptides with an ynamine-desthiobiotin probe.

The trend of superior ynamine reactivity continued using fluorescent “turn on” azide reagents in buffer and cell lysate, where 80% conversions were reached after 2 h with as little as 1 μM $\text{Cu}(\text{OAc})_2$ and over 80% conversion in <15 min with 30 μM copper in cell lysate. Conventional alkynes remained unreactive under these conditions.

After these promising results the ynamine is poised for *in vivo* bioconjugation, which will be explored in the future.



Scheme. Reaction of an aromatic ynamine with an azide to form a triazole.

Abbreviations

ADC	Antibody-drug conjugate
Aha	Azidohomoalanine
AMTC	2-{4-[(dimethylamino)methyl]-1,2,3-triazol-1-yl}cyclohexan-1-ol
BCN	Bicyclononyne
Birch A	Biotin ligase
BODIPY	Dipyrrrometheneboron difluoride
BTAA	2-(4-((bis((1-(tert-butyl)-1H-1,2,3-triazol-4-yl)methyl)amino)methyl)-1H-1,2,3-triazol-1-yl)acetic acid
BTES	3-(4-((Bis((1-(tert-butyl)-1H-1,2,3-triazol-4-yl)methyl)amino)methyl)-1H-1,2,3-triazol-1-yl)propane-1-sulfonic acid
CHO	Chinese hamster ovary
CMC	Critical micellular concentration
COSY	Correlation Spectroscopy
CTAB	Cetrimonium bromide
CuAAC	Copper catalysed azide-alkyne cycloaddition
DBCO	Dibenzocyclooctyne-amine
DFT	Density functional theory
DIC	<i>N,N'</i> -Diisopropylcarbodiimide
DIFO	Difluorinated cyclooctyne
DIPEA	<i>N,N</i> -Diisopropylethylamine
DMAP	4-dimethylaminopyridine
DMSO	Dimethylsulfoxide
DNA	Deoxyribonucleic acid
DoE	Design of Experiments
DPBS	Dulbecco's phosphate-buffered saline
DTAB	Dodecyltrimethylammonium bromide
DTT	Dithiothreitol
<i>E. coli</i>	<i>Escherichia coli</i>
EDC	1-Ethyl-3-(3-dimethylaminopropyl)carbodiimide
EDG	Electron donating group
EDTA	Ethylenediaminetetraacetic acid
EGFR	Epidermal growth factor receptor
EPR	Electron Paramagnetic Resonance

EtOH	Ethanol
EWG	Electron withdrawing group
FBS	Fetal bovine serum
FGE	Formylglycine generating enzyme
FITC	Fluorescein isocyanate
GFP	Green Fluorescent Protein
GSH	Glutathione
GSSG	Glutathione disulfide
hAGT	Human O ⁶ -alkylguanine-DNA alkyltransferase
HATU	Hexafluorophosphate Azabenzotriazole Tetramethyl Uronium
HEK	Human embryonic kidney
HeLa	Helacyton gartleri
HEPES	4-(2-hydroxyethyl)-1-piperazineethanesulfonic acid
HFIP	hexafluoroisopropanol
HMBC	Heteronuclear Multiple-Bond Correlation Spectroscopy
HOMO	Highest occupied molecular orbital
HPG	Homopropargylglycine
HPLC	High Performance Liquid Chromatography
HSQC	Heteronuclear Single Quantum Coherence
HUVEC	Human umbilical vein endothelial cells
IEDDA	Inverse electron demand Diels-Alder
IPA	Isopropanol
IR	Infrared
LUMO	Lowest occupied molecular orbital
ManNAz	Azido-acetyl mannosamine
MCF-7	Michigan Cancer Foundation-7
MeCN	Acetonitrile
MES	2-(<i>N</i> -morpholino)ethanesulfonic acid
MeTHF	Methyl-tetrahydrofuran
MOF	Metal-organic framework
NaAsc	Sodium ascorbate
NBS	<i>N</i> -bromo-succimide
NHC	<i>N</i> -heterocyclic carbene
NHS	<i>N</i> -hydroxysuccimide

NMP	<i>N</i> -methyl-2-pyrrolidinone
NMR	Nuclear Magnetic Resonance
nnAA	Non-natural amino acid
NOSEY	Nuclear Overhauser Effect Spectroscopy
ODN	Oligodeoxyribonucleotide
OMNP	Organometallic nanoparticle
PB	Phosphate buffer
PBS	Phosphate-buffered saline
qPCR	Quantitative polymerase chain reaction
RNA	Ribonucleic acid
ROS	Reactive oxygen species
SCNP	Short-chain nanoparticle
SDS	Sodium dodecyl sulfate
SiaNAz	Azido-sialic acid
SPAAC	Strain-promoted azide-alkyne cycloaddition
TBAF	Tetra- <i>n</i> -butylammonium fluoride
TBTA	Tris(benzyltriazolymethyl)amine
TCEP	Tris(2-carboxyethyl)phosphine)
TCO	<i>trans</i> -cyclooctene
TEMPO	(2,2,6,6-Tetramethylpiperidin-1-yl)oxyl
TFE	Trifluoroethanol
TG	Transglutaminase
THF	Tetrahydrofuran
THPTA	Tris(3-hydroxypropyltriazolymethyl)amine
TIPS	Triisopropyl
TLC	Thin-layer chromatography
TP2	Translocating peptide 2
TPP	Triphenyl phosphonium
Tris	Tris(hydroxymethyl)aminomethane
tRNA	Transfer ribonucleic acid
UPLC-MS	Ultra Performance Liquid Chromatography
VTNA	Visual Time Normalised Analysis

Chapter 1

Introduction

1.1 Native Enzymatic and Chemical Ligation

1.1.1 Green Fluorescent Protein

The discovery of green fluorescent protein (GFP) was a major revolution in cell imaging and allowed, for the first time, imaging and tracking of certain protein functions in living cells.^{1,2} The usefulness of GFP led to its widespread adoption and utilization. However, the GFP reporter strategy is limited to proteins and cannot be expanded to other biomolecules such as lipids or carbohydrates. Moreover, the large size of the GFP domain could interfere with the targeted protein's structure and function.^{3,4}

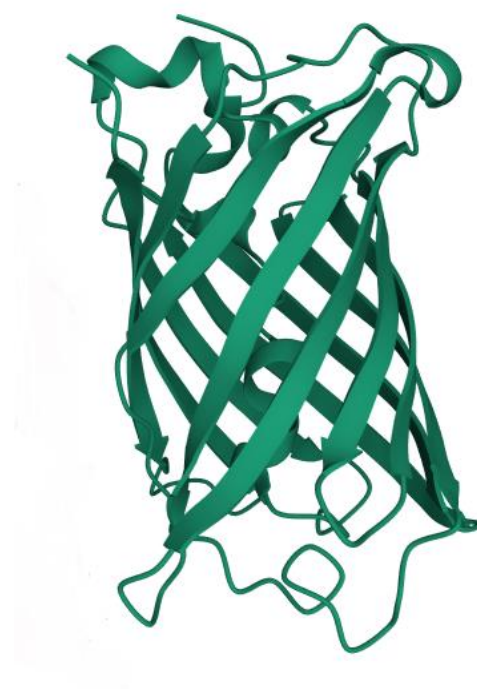


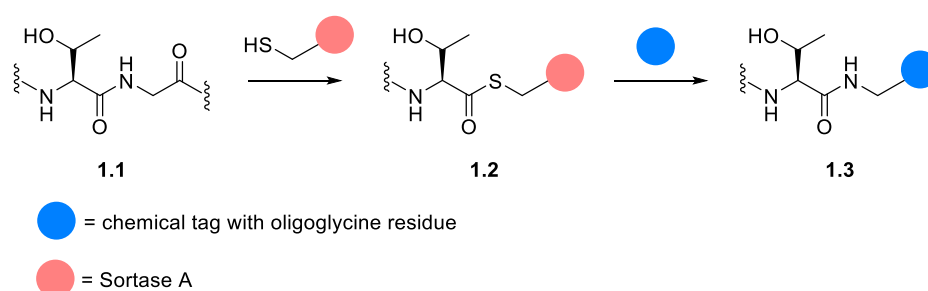
Figure 1.1. Crystal structure of GFP (PDB code: 1GFL).⁵

The development of GFP highlighted the need to overcome its limitations. Researchers then focused on developing chemical tools to introduce covalent modifications in biomolecules within living systems. Numerous methods have been developed allowing the ligation and labelling of proteins, lipids, and nucleic acids; a process called bioconjugation.^{6–10} The following will introduce common concepts and reactions that have been developed to perform bioconjugation.

1.1.2 Native Enzymatic Ligation

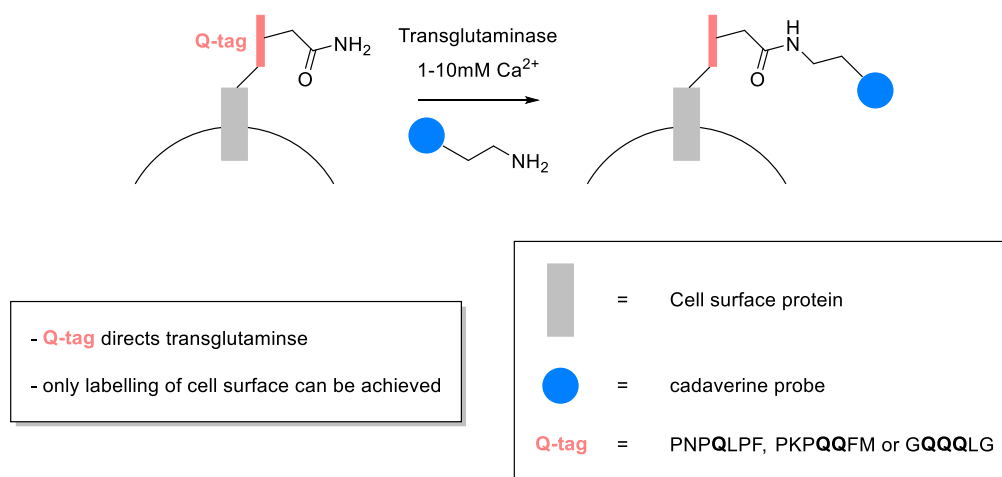
Several classes of enzymes have been used to carry out ligation of native functional groups; among them are peptidases, transglutaminases, oxidoreductases, and ligases.¹¹

Sortase A is a Gram-positive bacterial transpeptidase which catalyses the reaction between an internal protein sequence (LPXTG) and the N-terminus of an oligoglycine peptide, anchoring the protein to the cell surface (Scheme 1.1).¹² The enzyme cleaves the threonine-glycine bond forming a peptide-enzyme conjugate (**1.2**) which can undergo aminolysis with the N-Terminus of oligoglycine.¹³ In this manner molecular probes (*e.g.*, peptides, biotin or fluorophores) featuring an oligoglycine tail can be conjugated to target proteins engineered with the LPXTG sequence.¹⁴



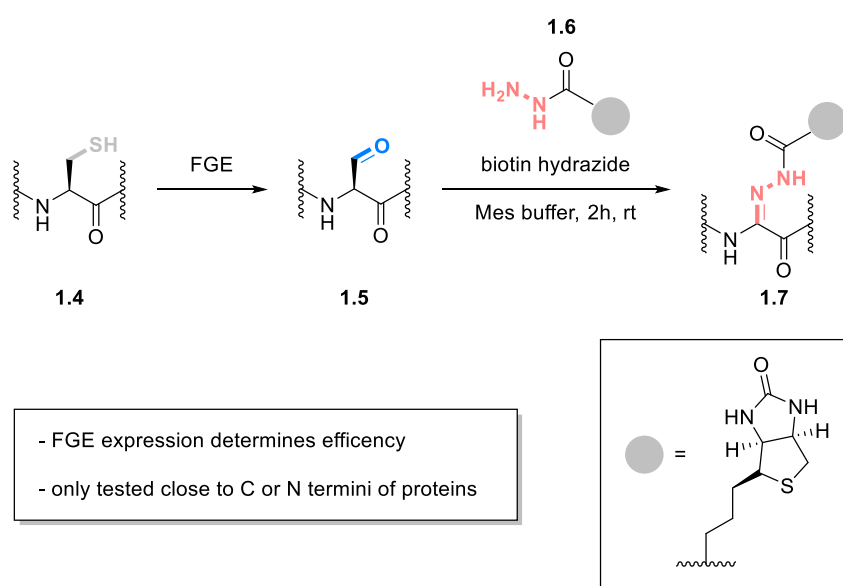
Scheme 1.1. Labelling of a target protein with an oligoglycine probe using Sortase A.

Transglutaminases (TG) are enzymes which catalyse the formations of isopeptide bonds between glutamine and lysine residues to crosslink proteins.¹⁵ In 2006, the Ting lab used a combination of guinea pig liver transglutaminase and a fusion cell membrane protein to label the cell surface of HeLa cells with either biotin cadaverine or Alexa 568 cadaverine (Scheme 1.2).¹⁶ Specific labelling was achieved by an amino acid sequence called Q-tag which directs the transglutaminase. The use of transglutaminases is generally restricted to cell surface labelling due to competing endogenous TGs and the high Ca^{2+} concentration needed for TG to function.



Scheme 1.2. Cell surface labelling by transglutaminase.

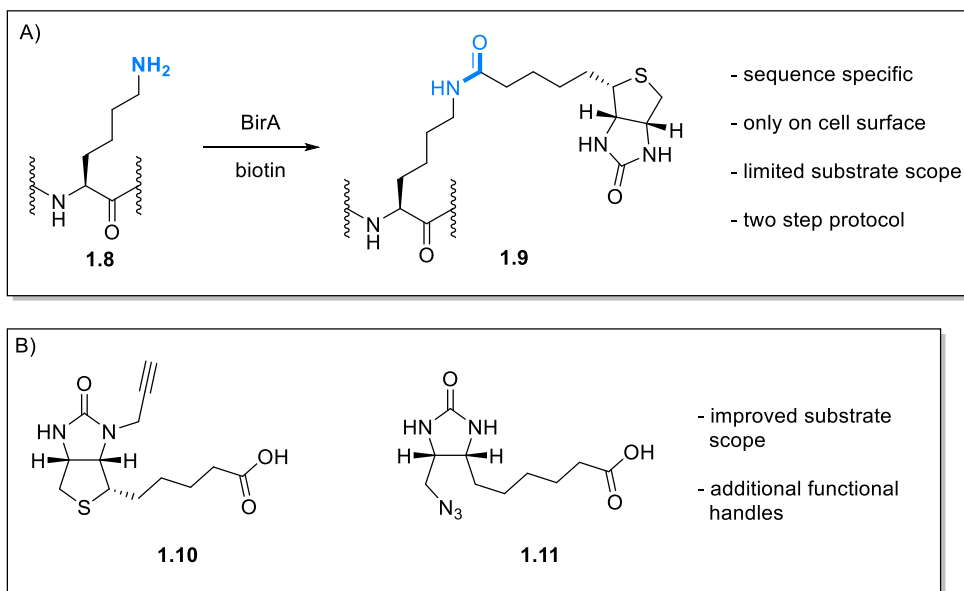
Formylglycine generating enzyme (FGE) is a oxidoreductase which converts cysteines into a formylglycine residue (**1.5**) and is guided by the five amino acid motif CXPXR.¹⁷ By incorporating this motif into a protein of interest, the generated aldehydes were selectively labelled with¹⁴ aminooxy or hydrazine probes (*e.g.*, **1.6**) (Scheme 1.3).⁸ Bertozzi *et al.* demonstrated that recombinant antibodies and cell surface proteins could be tagged successfully with either aminooxy or hydrazide probes.¹⁸



Scheme 1.3. Transformation of cysteine to formylglycine and subsequent labelling with biotin hydrazide.

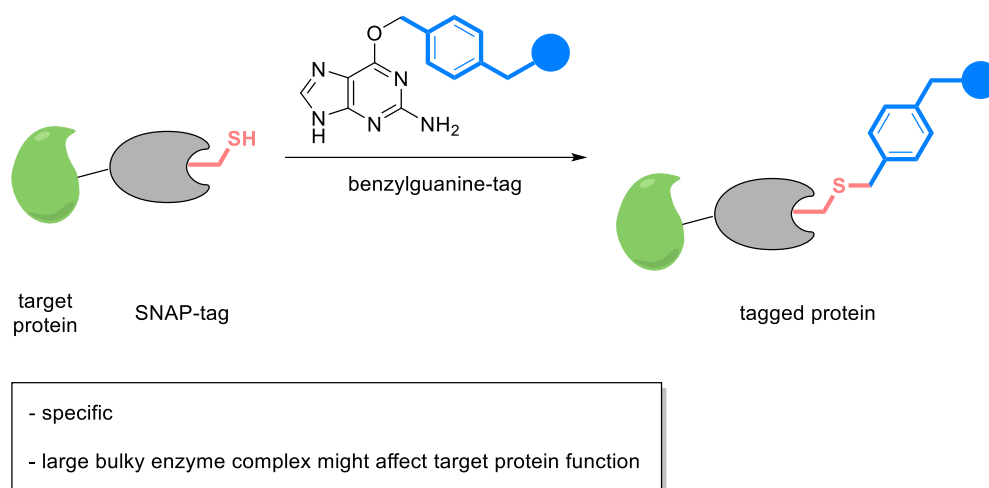
Biotin ligase (BirA) is a ligase from *E. coli*, which selectively attaches biotin to a lysine residue (Scheme 1.4A) and is directed by a 15 amino acid sequence called acceptor peptide.¹⁹ The high affinity of biotin for avidin proteins can be exploited for labelling and subsequent

purification or isolation of the target peptides by pull down assays. The original narrow substrate scope (due the specificity of *E. coli* BirA) was expanded by screening other organisms' biotin ligases and extended to alkyne or azide modified biotin analogues **1.10** and **1.11** (Scheme 1.4B).²⁰



Scheme 1.4. (A) Biotin ligase used to conjugate biotin to a lysine residue. (B) Improved substrate scope by using a yeast biotin ligase.

Human O⁶-alkylguanine-DNA alkyl transferase (hAGT) catalyses the transfer of an alkyl residue attached to the O⁶ position of guanine to a cysteine in the active site of hAGT.¹⁵ Through genetic engineering, hAGT was modified to exhibit higher affinity for benzyl guanine substrates, the so called SNAP-tag can be theoretically¹³ fused to any protein of interest²¹ and labelled with modified benzyl guanine substrates (Scheme 1.5). The major disadvantage of the SNAP-tag fusion protein is the large size of the tag relative to the target protein which could cause the natural function of the protein might be disturbed.¹⁵ Among others, SNAP tag has been used to study protein function²², protein half life²³ and protein complexes.²⁴



Scheme 1.5. Tagging of a target protein via the SNAP-tag methodology.

Most enzymatic methods for protein labelling presented above rely on genetic modification of the target organism to achieve specificity. As such, they all share certain disadvantages. Firstly, the need to genetically modify the organism limits the use of these techniques to bacteria and yeast, which are readily genetically modified. Secondly, expanding the amino acid sequence of a protein will change the structure and might impact function. To overcome these limitations, small molecule probes have been developed.

1.1.3 Bioconjugation using NHS Esters

Out of the proteinogenic amino acids lysine, cysteine, serine, and tyrosine (Figure 1.2A) can act as nucleophiles and lend themselves to modification.²⁵ Due to the substantial number of nucleophiles, controlling selectivity is challenging and important. The reactivity of cellular nucleophiles depends on their protonation state *in vivo*. Therefore, pH is one of the biggest factors to control selectivity and can be tuned to fit to the nucleophile in question. Additionally, the targeted amino acid must be present on the protein surface, otherwise successful conjugation is impossible.

One of the earliest small molecule protein modification reagents to be developed was the *N*-hydroxysuccimide (NHS) ester (Figure 1.2B).²⁶ This activated ester was designed to target lysine residues on proteins. The reaction works well at pH 7 to 8, which makes it ideal for physiological conditions.²⁵ However, since the pK_aH of the NH_2 of lysine is around 10,²⁷ the amino acid is predominantly present in its protonated form at physiological pH thereby reducing the nucleophilicity. The rate of NHS ester conjugation increases with higher pH, as the lysine protonation equilibrium shifts towards the unprotonated amine. However, the

increased reactivity comes at the cost of reduced stability. The half-life of NHS esters at pH 8.6 is approximately 10 minutes²⁸ compared with 4 hours at physiological pH.²⁹

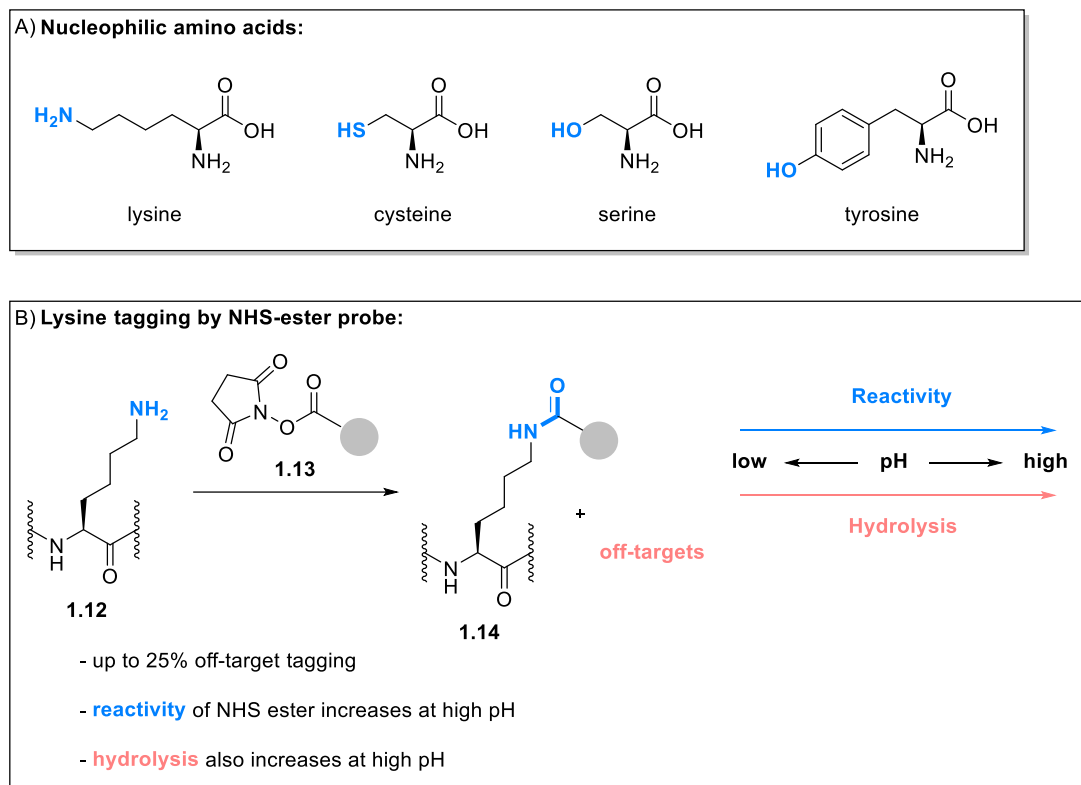


Figure 1.2. (A) Proteogenic amino acids which can act as nucleophiles. (B) Tagging of lysine residue with functionalised NHS-ester probe.

Further, off-target reactivity of up to 25%³⁰ was observed with solvent exposed serines, tyrosines and threonines.^{30,31} The degree of off-target labelling depended on the chemical environment, as a proximal histidine residue was shown to increase the reactivity of serine and tyrosine considerably through neighbouring group catalysis.³¹

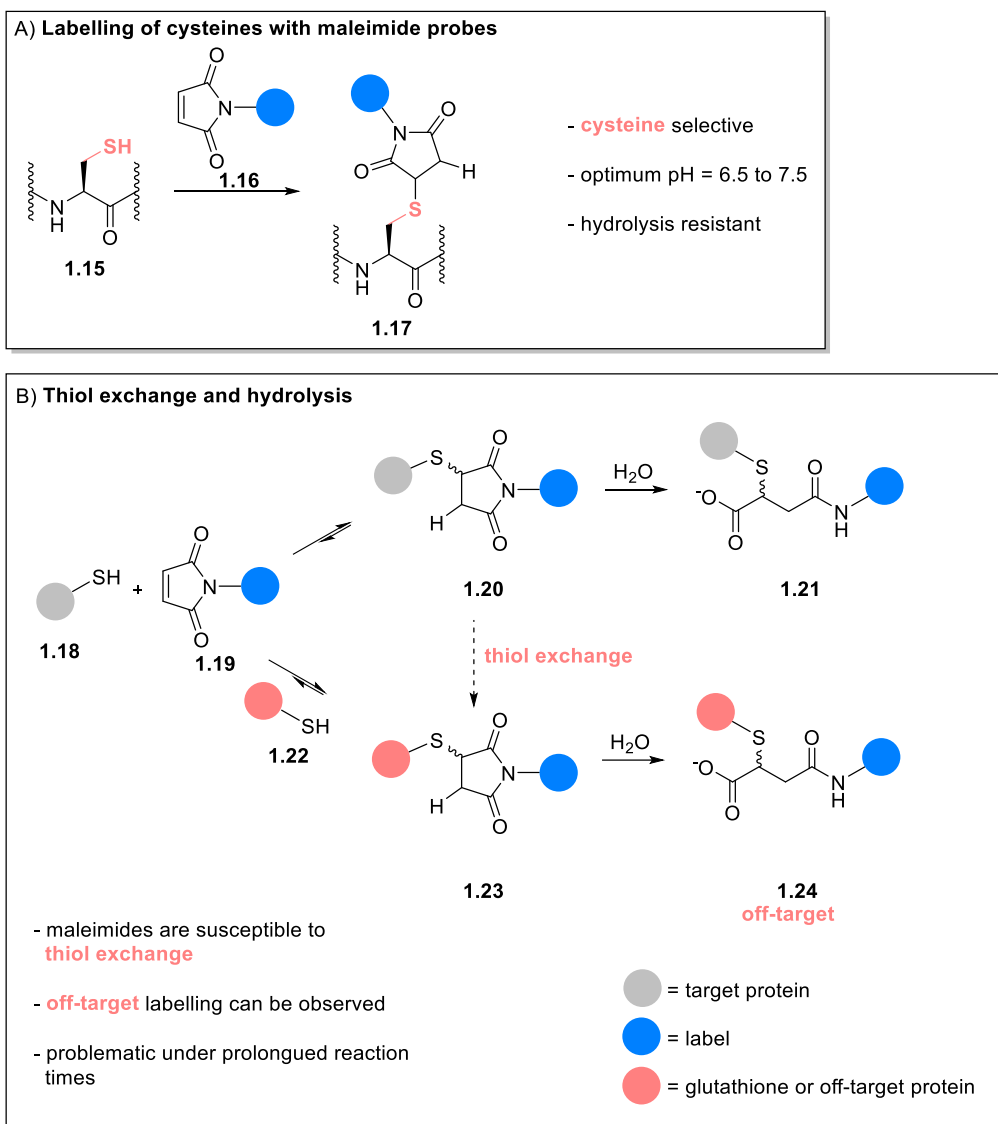
NHS esters present a convenient way to label proteins. They are straightforward to make and easy to deploy. However, this ease of use comes with several drawbacks. The high degree of off-target reactivity makes them a poor choice when specificity is required, and their limited aqueous stability restricts their use to applications which do not require extended reaction times. As such, they are frequently used either for cell lysate experiments or cell surface functionalization.

1.1.4 Bioconjugation using Maleimides and Bromomaleimides

Maleimides are comprised of a 5 membered 2,5-dione ring system with a double bond and are a popular alternative to NHS esters to label cysteines (Scheme 1.6A). The reactivity of the alkene is increased by added ring-strain and adjacent electron withdrawing groups (carbonyls) which decrease the LUMO energy when compared with NHS esters and make them excellent electrophiles (*i.e.* Michael-acceptors).³² Due to the soft nature of the maleimide system (diffuse charges) the moiety preferentially reacts with other soft nucleophiles such as cysteine.²⁵ The rarity of cysteine (~2%)³³ lends itself to targeted mutagenesis which can introduce a cysteine residue at the positions of interest while still ensuring selective labelling.²⁵

The main drawback of maleimide labelling is the susceptibility of the thiosuccinimide adducts (**1.20**) to thiol exchange (Scheme 1.6B).³⁴ The presence of excess thiols – such as glutathione (GSH) – can lead to off target labelling via retro-Michael addition. Through hydrolysis these off-target conjugates can be trapped as stable products (**1.24**).

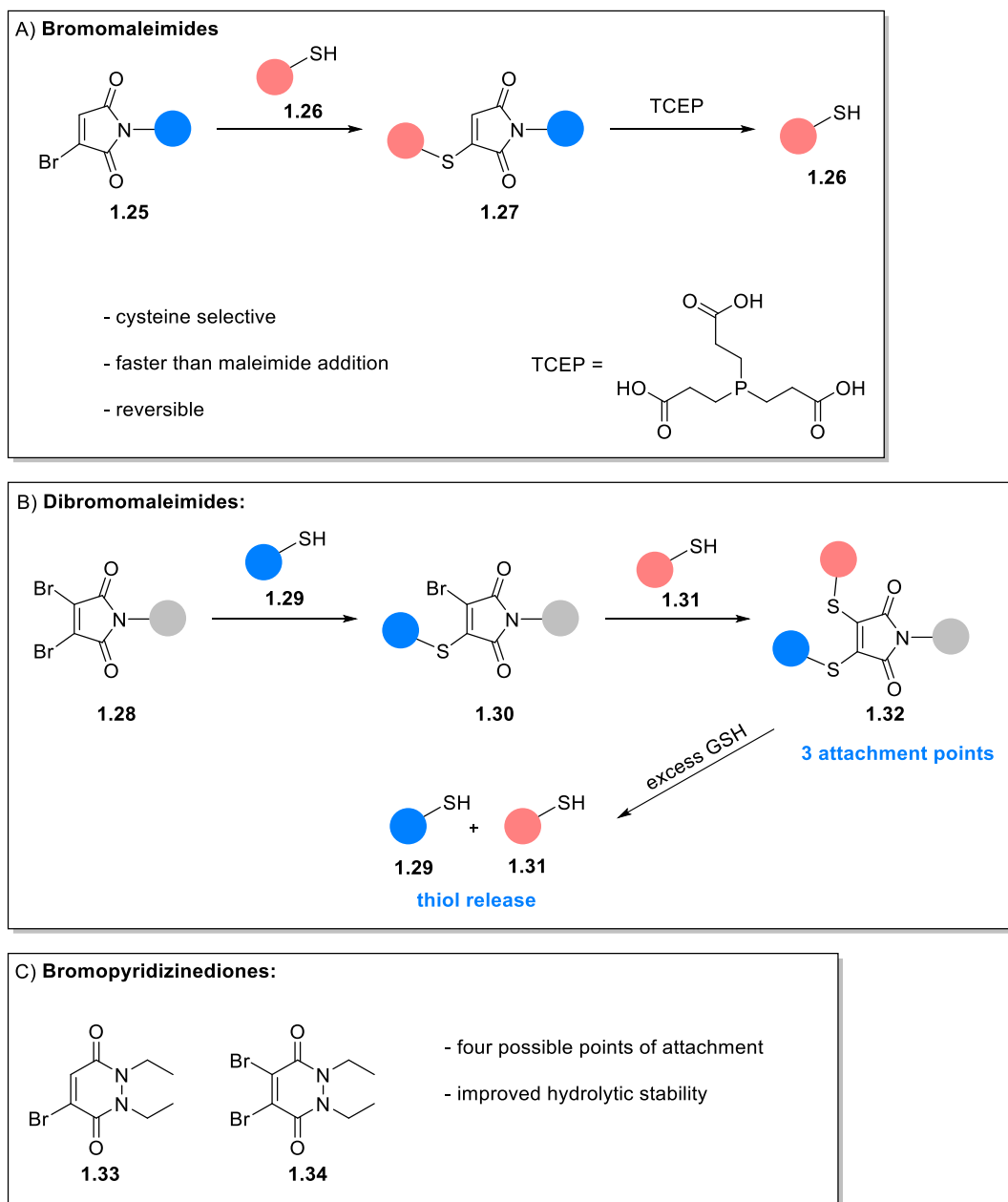
The stability of the maleimide conjugate is determined by the substituents on the nitrogen.³⁵ Thiol conjugates of *N*-alkyl maleimides (**1.20**) are resistant to hydrolysis and are prone to thiol exchange upon prolonged reaction times or high concentrations of competing thiols. The rate of hydrolysis to **1.21** is accelerated by electron withdrawing substituents. This can be beneficial to avoid the retro-Michael addition and trap the desired conjugate in the ring opened form (**1.21**).



Scheme 1.6. (A) Reaction of maleimide probe with cysteine residue. (B) Maleimides undergoing thiol exchange leading to off-target reactions.

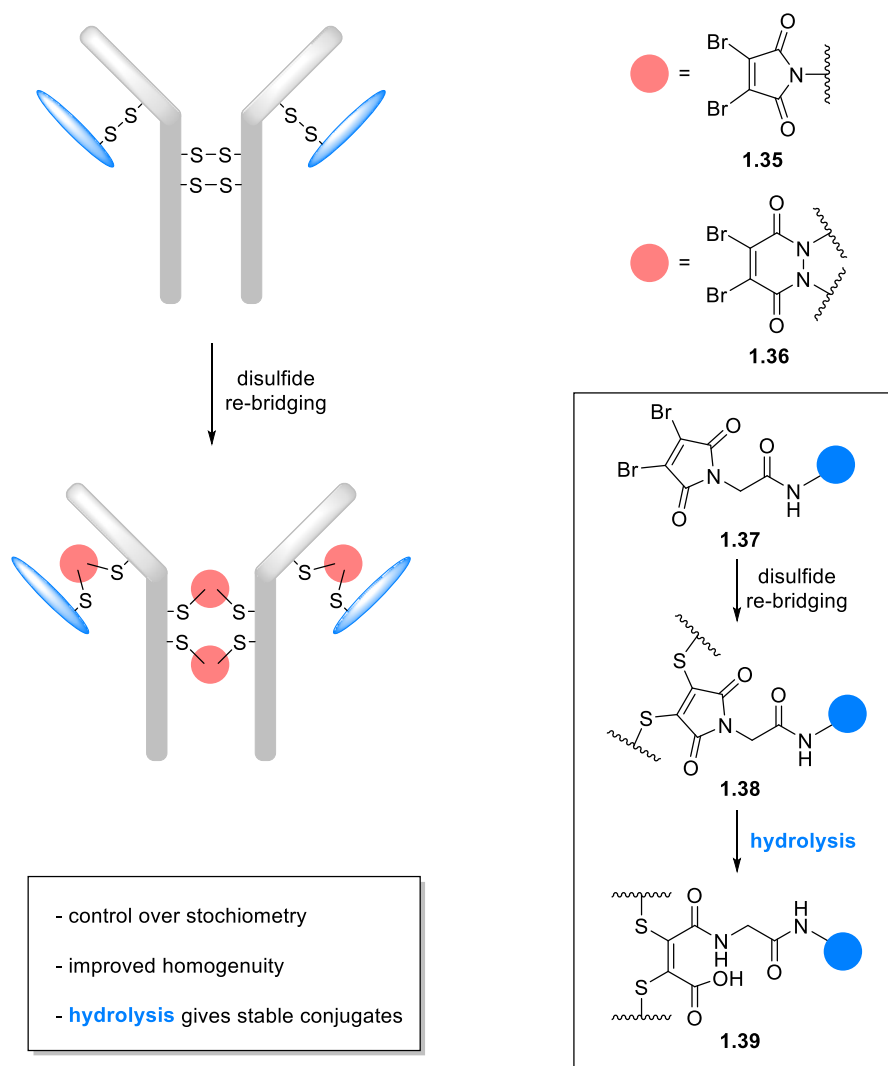
In 2009, Tedaldi *et al.* introduced the bromomaleimide (**1.25**), which was designed to improve on the stability, kinetics, and utility of the maleimide moiety while exploiting the reversibility of the reaction (Scheme 1.7A).³⁶ The functionality of the bromomaleimide was extended further in 2010.³⁷ The dibromomaleimide (**1.28**) offers three points of attachments and can undergo thiol release from di-thiolmaleimide **1.32** by the addition of excess thiols such as glutathione or mercapto-ethanol (Scheme 1.7B).

Bromopyridizinediones (**1.33** and **1.34**) were developed a year later, improving hydrolytic stability and offering four points of attachment (Scheme 1.7C).³⁸



Scheme 1.7. (A) Conjugation of cysteine to a bromomaleimide and subsequent thiol release with TCEP. (B) Di-functionalisation of dibromomaleimides with two thiols and subsequent release. (C) Bromopyridizinediones offer four points of attachment.

Bromomaleimides and bromopyridizinediones have found applications in antibody drug conjugates. The ability to insert into disulfide bonds between the light and heavy chain or the hinge region (Scheme 1.8) gives these reagents the ability to control the stoichiometry of the conjugates which is of utmost importance in ADCs as this affects efficacy, toxicity, and pharmacokinetics.^{39,40} Controlled hydrolysis of the bridging conjugate (1.38 into 1.39) can be used to prevent side reactions and increase ADC homogeneity further.⁴¹



Scheme 1.8. Dibromomaleimides or pyridazines can insert into antibodies and be used to attach a controlled number of drug molecules. Hydrolysis of the bromomaleimides furnishes stable conjugates.

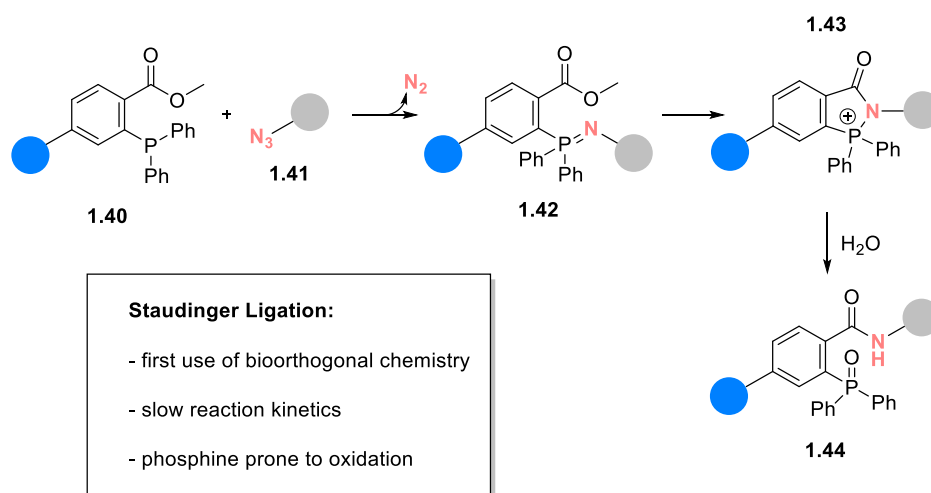
Maleimides and NHS esters present a straightforward way of labelling native protein residues. *In vitro* labelling of specific protein residues, broad spectrum protein labelling, cross linking proteins in cell lysate and assembly of ADCs are where NHS esters and maleimides shine^{9,42}. However, their limited water stability and the abundance of reactive sites in cells make them unsuitable for *in vivo* applications. Therefore, further reactions that are selective in *in vivo* conditions are needed.

1.2 Bio-orthogonal Methods and Strategies

The limitations of enzymatic and bioconjugation *via* NHS esters and maleimides have prompted the development of novel chemical strategies to label biomolecules *in vivo*. The main requirement for these reagents is high stability, reactivity, and stability.⁸ A variety of reagents has been developed and the most common will be introduced in the following section.

1.2.1 Staudinger Ligation for Bioconjugation

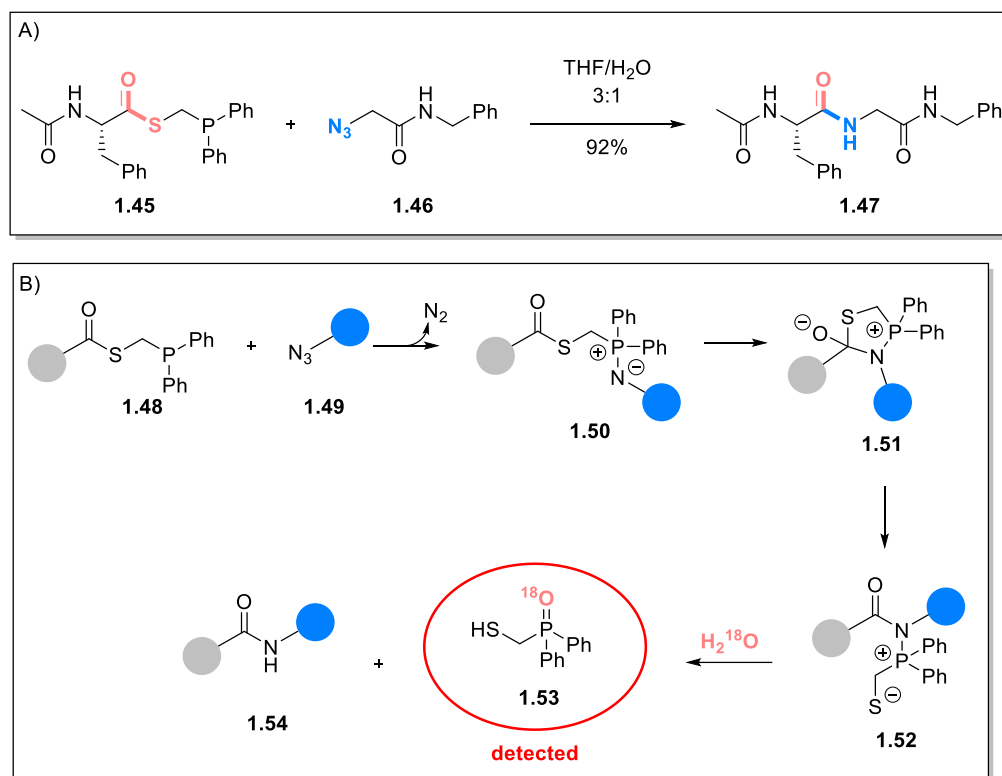
The reaction of an azide with a phosphine to produce iminophosphoranes was discovered in 1919 by Herman Staudinger.⁴³ Staudinger described that the reaction occurred “like an explosion” and released only nitrogen as a by-product. In 2000, the group of Bertozzi adapted the Staudinger reduction for bio-orthogonal tagging methods.⁴⁴ The reactive iminophosphorane **1.42** was trapped with a proximal electrophilic methyl ester to produce a 5-membered ring intermediate (**1.43**) which, after hydrolysis, resulted in a new amide bond between the two starting materials (Scheme 1.9). In this manner, azidoglycans on the surface of Jurkat cells were tagged with a biotin modified phosphine. This report demonstrated the first use of non-native chemical moieties in a cellular context and forms the basis of the field of bio-orthogonal chemistry.



Scheme 1.9. Labelling of azides with fluorescent probes via the Staudinger ligation.

The rate of the Staudinger ligation varies between $1.9 \times 10^{-3} \text{ M}^{-1}\text{s}^{-1}$ and $2.5 \times 10^{-3} \text{ M}^{-1}\text{s}^{-1}$ and the reaction rate increases with polar solvents (THF < acetone < MeCN < MeOH < DMSO) and increased water content.⁴⁵ Substituents on the ester had negligible influence on the reaction, while electron-donating groups on the phenyl groups increased reaction rates concurrent with the fact that the nucleophilic attack of the phosphine on azide was rate limiting.⁴⁵

Several modifications to the Staudinger ligation have been developed since its inception. In 2000 and 2001, Nilsson *et al.* developed the “traceless” Staudinger ligation (Scheme 1.10A).^{46,47} The reaction is termed “traceless” as the final product (**1.47**) does not contain the phosphine oxide. In 2006, the same group investigated the mechanism of the traceless Staudinger reaction.⁴⁸ Through the use of isotopically labelled water (H_2^{18}O) they concluded that the reaction proceeds through the formation of the amidophosphonium salt **1.52** and subsequent hydrolysis (Scheme 1.10).



Scheme 1.10. (A) Amide bond formation via the traceless Staudinger ligation. (B) Proposed mechanism of the traceless Staudinger ligation.

A further evolution of the Staudinger ligation is the light-triggered Staudinger ligation. In this approach, the phosphine is caged with a photoactivatable group (*e.g.*, **1.55**⁴⁹ or **1.56**⁵⁰) which can be cleaved upon irradiation with light (Figure 1.3A and B). This allows precise control over the initiation of the reaction as well as giving spatial resolution. A further advantage is that photocaged phosphines are not susceptible to oxidation *in vitro* and *in vivo*. A drawback of this approach is need for UV-light, which can be cytotoxic. Through increasing the conjugation of the anthracene photocaging group (**1.58**), the wavelength needed for successful decaging could be shifted to the visible spectrum (Figure 1.3B).⁵¹

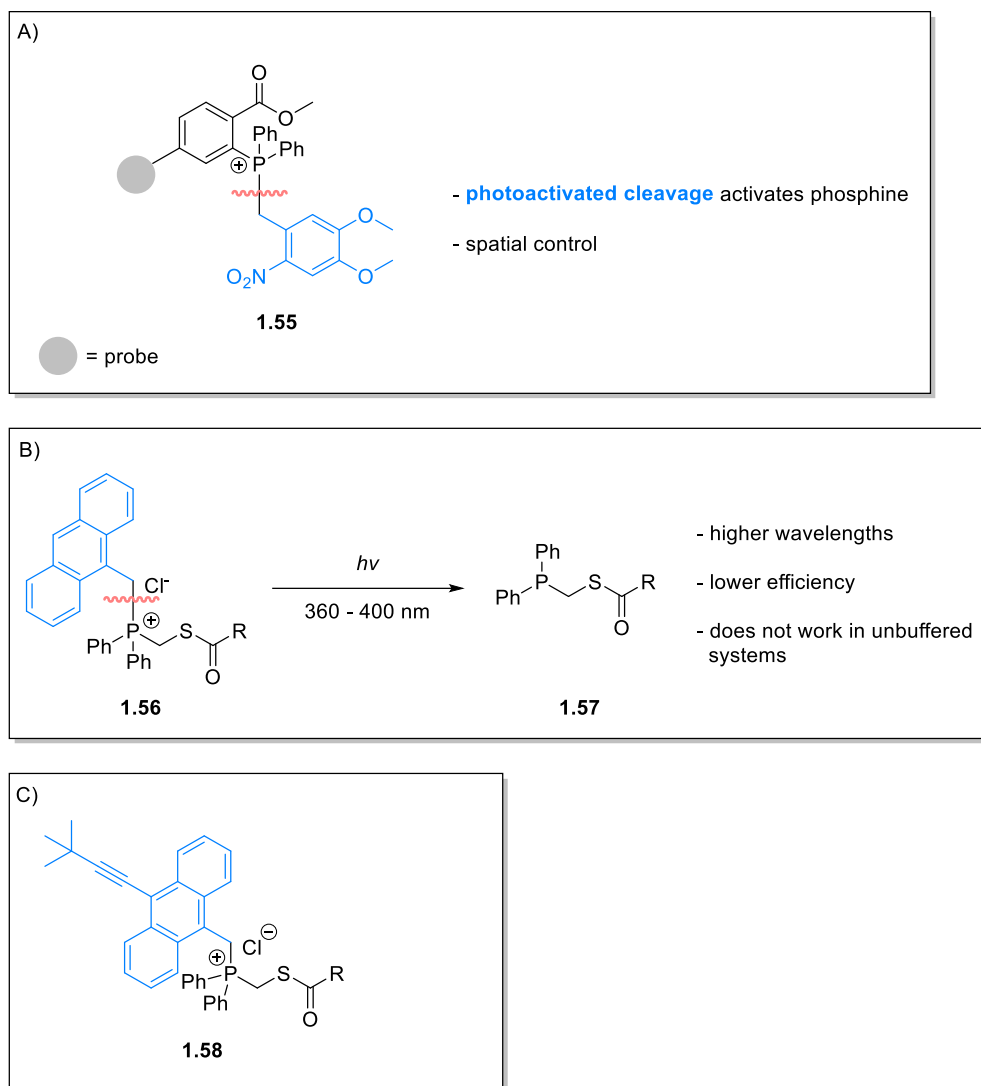


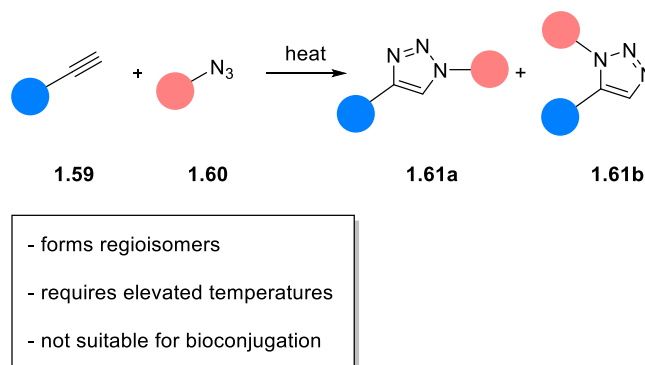
Figure 1.3. (A) Use of the 4,5-dimethoxy-2-nitrobenzyl photocaging group. (B) Anthracene photocaging group shifts activation to higher wavelengths. (C) Visible light-activated Staudinger ligation.

The development of the Staudinger ligation was the genesis of bio-orthogonal chemistry and allowed small molecular probes to label cellular organisms.⁴⁴ However, the reaction has several drawbacks and has been superseded by other bio-orthogonal reactions. First, the reaction kinetics are slow. Secondly, the phosphine starting material can be oxidised to the unreactive oxide. Both issues open the possibility to side reactions and degradation. Furthermore, slow kinetics necessitate higher reagent concentrations to achieve satisfactory conjugation which can increase toxicity or other off-target issues. Lastly, the reagents used for the Staudinger ligation tend to be bulky and hydrophobic. This can disturb natural function, cause unspecific binding and lead to solubility problems. Due to these problems, new bio-orthogonal reactions were actively sought out.

1.2.2 Copper Catalysed Azide Alkyne Cycloaddition (CuAAC)

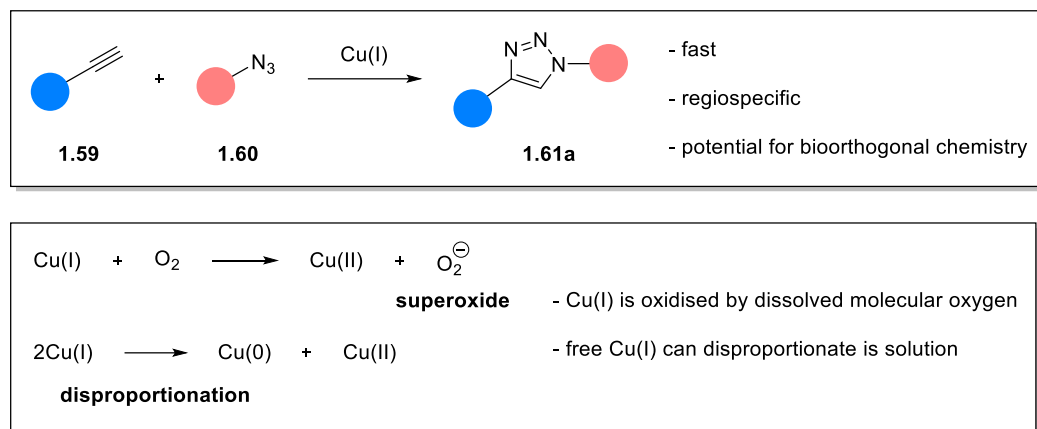
The 1,3 dipolar cycloaddition between an alkyne and an azide was first described by Huisgen in 1963.⁵² The reaction proceeds rather slowly at room temperature and the rate could be increased by heating. This reaction is not regioselective and both the 1,4 (**1.61a**) and 1,5 (**1.61b**) triazole products are formed (Scheme 1.11).

Huisgen Cycloaddition:



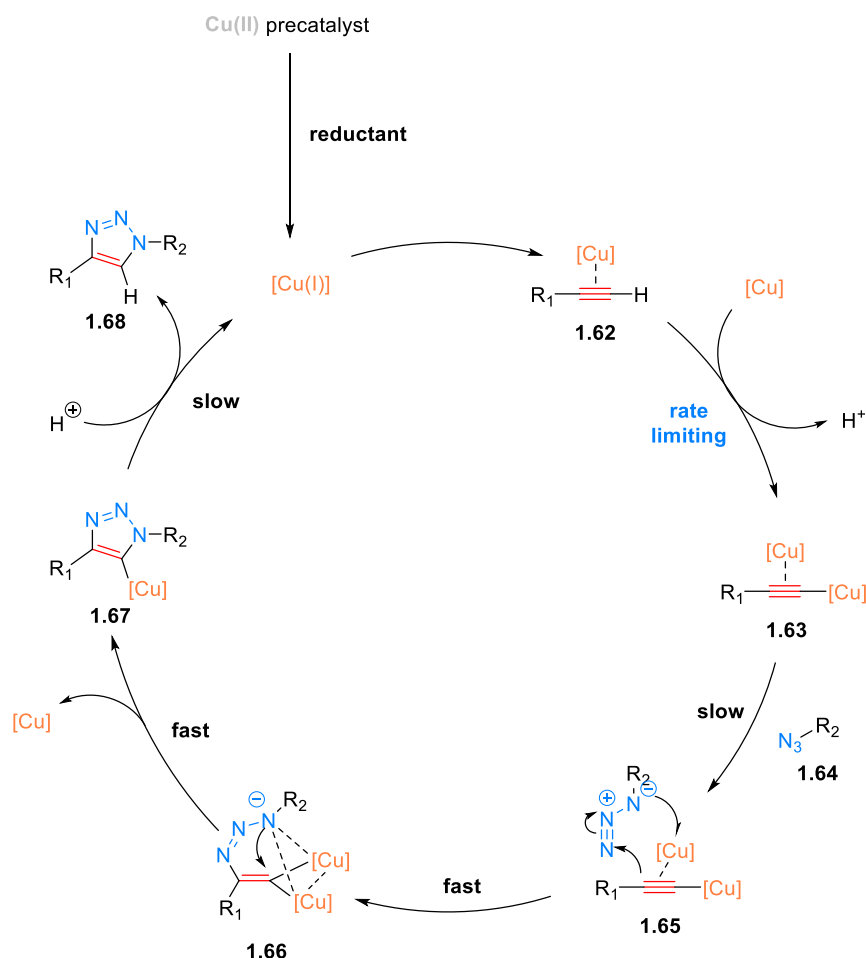
Scheme 1.11. Thermal Huisgen-Cycloaddition.

In 2002 the groups of Meldal⁵³ and Sharpless⁵⁴ both independently discovered that the reaction could be catalysed by the addition of copper salts. Copper catalysis increased the reaction rate significantly and led to the exclusive formation of the 1,4 triazole (**1.61a**) (Scheme 1.12). Cu(I) was proposed as the active species and could either be formed *in situ* by reduction of Cu(II) or through the use of Cu(I) salts. It is vital to maintain the copper in its first oxidation state throughout the reaction. This is complicated by the fact that dissolved molecular oxygen can oxidise Cu(I) to Cu(II) or the metal can disproportionate in solution to form Cu(II) and elemental copper. Therefore, the reaction is usually run under inert atmosphere or with an excess of reducing agent. The CuAAC reaction fits the described criteria⁵⁵ for a “click reaction”, which require reactions to be modular, wide in scope, high yielding, generate minimal side products and be stereospecific. Therefore, the CuAAC reaction is also known as the “copper click reaction”.

Copper catalysed azide-alkyne cycloaddition:**Scheme 1.12.** The CuAAC reaction and routes to Cu(II) in solution.*1.2.2.1 Mechanism of the CuAAC Reaction*

The first tentative mechanism was proposed by Sharpless in 2002,⁵⁴ followed by a series of investigations stretching over several years to elucidate the mechanism of the CuAAC reaction leading to the current accepted mechanism depicted in Scheme 1.13. The reaction is initiated by co-ordination of Cu(I) to the alkyne triple bond (**1.62**). This lowers the $\text{p}K_{\text{a}}$ of the acetylide proton and facilitates the formation of the π,σ -bis(copper) acetylide complex (**1.63**).^{56,57} The azide then co-ordinates to the dinuclear complex (**1.65**)⁵⁸ and forms intermediate^{59,60} **1.66** which then contracts to form the mononuclear copper triazole (**1.67**).⁶¹ Proto-demetalation then furnishes the triazole product (**1.68**) and Cu(I) can re-enter the catalytic cycle.

The formation of bis-acetylide complex **1.62** is regarded as the rate limiting step⁵⁷ and is determined by the acidity of the alkyne proton ($\text{p}K_{\text{a}} \sim 25$ in water), which can be lowered by adjacent electron withdrawing groups. The proto-demetalation can be accelerated by the use of copper salts such as $\text{Cu}(\text{OAc})_2$ where the acetate is assumed to act as a proton shuttle.⁶² The formation of intermediate **1.67** is assumed to be extremely fast, as no intermediates could be isolated.



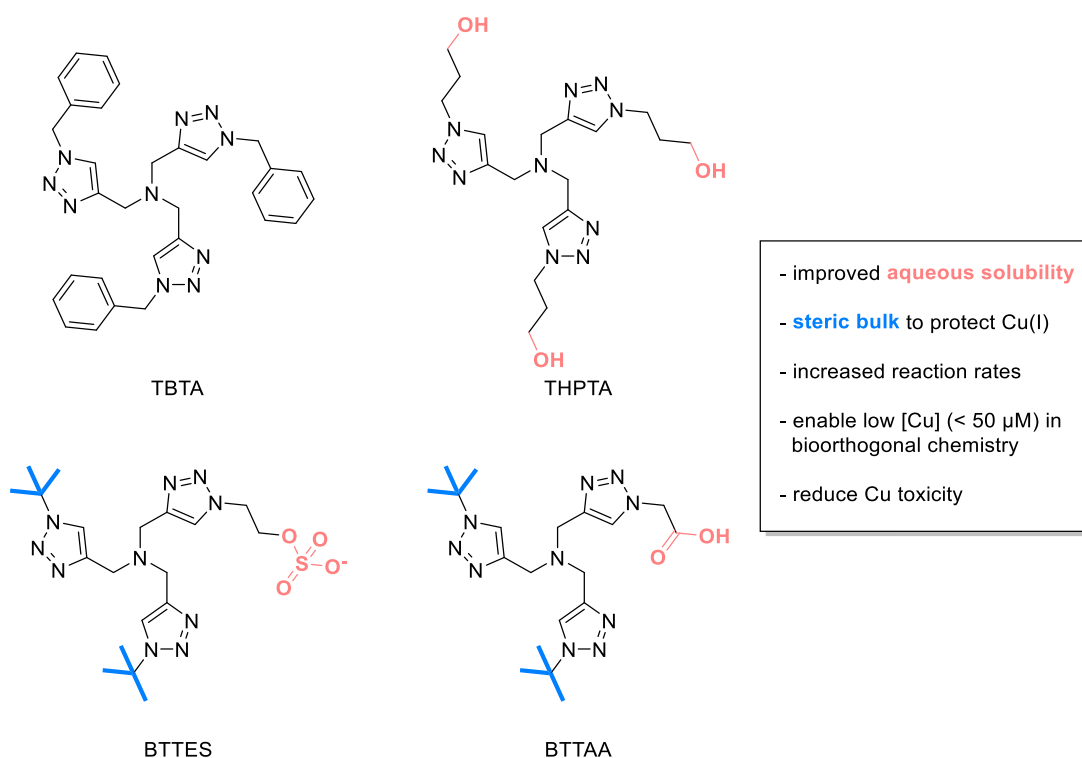
Scheme 1.13. Current accepted mechanism of the CuAAC reaction.

The CuAAC reaction has attracted a lot of attention in the field of bioconjugation due to the fast reaction kinetics and regioselectivity.⁶³ The reaction requires only small reactive handles such as alkynes and azides, which are unlikely to disturb the biological function of a molecule. Both moieties are non-natural and generally not reactive with endogenous molecules. All these factors make the CuAAC an ideal candidate for bio-orthogonal chemistry. However, the reaction has one significant drawback. The need for Cu(I) to catalyse the reaction limits the use *in vivo* due to copper's cytotoxicity. While copper is an essential trace element in biology, its potential to catalyse the formation of reactive oxygen species means that its cellular transport and location are tightly controlled by chelation with enzymes and small molecules such as glutathione.⁶⁴ Consequently, free Cu(I) is essentially non-existent in a cellular environment.⁶⁵ To perform the CuAAC reaction *in vivo*, large concentrations of copper ($> 100 \mu\text{M}$) must be added to the system which significantly affects the viability of living

organisms. Researchers have devised several strategies to combat the cytotoxicity of copper and enable its use *in vivo*.

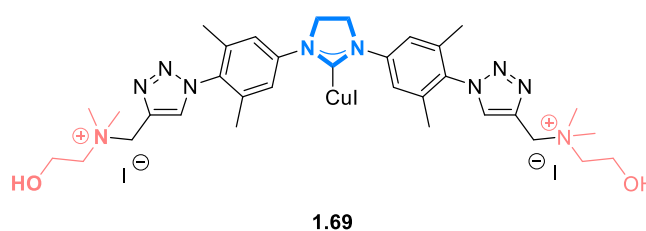
1.2.2.2 Developments of Ligands for the CuAAC Reaction

To increase catalytic efficiency and limit toxicity, several CuAAC ligands were developed for biological applications. At first, polytriazoleamine ligands such as TBTA (Figure 1.4) were shown to accelerate the CuAAC reaction and stabilise Cu(I) in its oxidation state by chelation and protection from disproportionation or oxidation through oxygen.⁶⁶ Multiple variations of tripodal amine ligands containing benzimidazole⁶⁷ and other copper chelating moieties (pyridyl, triazolyl)⁶⁸ were then investigated and THPTA emerged as a more effective and soluble ligand.⁶⁹ The next iteration of ligands led to the discovery of the ligand BTTES.⁷⁰ This ligand enabled effective cell surface labelling without significant toxicity at low Cu(I) concentrations (50 μ M). Furthermore, fucosides of living zebrafish could be labelled for the first time. Encouraged by these results, the same researchers developed an improved variation the following year.⁷¹ The ligand BTTAA, which features a carboxylic acid moiety instead of a sulphate, yielded larger reaction rates in fluorescent assays and showed better or comparable labelling of proteins in various cell lysate assays when compared against cyclooctyne DBCO.⁷¹ Furthermore, BTTAA outperformed SPAAC labelling of cell surface glycans and zebrafish and also outperformed BTTES in fucoside labelling in zebrafish by approximately 2.5 times.⁷¹

CuAAC accelerating ligands:**Figure 1.4.** Structure of common CuAAC ligands used for bioconjugation.

NHC ligands with their strong electron donating properties were envisioned to stabilise Cu(I) in an aqueous environment without the need of reducing agents such as NaAsc. But their poor water solubility was a hurdle that had to be overcome by Gaulier *et al.* in 2012.⁷² They modified the mesityl core with choline groups linked by a triazole (**1.69**) to increase water solubility (Figure 1.5) and the iodide counterion was crucial to ensure stability and reactivity and buffers containing chloride diminished reactivity. The ligand was then used to functionalise short peptides and showed good activity unless chelating amino acids such as cysteine or histidine were present.

NHC ligands for CuAAC:



- carbene **stabilises Cu(I)** in aqueous environment
- choline substituents **improved solubility**
- chloride containing buffers reduce efficiency

Figure 1.5. Structure of water soluble NHC-ligand.

The use of preformed ligands avoids the use of reducing agents and eliminates possible interference side products.⁷³ Therefore, the group of Mascarenas screened the reactivity of various preformed copper-ligand complexes *in vitro* and *in vivo*.⁷⁴ While the preformed copper complexes performed worse *in vitro*, compared with the standard protocol (Cu(II) source, ligand and sodium ascorbate), they showed better reactivity *in vivo* activity – the BTTE-Cu(I) complex (1.70) in particular (Figure 1.6). It was found that preformed copper complexes were superior to elevate the cellular copper concentration.

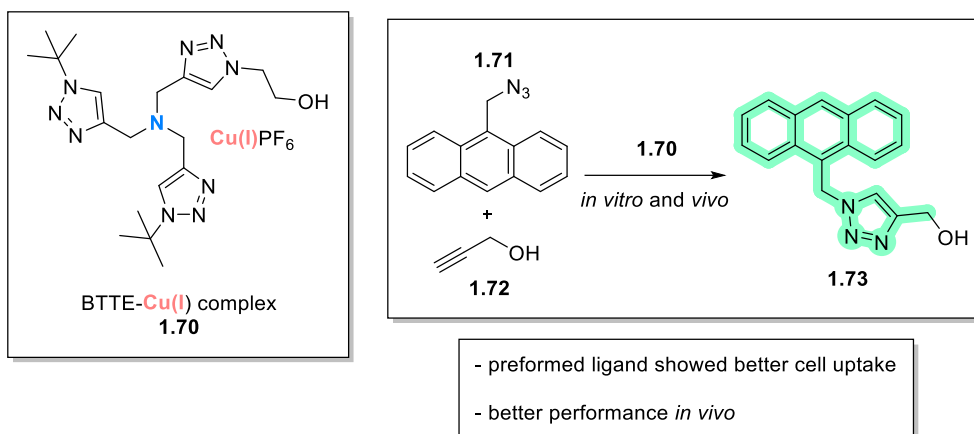


Figure 1.6. Structure of the preformed ligand. Fluorescent “turn on” CuAAC reaction *in vitro* and *in vivo*.

1.2.2.3 Organometallic Nanoparticles for CuAAC Bioconjugation

Protecting Cu(I) in an aqueous environment is key for successful CuAAC bioconjugation. Organometallic nanoparticles (OMNP), which are single chain crosslinked polymers containing metal centres are designed to mimic metalloenzymes. In a first study such an

OMNPs successfully catalysed the CuAAC reaction with ppm levels (5 - 30) of copper between various alkynes and azides in water (Figure 1.7).⁷⁵ Hydrophilic substrates required higher catalyst loadings which was attributed to their decreased binding to the polymer surface. The same OMNP was also effective in catalysing the CuAAC between 3-azido-7-hydroxycoumarin (**1.74**) and *p*-ethynyl anisole (**1.75**) in human breast cancer cells at a concentration of only 0.5 μ M.

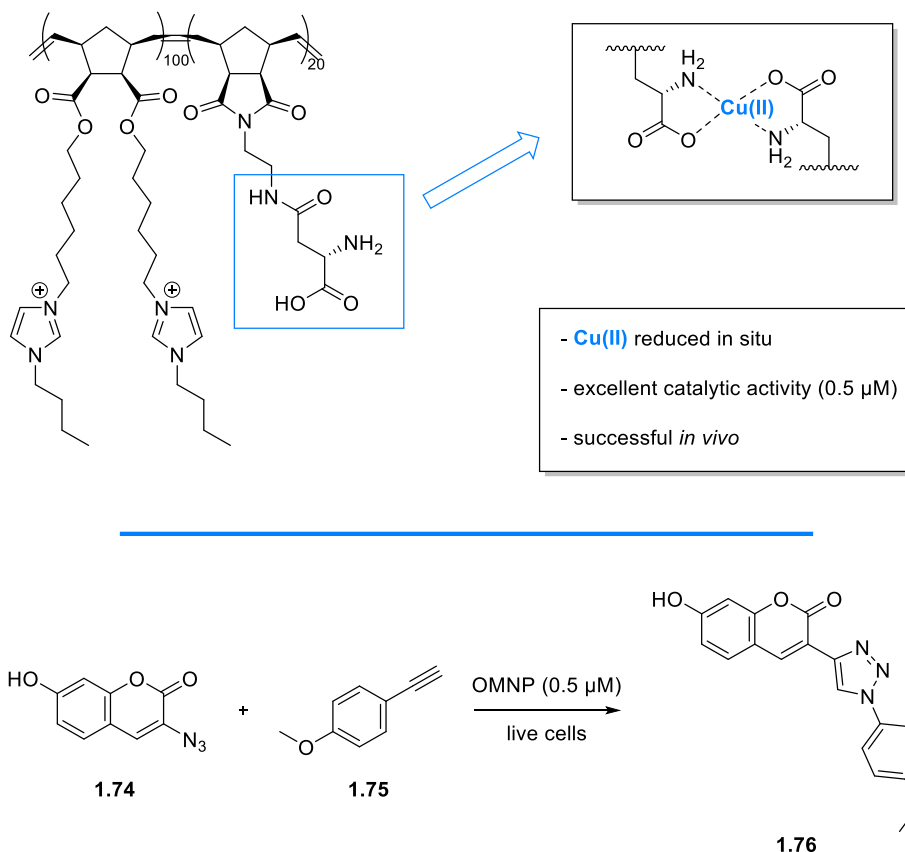
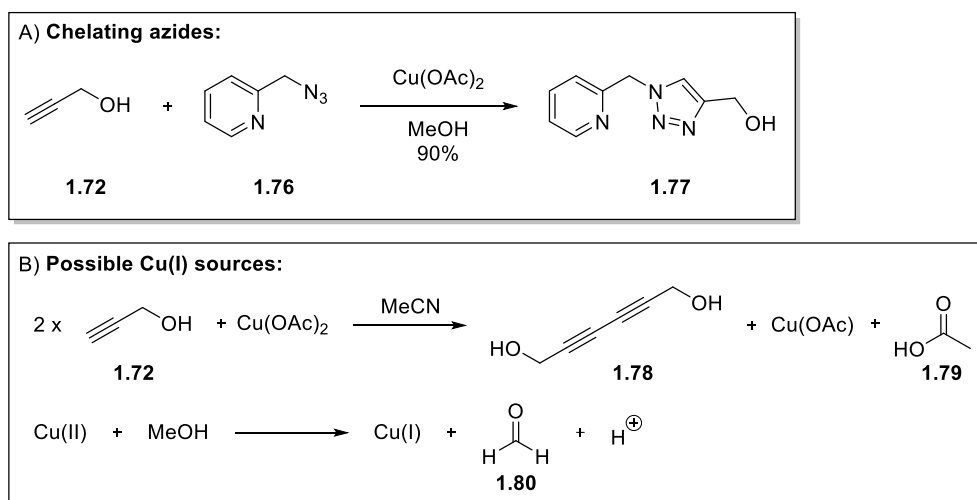


Figure 1.7. Structure of OMNP which catalyses reaction between azide **1.74** and alkyne **1.76** in live cells.

The same group then investigated the influence of lipophilicity, charge, size and copper loading on catalysis.⁷⁶ Substrate binding affinity to the short-chain nanoparticle (SCNP) largely determined reactivity. An overall positively charged SCNP increased reaction rates for negatively charged substrates and *vice versa*. When the SCNP was zwitterionic, the reaction rate did not depend on charge but on lipophilicity. Size did not affect reaction rate significantly and medium sized SCNP (4 - 7 nm diameter) were the most reactive. Similarly, higher copper loading did not increase reaction rate.

1.2.2.4 Copper Chelating Azides for CuAAC Reactions

In 2009, the group of Zhu discovered that copper chelating azides – such as picolyl azide **1.76** – accelerated the CuAAC reaction (Scheme 1.14A).⁷⁷ Cu(OAc)₂ was the only Cu(II) source which showed good conversion in aprotic and protic solvents. As none of these reactions required reducing agents, the researchers speculated that Cu(I) could either be produced by oxidative homocoupling in acetonitrile (creating the diyne **1.78**) or from alcohol oxidation in protic solvents (Scheme 1.14B).



Scheme 1.14. (A) CuAAC reaction accelerated by chelating azides. (B) Alkyne homocoupling and MeOH oxidation to provide Cu(I) sources for CuAAC catalysis.

The potential of chelating azides to achieve high reaction rates under reduced copper loadings in bioconjugation was recognised in 2012 by Alice Ting and researchers.⁷⁸ Screening of various picolyl azide derivatives revealed that electron donating groups accelerated the chelation assisted CuAAC while electron withdrawing groups reduced reaction rate (Figure 1.8). The chelation assisted CuAAC could be further enhanced by the addition of ligands such as THPTA. Compared to non-chelating azides, the extent of cell surface labelling increased by 3 to 25 times when copper chelating azides were used and the surface of modified HEK cells could be labelled using only 40 μ M copper.

However, higher concentrations of CuSO₄ (2 mM) were needed to label alkyne modified RNA inside cells. The use of chelating azides has now enabled the labelling of proteins,⁷⁹ oligosaccharides in live cells⁸⁰ and the EGFR on living cells.⁸¹

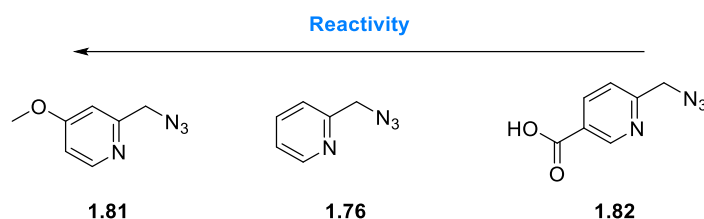


Figure 1.8. Electron-donating groups improve the chelating azide assisted CuAAC.

Taking inspiration from both the ligand and chelating azide accelerated CuAAC reaction, Bevilacqua *et al.* fused both concepts to achieve an even more effective catalyst.⁸² Their “all in one” azide (**1.83**) (Figure 1.9) achieved conversion of ~65% in 40s at a reactant concentration of 17.5 μM (alkyne, azide, ligand 1:1:1). In cell lysate, the conversion was reduced to 40%. The *in vivo* applicability of this azide was demonstrated by labelling microtubules inside HuH-7 cells at a concentration of 50 μM of the azide-copper complex.

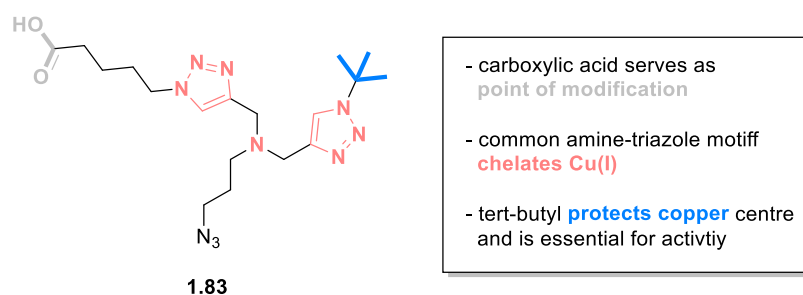
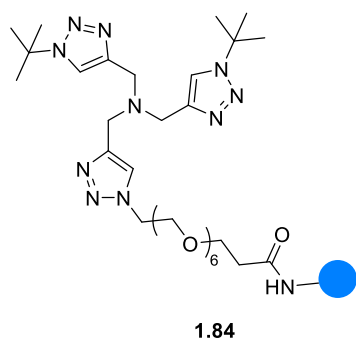


Figure 1.9. Structure of chelating “all in one” azide.

1.2.2.5 Applications of CuAAC Reactions inside Living Cells

Despite the many advancements for the CuAAC in bioconjugation, *in vivo* applications inside live cells are still rare. The first example makes use of the classical strategy of employing copper ligands to limit cytotoxicity.⁸³ To increase cellular copper uptake, the group of Cai attached Tat, a cell penetrating peptide, to a BTAA derivative (Figure 1.10) to form ligand **1.84** which doubled the cellular copper concentration in HUVEC and OVCAR5 cells. The ligand also protected cells from copper induced apoptosis (60% remaining after 24 h vs <5% in the presence of unchelated 100 μM CuSO_4). Notably, a NaAsc concentration of larger than 500 μM also induced cell death. *In vivo*, the labelling yield when using ligand (**1.84**) was only ~0.8%. Targeted depletion of GSH increased the yield to 14%, which signifies the impact the cellular thiol can have on the CuAAC reaction.

Cell-penetrating CuAAC ligands:



- increased cellular copper uptake
- better performance *in cellulo* than BTAA
- reduced copper toxicity
- *in vivo* CuAAC yield affected by GSH

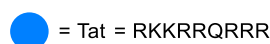
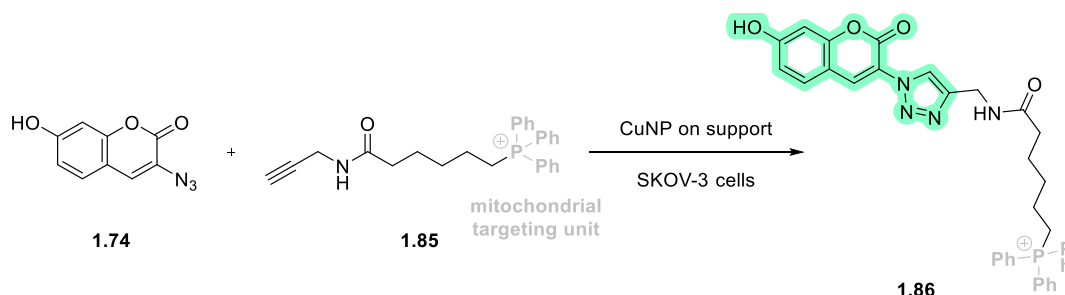


Figure 1.10. Structure of cell penetrating ligand.

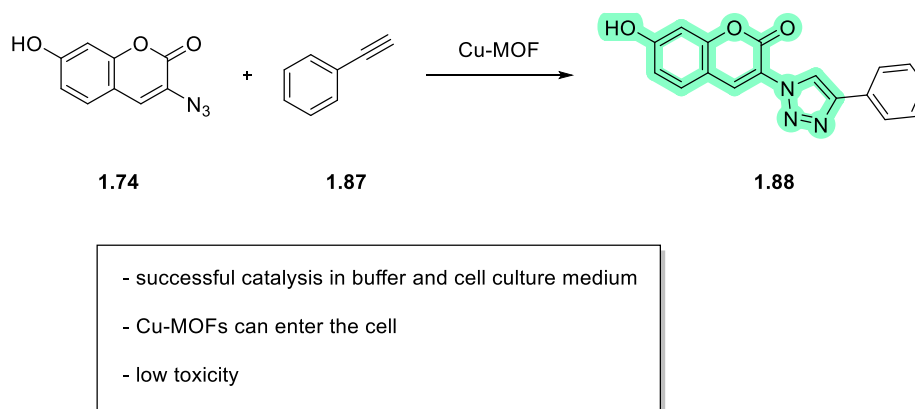
A second approach to *in vivo* CuAAC reactions is heterogenous catalysis. The group of Bradley used copper nanoparticles on solid support to perform the CuAAC *in vivo*.⁸⁴ The aim was to reduce copper toxicity by trapping copper ions in TentaGel® resin beads, thereby creating nanoparticles which enhanced biocompatibility. They were able to catalyse the fluorogenic CuAAC reaction between **1.74** and **1.85** (Scheme 1.15) in a variety of media (PBS, 5% FBS and HeLa cell lysate) and obtained comparable conversion to the traditional CuSO₄/THPTA system. The cell viability of SKOV-3 (ovarian adenocarcinoma) cells was not compromised by the nanoparticles (compared with ~20% viability after 24 h with 20 μM CuSO₄). Due to the size of the particles (~160 μm), the microbeads needed to be implanted into the yolk sac of zebrafish to catalyse the fluorogenic reaction between **1.74** and **1.85**. No significant toxic or developmental effects were observed for the embryo.



- comparable conversions to CuSO₄/THPTA protocol
- successful in medium and cell lysate
- better cell viability compared to CuSO₄/THPTA protocol

Scheme 1.15. Reaction between **1.74** and **1.85** catalysed by copper nanoparticles on solid support.

The main drawback of the previous approach was that the particles were too big to enter cells. Wang *et al.* envisioned that metal organic frameworks (MOF) could accomplish the task of protecting copper while being able to pass the cell membrane.⁸⁵ They synthesised MOFs of a 51 nm diameter and were able to successfully catalyse the fluorogenic CuAAC reaction between **1.74** and **1.87** (Scheme 1.16) in water, PBS and cell culture medium. Additionally, the MOFs were able to enter cells via endocytosis and when functionalised with a triphenylphosphonium (TPP) moiety localised in the mitochondria, where they catalysed the click reaction between **1.74** and **1.87** inside MCF-7 cells. They also showed negligible cytotoxicity up to a level of 100 µg/mL. They further demonstrated the *in situ* synthesis of a triazole resveratrol analogue which more effectively increased cell apoptosis compared with supplementing the cell medium with the drug.



Scheme 1.16. Fluorogenic reaction between **1.74** and **1.87** catalysed by Cu-MOFs.

1.2.2.6 The Main Drawbacks of the CuAAC for Bioconjugation: Oxidative Damage and Cytotoxicity

The main drawbacks of the CuAAC for bioconjugation are the cytotoxicity and availability of copper. Copper is an essential trace element that is found in every cell of the organism and forms the active centres of vital enzymes.⁸⁶ The cellular concentration of copper depends on organisms and cell types. For example, the copper concentration is estimated to be around 70 µM in yeast cells.⁸⁷ While these levels are theoretically enough to catalyse the CuAAC reaction, virtually no measurable levels of unbound copper are present in cells.⁸⁸

The toxicity of free copper is attributed to the production of reactive oxygen species (Figure 1.11A). Cu(I) can react with dissolved molecular oxygen to form superoxide which can be converted to hydroxy radicals.⁸⁹ These free radicals can also damage DNA through base

oxidation or scission of the DNA backbone. The most susceptible nucleobase is guanine **1.89**. From a variety of degradation pathways the most prominent is shown in Figure 1.11B.⁹⁰ This damage can occur rapidly as measured by qPCR with only 1 in 5000 DNA strands (3.5 kb long) remaining intact after 5 minutes of exposure to 50 μM Cu(I).⁹¹ Higher concentrations of ligand or NaAsc reduced the DNA damage slightly. In contrast, the addition of 10% DMSO to the reaction medium had a pronounced effect on DNA stability. After 25 minutes, about 40% of the DNA remained intact. This was attributed to the ability of DMSO to scavenge superoxide and hydroxyl radicals.

The hydroxyl radicals generated from free Cu(I) can also oxidise the most susceptible amino acids such as histidine, cysteine, and methionine (Figure 1.11C).⁹² Again, oxidative damage can be reduced by CuAAC-ligands and is dependent on the surface accessibility of amino acid. Other mitigation strategies involve carrying out the reaction under argon or the addition of sacrificial cysteine, which has been shown to reduce the oxidative damage to interferon beta-1b (~ 20 kDa) from around 7% to less than 1%.⁹³

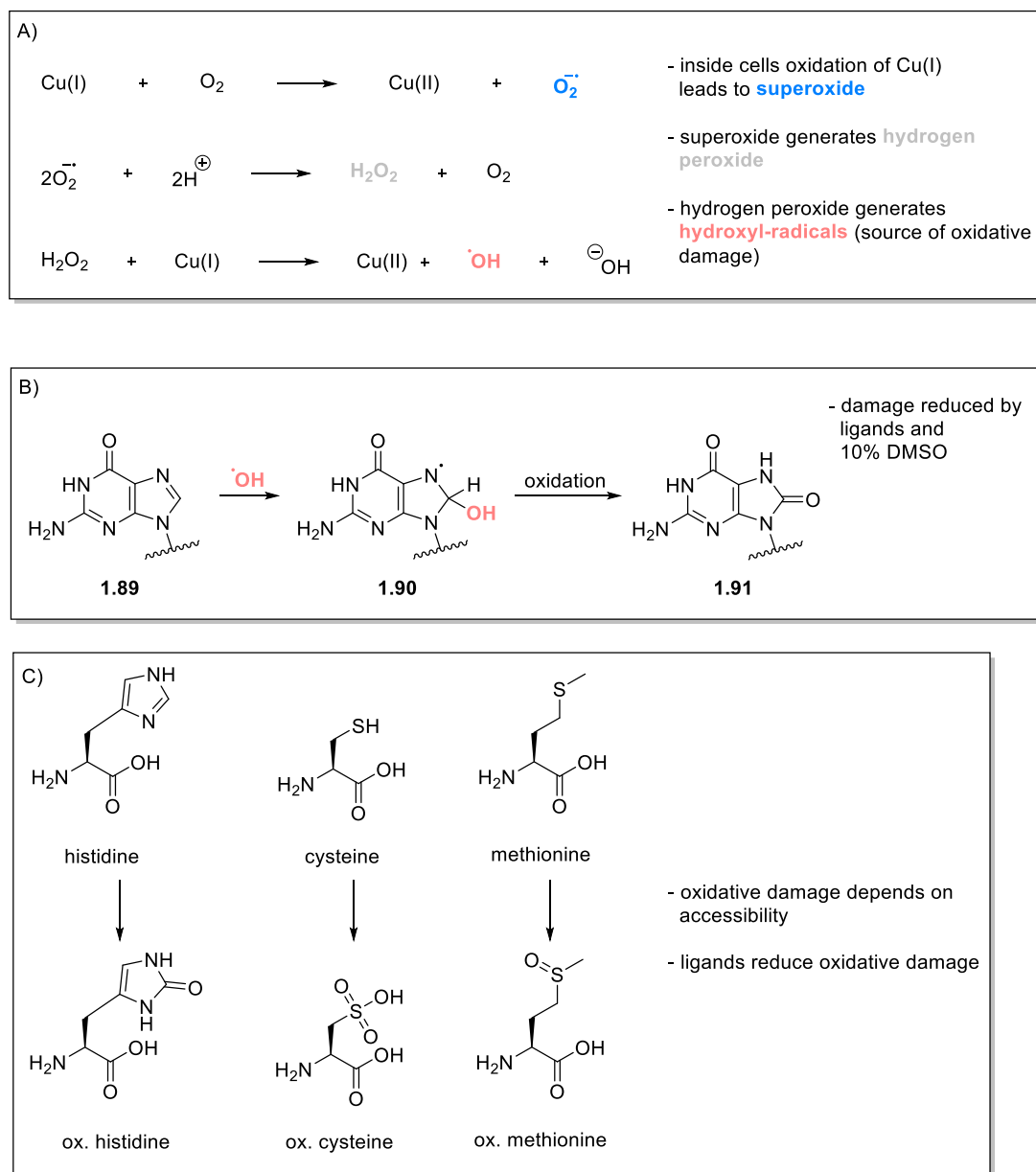


Figure 1.11. (A) Production of hydroxyl radicals by Cu(I) redox cycling. (B) Oxidation of guanine. (C) Oxidised amino acids histidine, cysteine, and methionine.

For *in vivo* applications, reduced cell viability is mainly caused by Cu(I), as exposure to 20 – 100 μM Cu(I) for 4 hours reduced cell survival to 10%. In contrast, Cu(II) showed no measurable toxicity under the same conditions.⁹⁴ Ligands can raise viability to around 75%^{94,95} depending on the exact conditions. Copper-complexes with histidine were especially effective in reducing toxicity as no drop in viability was observed after exposure to 50 μM Cu(I) for three days.⁸⁹ However, these promising results have not been applied in further applications by other groups and histidine has been reported to only be moderately effective at catalysing

the CuAAC reaction.⁹⁶ The solvent and NaAsc concentration vary between the different publications, which might explain the different observed reactivity.

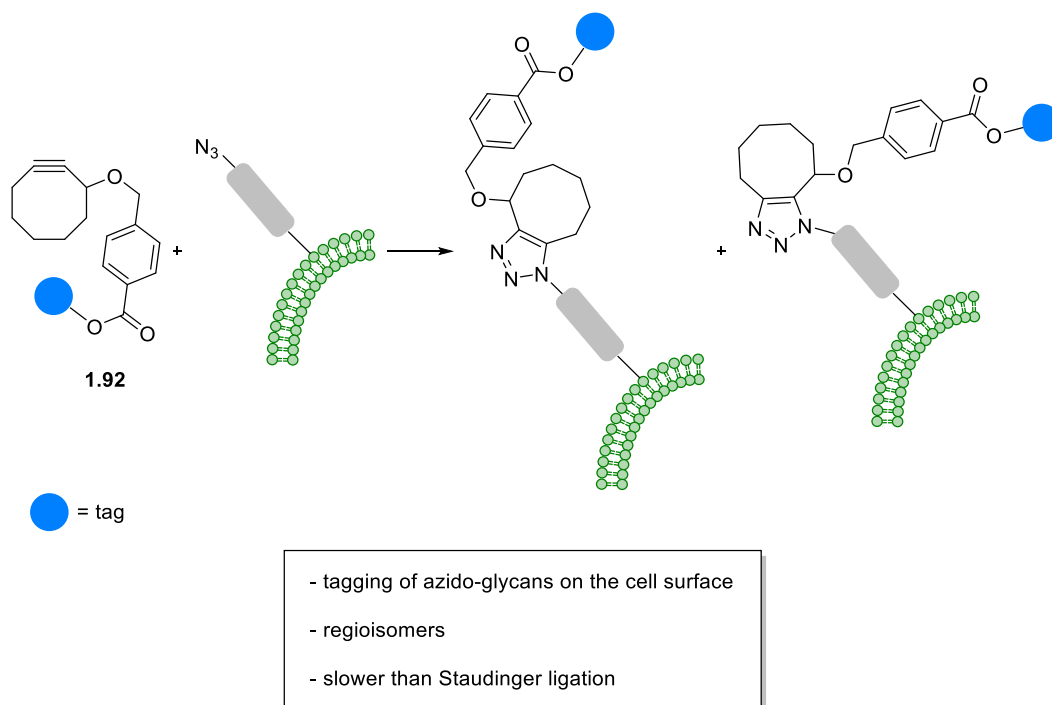
In summary, the ideal for a CuAAC conditions for *in vivo* application is as follows: [Cu] under 50 μM ,^{74,78,83,97,98} excess ligand⁹⁹ and the least amount of reducing agent¹⁰⁰ necessary. These conditions successfully mitigate toxicity; however, oxidation is still likely to occur under these conditions.^{100,101} To minimise oxidation further, the CuAAC reactions should be performed under the exclusion of oxygen.¹⁰²

1.2.3 Strain-Promoted Azide-Alkyne Cycloaddition (SPAAC)

1.2.3.1 First Generation Cyclooctynes

After the development of the Staudinger reaction for bio-orthogonal chemistry, Bertozzi recognised the suitability of the azide moiety as a functional handle for bioconjugation. In 2004, the Bertozzi group reported the first 1,3 dipolar cycloaddition between an azide and cyclooctyne (**1.92**) for bioconjugation, which was termed the strain-promoted alkyne-azide cycloaddition (SPAAC).¹⁰³ The SPAAC reaction avoids the use of cytotoxic copper and the surface of Jurkat cells could be labelled in a dose-dependent and selective manner (Scheme 1.17). However, labelling was not as efficient when compared to the Staudinger ligation.

In vivo use of the SPAAC reaction:



Scheme 1.17. Tagging of cell surface glycan via the SPAAC reaction.

To improve the kinetics of the cyclooctyne process, several modifications were explored (Figure 1.12).¹⁰⁴ Removal of the phenyl group in **1.94** served to reduce potential a steric clash, while the addition of a fluorine atom in **1.96** lowered the LUMO energy of the alkyne reducing the HOMO_{azide}-LUMO_{alkyne} gap. Rate constants were determined in CD₃CN and the addition of a fluorine atom doubled the rate (4.3 vs $2.4 \times 10^{-3} \text{ M}^{-1}\text{s}^{-1}$) while the removal of the phenyl group did not increase the rate constant. Further rate enhancements could be achieved by the synthesis of **1.97**, increasing the rate to $76 \times 10^{-3} \text{ M}^{-1}\text{s}^{-1}$.¹⁰⁵

First Generation Cyclooctynes:

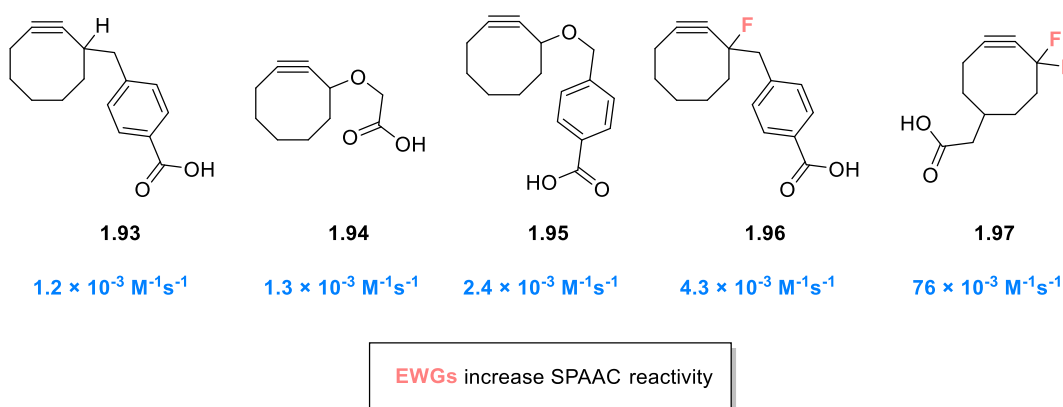


Figure 1.12. Structures and second order rate constants of SPAAC analogues.

The improved analogue (**1.97**) enabled labelling of isolated azido-modified protein (dihydrofolate reductase) that was on par with CuAAC labelling under pseudo first-order conditions and labelling of azido-modified glycans on Jurkat cells that was 20 times greater than that of Staudinger ligation or non-fluorinated cyclooctyne SPAAC. The faster reaction kinetics also allowed dynamic imaging of cell surface trafficking in CHO cells. Due to the low toxicity and the improved reaction kinetics, Laughlin *et al.* could utilise **1.97** for *in vivo* labelling of azide modified glycans in zebrafish.¹⁰⁶

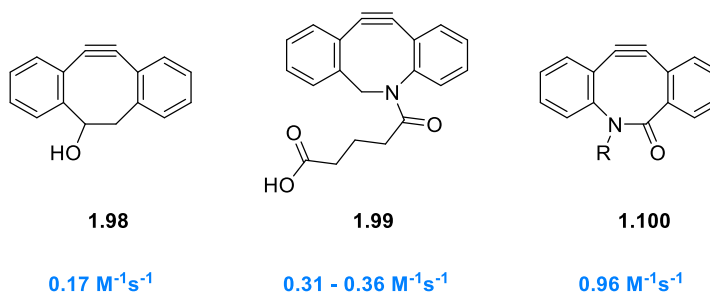
1.2.3.2 Second Generation SPAAC Reagents

Boons and co-workers explored further rate enhancements by increasing ring strain through the addition of aromatic rings to the cyclooctyne to form compound **1.98** (Figure 1.13).¹⁰⁷ They hypothesised that the increased ring strain would increase reaction rate and the ortho hydrogens might increase stability by preventing nucleophilic attack through a steric clash. Indeed, the measured rate constants for the reaction of **1.98** with benzyl azide were several orders of magnitude higher (0.17 or $2.3 \text{ M}^{-1}\text{s}^{-1}$ in MeOH or MeCN:H₂O = 4:1) than for the

original cyclooctyne **1.93** and on par with difluoro-cyclooctyne **1.97**. Using a biotin modified analogue the azide modified glycans on the surface of Jurkat cells could be imaged through fluorescent avidin-FITC staining. However, the solubility of **1.98** was limited to 100 μM in their system.

Taking this concept further, the group of van Delft tried to increase solubility and reaction rate by adding a nitrogen into the eight-membered ring (Figure 1.13).¹⁰⁸ The rate constant for their dibenzocyclooctyne-amine (DBCO) **1.99** was determined to be $0.31 \text{ M}^{-1}\text{s}^{-1}$ in CD_3OD and $0.36 \text{ M}^{-1}\text{s}^{-1}$ in D_2O , which was a slight improvement over **1.98**. They demonstrated the biological applicability by attaching PEG chains to different enzymes and proteins.

Second Generation cyclooctynes:



- Fused phenyl-rings increase ring strain and reactivity
- incorporation of sp^2 hybridised ring-atoms increases reactivity further
- **1.100** reaches the limit stability and reactivity balance

Figure 1.13. Structure and second order rate constants of benzene ring-fused cyclooctynes to increase ring strain and reactivity.

The final evolution of this aromatic ring strained system was developed by Bertozzi *et al* later in 2010.¹⁰⁹ They aimed to introduce an additional sp^2 carbon centre into the eight-membered ring to increase ring strain further (Figure 1.13). The resulting compound **1.100** had a rate constant of $0.96 \text{ M}^{-1}\text{s}^{-1}$ in acetonitrile and labelled the cell surface of Jurkat cells about three times more effectively than **1.97** and **1.98**. The high reactivity also allowed labelling at low concentrations (250 nM) which meant that washing after labelling could be eliminated. However, the increased reactivity came at the price of decreased stability. The half-life of **1.100** in the presence of a 2.5-fold excess (relative to **1.100**) of GSH was only 24 h, which is considerably less than for other cyclooctynes.

Most strained cyclo-alkynes presented so far suffer a lengthy and low yielding synthesis and are prone to nonspecific interactions with biomolecules due to high lipophilicity.¹¹⁰ To combat these problems, van Delft and co-workers developed the strained alkyne bicyclo[6.1.0]nonyne (BCN) (Figure 1.14).¹¹¹ The alkyne was synthesised in three-steps, yielding *endo*-BCN (**1.101**) in an overall yield of 61% and *exo*-BCN (**1.102**) in 53% yield (reduced separately from ester). *Endo*-BCN had a second order rate constant of $0.29 \text{ M}^{-1}\text{s}^{-1}$ while *exo*-BCN had a rate constant of $0.19 \text{ M}^{-1}\text{s}^{-1}$ in $\text{CD}_3\text{CN}/\text{D}_2\text{O}$ (1:2). Unlike **1.100**, both diastereomers were stable in the presence of GSH over a period of 48 hours.

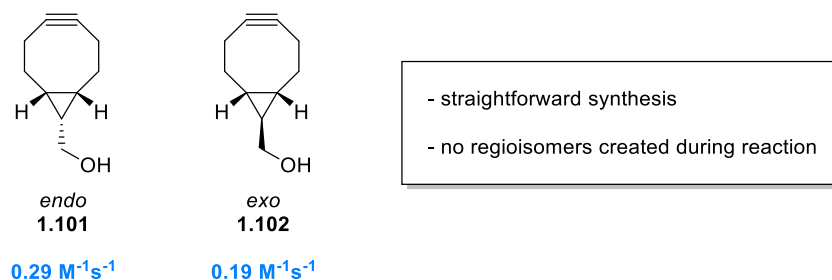
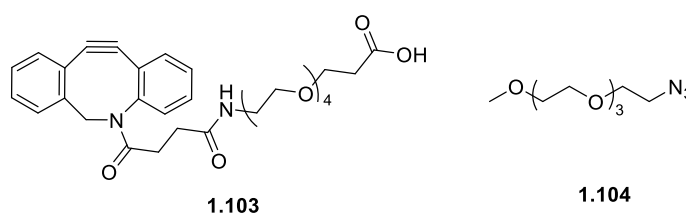


Figure 1.14. Structure and rate constants of *endo*- and *exo*-BCN.

1.2.3.3 Solvent Effect on the SPAAC Reaction

The group of Heemstra analysed the effect of the solvent on the SPAAC reaction.¹¹² For their study, they used hydrophilic DBCO (**1.103**) and hydrophilic azide (**1.104**) (Figure 1.15), which are commonly used in biological applications. The type of buffer (PBS, Tris, HEPES, etc) or ionic strength (additional NaCl to buffers, 0 – 500 mM) had negligible effect on the measured rate constants ($k_2 = \sim 1 \pm 0.2 \text{ M}^{-1}\text{s}^{-1}$) which were also not affected by pH (6.5 – 8). They attributed this to the fact that their reagents were hydrophilic, and a more pronounced effect would be observed with more hydrophobic reagents.

Solvent effect on SPAAC:



- ionic strength, buffer type and pH **do not affect** reaction rate
 - **higher water %** increases reaction rate

Figure 1.15. Structure of DBCO **1.103** and azide **1.104** used to investigate effect of solvent on the SPAAC reaction.

In contrast, the concentration (10, 40 and 70%) of the co-solvent (MeOH, MeCN, DMSO, NMP, EtOH) profoundly affected reaction rate. As is common for cycloadditions,^{113–115} the rate decreased with higher percentages of co-solvents which was especially pronounced for MeCN with rate constants halving going from 10 to 70% co-solvent. This was attributed to the loss of stabilising hydrogen bonding from water during the transition state. The only exception to this were DMSO and EtOH, where intermediate concentrations (~40%) increased rate constants (1.29 vs 1.56 M⁻¹s⁻¹, 10% vs 40% DMSO) up to a maximum of 1.8 M⁻¹s⁻¹ in 50 - 60% DMSO.

1.2.3.4 Micellar Catalysis for the SPAAC Reaction

Another approach to increase reaction rates in water is micellar catalysis.¹¹⁶ Micellar catalysis works by concentrating the hydrophobic reactants in the micelle centre, increasing the effective concentration. Since SPAAC reagents are usually hydrophobic, Grant *et al.* investigated the effect of ionic and non-ionic surfactants on the SPAAC reaction between (**1.103**) and benzyl azide **1.105**.¹¹⁷ The surfactants were employed at double the critical micellar concentration (CMC) and non-ionic surfactants (Tween 80 and Triton X-100) resulted in a modest (6.4 and 11-fold) increase in reaction rate. Both SDS (anionic) and DTAB (cationic) spurred large rate increases (92-fold), and CTAB (cationic) increased the rate constant 179-fold to 78 M⁻¹s⁻¹ (Figure 1.16). In contrast, when hydrophilic azide (**1.104**) was used, only small increases in reaction rate were found. Similarly, when a DBCO modified DNA strand was labelled with benzyl azide, only a modest increase in rate (~10-fold) was observed when CTAB was used as surfactant. This was attributed to the hydrophilicity of DNA and shows the limits and problems for this approach for *in vitro* or *in vivo* labelling.

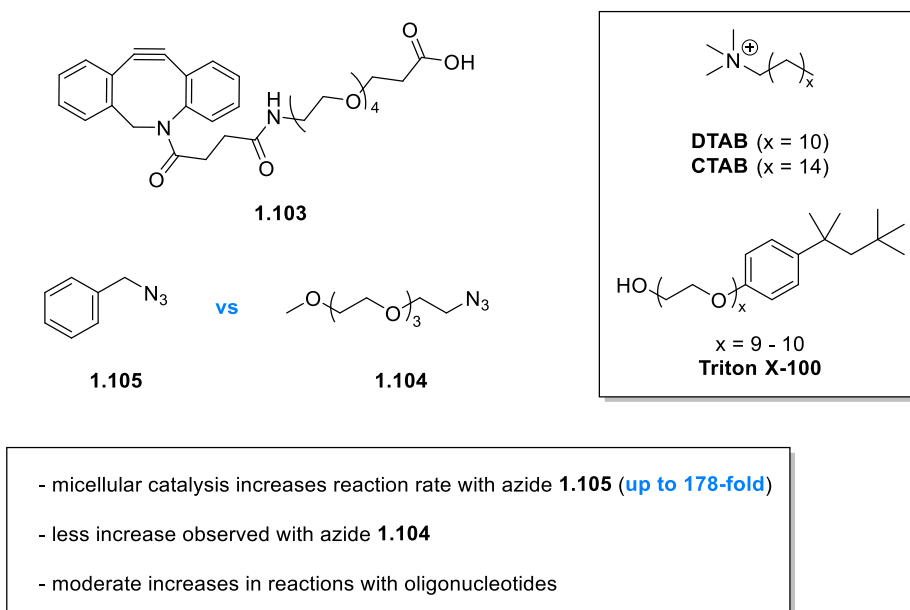
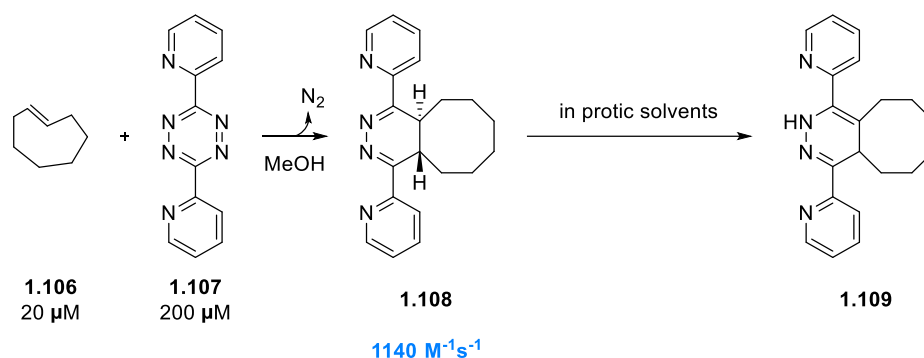


Figure 1.16. Structures of reagents and surfactants used to investigate micellar catalysis.

The development of the SPAAC allowed the labelling of biomolecules in a transition metal free fashion, circumventing possible toxicity issues. However, despite numerous developments, the observed rate constants reach limits of $\sim 1 \text{ M}^{-1}\text{s}^{-1}$ and further improvements are challenging as increasing ring strain leads to higher instability of the SPAAC reagent. Further drawbacks include the often-bulky size, lipophilicity, lengthy synthesis, and the formation of regio-isomers.

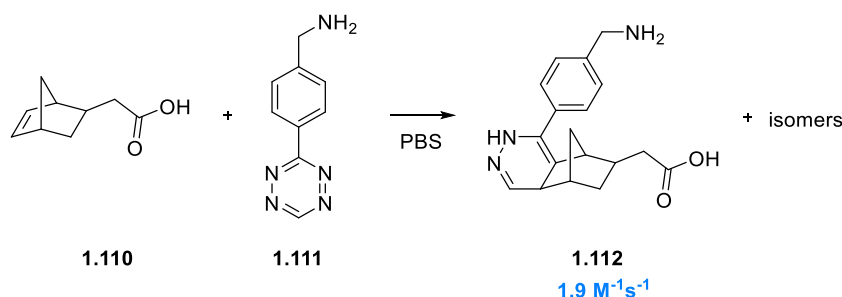
1.2.4 Inverse Electron Demand Diels Alder Reaction

A significant advance for copper-free click reactions was made in 2008, when the inverse electron demand Diels-Alder (IEDDA) reaction was used in a biological context for the first time. The hunt for increased reaction kinetics led the researchers of Fox *et al.* to the reaction of tetrazines and *trans*-cyclooctenes (TCO).¹¹⁸ Based on the work of Sauer *et al.* in 1990¹¹⁹ they surmised that the IEDDA would be applicable for biology. The reaction between TCO **1.106** and tetrazine **1.107** (Scheme 1.18) was successful in cell media (DMEM + 5% FBS) and cell lysate, which proved the biocompatibility of the reaction. The rate constant measured in MeOH was $1140 \text{ M}^{-1}\text{s}^{-1}$ which increased to $2000 \text{ M}^{-1}\text{s}^{-1}$ in MeOH/H₂O (9:1) and was unprecedented for bio-orthogonal reactions. The applicability of the IEDDA was demonstrated by tagging thioredoxin (single accessible cysteine residue) with a maleimide-TCO-conjugate and reacting the modified protein (15 μM) with a two-fold excess of **1.107**.



Scheme 1.18. First use of the IEDDA reaction in biological context.

In parallel, Devaraj *et al.* investigated the reaction between norbornene **1.110** and tetrazine **1.111** (Scheme 1.19) as a potential substrate pair for bioconjugation.¹²⁰ They determined rate constants of $1.9 \text{ M}^{-1}\text{s}^{-1}$ in buffer and of $1.6 \text{ M}^{-1}\text{s}^{-1}$ in FBS, which were significantly slower when compared to the IEDDA reaction with TCO. Another drawback is that the reaction created four isomeric products.



Scheme 1.19. Reaction between norbornene **1.110** and tetrazine **1.111** in buffer.

1.2.4.1 Cyclopropenes for IEDDA Reaction

Further substrates for the IEDDA were investigated by Prescher¹²¹ and Devaraj¹²² in 2012 to address the problems of stability, size and lipophilicity of the TCO. Unsubstituted cyclopropenes are unstable at room temperature and tend to dimerize easily even if stored in the freezer overnight. Therefore, Devaraj investigated cyclopropene derivatives (**1.113** and **1.114**) to find a good balance between stability and reactivity (Figure 1.17A).¹²² Both cyclopropenes were stable in aqueous solution and in the presence of 1 mM L-cysteine over a period of 24 hours. The influence of the electron withdrawing carboxylic group on the reaction rate was significant with a rate constant obtained of $0.137 \text{ M}^{-1}\text{s}^{-1}$ at 37°C versus **1.114** with a

rate constant of $13 \text{ M}^{-1}\text{s}^{-1}$. In the same year, the group of Prescher also investigated a range of potential cyclopropenes (**1.115** – **1.118**) for bio-orthogonal labelling.¹²¹ They observed the same trends as Devaraj *et al.* with cyclopropenes possessing electron-withdrawing carbonyl groups being more stable and less reactive than their counterparts (Figure 1.17).

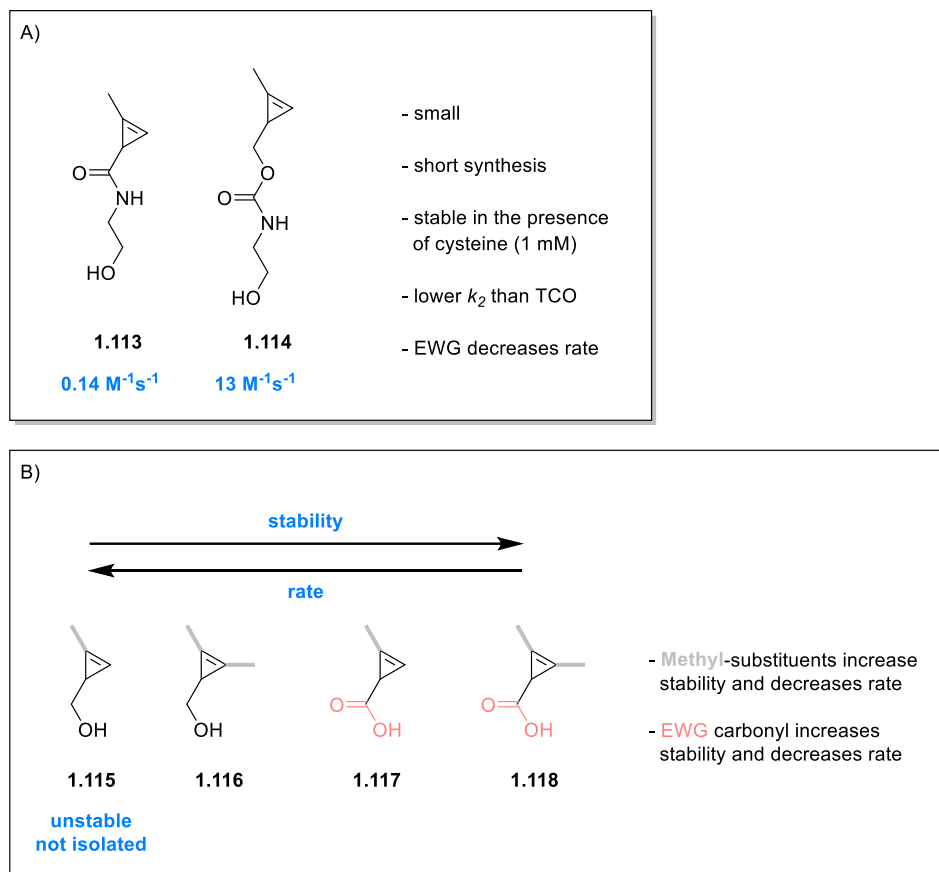


Figure 1.17. (A) Cyclopropenes investigated by the group of Devaraj. (B) Cyclopropenes investigated by the group of Prescher.

1.2.4.2 Factors which Influence IEDDA Reactivity

The IEDDA proceeds in a 4+2 cycloaddition between an electron rich-diene and electron-deficient dienophile.¹²³ Unlike the Diels Alder reaction, the IEDDA is not reversible due to the evolution of nitrogen, making it ideal for bioconjugation. In the IEDDA the LUMO of the electron-poor diene reacts with the HOMO of the electron rich dienophile. Therefore, the reactivity of the IEDDA reaction can be modulated by decreasing the HOMO-LUMO gap (Figure 1.18).

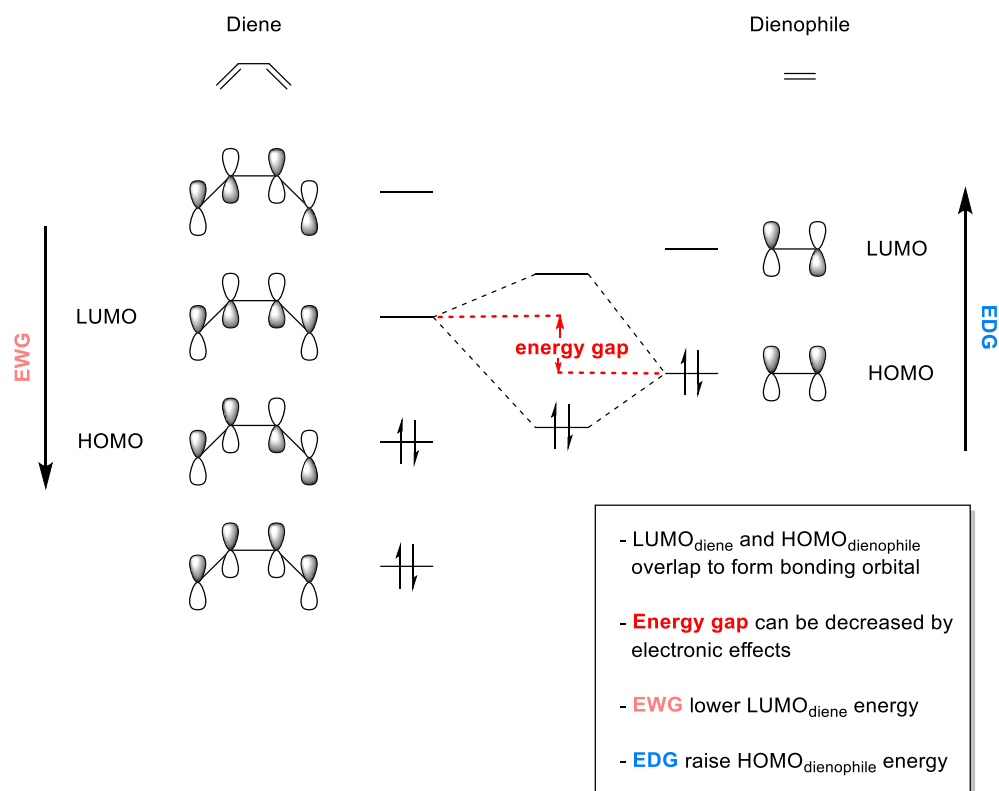


Figure 1.18. Figure showing the FMO theory of the IEDDA reaction.

Electron-withdrawing groups (EWG) on the diene lower LUMO energy and electron-donating groups (EDG) in the dienophile increase HOMO energy (Figure 1.19A and C). Alkynes are generally less reactive than alkenes due to the lower HOMO energy.¹²⁴

The second handle to modulate reactivity is to increase diene strain which raises the HOMO energy and distorts the geometry closer to the transition state, which lowers the activation energy (Figure 1.19B).¹⁰

Apart from electronics and ring strain, stereochemistry also plays a vital role. For example, TCO functionalised with electron-donating groups to increase the HOMO energy can be either present as the equatorial (**1.125**) or axial (**1.126**) isomers (Figure 1.19 D). The axial isomer (**1.126**) is about four times more reactive.

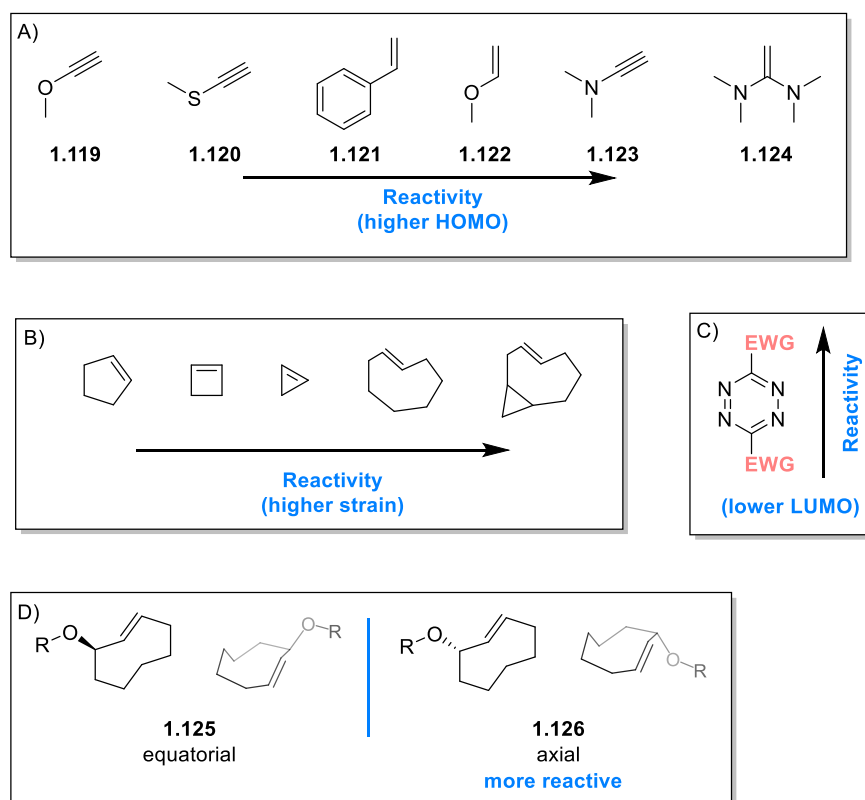


Figure 1.19. (A) Reactivity of alkenes and alkynes in the IEDDA reaction. (B) Reactivity of strained alkenes in the IEDDA reaction. (C) EWG increase tetrazine reactivity. (D) Axial TCO isomer is more reactive.

Steric effects of tetrazines can also influence the reaction rate of the IEDDA reaction. Monosubstituted tetrazines are generally more reactive than their disubstituted counterparts. However, the increased reactivity is usually offset by diminished stability. Karver *et al.* synthesised a panel of tetrazines and determined the second order rate constants as well as the stability in FBS after 10 h (Figure 1.20).¹²⁵ Generally, the most reactive tetrazines also displayed lowest stabilities. Monosubstituted tetrazines (**1.128** and **1.111**) were most reactive, followed by pyrimidyl-substituted tetrazines (**1.129** and **1.131**), then pyridyl-substituted (**1.130** and **1.132**) and finally methyl-substituted tetrazines (**1.133**). Pyrimidyl-substituted tetrazines especially suffered from significant instability (only 20 or 40% remaining after 10 h). One exception was tetrazine **1.128**, which displayed the highest reactivity ($k_2 = 30000 \text{ M}^{-1} \text{s}^{-1}$) and maintained good stability (70%). Another noteworthy point is the poor solubility of tetrazines. Especially diaryl substituted tetrazines are frequently insoluble, obstructing their use in biology.

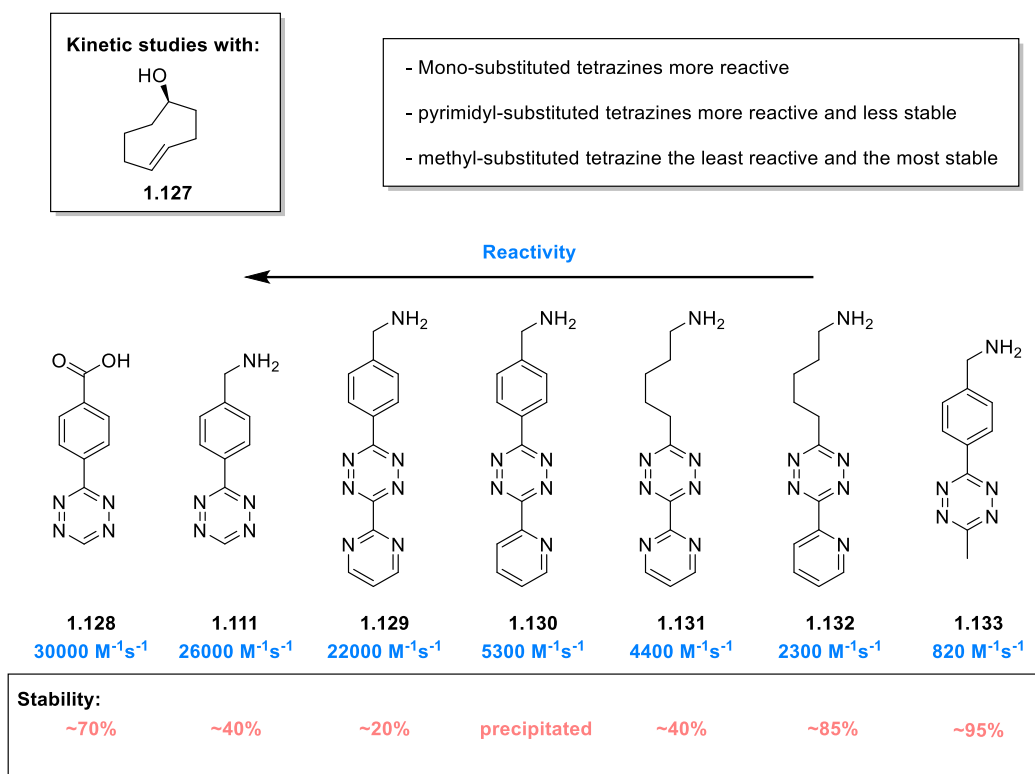


Figure 1.20. Reactivity and stability of a range of tetrazines. Stability studies performed in FBS over 10 h at 37 °C.

The high reaction rates also translate to *in vivo* experiments (Figure 1.21).¹²⁶ Genetically encoded tetrazine **1.134** could be labelled with a the second-order rate constant of 72500 M⁻¹s⁻¹ which compares to a rate constant of 87000 M⁻¹s⁻¹ *in vitro*. Due to the high reaction rates ($t_{1/2}$ = 12 -14 sec) real-time monitoring was possible for the first time.

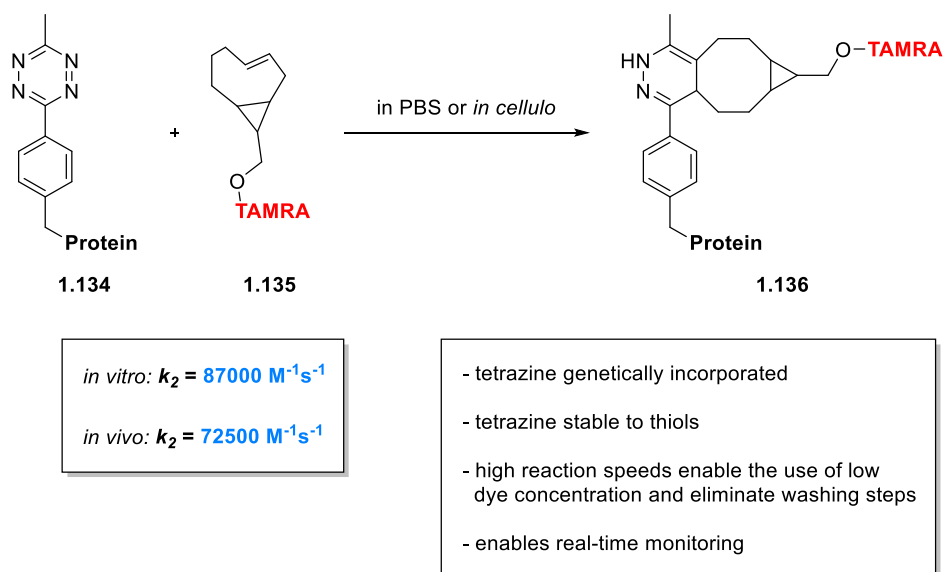


Figure 1.21. Labelling of genetically encoded tetrazine with strained TCO leading to comparable reaction rates *in vitro* and *in vivo*.

1.2.4.3 IEDDA Reaction for ‘Click to Release’ Applications

Apart from highly efficient fluorescent labelling, the IEDDA reaction has also found use in targeted and timed drug release. In 2013, the group of Robillard evaluated a range of tetrazines for its ability to release amine-cargo from carbamate modified TCO (**1.137**) (Figure 1.22A).¹²⁷ The cleavage yield depended on the steric size of the tetrazine substituents with smaller methyl-substituents (**1.138**) affording superior release (79% after 4 h in 25% CD₃CN at 37°C). The axial TCO isomer (**1.142**) (Figure 1.22B) was more reactive and the rates of release increased in an aqueous environment. Good release was also observed in 50% serum (Figure 1.22 C) and release was also demonstrated in cell culture (A431 tumor cells).

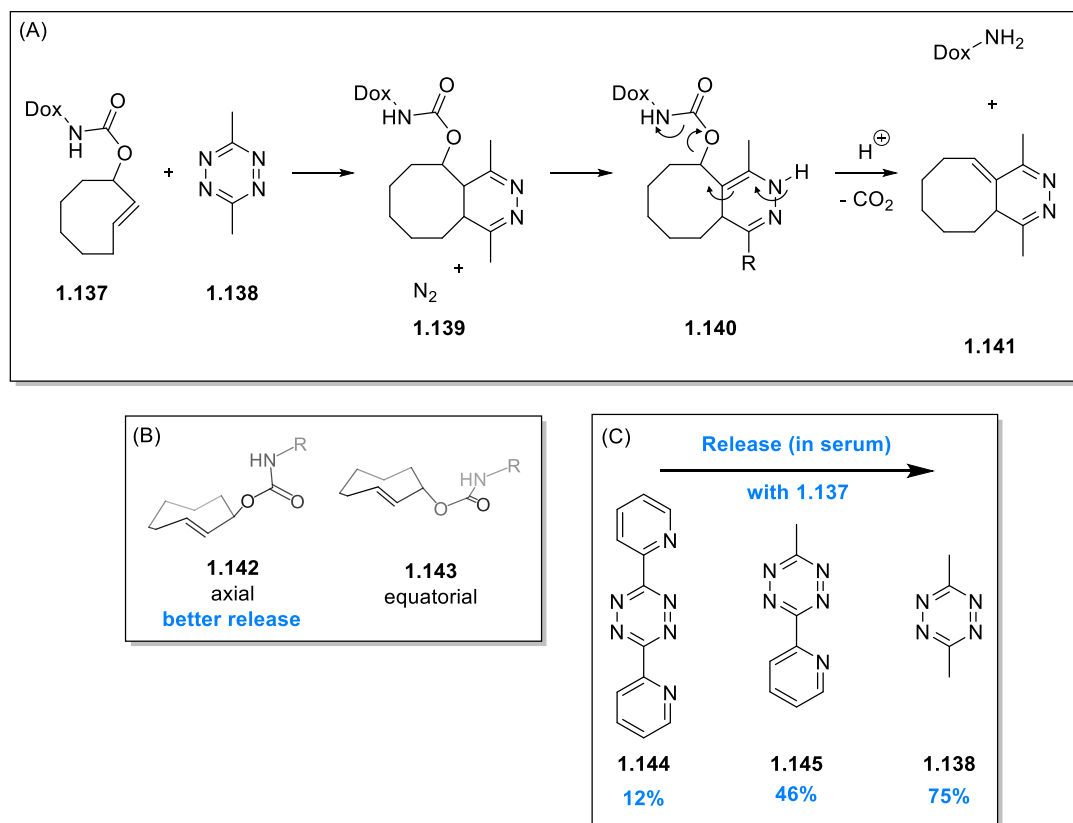


Figure 1.22. (A) Mechanism of release, Dox = doxorubicin (a common cancer drug), (B) Axial TCO isomers afford better release yields (in 50% serum at 37 °C after 4 h); (C) unhindered tetrazines yield better release; (D) Better drug release also correlates with increased drug efficiency.

Further studies investigated the click to release applications of the IEDDA reaction. In 2014, the group of Chen applied the IEDDA click reaction to uncage lysine residues in GFP (**1.146**) *in vitro* (80% after 15 mins) and in luciferase *in vivo* (>80% after 15 mins).¹²⁸ Their study confirmed the previously observed trends that unhindered tetrazines (**1.138**) and the axial TCO isomer afford better release yields (Figure 1.23A). In a follow-up study in 2016, the same group investigated the factors that influence release (Figure 1.23B).¹²⁹ In agreement with earlier results, they found that smaller substituents performed better and that electron-poor tetrazines afforded higher cycloaddition yields. Tetrazine **1.149** showed excellent performance and was able to decage 90% of TCO-lysine residues in modified GFP and luciferase proteins, within 5 minutes.

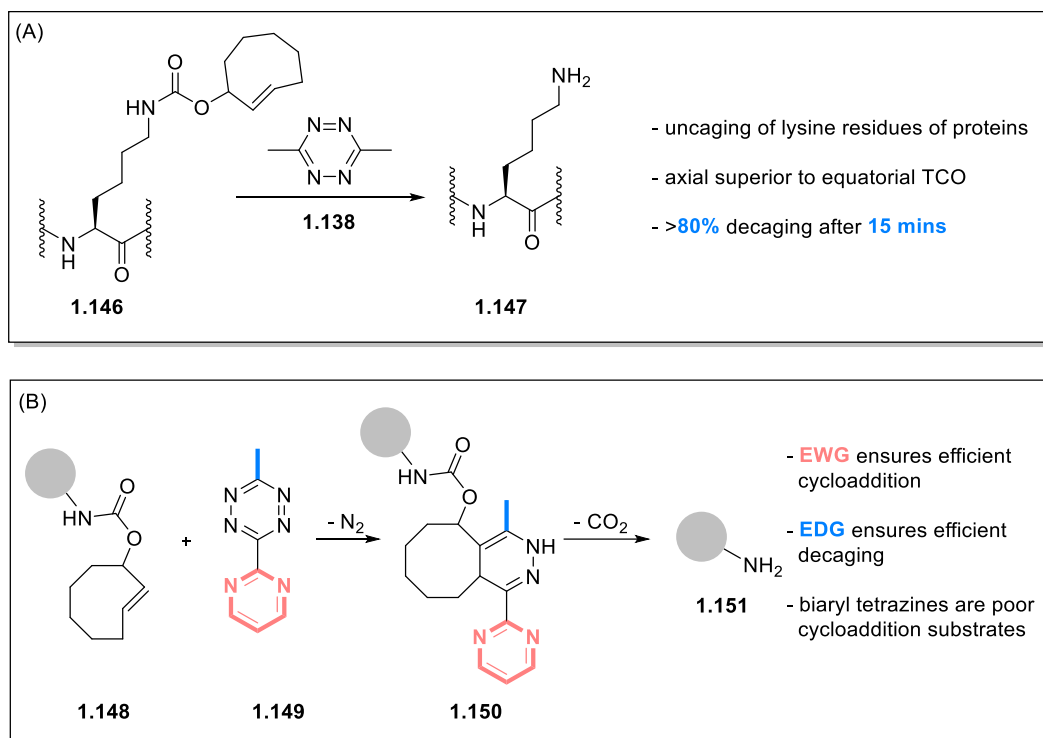


Figure 1.23. (A) Decaging of TCO-lysine incorporated into proteins. (B) Tetrazines must strike a balance between electron-rich and electron-poor to allow the cycloaddition and decaging to proceed efficiently.

The group of Weissleder investigated the TCO click to release reaction under physiologically relevant conditions in 2018.¹³⁰ They discovered that pH was an important factor and a pH of 5 or 6 accelerated the release. Further, they could identify the formation of cyclised product **1.157** as the cause of low release yields (Figure 1.24A). The formation of this product was favoured at higher pH. At lower pH, the tautomerisation to **1.153** and **1.154** proceeded quickly and in the case of **1.153** led to fast release. While tautomer **1.154** was not a dead end, it could not undergo release of the carbamate and had to tautomerize to **1.153** before release was possible. This process was slow and competed with the slow oxidation to product **1.156**, which formed a reactive dead end.

Therefore, to achieve efficient release, the formation of **1.154**, **1.156** and **1.157** had to be prevented or minimised. The group of Weissleder achieved this by employing a carboxylic acid functionalised tetrazine to form cycloaddition product **1.158** (Figure 1.24B). Through proximal proton transfer, the rate of release could be enhanced considerably (too fast to quantify) up to a release of 50%. Then the release rate slowed. The initial fast release was attributed to isomer **1.158**, while the second slower release was attributed to **1.160**, highlighting the importance of regioselectivity. Formation of **1.157** could also be reduced by

methyating the amide nitrogen of the carbamate (**1.161**) to block ring formation (Figure 1.24C).

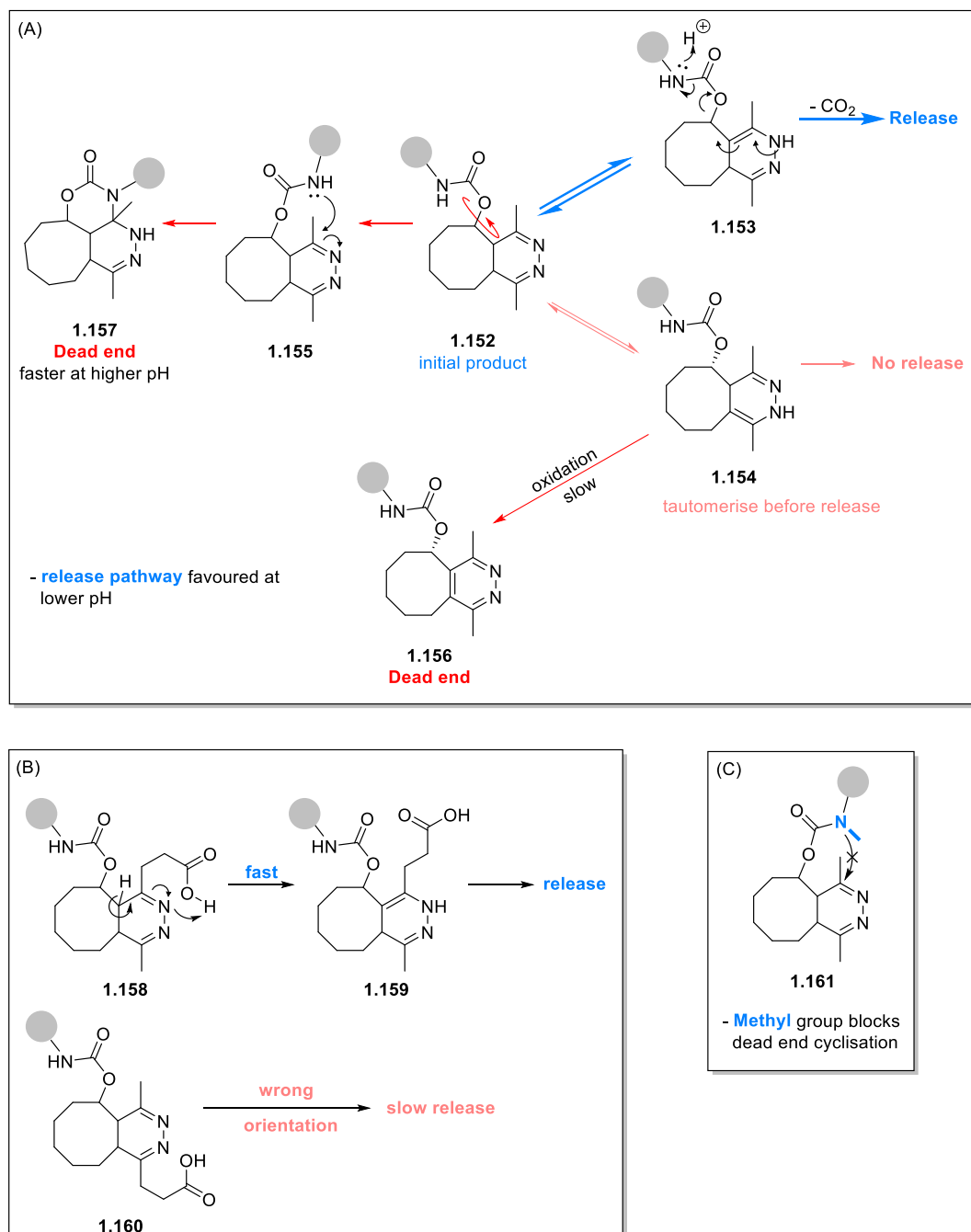


Figure 1.24. (A) Mechanism of “Click to Release”. (B) Acid assisted accelerated release. (C) Methylated nitrogen prevents formation of ‘dead-end’ product.

To sum up, the IEDDA achieves unparalleled reaction rates for bio-orthogonal chemistry and allows the use of low reagent concentrations while still enabling real-time monitoring. The rate of the reaction can be increased by attaching electron-withdrawing groups to the tetrazine

and thereby lowering the LUMO energy. A balance between reactivity and stability must be struck, as biaryl tetrazines are prone to degradation. The HOMO energy of the dienophile partner can be either raised through electron-donating groups or by increasing ring strain. The two most common dienophiles are the cyclopropene and TCO. Cyclopropenes display good reactivity and stability but are outperformed by TCO in terms of reactivity. However, TCO is prone to *trans-cis* isomerisation by intracellular thiols,¹³¹ which deactivated the highly strained system and abolishes IEDDA reactivity. Furthermore, the IEDDA reaction produces several regio-isomers and tetrazines are frequently insoluble which can limit their applications in bioconjugation.

1.3 Incorporation of Unnatural Moieties

1.3.1 Incorporation of Unnatural Moieties by Native Enzymes

Bio-orthogonal functional groups must be introduced into the organism of interest, as they are typically non-canonical. One approach exploits the promiscuity of the natural cellular machinery to incorporate non-canonical amino acids into biomolecules into proteins during translation.

Translation is part of the “Central Dogma of Biology” which was first proposed by Francis Crick in 1957 (Figure 1.25).¹³² It describes the process of converting the information stored in DNA through RNA into proteins via transcription and translation.

Central Dogma of Biology:

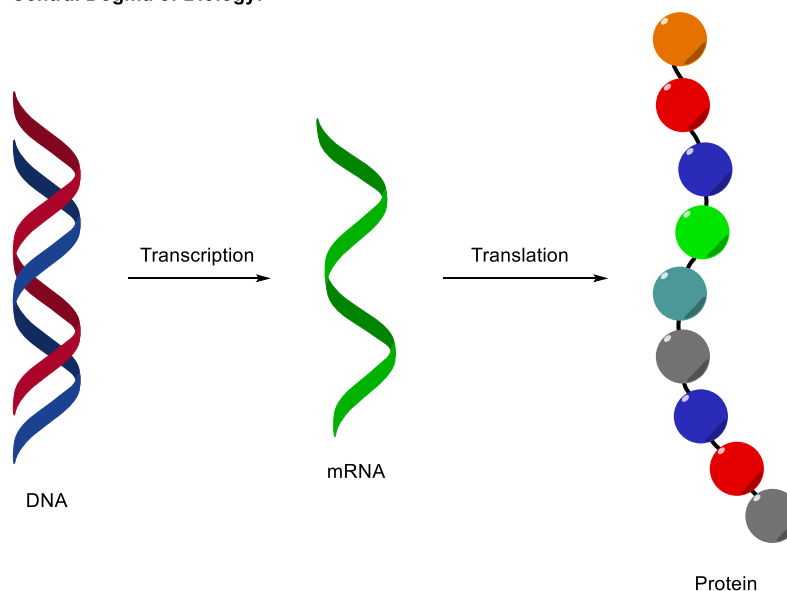


Figure 1.25. Schematic of the coded protein synthesis going from DNA to RNA and finally to protein via transcription and translation.

During transcription, the information of the DNA template strand is copied to RNA by the enzyme RNA polymerase. Before leaving the nucleus, the RNA is processed by capping the 5' end (with guanine) and attaching a 3' poly-adenosine tail to form pre-messenger RNA (pre-mRNA). Then non-coding pieces of RNA (introns) are removed from the strand and coding pieces of RNA (exons) spliced together to form a mature messenger RNA (mRNA) strand which can leave the nucleus.¹³³

Once in the cytosol, the mRNA is translated into a string of amino acids by the ribosome complex. Each amino acid is encoded by a unique three letter sequence of nucleotides, called codon. In the ribosome, the amino acids are delivered to the growing peptide chain by transfer RNA molecules (tRNA). These singled stranded RNA molecules feature an anti-codon, which is complementary to the codon in the mRNA.¹³³

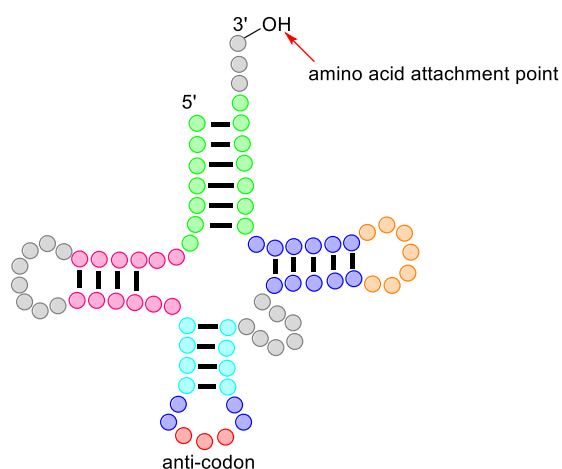
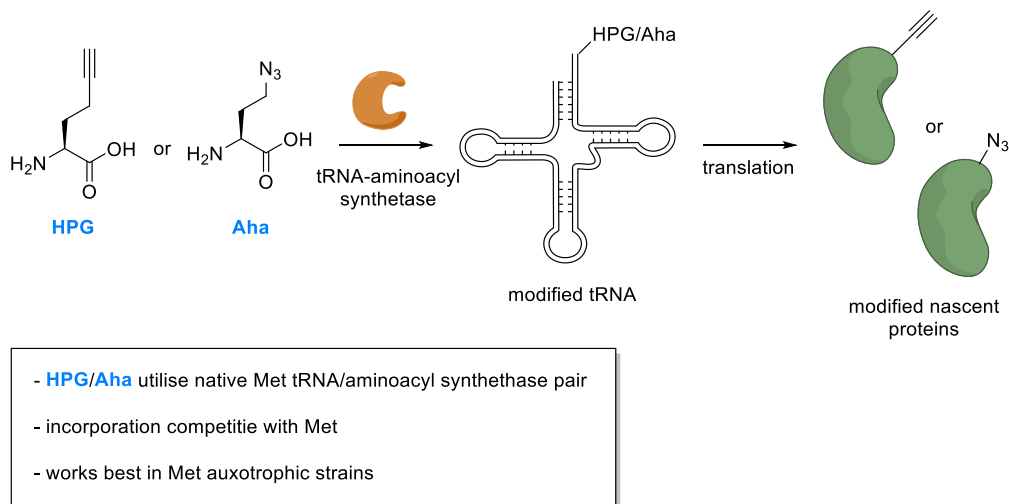


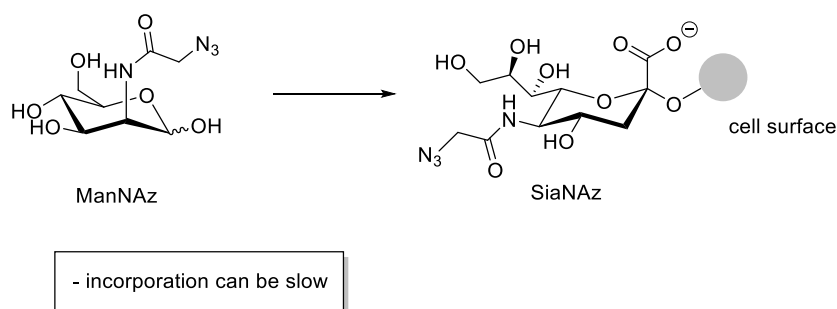
Figure 1.26. Schematic of tRNA.

The amino acids are loaded onto the tRNA by an enzyme called t-RNA aminoacyl synthetase. It is the promiscuity of this enzyme, that researchers have exploited to incorporate alkyne (HPG)¹³⁴ or azido-modified (Aha)¹³⁵ amino acids into nascent proteins (Scheme 1.20). Native methionine tRNA-aminoacyl synthetase incorporates these analogues into the tRNA coding for methionine. The incorporation efficiency of the non-natural amino acids (nnAAs) is reduced when in competition with methionine and incorporation was found to perform best in methionine auxotrophic strains of *E. coli*. Another drawback of this method is the uncontrolled incorporation of the unnatural amino acid, which leads to methionine replacement throughout the proteome.



Scheme 1.20. Incorporation of HPG or Aha via the native methionine tRNA-aminoacyl synthetase/tRNA pair.

Another approach is the incorporation of azides into the sialic acid found on the surface of glycoproteins. By supplementing the cellular growth media, the sialic acid precursor *N*-azido-acetyl-mannosamine (ManNAz) is taken up, converted into azido-sialic acid (SiaNAz) and incorporated into glycans on the cell surface of mammalian cells (Scheme 1.21).⁴⁴



Scheme 1.21. Incorporation of azide modified mannose into cell surface glycans of cells.

1.3.2 Genetic Code Expansion for the Incorporation of Bio-orthogonal Reagents

The approaches described in Section 1.3.8 are convenient methods to incorporate bio-orthogonal functionalities into proteins or cells but lack specificity. Ideally, the incorporation of novel amino acids should be directed to a specific, predetermined site in the target protein. To achieve this level of precision, several requirements must be met.¹³⁶ The non-natural amino acid should have a unique codon which does not encode for any of the native amino acids. Additionally, the non-natural amino acid should use a unique pair of aminoacyl-tRNA synthetase and tRNA. To ensure specificity, the nnAA must not be a substrate for a canonical tRNA/aminoacyl-synthetase pair and the unique aminoacyl-tRNA must not recognise

canonical codons. In short, to meet these conditions an orthogonal translational machinery has to be introduced into the cell and a codon has to be reprogrammed to accept the novel aminoacyl tRNA.

The initial efforts were focused on *E. coli*, which is easily genetically manipulated, and the amber stop codon (UAG) is only found rarely which makes it an ideal target codon for reprogramming. Initial attempts tried developing an orthogonal pair from *E. coli* but failed to achieve the desired specificity.¹³⁷ The breakthrough came in 2001, when the first orthogonal tRNA/synthetase pair from archaea was used in *E. coli* to selectively incorporate a range of nnAAs.¹³⁸ The advantages of using this tRNA/synthetase pair include that archaea tRNA are poor substrates for *E. coli* aminoacyl-synthetases and their expression is on par with nascent pairs.

Due to directed evolutionary mutagenesis¹³⁹ it is now possible to incorporate a plethora (150 +) nnAA into bacteria, eukaryotic cells and whole living organisms.¹⁴⁰ These range from azides to alkynes and from SPAAC to IEDDA reagents (Figure 1.27).^{140,141}

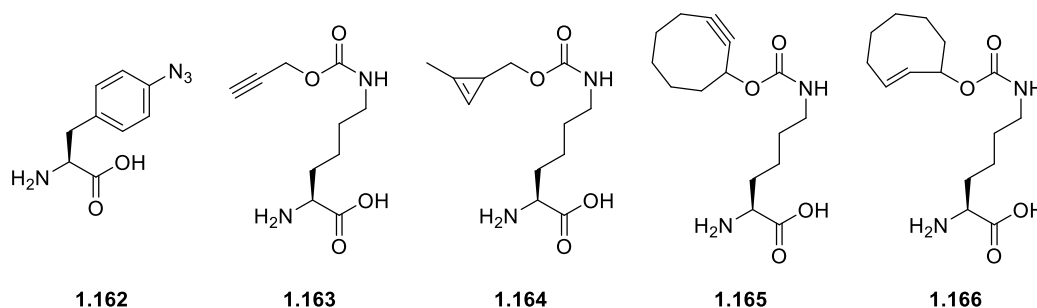


Figure 1.27. Selection of nnAA that have been incorporated into living organisms.

Nevertheless, certain problems remain. The use of the rare amber stop codon in *E. coli* reassigns a codon but can come at the cost of compromised fitness of the modified bacterial mutants. Secondly, while genetic code expansion is practised in several species, *E. coli* remains the dominant platform due to the biotechnological tools available. Incorporation of nnAA in eukaryotes is still far from common which restricts the use of this platform, but progress is being made and genetic code expansion is now also employed in animals.^{142,143} Further progress in this area involves the use of multiple orthogonal tRNA/synthetase pairs to incorporate more than one nnAA into organisms.^{144,145}

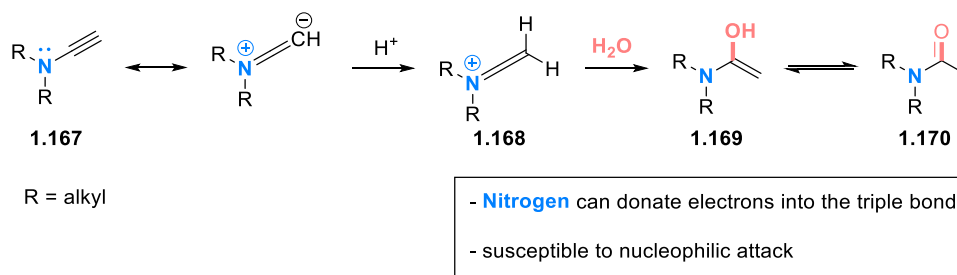
Finally, the problem of codon assignment is being tackled. Recently, it was possible to free up three codons by the deletion of two serine synonymous codons and one stop codon.¹⁴⁶ This was made possible by advances in genetical engineering which allowed the replacement of large parts of the *E. coli* genetic code.¹⁴⁷ In this manner, the three codons could be reassigned

to three nnAA and as a proof of work, the group was able to synthesise several variants of ubiquitin containing several different nnAAs.

This work points the way for future improvements in genetic code expansion. Whole genome editing as well as ribosomal editing¹⁴⁸ (to improve incorporation efficiency) could open new ways to create bespoke modified proteins or even biopolymers in living systems.

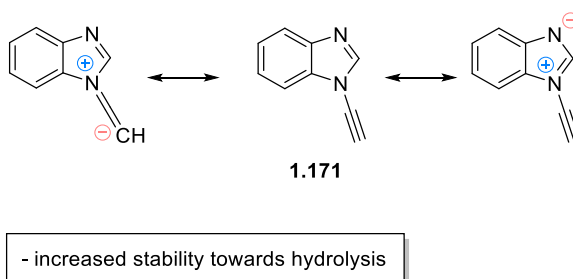
1.4 Aromatic Ynamines as Unique Bio-orthogonal Reagents

The triple bond of conventional ynamines (**1.167**) is polarised due to the ability of the nitrogen to donate an electron pair into the triple bond, activating it for protonation and subsequent nucleophilic attack of water. Unfortunately, this makes ynamines inherently susceptible towards degradation (Scheme 1.22).¹⁴⁹



Scheme 1.22. Hydrolysis of an ynamine.

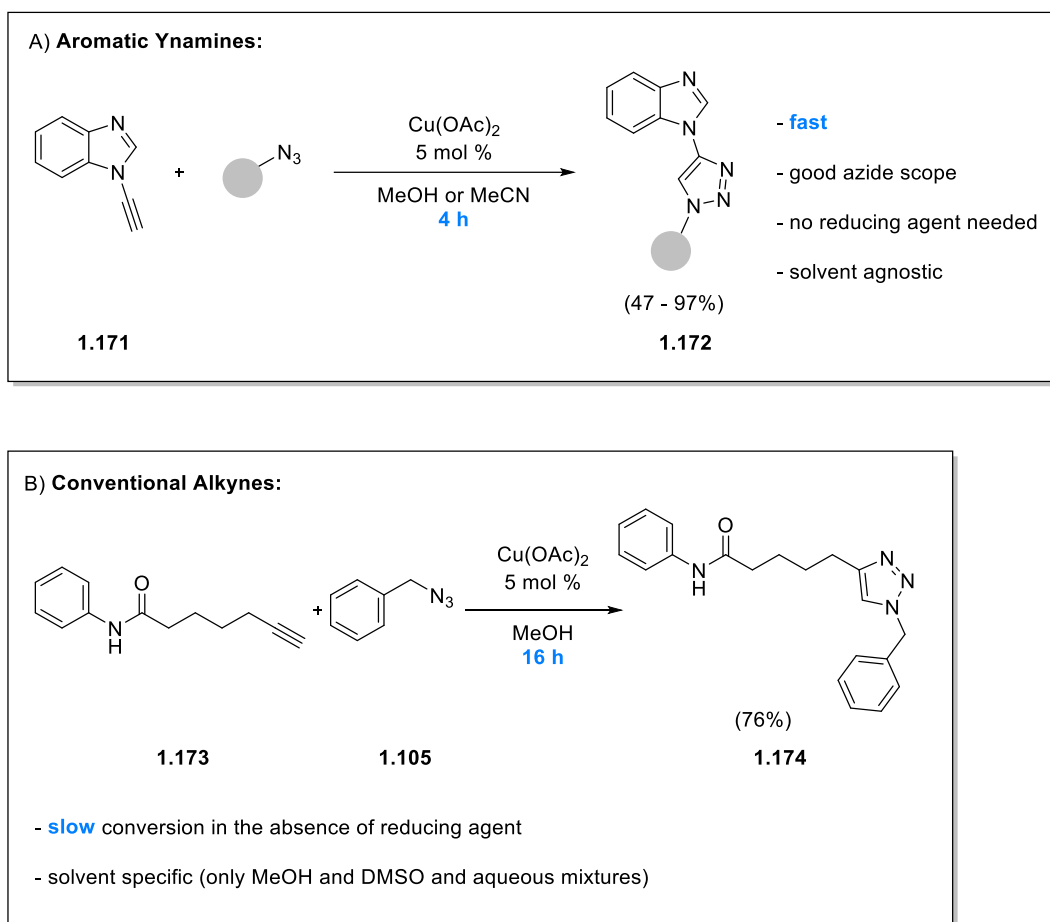
In contrast, Burley *et al.* showed in 2010 that aromatic ynamines (e.g., **1.171**) were more stable towards hydrolysis and also highly reactive in CuAAC reactions.¹⁵⁰ The nitrogen's ability to donate electron density into the triple bond is reduced by the delocalisation of its lone pair in the aromatic ring.



Scheme 1.23. Resonance forms of the aromatic ynamine. Stability towards hydrolysis is increased due to delocalisation of nitrogen lone pair into aromatic ring.

1.4.1 Sequential Bio-orthogonal Labelling using Ynamines

In 2016, Hatit *et al.* showed that **1.171** exhibited good reactivity with a wide range of azides (Scheme 1.24A) without the need for a reducing agent such as sodium ascorbate.¹⁵¹ In contrast, a conventional alkyne, *N*-phenylhept-6-ynamide (**1.173**), did not react in MeCN under the same conditions and reached lower conversion in MeOH than the ynamine **1.171** (Scheme 1.24B). The reactivity of the alkyne (**1.173**) could be increased by the addition of NaAsc and the ligand TBTA.

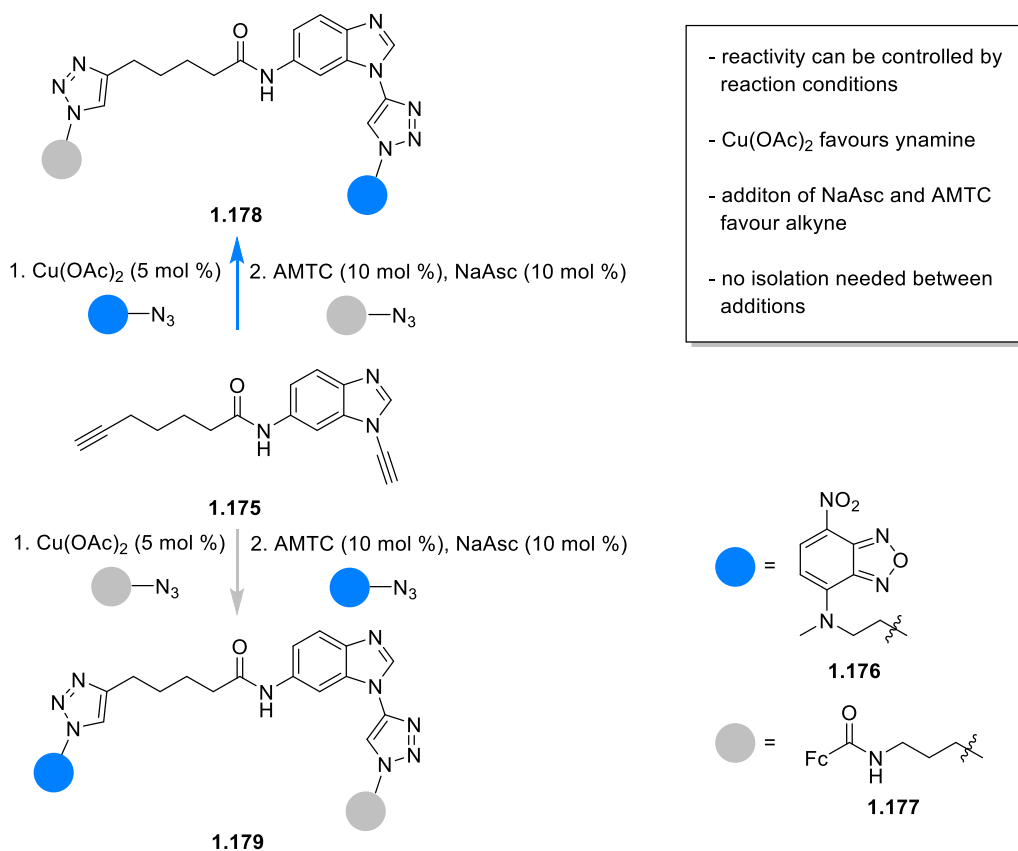


Scheme 1.24. (A) Aromatic ynamine **1.171** displays good azide scope and reactivity in the absence of reducing agent. (B) Conventional alkyne **1.173** only reactive in MeOH and DMSO in the absence of reducing agents.

The difference in reactivity was then exploited in the bifunctional system (**1.175**) to first react the *N*-ethynyl moiety with azide **1.176** and then the aliphatic alkyne with a second azide **1.177** to form **1.178** (Scheme 1.25). By changing the addition order of the azides the other regioisomer (**1.179**) could be formed selectively. The key to this strategy was the addition of NaAsc

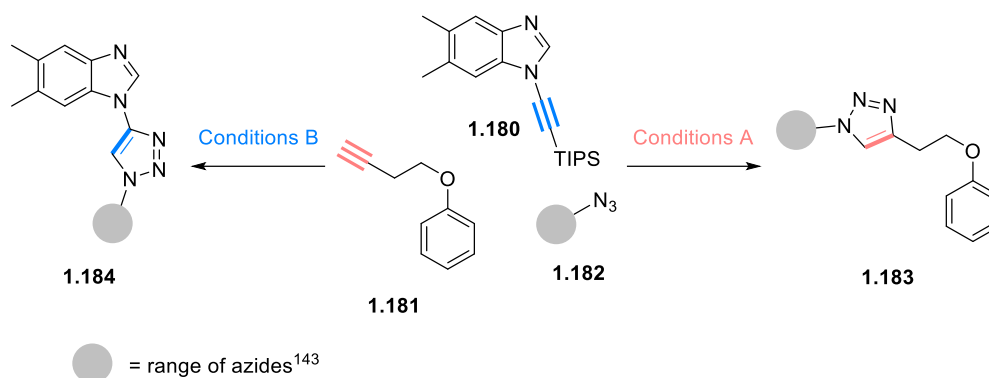
and AMTC (CuAAC ligand) to accelerate the click reaction of the aliphatic alkyne with the second azide.

Sequential CuAAC Reaction:



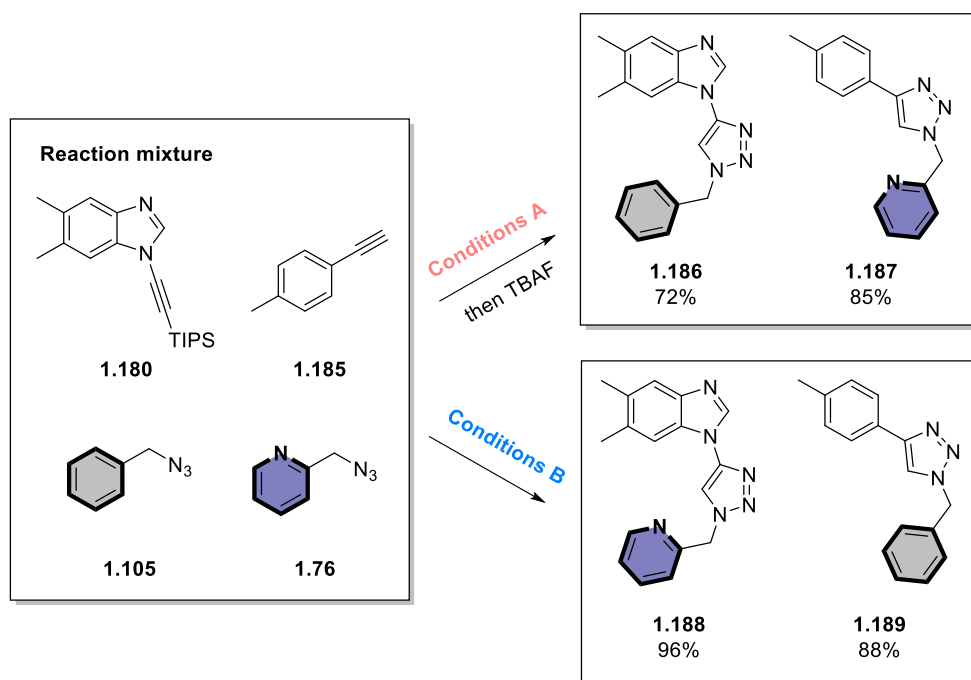
Scheme 1.25. Sequential CuAAC reaction of alkyne **1.178** with azide **1.176** and azide **1.177** in MeOH/H₂O (16 h).

In 2017, this method was extended to achieve orthogonality in a system with two alkynes.¹⁵² In competition experiments, the aromatic ynamine reacted first in the presence of a variety of alkynes and in the absence of reducing agents. It was envisioned that by using TIPS-protected ynamine **1.180** the selectivity could be controlled by *in situ* deprotection (Scheme 1.26). The solvent choice was crucial for selectivity as ynamine triazole **1.184** could only be obtained selectively using TBAF in MeCN. Triazole **1.183** could be selectively obtained using AMTC and NaAsc in DMSO/H₂O mixture.



Scheme 1.26. Reaction scheme for orthogonal click reaction. *Conditions (A)*: alkyne-selective, $\text{Cu}(\text{OAc})_2$ (5 mol %), NaAsc (10 mol %), AMTC (10 mol %), DMSO/ H_2O (1:1), rt, 16 h. *Conditions (B)*: ynamine selective, $\text{Cu}(\text{OAc})_2$ (5 mol %), TBAF (1.1 equiv), MeCN, rt, 16 h.

After further development, it proved possible to achieve full control over the desired product formation from a four-component reaction mixture (Scheme 1.27). Azide selectivity was achieved by usage of a chelating azide (picolyl azide **1.76**) with which alkynes reacted preferentially over benzyl azide. By employing the conditions described above, it was possible to selectively react either **1.180** or **1.185** with **1.105** or **1.76**.



Scheme 1.27. Reaction scheme for sequential click reactions. *Conditions (A)*: alkyne-selective, $\text{Cu}(\text{OAc})_2$ (5 mol %), NaAsc (10 mol %), AMTC (10 mol %), DMSO/ H_2O (1:1), rt, 16 h. *Conditions (B)*: ynamine selective, $\text{Cu}(\text{OAc})_2$ (5 mol %), TBAF (1.1 equiv), MeCN, rt, 16 h.

1.4.2 Mechanistic Investigations of the Ynamine-CuAAC

To discover the cause of the chemoselectivity, a series of NMR competition experiments was performed between ynamine **1.190** and a set of alkynes (**1.191** – **1.195**) (Figure 1.28).¹⁵³ The ynamine outperformed the selection of alkynes in competition experiments. However, when the rates of the reactions were determined in isolation, **1.191** displayed a significantly faster rate than ynamine **1.190**.

Substrate Scope:

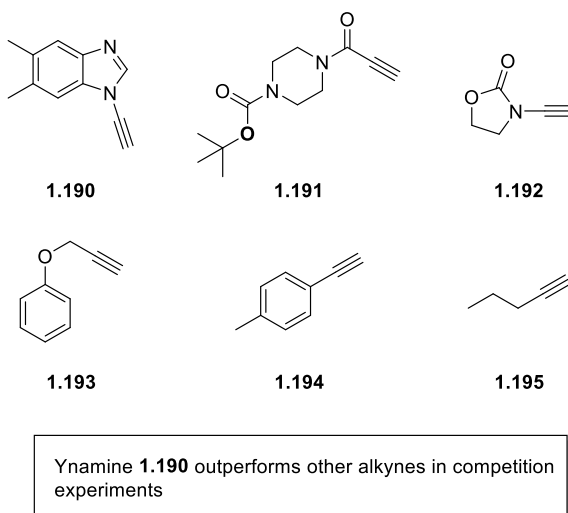
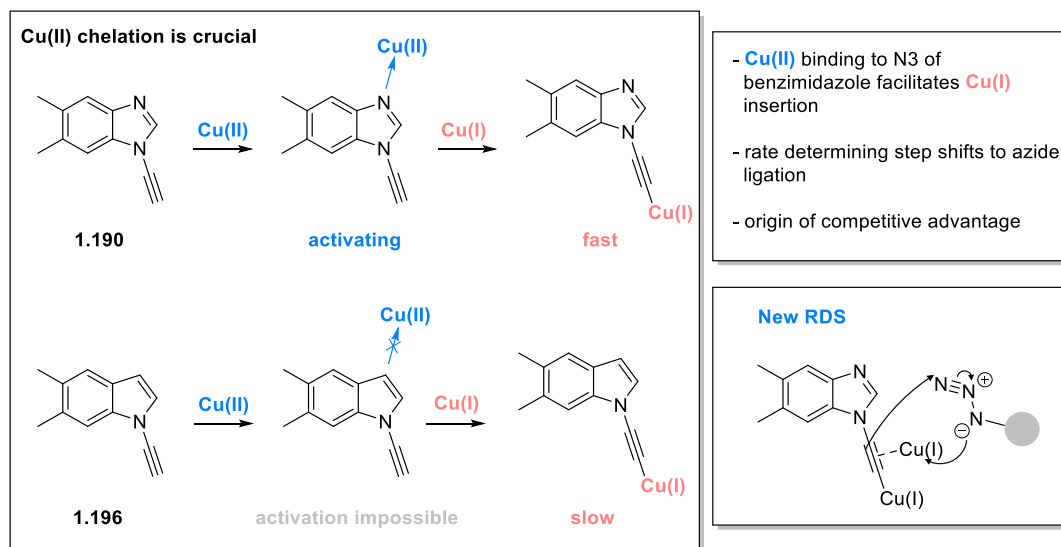


Figure 1.28. Substrate scope for the competition experiment.

Further NMR experiments revealed that the rate of the reaction was zero order dependant on the alkyne and second order dependant on the azide. This is in contrast to other alkynes, which are usually second order in copper concentration when the transition metal is present in catalytic amounts.¹⁵⁴ Furthermore, kinetic data suggested that the copper acetylide formation was rapid when compared to other alkynes which is usually regarded as the rate determining step. It was hypothesised that this shift could be a direct consequence of the co-ordination of copper to the N3 of the benzimidazole ring (Scheme 1.28). Indeed, control experiments showed that indole **1.196** lost in competition experiments to **1.190**. Copper co-ordination could not be monitored due to rapid C-H insertion but control experiments with other Lewis acids such as $\text{Sc}(\text{OTf})_3$ also showed a decrease in $\text{p}K_{\text{a}}$ of the acetylide proton. Notably, Cu(I) did not coordinate to N3, potentially explaining why the click reaction with the ynamine performed so well in the absence of a reductant. From this series of experiments, it was postulated that the competitive performance of the ynamine **1.190** stems from a shift in the RDS.¹⁵³



Scheme 1.28. Origin of chemo-selectivity. Cu(II) co-ordination to N3 and activates the triple bond for Cu(I) insertion. Rate determining step shifts to the azide insertion.

1.1 Glutathione

Glutathione (GSH) is a tripeptide made from glutamic acid (γ -glutamyl linkage), cysteine and glycine (Figure 1.29). It is one of the most abundant peptides in many organisms and is present in cells in concentrations ranging from 0.1 mM to 10 mM while the extracellular concentration is significantly lower.¹⁵⁵

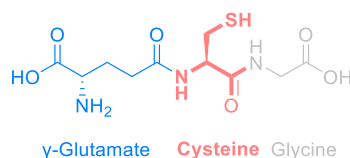
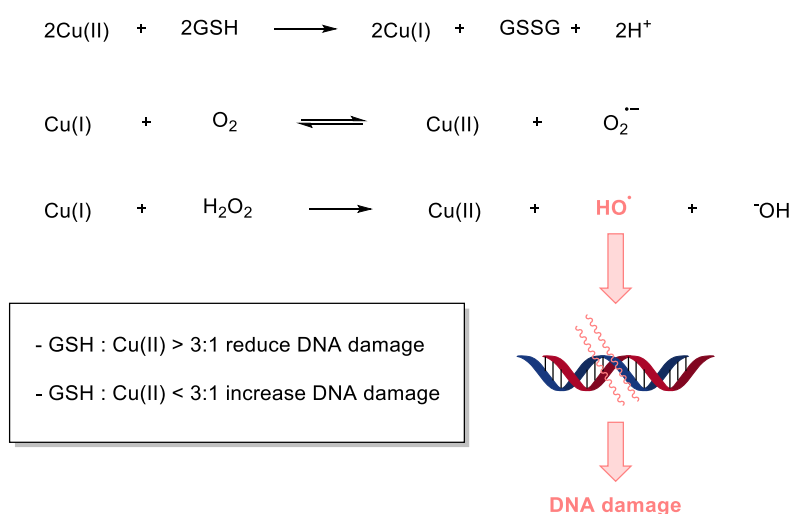


Figure 1.29. Structure of GSH.

GSH is involved in many cellular processes such as antioxidant processes, detoxification, redox signalling, regulation of immune response and cellular proliferation and also post-translational protein modification.^{156–158} Reviewing all GSH functions is beyond the scope of this introduction, therefore, this part will focus on two aspects which are likely to have impact on bio-orthogonal reagents: copper binding and nucleophilic attack on bio-orthogonal reagents.

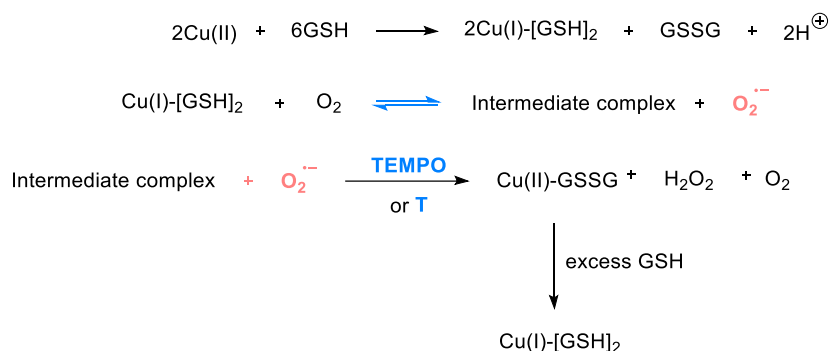
1.1.1 Glutathione and Copper Redox Chemistry

In cells, GSH binds copper readily. In fact, when ^{67}Cu was added to cells, more than 60 % was recovered as a Cu-GSH complex.¹⁵⁹ Furthermore, GSH readily reduces Cu(II) to Cu(I)^{160,161} to form a very stable complex.¹⁶² For a long time, it was thought that this complex prevented Cu(I) from producing superoxide radicals. However, it was shown that sub stoichiometric amounts of GSH actually could accelerate DNA cleavage¹⁶³ (Scheme 1.29). This was further investigated by Spear and Aust in 1995, who found that GSH-Cu ratios exceeding a 3:1 ratio prevented oxidative damage, while lower ratios induced DNA damage.¹⁶⁴ The ability to break DNA strands is usually attributed to hydroxyl radical and not superoxide or hydrogen peroxide.



Scheme 1.29. Generation of hydroxyl radicals in the presence of GSH and Cu(II) which can lead to DNA damage.

As DNA damage was prevented by a higher GSH-Cu ratio, it was assumed that superoxide formation was suppressed. However, Speisky and co-workers showed that, in fact, superoxide was continuously created even at high ratios of GSH-Cu.¹⁶⁰ In later investigations, they discovered that, while superoxide is continuously produced, GSH is not consumed, so they concluded that the reaction was reversible.¹⁶⁵ Only when superoxide was removed with TEMPO or by auto-dismutation at elevated temperatures did the GSH concentration decline, and they detected the formation of a Cu(II)-GSSG complex (Scheme 1.30). This complex can be reduced back to Cu(I)-GSSG (1 equiv of GSH added) or to a Cu(I)-[GSH]₂ complex (> 2 equiv of GSH added).¹⁶⁶

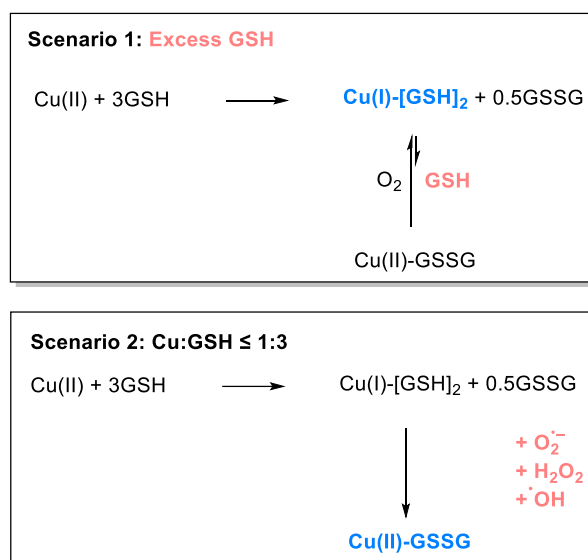


- **superoxide** is continuously produced at high Cu:GSH ratios
- formation of **reversible** complex
- by **trapping** superoxide equilibrium is broken and GSH is consumed

Scheme 1.30. Formation of Cu-GSH complex upon addition of GSH. This complex can generate superoxide but reaction is reversible. The removal of superoxide drives consumption of complex to Cu(II)-GSSG.

From this series of studies it can be concluded that the nature of Cu(II)-GSH chemistry is highly dependent on the reaction stoichiometries and conditions. Two scenarios can be imagined. In one scenario the GSH concentration far exceeds the Cu(II) concentration (> 3:1)(Scheme 1.31A). In this case, Cu(II) will be reduced using 3 equivalents of GSH to form a Cu(I)-GSH₂ complex and 0.5 equivalents of GSSG. This complex can produce superoxide, but the reaction is reversible if superoxide is not consumed in a secondary reaction. If superoxide is consumed, then oxidation of the Cu(I)-GSH₂ complex will occur and a Cu(II)-GSSG complex will be formed. This complex is exceptionally stable and cannot be reduced by conventional reductants such as NaAsc.¹⁶⁵ Only GSH can reduce this complex and therefore in a large excess of GSH, Cu(I) will be present in the system and little GSSG produced.

In a scenario where GSH is only in small excess to Cu(II) ($\leq 3:1$), the Cu(I)-GSH₂ complex will again be formed and GSSG produced (Scheme 1.31B). However, this time, consumption of superoxide leads to the continuous oxidation of the Cu(I)-GSH₂ complex to form Cu(II), GSSG and hydrogen peroxide. Once the stoichiometry of GSH drops below double that of copper (2:1), hydroxyl radicals will be formed. The production seems to be contingent on the presence of hydrogen peroxide and Cu(II) as the addition of catalase reduced hydroxyl radical production.¹⁶⁷



Scheme 1.31. Scenario 1: Cu(I)-[GSH]₂ is the major copper species; Scenario 2: Cu(II)-GSSG is continuously produced.

The nature of the exact complex formed by GSH and Cu(I) was subject to multiple investigations and debates. While a 1:1 or 2:1 stoichiometry was often indicated, the exact structure remained elusive and dependant on analytical techniques.^{168,169} For example, using NMR and x-ray absorption, Corazza *et al.* determined a 1.2 stoichiometry where 3 sulphur atoms co-ordinate to one copper forming a polycluster.¹⁷⁰ Measurements of thiol consumption after Cu(II) addition indicated either a 1:1 complex¹⁶⁷ (absence of oxygen) or a 1:2 complex^{167,171} (presence of oxygen).

Morgan *et al.* set out to investigate copper-GSH complex formation under physiologically relevant conditions.¹⁶¹ Previously, they had developed a set of potent copper ligands, with binding constants ranging from femto- to attomolar levels. These ligands allowed them to monitor Cu-GSH complex formation by UV. Through back titration and curve fitting they elucidated the presence of a tetranuclear Cu-GSH cluster with adamantane geometry (Figure 1.30). This cluster also showed similar phosphorescent properties as previously reported of Cu₄S₆ clusters¹⁷², further confirming their theory. Additionally, they were able to calculate a Cu-GSH binding affinity of $\log\beta_{46} = 85$ which effectively means that GSH can limit the copper concentration to femtomolar levels in cellular environments, which is considerably lower than previously reported.¹⁶⁸ In combination with the previous results, the acute toxicity of a copper-GSH complex *in vivo* is likely minimal. GSH is present in large excess over copper in a cellular environment and if oxidised to GSSG can be continuously regenerated. As seen above, the

ability of Cu-GSH complexes to produce hydroxyl radicals, and therefore toxicity, is minimal at large Cu:GSH ratios.

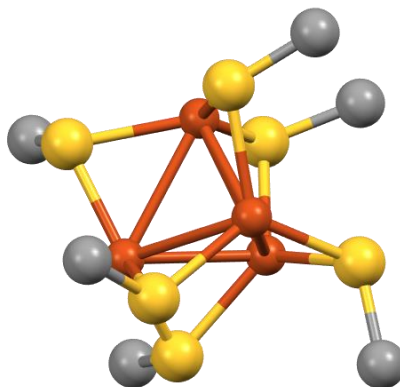


Figure 1.30. Structure of Cu-GSH cluster (PDB Code = TPHCUB).^{161,173}

1.1.2 GSH as a Nucleophile to Deactivate Bio-orthogonal Reagents

Apart from co-ordinating copper, GSH can also react with electrophilic compounds. In fact, GSH is regularly used to simulate *in vivo* stability of novel compounds or drugs.^{174,175} In the case of bio-orthogonal reactions, GSH can act as a nucleophile towards the alkyne in a thiol-yne type of reaction. Van Geel *et al.* investigated a range of common SPAAC for off-target reactivity with cysteines on the protein surface (Figure 1.31).¹⁷⁶ Indeed, when the strained alkynes were incubated in cell lysate devoid of an azide functionality, significant off-target protein labelling was observed (**1.201**). The off-target labelling could be reduced by the addition of iodoacetamide (**1.203**) indicating that most side reactions were due to reactive thiols. This trend was confirmed on recombinant heat shock displaying a surface cysteine and azide moiety. While SPAAC reaction was the major product, some cysteine labelling was also observed which could be reduced by the preincubation with iodoacetamide. DBCO and BCN showed higher degrees of off-target reactivity, consistent with their increased SPAAC reactivity.

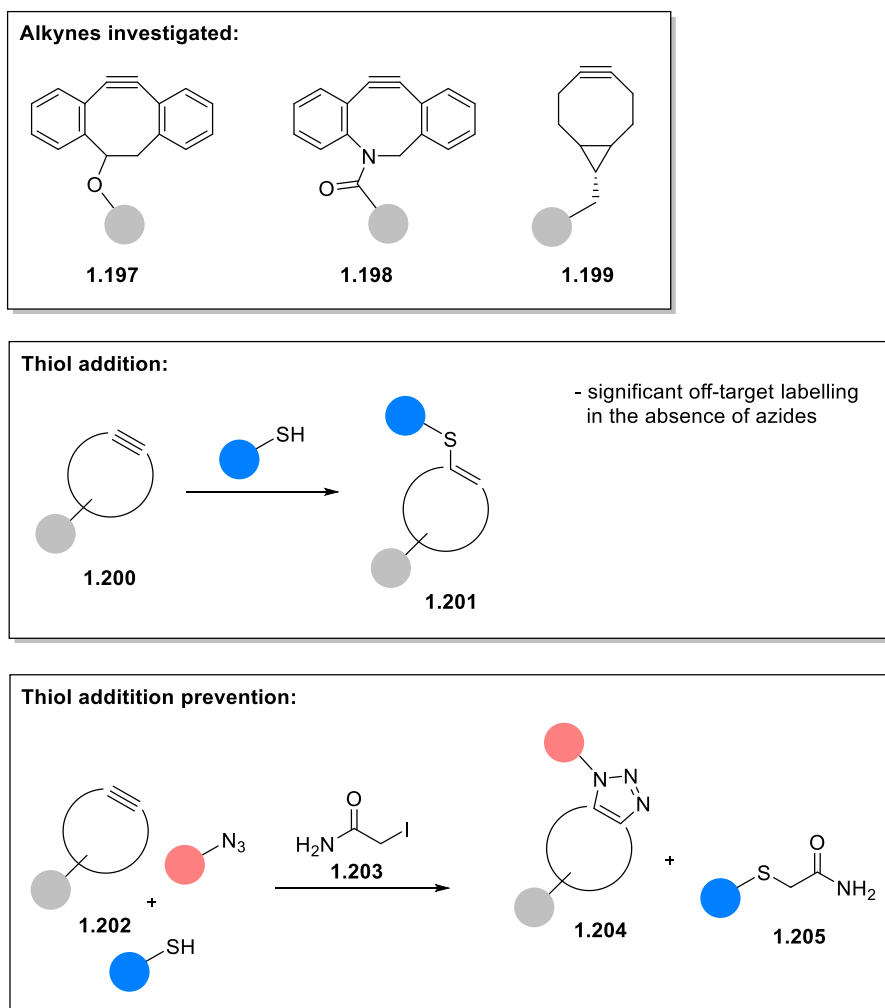
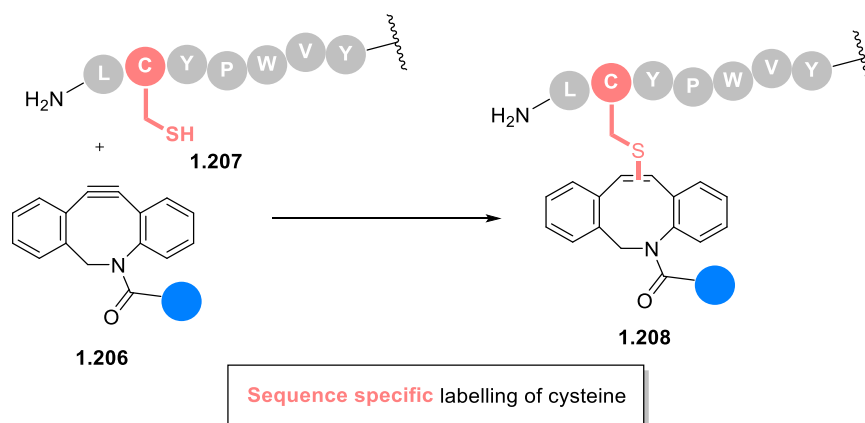


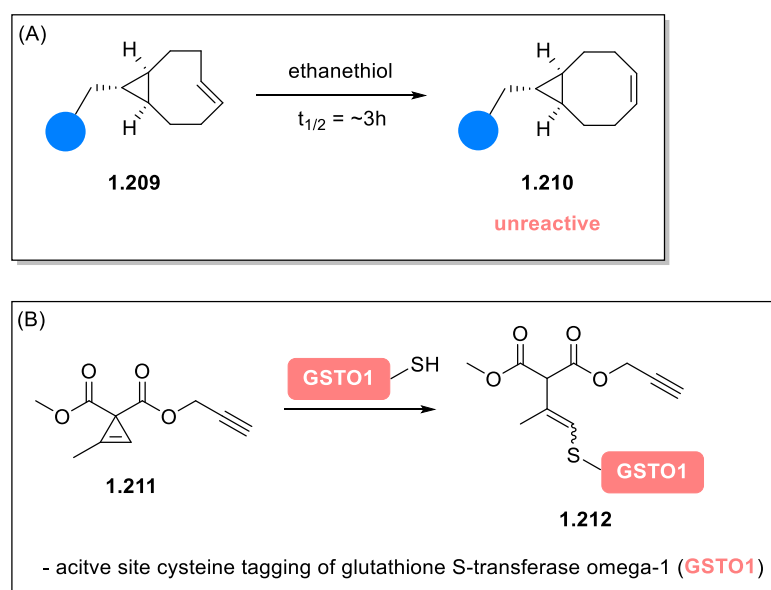
Figure 1.31. Structures of alkyne investigated. Alkyne-thiol adducts and reduction of thiol-addition by covalent capping.

Zhang *et al.* exploited the tendency of DBCO (**1.206**) to react with thiols and turned the strained alkyne into a targeted thiol tagging reagent. The amino acid sequence (LCYPWVY) accelerated the thiol reaction up to 220-fold and enabled the targeted cysteine conjugation (**1.208**) in the presence of other thiols with various functional groups.¹⁷⁷



Scheme 1.32. Sequence specific labelling of cysteines with DBCO.

GSH can also affect the IEDDA reagents. Thiols can isomerise TCO from the reactive *trans* to the inactive *cis* isomer (**1.210**) with an approximate half-life of 3 h.¹³¹ Similar to DBCO, the cyclopropene moiety (**1.211**) has also been exploited as a covalent warhead to inhibit glutathione S-transferase (GSTO1).¹⁷⁸



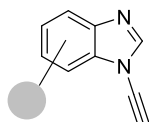
Scheme 1.33. (A) Isomerisation of TCO by thiols. (B) Electrophilic cyclopropene warhead reacts with active site cysteine.

1.2 Hypothesis

The main issue of the CuAAC reaction for bioconjugation and bio-orthogonal chemistry is the cytotoxicity of copper. Reducing copper concentration *in vitro* and *in vivo* to counteract the toxicity invariably results in reduced reaction rates. Researchers have developed copper-

chelating azides and ligands to increase the CuAAC reactivity at low copper concentrations.^{66,71,78} In contrast, little progress has been made on the alkyne side. The aromatic ynamine was shown to be more reactive than traditional alkynes, which would be beneficial for bioconjugation.^{151–153} The main hypothesis is that the aromatic ynamine would be uniquely reactive and undergo bioconjugation at reduced copper loadings.

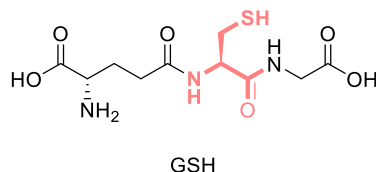
Aromatic Ynamines:



- more reactive than conventional alkynes
- can be combined with ligands and chelating azides
- superior novel alkyne for bioconjugation?

Figure 1.32. Aromatic ynamines have the potential for a new bio-orthogonal reagent.

Additionally, the impact of GSH on either CuAAC or copper-free click reactions has not been investigated extensively.^{109,111,179–181} It is hypothesised that GSH will impact the CuAAC significantly through copper co-ordination and of also degrade bio-orthogonal reagents. As such, GSH could be a useful tool to compare the performance bio-orthogonal reagents.



- can chelate copper
- can degrade bio-orthogonal reagents
- impact not explored extensively

Figure 1.33. GSH can be used to evaluate and compare the performance of bio-orthogonal reagents.

1.3 Thesis Aims

The specific aims of this thesis are to:

- (i) Explore ynamine reactivity and susceptibility to side-reactions with GSH.
- (ii) Compare ynamine reactivity in the presence of GSH to a range of alkynes and other classes of bio-orthogonal reactions.
- (iii) Develop conditions for a fast ynamine-CuAAC reaction in the presence of GSH and apply them to biomolecules
- (iv) Determine and optimise the application of ynamine-CuAAC reactions in cell lysate.

In detail, the second chapter will explore the susceptibility of aromatic ynamines and alkynes towards reactivity with GSH at the highest physiological GSH concentration (10 mM). The

influence of redox active metal ions such as copper will also be examined. The chapter will end with examining the influence of high GSH concentrations on the CuAAC reaction.

The third chapter will explore the influence of GSH on the CuAAC reaction in detail, specifically at Cu:GSH ratios of less than 1:3.

The fourth chapter will use the optimised conditions for the Ynamine-CuAAC reaction in the presence of GSH to ligate functionalised ynamines to cell penetrating peptides and explore the synthesis of an ynamine modified synthetic oligonucleotide.

The final chapter will optimise the reaction between an aromatic ynamine and a “turn on” fluorescent azide to first in buffer and then in cell lysate. These conditions will serve as a basis for future *in vivo* experiment.

Chapter 2

Influence of Glutathione on Alkyne Stability and Reactivity in Copper- Catalysed Alkyne-Azide [3+2]Cycloadditions

2.1 Introduction

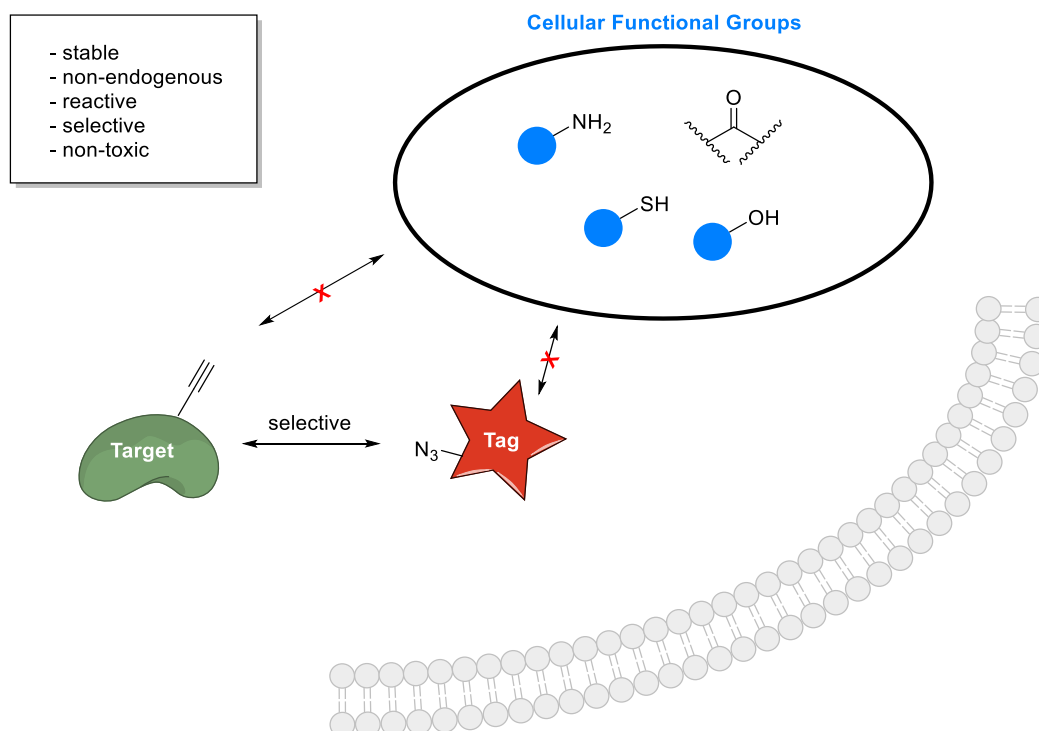
2.1.1 Requirements of Bio-orthogonal Reagents

Bio-orthogonal reactions use reagent pairs that selectively react with each other in cellular environments. These reagents have unique requirements that set them apart from standard reactions used in synthetic organic chemistry.^{6,182} These reagents must be stable under physiological conditions, selectively react with each other, display reasonably fast reaction kinetics, and be non-toxic when used in live cells. Each attribute comes with a cost (*i.e.*, high reactivity decreases stability under physiological conditions) and to achieve the ideal bio-orthogonal reaction set, all these attributes must be balanced appropriately.¹⁸³

The archetype of bio-orthogonal reagents is the alkyne and azide combination (Scheme 2.1). Both moieties are predominantly absent in biological organisms, do not readily cross-react with native functional groups (thiols, amines, hydroxyl groups, carbonyls, etc.), are stable under cellular conditions (pH ranges and resistant to hydrolysis), and form non-reversible adducts.¹⁸⁴ A further advantage of the alkyne/azide pair are their small sizes. In comparison to the traditional fluorescent reporter system (GFP), the small molecules minimally perturb the function of a biomolecule they are incorporated into due to their small size.

Designing new reagents that meet these requirements and withstand cellular conditions is challenging. The development and optimization of existing classes of bio-orthogonal reagents have commonly been derived from traditional organic chemistry reactions and have been tailored for use in more complex environments (aqueous buffer and cellular components) and finally into *in vivo* situations.^{44,103}

A typical workflow for bio-orthogonal optimization focuses on stability under physiological conditions, chemoselectivity and reaction kinetics.⁹⁹ Poor stability/selectivity can lead to side reactions and off-target effects which can compromise applications, such as fluorescent tagging, by increasing the background signal.¹⁸⁵ Keeping the reagent concentration low can minimise these issues and requires fast reaction kinetics (*i.e.* large rate constants)¹⁸⁶ to still ensure efficient conjugation.

The Ideal Bioorthogonal Reagent:**Scheme 2.1.** Schematic of the ideal bio-orthogonal reagent.**2.1.2 Glutathione as a Source of Side-reactivity with Bio-orthogonal Reagents**

Glutathione (GSH) is an abundant tripeptide which regulates redox processes in a cell and is used to detoxify exogenous compounds.¹⁵⁶ Present in millimolar concentrations, exploring the susceptibility of bio-orthogonal reagents to reactions with GSH is therefore a key step in their application as tagging tools in biological systems (Figure 2.1).^{109,111,187–190} The concentration of GSH can fluctuate by two orders of magnitude (0.1 - 10 mM), and GSH can form addition adducts either through nucleophilic (*e.g.*, Michael) additions (alkynes)¹⁷⁶ or isomerisation¹³¹ (strained alkenes) thereby deactivating them.

In the case of the CuAAC reaction, GSH is known to reduce the formation triazole products *in vitro*¹⁷⁹ and has been identified as the cause of reduced conversion *in vivo*.⁸³ The cause of this inference is attributed to copper co-ordination by GSH ($K_D \sim 9 \times 10^{-12} \text{ M}^{-1}$).¹⁶⁸ Experiments that evaluate novel copper ligands in the presence of GSH support this hypothesis as increased conversions are achieved using these ligands.^{191,192} Notably, TBTA (a common CuAAC ligand) is not effective in shielding Cu(I) from GSH and negligible conversion in the presence of the thiol is observed, on par with the absence of any ligand.

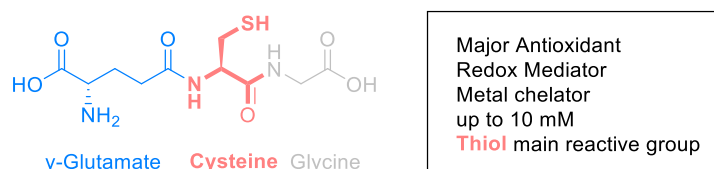


Figure 2.1. Structure of GSH.

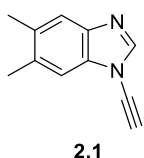
Biological thiols such as cysteine^{121,122} or GSH¹⁷⁶ have been used to evaluate the stability of novel bio-orthogonal reagents. However, comparing these studies is difficult as a wide range of conditions is used. The thiol concentration varies from 1 equiv¹⁸⁹ to large excesses (5 – 10 mM)^{187,193} and bio-orthogonal reagent concentration is either high (2 mM)¹⁰⁹ or sometimes not reported.^{187,190} As solvent systems, buffer or water (either deuterated or not) are commonly used and the co-solvent also varies.^{109,176,187,193} Some studies even use DMSO as a co-solvent,^{188,194} which should be avoided as DMSO was known to oxidise GSH.¹⁹⁵

To really evaluate and compare the stability of bio-orthogonal reagents, a workflow using a standardised set of conditions is needed, which is currently lacking. Ideally, this assay would use the highest physiological concentration of GSH (10 mM), employ low reagent concentrations, use a single buffer, and avoid DMSO as a co-solvent.

2.2 Hypothesis to be tested in this Chapter

Previous work has shown that ynamines (*e.g.*, **2.1**, Figure 2.2), are more reactive in CuAAC reactions relative to conventional alkynes.¹⁵³ As such, ynamines have significant potential for use as a novel bio-orthogonal reagent.

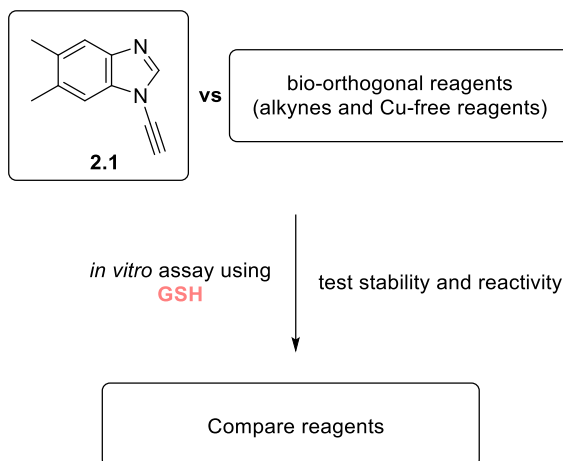
Aromatic Ynamines:



- outcompete conventional alkynes
- no reducing agent needed
- potential for new bio-orthogonal reagent

Figure 2.2. Structure of aromatic ynamine **2.1**. This ynamine (**2.1**) was shown to outcompete a range of conventional alkynes through a shift in the rate determining step from the acetylide formation to azide insertion.¹⁵³

To date, the stability of ynamines to physiological conditions has not been evaluated. The development of a high-throughput *in vitro* assay using GSH to evaluate the suitability of ynamines as novel bio-orthogonal reagents and compare them to other alkynes as well as copper-free bio-orthogonal reactions such as the SPAAC or IEDDA reaction (Scheme 2.2) would be a valuable tool.

Workflow:

Scheme 2.2. Schematic of workflow in for studies contained within Chapter 2. First, bio-orthogonal reagents will be synthesised and then their stability and reactivity in the presence of GSH compared in an *in vitro* assay.

2.3 Aims of Chapter 2

The specific aims of this chapter are:

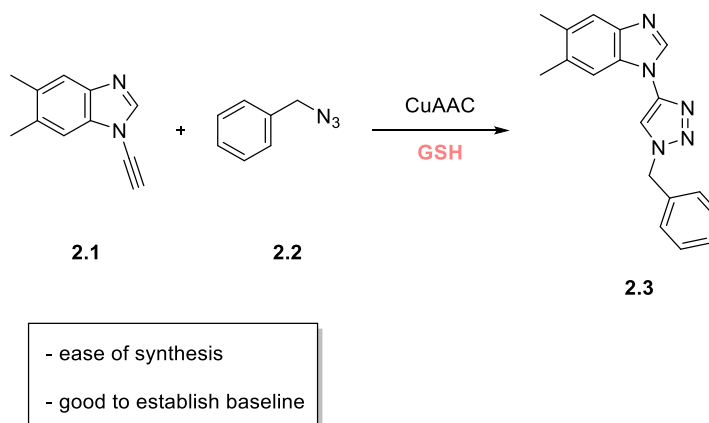
- (i) Develop a high-throughput assay to determine the reactivities of alkyne reagents with GSH.
- (ii) Probe stabilities of alkynes and biorthogonal reagents at biologically relevant GSH concentrations.
- (iii) Determine the effects of GSH on a range of bio-orthogonal reactions (*e.g.*, CuAAC, ynamine-CuAAC, SPAAC and IEDDA) under physiological conditions.

2.4 Results & Discussion

2.4.1 Synthesis of Aromatic Ynamines

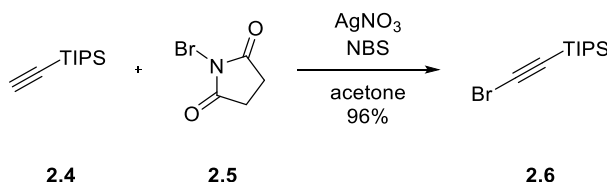
Ynamine **2.1** was chosen as the model substrate to test stability and the CuAAC reactivity with benzyl azide (**2.2**) in the presence of GSH (Scheme 2.3).

Model Reaction:



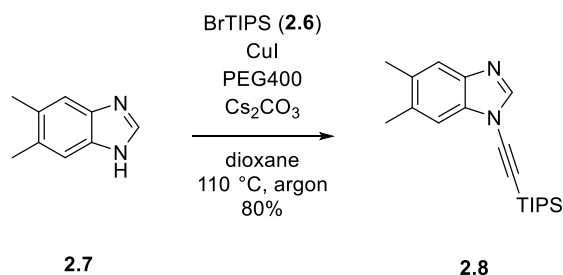
Scheme 2.3. Scheme of the model reaction used at the start of the investigation.

Ynamine **2.1** was synthesised via an Ullman-type coupling between a benzimidazole (commercial) and a bromo-alkyne. The bromo-alkyne (**2.6**) was prepared via a silver-catalysed bromination of TIPS-alkyne **2.4** (Scheme 2.4).¹⁹⁶ The reaction proceeded smoothly, and the product could be isolated in a 96% yield.



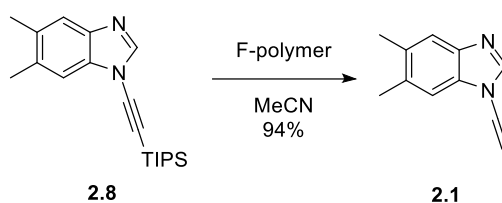
Scheme 2.4. Synthesis of **2.6**. *Conditions:* **2.4** (1 equiv), NBS (1.1 equiv), AgNO₃ (0.1 equiv), rt, overnight.

Ynamine **2.8** was synthesised from 5,6-dimethylbenzimidazole (**2.7**) and bromo-alkyne **2.6** (Scheme 2.5).¹⁹⁷ The standard procedure employed microwave heating but due to the amounts of material required (> 1 g), the use of a microwave was not possible, and the reaction was heated to 110 °C for two days. The product **2.8** was obtained in good yield (80%).



Scheme 2.5. Synthesis of **2.8**. Conditions: **2.7** (1 equiv), **2.6** (1.1 equiv), CuI (0.05 equiv), PEG400 (0.1 equiv), Cs₂CO₃ (1.2 equiv), 110 °C, argon, 2 days.

Finally, removal of the TIPS group with polymer-immobilised fluoride afforded **2.1** in 94% yield (Scheme 2.6).



Scheme 2.6. Synthesis of **2.1**. Conditions: **2.8** (1 equiv), fluoride on polymer (1 equiv), rt, overnight.

2.4.2 Synthesis of Alkynes and Bio-orthogonal Reagents

Previous work has demonstrated that ynamines (*e.g.*, **2.1**) display enhanced reaction kinetics relative to conventional alkynes.¹⁵³ As reactivity and stability are usually inversely correlated it was expected that the ynamine stability would decrease when compared to other non-activated alkynes.¹⁹⁸ To explore this hypothesis, three further alkynes (**2.9** – **2.11**) spanning a range of reactivities were synthesised (Figure 2.3).^{151,153} Alkyne reactivity has been shown to increase when an electron withdrawing group is placed adjacent to the triple bond due to lowering the alkyne LUMO energy.¹⁹⁹ Furthermore, all alkynes needed to contain a chromophore, so they could be analysed by HPLC.

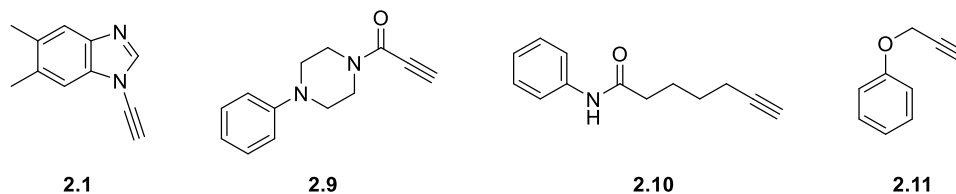


Figure 2.3. Representative alkynes to profile CuAAC reactivity and stability under physiological conditions.

The SPAAC and IEDDA reactions are popular copper-free alternatives to the CuAAC reaction for bio-orthogonal labelling. These reactions do not require copper for catalysis and have

become the tool of choice for *in vivo* labelling.^{10,200} While the SPAAC and IEDDA substrate reactivities have been investigated, their metabolic stabilities have not been explored extensively. Although several publications have used GSH to test stabilities of SPAAC or IEDDA reagents, the results do not always agree and seem to depend on the conditions used.^{109,111,188,190} As such, to draw proper comparisons between CuAAC and SPAAC/IEDDA reagents in this study, it was decided to synthesise or purchase a selection of common strain promoted cycloaddition reagents (Figure 2.4) and test stabilities under comparable conditions. Cyclooctynes **2.12** and **2.13** were chosen as common representatives for the SPAAC reaction. Tetrazine **2.14** has been shown to be highly reactive with TCOs and the stability in FBS at 37 °C after 10 h is reported,²⁰¹ which would enable comparisons with the stability in the presence of GSH in this study. Cyclopropene **2.15** was chosen as a reaction partner for tetrazine **2.14**.

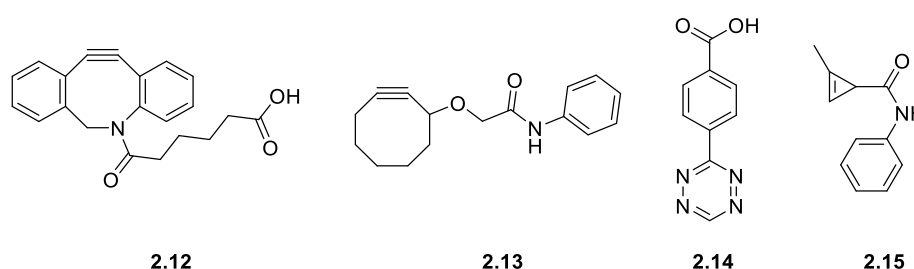
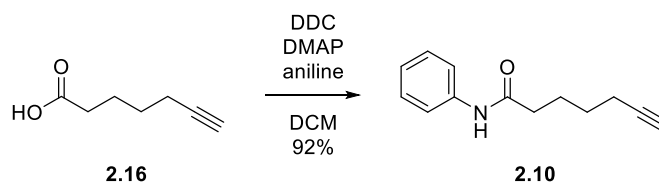


Figure 2.4. Structures of SPAAC or IEDDA reagents selected for this study.

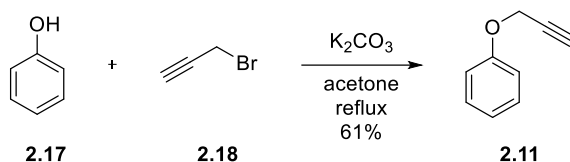
2.4.2.1 Synthesis of Alkyne Series for Bio-orthogonal Profiling

Alkyne **2.10** was prepared from a coupling reaction of hept-6-ynoic acid with aniline using DCC in 92% yield (Scheme 2.7).



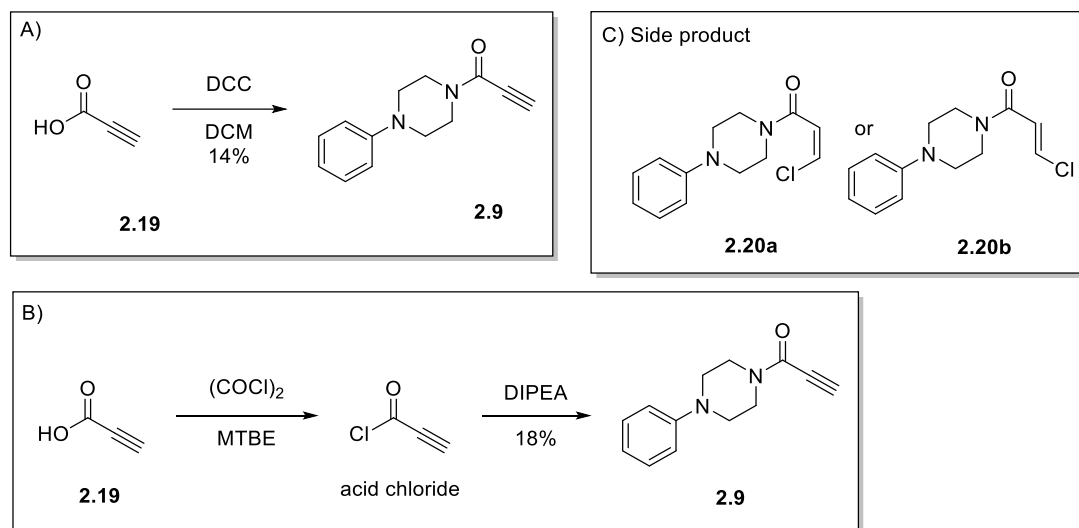
Scheme 2.7. Synthesis of **2.10**. Conditions: **2.16** (1 equiv), DCC (1 equiv), DMAP (0.1 equiv), aniline (1.1 equiv), rt, 4 h.

Compound **2.11** was obtained in 61% yield via etherification from phenol (**2.17**) and propargyl bromide **2.18** (Scheme 2.8).



Scheme 2.8. Synthesis of **2.11**. Conditions: **2.17** (1 equiv), **2.18** (1 equiv), K₂CO₃ (1 equiv), reflux, overnight.

Compound **2.9** was synthesised using the same procedure as for compound **2.10** (Scheme 2.7). However, the reaction gave a significantly lower yield of 14% (Scheme 2.9A). The low coupling efficiency might be due to the electron rich carboxylic acid and the sterically hindered amine. The reaction was repeated using oxalyl chloride to first generate the acid chloride and then subsequently coupled to phenylpiperazine (Scheme 2.9B). This improved the yield marginally to 18%. The chloride addition product could also be isolated as a major side product. The ¹H-NMR spectrum showed a vinylic coupling constant of 13 Hz, which indicates either the *Z*- or *E*-isomer (**2.20a** or **2.20b**, Scheme 2.9C).

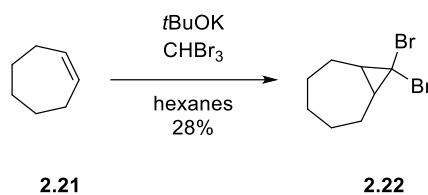


Scheme 2.9. (A) Initial synthesis of **2.9**. Conditions: **2.19** (1 equiv), DCC (1 equiv), DMAP (0.1 equiv), aniline (1.1 equiv), rt, overnight; (B) Improved synthesis of **2.9**. Conditions: **2.19** (1 equiv), oxalyl chloride (1.2 equiv), 1-phenylpiperazine (1.2 equiv), DIPEA (5 equiv), rt, 1.5 h; (C) Structure of side product (**2.20a** or **2.20b**) isolated during improved synthesis (B).

2.4.2.2 Synthesis of Bio-orthogonal Reagents

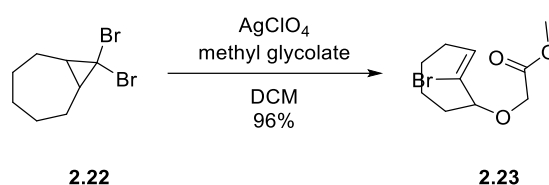
Burk *et al.* published an improved, large-scale synthesis of cyclooctyne **2.24** (Scheme 2.12).²⁰² The first step to form **2.22** gave significantly lower yields (28% vs 95%) than previously reported (Scheme 2.10).²⁰² When the reactions were carried out in a round bottom flask a thick

suspension formed which could not be mixed efficiently with a magnetic stirring bar. Overhead stirring might alleviate this problem if the reaction is repeated.



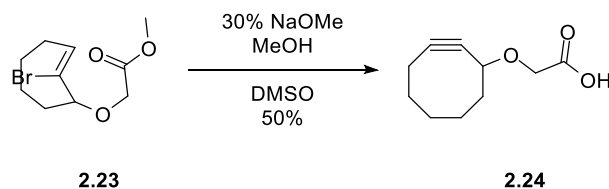
Scheme 2.10. Synthesis of **2.22**. Conditions: **2.21** (1 equiv), *t*BuOK (2.5 equiv), bromoform (1.5 equiv), –10 to 20 °C, 2 days.

The electrocyclic ring opening of **2.22** and subsequent reaction with methyl glycolate yielded **2.23** in excellent yield of 96% (Scheme 2.11).²⁰²



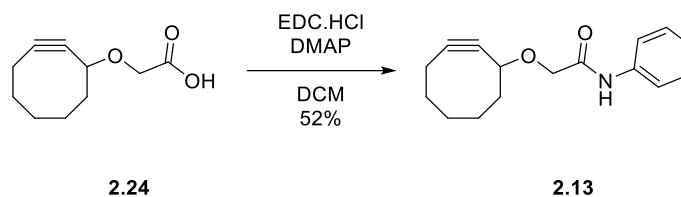
Scheme 2.11. Synthesis of **2.23**. Conditions: **2.22** (1 equiv), methyl glycolate (9 equiv), AgClO₄ (2 equiv), rt, 3 h.

Vinyl bromide **2.23** was then converted to the cyclooctyne through base mediated elimination (Scheme 2.12).²⁰² This step yielded the product **2.24** in 50%, although full consumption of the starting material was observed.



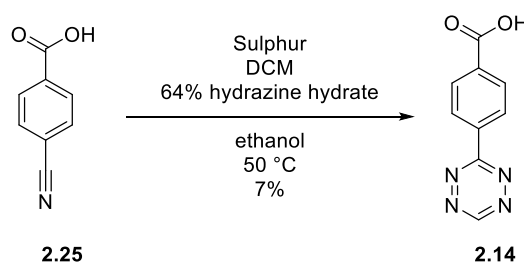
Scheme 2.12. Synthesis of **2.24**. Conditions: **2.23** (1 equiv), NaOMe (6.8 equiv), rt, overnight.

With sufficient crude material in hand, **2.24** could be coupled with aniline to synthesize a compound that would be UV active and facilitate analysis in the HPLC assay (Scheme 2.13). The amide coupling was performed using EDC.HCl and a catalytic amount of DMAP to afford **2.13** in a 52% yield. The lower yield was due to some co-elution with an unknown side-product during column chromatography, but some pure product could be obtained.



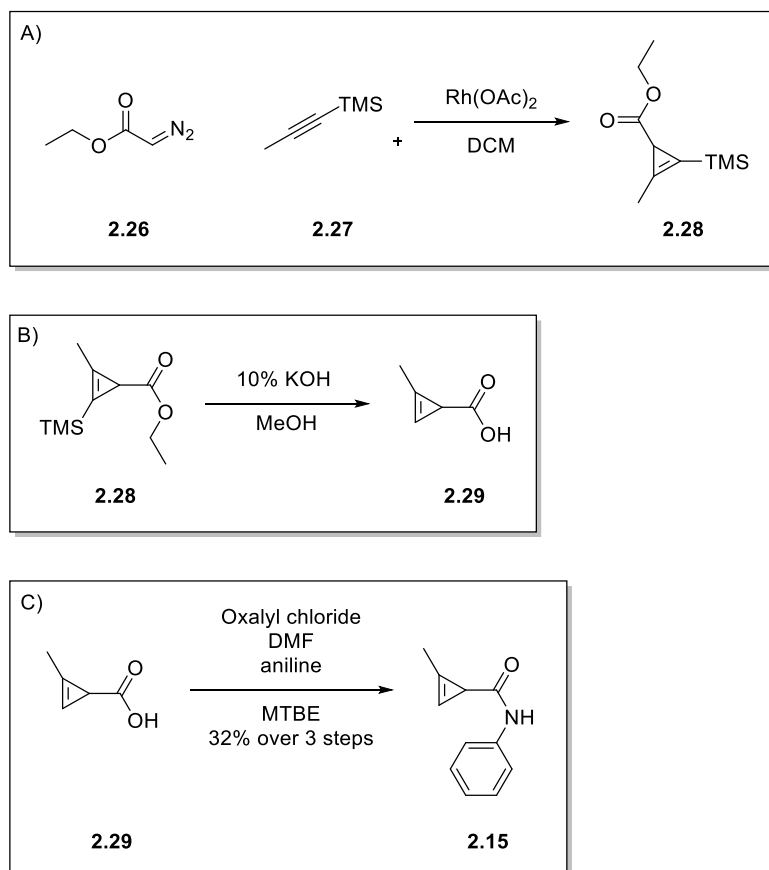
Scheme 2.13. Synthesis of **2.13**. *Conditions:* **2.24** (1 equiv), EDC.HCl (1.1 equiv), DMAP (0.05 equiv), aniline (1.5 equiv), 0 °C to rt, overnight.

Recently, an improved synthesis of mono-substituted tetrazines was published that avoided the use of pure hydrazine hydrate, which is a considerable safety hazard and very difficult to source.²⁰³ Instead, the synthesis used elemental sulphur as an activating agent, DCM as a carbon source and aqueous hydrazine hydrate (64% wt). The synthesis proceeded as expected (Scheme 2.14), however, purification of **2.14** proved to be challenging. The tetrazine was insoluble in all solvents tested (toluene, DCM, ethyl acetate, methanol, ethanol, isopropanol, water, etc.) apart from DMSO and only moderately soluble in DMF. After column purification **2.14** was obtained in only 7% yield and considerable amounts of product were likely lost on the column as the compound exhibited considerably streaking. In the future, recrystallisation might be a better purification strategy.



Scheme 2.14. Synthesis of **2.14**. *Conditions:* **2.25** (1 equiv), sulphur (2 equiv), DCM (2 equiv), hydrazine hydrate (8 equiv), 50 °C, 24 h.

The protected cyclopropene **2.28** was formed *via* a cycloaddition catalysed by rhodium acetate (Scheme 2.15A).²⁰⁴ The resulting crude product was directly used in the next step in which the alkene and ester were simultaneously deprotected to give **2.29** (Scheme 2.15B). After an aqueous work up, the crude acid was used directly in the next step and coupled to aniline by formation of the acid chloride¹⁹⁴ with oxalyl chloride and subsequent reaction with an excess of aniline. After purification, the product **2.15** was isolated in 32% yield over 3 steps (Scheme 2.15C).



Scheme 2.15. (A) Synthesis of **2.28**. Conditions: **2.26** (1 equiv), **2.27** (3 equiv), Rh(OAc)₂ (0.1 equiv), rt, 1 hour.

(B) Synthesis of **2.29**. Conditions: **2.28**, 10% KOH in MeOH (1:1), rt, overnight. (C) Synthesis of **2.15**.

Conditions: **2.29** (1 equiv), oxalyl chloride (1 equiv), aniline (2.5 equiv), rt, 2 h.

2.4.3 Development and Optimisation of a HPLC Assay to Determine the Stability of Bio-orthogonal Reagents

Reagent stability or reaction progress is routinely monitored by either NMR spectroscopy or HPLC. The advantage of NMR is that additional structural data can be gathered alongside time course data. Drawbacks are the reliance on deuterated solvents (which can influence reaction kinetics²⁰⁵) and the need for high reagent concentrations (in the mM range). Most bio-orthogonal chemistry is carried out at micromolar concentrations and ideally *in vitro* studies should mimic these concentrations. In contrast, HPLC offers greater flexibility in terms of solvent choices, concentration ranges and availability at the cost of structural information. It was anticipated that HPLC would meet the needs of the investigation better and was adopted as the analytical method of choice.

Several publications used HPLC to investigate the stability of small molecules in the presence of GSH and were chosen as a starting point for the development of the HPLC assay.^{174,175,206}

An appealing feature of the published HPLC assay was the fact that reactions were run in an HPLC vial, left in the autosampler, and sampled continuously over a specified period. This eliminated the need for manual sampling of the reaction mixture, increased throughput, removed sampling inconsistencies, enabled more frequent and consistent timepoints and ultimately lead to increased reproducibility.

The assay was further optimised by developing a fast HPLC method (10 min) – utilising a short, small particle size (2.6 μm) core-shell column – maximising the capabilities of the HPLC instrument (~ 144 samples/24 h). A typical chromatogram is shown in Figure 2.5.

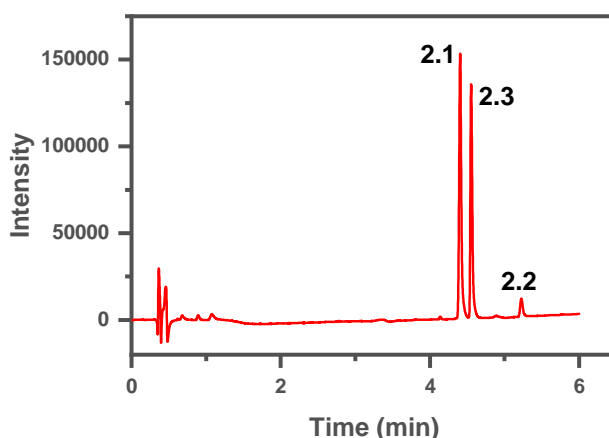


Figure 2.5. Example of a typical UV-trace obtained. Only elution gradient shown (up to 6 min). No further compounds eluted after 6 min.

Consideration was given as to whether to employ an internal standard for quantification or an external calibration curve. An internal standard is commonly used to correct for sampling error. Sampling errors can be introduced during sample transfer (*i.e.*, taking aliquots from a reaction mixture or performing a sample work-up) or by the autosampler of the HPLC system. As no sample transfer occurred in the developed protocol (reaction was carried out directly in the HPLC vials) and the sampling error of the Shimadzu HPLC systems was extremely low ($\text{SD} = <1\%$ after reaching full conversion, as observed in Figure 2.16C; see Experimental for details) it was decided that an internal standard would not offer any benefits over an external calibration curve. Furthermore, an internal standard itself can be the source of errors, as errors during IS addition can propagate into quantification errors.²⁰⁷

Therefore, external calibration was deemed appropriate and a calibrations curves were constructed for ynamine **2.1** corresponding triazole **2.3** (Figure 2.6). Each calibration curve was measured in triplicate and an excellent linear relationship ($R^2 > 99\%$) was obtained in each case.

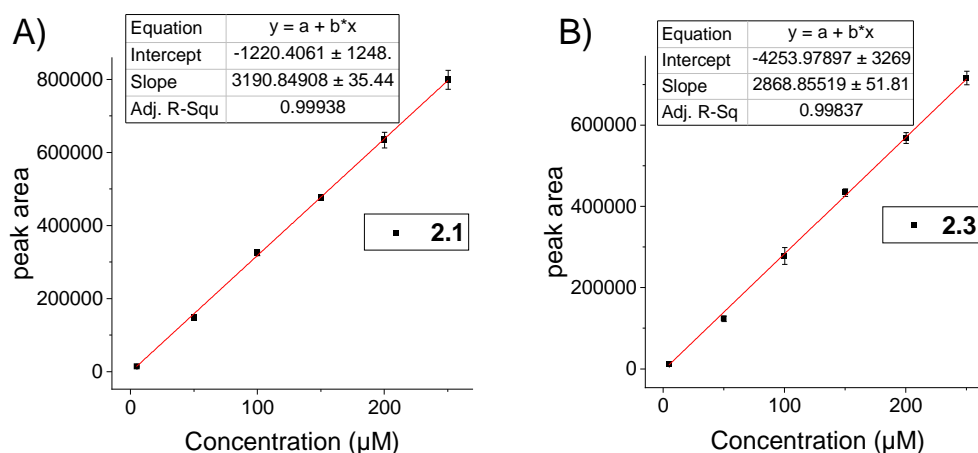


Figure 2.6. (A) Calibration curve for ynamine **2.1**. (B) Calibration curve for triazole **2.3**. Each calibration curve was measured in triplicate. The averaged peak area for each concentration was used to construct the calibration curves. Error bars represent the standard deviation.

Conversions for the other substrates were calculated by absolute peak areas by dividing the peak area of the starting material or product by the sum of the peak area of starting material and product. Deviations from this protocol are clarified in the corresponding experimental sections.

Calculating conversions in this way relied on several assumptions to obtain valid results. First, it was assumed that the starting material was quantitatively converted to product, and no side reactions occurred. In the experiments performed, no significant amount of side products was observed in the HPLC chromatograms. Therefore, the first assumption was deemed appropriate.

The second assumption of this approach relied on the fact that the detector response of the starting material and product was similar at the monitored wavelength. If this was not the case, then calculated conversions would not be accurate, as a stronger UV response of either substrate would skew the ratio. For quantitative measurements, this would be a problem. However, the aim of this HPLC assay was to compare the relative reaction kinetics of bio-orthogonal reactions and constructing calibration curves for the large number of compounds of this study would be time consuming. Calculating conversion by peak area preserved the qualitative aspect and therefore was deemed appropriate to fulfil the intentions of this study. However, the results obtained are not suitable for a quantitative analysis.

The standard reagent concentrations were chosen to be 200 μM as this gave a good HPLC UV-detector response while keeping the concentration as low as possible. Unless otherwise noted, reactions were carried out in triplicate and the standard deviation plotted either as error bars for bar charts or as shaded bands for line graphs.

2.4.4 Ynamine Stability in the Presence of Glutathione

Stability was an important prerequisite for a bio-orthogonal reagent. If ynamine reactivity with GSH is high, then side reactions could reduce the versatility in biological applications or give unreliable results (*e.g.*, increased background fluorescence).^{185,208} The goal of this first section was to investigate the susceptibility of ynamine **2.1** to react with GSH.

2.4.4.1 Influence of Buffer Conditions on Ynamine Stability

The first parameter investigated was the reaction medium. The media chosen were sodium phosphate buffers (PB) (0.1 M and 0.2 M), commercial Dulbecco's phosphate buffered saline (DPBS; 1X and 10X DPBS, equates to 0.01 M and 0.1 M) and water serving as a control. The buffers differ in their salt composition (Experimental Table 2.2); the phosphate buffers only contain sodium and phosphate ions whereas the DPBS buffers contains potassium, sodium chloride, magnesium, and calcium as well. The phosphate buffer is commonly employed in biology whereas the DPBS adds additional salts which are commonly found in cells. All buffers were adjusted to pH 7.4 before use. Unless otherwise stated, this pH was used throughout the thesis.

The stability of the ynamine **2.1** was monitored in the different buffer systems over 24 h in the presence of 10 mM GSH (Figure 2.7). About 80% of ynamine **2.1** remained intact in water and 1X DPBS and about 75% in 10X DPBS after 24 h. In contrast, only ~15% and ~10% of ynamine **2.1** remained in 0.1 M and 0.2 M phosphate buffer, respectively.

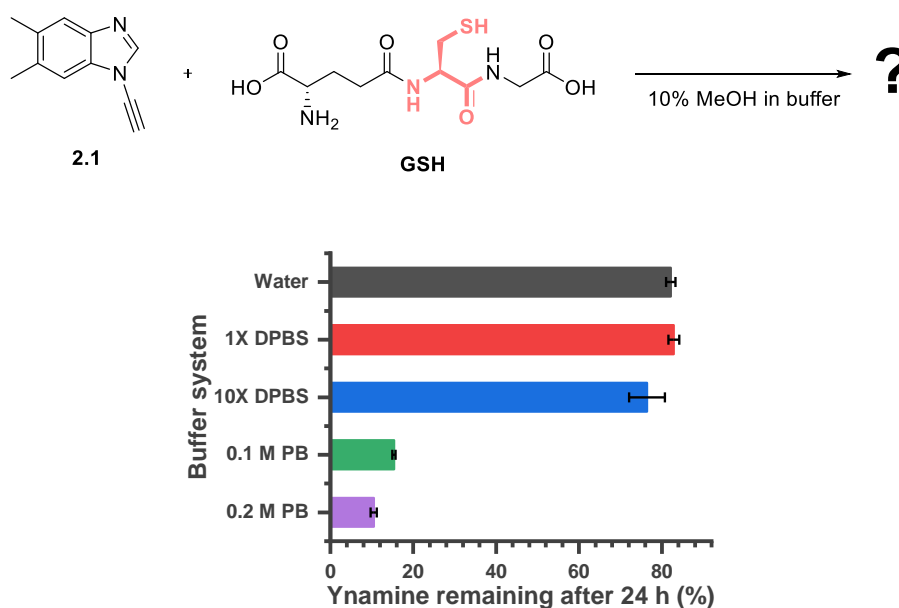
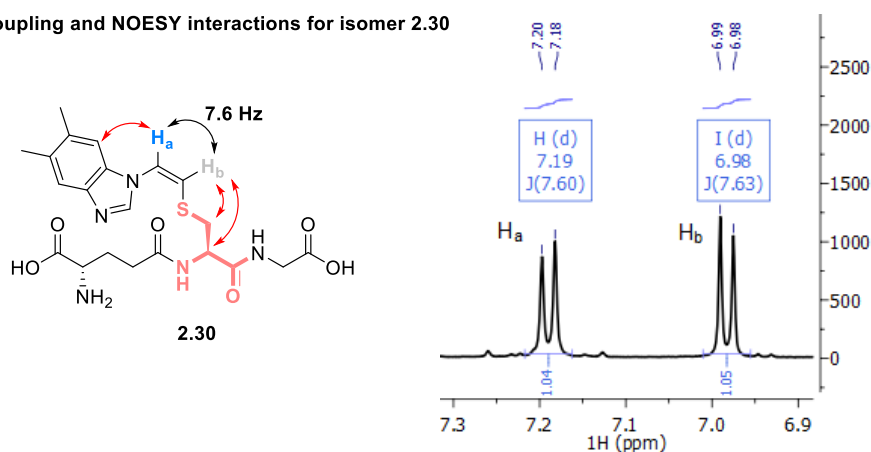
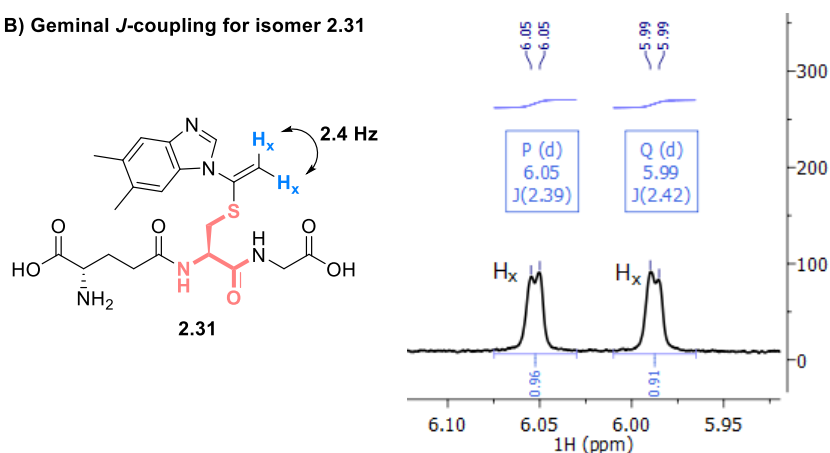


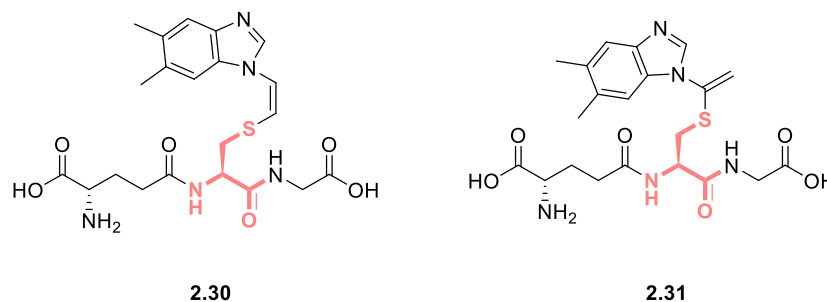
Figure 2.7. Stability of ynamine (**2.1**) in the presence of GSH (10 mM) after 24 h in different buffer systems. *Conditions:* **2.1** (200 μ M), GSH (10 mM), 10% MeOH in aqueous buffer (for composition of each buffer see Experimental Table 2.2), rt, 24 h. Buffer pH = 7.4. Error bars represent the standard deviation calculated from three experiments.

The difference in stability is not caused by buffer concentration or ionic strength, as there was negligible difference between either 1X DPBS and 10X DPBS or 0.1 M and 0.2 M phosphate buffer. When the concentrations of the buffers match (10X DPBS and 0.1 M phosphate buffer) a drastic difference in stability was observed. Therefore, the difference was likely caused by buffer composition. The DPBS buffer contains both magnesium and calcium (albeit low, ~0.5 and ~0.7 mM in 1X DPBS) which could interact with GSH and reduce its reactivity. On the basis of these results, 1X DPBS was used in further experiments.

Two new species were observed in the HPLC chromatogram, which were assumed to be the degradation products. After a scale up reaction, compounds **2.30** and **2.31** (Table 2.1) were isolated. The ^1H -NMR spectrum of **2.30** showed an AB-type coupling of 7.6 Hz, which is diagnostic for *Z*-alkenes whereas a coupling constant of 2.4 Hz for **2.31** was indicative of the geminal isomer (Figure 2.8).

A) *J*-coupling and NOESY interactions for isomer **2.30**B) Geminal *J*-coupling for isomer **2.31****Figure 2.8.** (A) *J*-coupling and NOESY interactions of isomer **2.30**. (B) *J*-coupling of isomer **2.31**.

In the studied buffers, a slight preference towards isomer **2.30** (ratio = 6:4) was observed (Table 2.1), except for 1X DPBS where **2.30** was heavily favoured (ratio = 4:1).

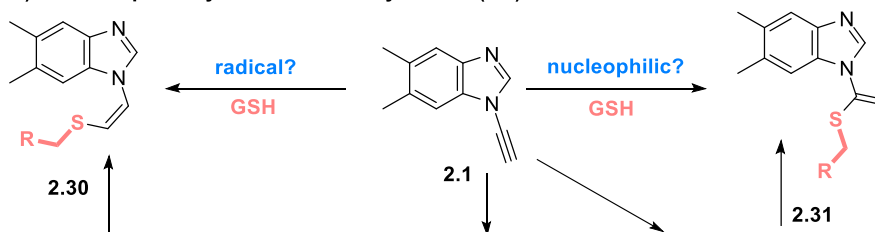
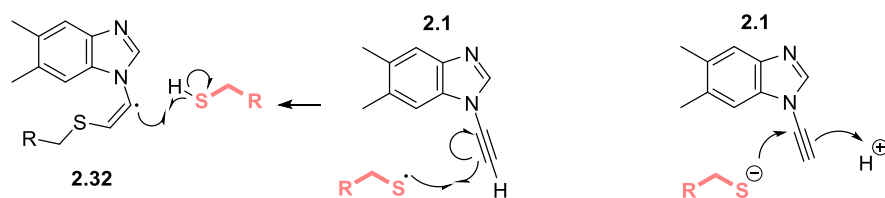
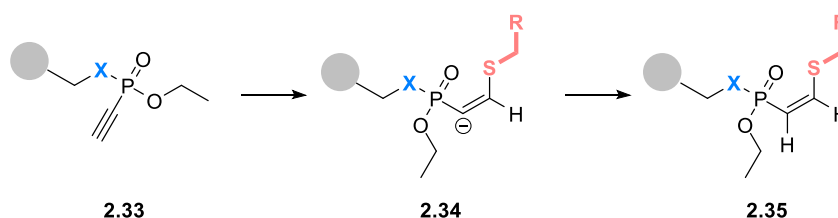
Table 2.1. Ratios and conversion of degradation products (**2.30** and **2.31**) in the different buffers.

Entry	Buffer	Ratio (2.30:2.31)	Conversion (%) 2.30/2.31
1	Water	~ 6:4	6/4
2	1X DPBS	~ 4:1	9/2
3	10X DPBS	~ 1:1	4/4
4	0.2 M PB	~ 6:4	43/31
5	0.1 M PB	~ 6:4	48/38

Conditions: **2.1** (200 μ M), GSH (10 mM), 10% MeOH in aqueous buffer (pH 7.4), rt, 24 h.

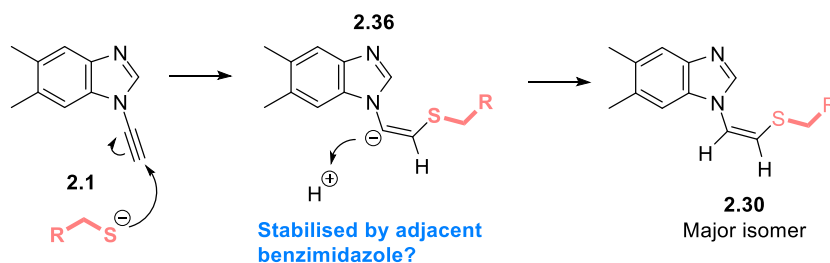
The two degradation products are likely produced through different mechanisms (Scheme 2.16A). Compound **2.31** is the classical Markovnikov product resulting from nucleophilic attack of the GSH thiol group at the ynamine C_{α} , whereas **2.30** is likely formed via an anti-Markovnikov addition at C_{β} (Scheme 2.16B).

If an electron withdrawing group is present adjacent to the triple bond, **2.30** could also be formed through nucleophilic addition as observed with phosphorus(V) alkynes (Scheme 2.16C).²⁰⁹ For the ynamine **2.1**, stabilisation of the negative charge by the adjacent benzimidazole could be conceivable (**2.36**, Scheme 2.16D).

A) Possible pathways for reaction of ynamine (2.1) with GSH:**B) Potential mechanisms:****C) Literature precedence of forming Z-isomers via nucleophilic addition:**

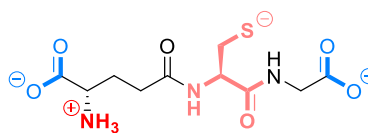
X: S, O or N

● = fluorescent probe

D) Potential mechanism for Z-isomer (2.30) via nucleophilic addition:

Scheme 2.16. (A) Possible pathways to degradation products **2.30** and **2.31**. (B) Proposed mechanism of either radical or nucleophilic degradation of **2.1** by GSH. GSH radicals could be formed through the presence of copper. (C) Literature example of formation of the anti-Markovnikov Z-isomer via nucleophilic addition.²⁰⁹ (D) Potential mechanism for formation of **2.30** via nucleophilic addition instead of radical degradation.

If this is indeed the case, then increasing the pH should increase the propensity of the thiolate (**2.37**) form of GSH (Figure 2.9)²¹⁰ and lead to increased degradation.



2.37

Figure 2.9. Thiolate form of GSH (**2.37**) present at pH 7 – 8 (1 – 10%). Percentage increases at higher pH.²¹¹

2.4.4.2 Influence of pH on the Susceptibility of Ynamines to Glutathione Addition

The pH dependence of the reactivity of ynamine **2.1** with GSH over 24 h was explored by adjusting the pH of a 1X DPBS solution to either 4, 7 and 11 with HCl or NaOH (Figure 2.10). The pH of these solutions had a negligible effect on the stability of **2.1**. This implied that the protonation state of the thiol did not play a key role in the degradation mechanism, which suggested a radical-mediated degradation pathway. However, the pH was not measured after the reaction and the buffering capacity of the system at pH 4 was likely limited. Therefore, more investigation might be needed to confirm these results.

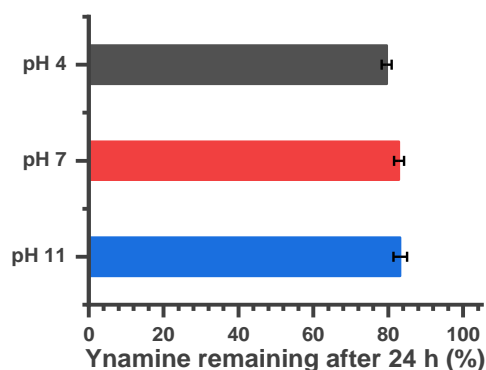
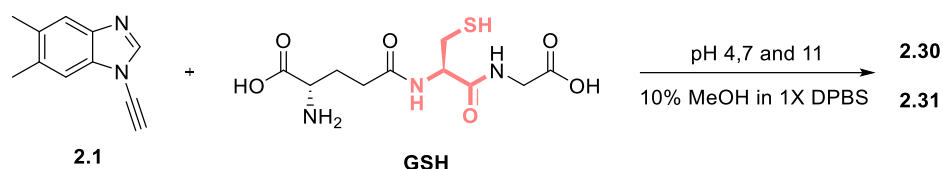


Figure 2.10. Influence of pH on the stability of ynamine **2.1** in the presence of GSH (10 mM) after 24 h. *Conditions:* **2.1** (200 μ M), GSH (10 mM), 10% MeOH in 1X DPBS, rt, 24 h. Error bars represent the standard deviation calculated from three experiments.

2.4.4.3 The Effect of Copper and Glutathione Concentration on Ynamine Reactivity

The concentrations of the Cu(II) source and GSH were then investigated. A final concentration of 350 μ M of Cu(OAc)₂ was used in the reaction relative to 200 μ M for ynamine **2.1**. The

concentration of GSH was varied (1, 2, 5 and 10 mM) and the experiments performed both in the presence and absence of a Cu(II) source (Figure 2.11A and B).

In the absence of a Cu(II) source, the amount of **2.30** and **2.31** formed generally correlated with GSH concentrations (Figure 2.11A). At 1 and 2 mM GSH, about 10% of **2.30** and **2.31** were formed in a ratio of 6:4. This increased to ~20% at 10 mM GSH and the ratio shifted towards **2.30** as the major degradation product. Peculiarly, at 5 mM GSH, less **2.30** (2%) and **2.31** (1%) were formed. Although this experiment was performed in triplicate it would be useful to repeat this experiment to confirm the findings.

The presence of Cu(OAc)₂ resulted in the exclusive formation of **2.30** and the amount correlated with the GSH concentration. At 1 – 2 mM GSH, about 3% of **2.30** was formed which increased to 25% (5 mM GSH) and 27% (10 mM). Closer inspection of the reaction time-course revealed that no further **2.30** was produced after 4 h in the presence of 1 – 2 mM GSH whereas **2.30** was continuously produced at higher GSH concentrations.

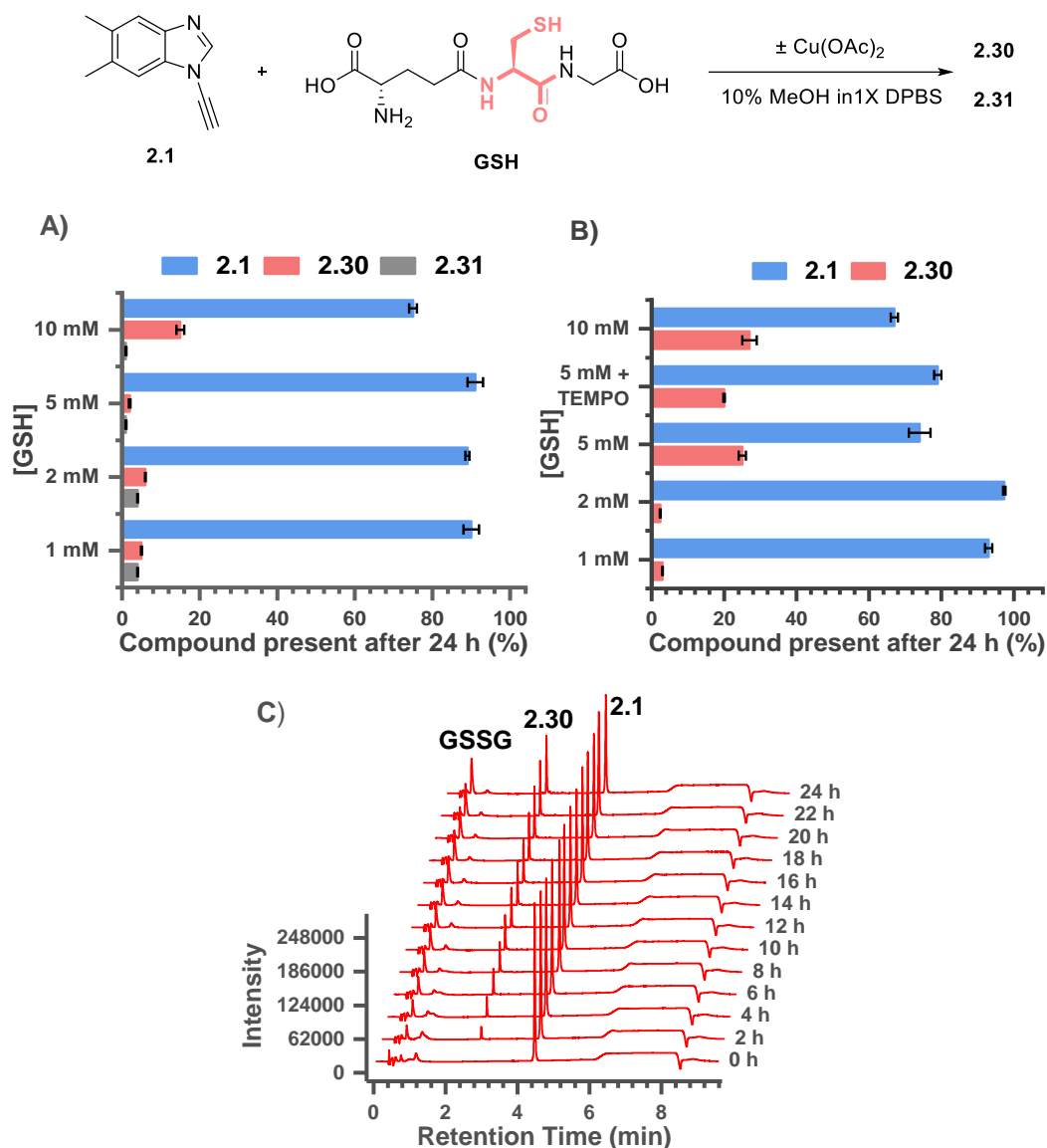
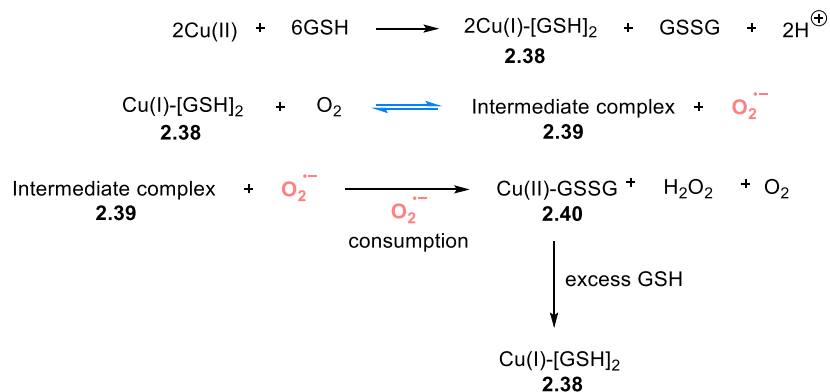


Figure 2.11. (A) Influence of a range of GSH concentrations (1, 2, 5 and 10 mM) on ynamine **2.1** stability after 24 h. *Conditions:* **2.1** (200 μ M), GSH (1, 2, 5 or 10 mM), 10% MeOH in 1X DPBS, rt, 24 h. (B) Influence of Cu(OAc)_2 (350 μ M) addition on ynamine **2.1** reactivity with GSH (1, 2, 5 and 10 mM). *Conditions:* **2.1** (200 μ M), Cu(OAc)_2 (350 μ M), GSH (1, 2, 5 or 10 mM), 10% MeOH in 1X DPBS, rt, 24 h. Buffer pH = 7.4. Error bars represent the standard deviation calculated from three experiments. (C) Waterfall plot of stacked chromatograms showing continuous production of GSSG and **2.30** in the presence of Cu(OAc)_2 (350 μ M). *Conditions:* **2.1** (200 μ M), Cu(OAc)_2 (350 μ M), GSH (1, 2, 5 or 10 mM), 10% MeOH in 1X DPBS, rt, 24 h. Buffer pH = 7.4.

Previous work had shown that mixing GSH with Cu(II) resulted in the formation of a Cu(I) -GSH complex and GSSG were produced (Scheme 2.17).¹⁶⁰ The Cu(I) -complex (**2.38**) can react with oxygen continuously to produce superoxide. This reaction is reversible unless superoxide is consumed (*i.e.*, auto-dismutation) and a Cu(II) -GSSG (**2.40**) complex is produced.¹⁶⁵

At high excesses of GSH, the Cu(II)-GSSG complex can be reduced back to the Cu(I)-GSH (2.38) complex by GSH.¹⁶⁶ Therefore, as long as superoxide is removed, GSH is continuously consumed to form GSSG. Once fully consumed, this cycle stops and no reduced GSH is present in the system.



- **superoxide** is continuously produced at high Cu:GSH ratios
- formation of **reversible** complex
- by **trapping** superoxide equilibrium is broken and GSH is consumed

Scheme 2.17. Summary of GSH and copper redox chemistry.^{165,166}

This is what is observed in experiments shown in Figure 2.11B (1 and 2 mM GSH), where the formation of GSSG plateaus after 4 h (see Experimental Figure 2.19) and coincides with no further formation of 2.30. In contrast, at high concentration of GSH (5 and 10 mM), GSSG is continuously formed over 24 h and presumably GSH radicals are also continuously formed which can react with ynamine 2.1 to form 2.30.¹⁶⁶

Finally, to explore if the reactivity of 2.1 could be due to a radical-based mechanism, the reaction with 5 mM GSH and Cu(OAc)₂ (350 μM) was repeated in the presence of the radical scavenger TEMPO (3.5 mM) (Figure 2.11B). Unexpectedly, the addition of TEMPO did not significantly reduce the amount of 2.30 formed (from ~25% to 20%). Contrary to previous experiments (pH and addition of copper) this would speak against a radical mechanism. However, TEMPO is also known to react with superoxide,¹⁶⁵ which is produced by GSH in the presence of copper. Further experiments are needed to conclusively confirm whether a radical-mediated mechanism is in place.

In summary, ynamine **2.1** reacts with GSH to form the addition products **2.30** and **2.31**, with the amount of these products influenced by the nature of the buffer system and the presence of a Cu(II) source.

2.4.5 Susceptibility of Common Bio-orthogonal Reagents to Reactivity with Glutathione

First, the stability of the alkynes (**2.1**, **2.9** – **2.11**) was monitored in the presence of GSH (10 mM) in 1X DPBS over 24 h (Figure 2.12). The concentration of 10 mM GSH was chosen to simulate the highest physiological concentration that could be encountered by these reagents. The results for ynamine **2.1** are added to the figure for comparison.

All alkynes displayed good stability after 24 h (> 80%). Alkyne **2.10** did not react with GSH and the propiolic alkyne **2.9** was also stable with around 93% remaining. Only ~80% of propargylic alkyne **2.11** remained after 24 h but the result displayed a large standard deviation. No new peaks were detected in the HPLC chromatogram therefore it is possible that the decrease in peak area was not due to degradation but precipitation.

Out of all the alkynes tested, GSH degraded the ynamine **2.1** the most (excluding **2.11**, where degradation was uncertain), which could indicate reduced *in vivo* stability. However, the amount ynamine **2.1** remaining after 24 h is still comparable to the other alkynes.

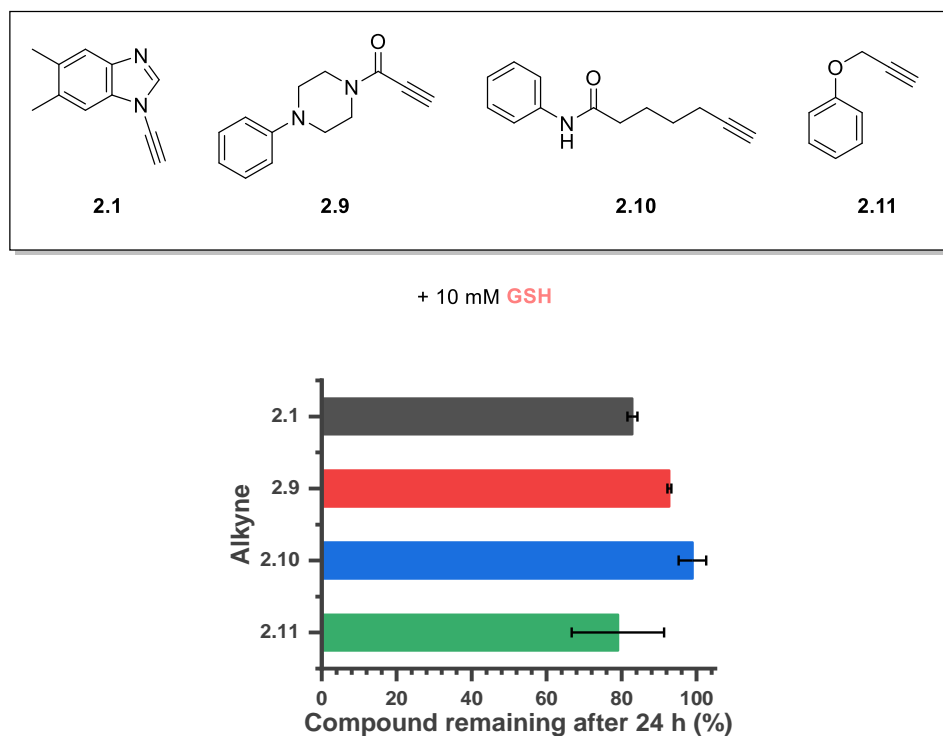


Figure 2.12. Stability of alkynes (**2.1**, **2.9** – **2.11**) in the presence of GSH (10 mM) after 24 h. *Conditions:* **2.1**, **2.9** – **2.11** (200 μ M), GSH (10 mM), 10% MeOH in 1X DPBS, rt, 24 h. Buffer pH = 7.4 Error bars represent the standard deviation calculated from three experiments.

The same experiment was repeated with bio-orthogonal reagents (**2.12** – **2.15**), which all displayed good stability in the presence of GSH (Figure 2.13). Especially DBCO **2.12** and cyclopropene **2.15** (91% and 93%) did not react much with GSH and cyclooctyne **2.13** and tetrazine **2.14** were slightly less stable (87% and 85%).

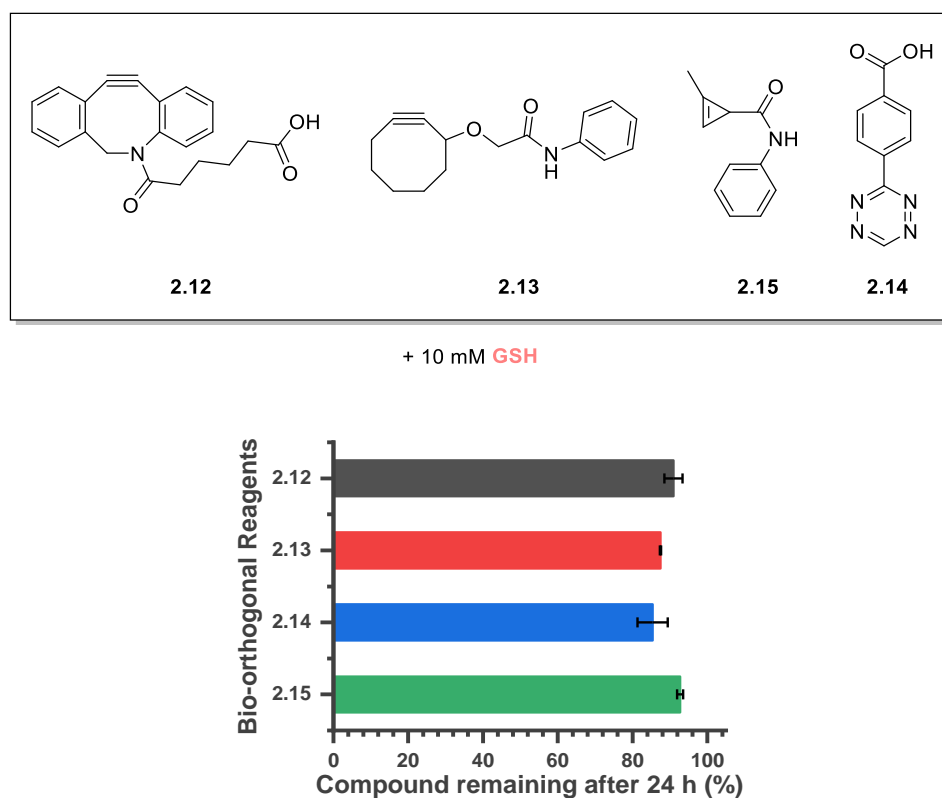


Figure 2.13. Stability of bio-orthogonal reagents (**2.12** – **2.15**) in the presence of GSH (10 mM) after 24 h. *Conditions:* **2.12** – **2.15** (200 μ M), GSH (10 mM), 10% MeOH in 1X DPBS, rt, 24 h. Buffer pH = 7.4. Error bars represent the standard deviation calculated from three experiments.

Cyclopropenes have been reported to be unreactive towards thiols (*i.e.*, 1 equiv of cysteine).^{121,122} This matches with the excellent stability towards GSH observed for cyclopropene **2.15**, although GSH was present in a 50-fold excess. The result for tetrazine **2.14** is also comparable to the stability reported in FBS where ~75% remained after 10 h at 37 °C.²⁰¹

Unexpectedly, DBCO **2.12** was very stable towards GSH, although it had previously been reported as thiol reactive,¹⁷⁶ but potentially stability can differ depending on reaction conditions or the local micro-environment (*i.e.* adjacent amino acids in protein) could influence stability.¹⁷⁷

2.4.6 Influence of Glutathione on the CuAAC Reaction

To increase the scope of the investigation of the CuAAC reaction in the presence of GSH, it was decided to expand the azide substrates from benzyl azide (**2.2**) to also include azido-ethanol (**2.41**) and picolyl azide (**2.42**) (Figure 2.14). This scope covers a range of chemical properties - hydrophobic, hydrophilic, and copper chelating - which should highlight any changes in reactivity.

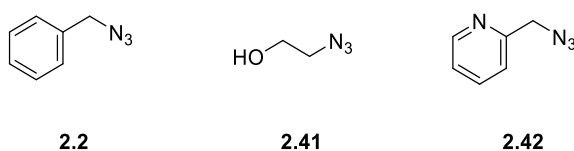
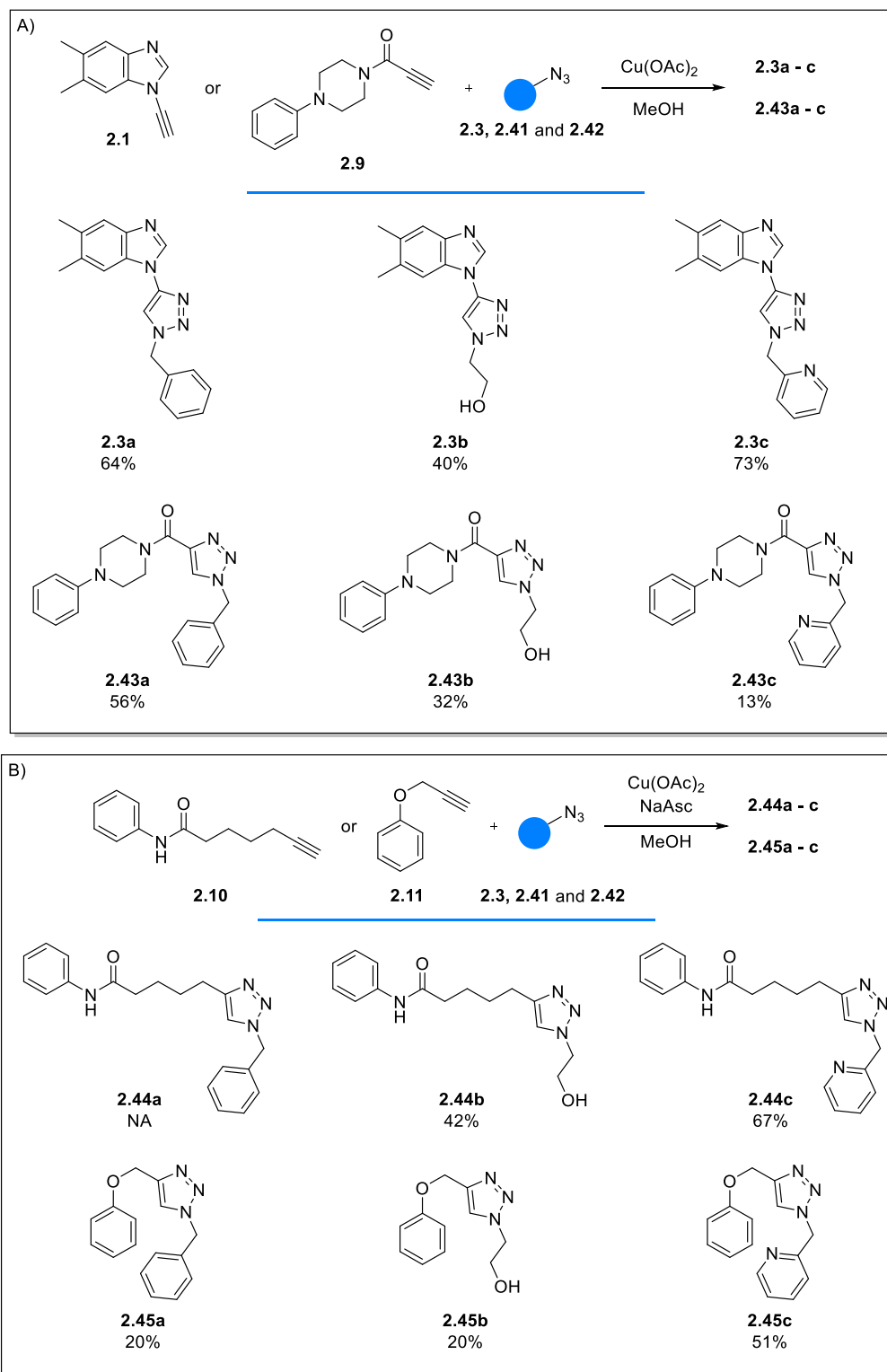


Figure 2.14. Structures of expanded azide scope.

Triazole products were first synthesised as reference compounds to determine retention times the HPLC assay. The CuAAC reactions with ynamine **2.1** were carried out according to the standard procedure used in the group (10% $\text{Cu}(\text{OAc})_2$ in MeOH) (Scheme 2.18A). No NaAsc was added as the ynamine is known to react without it.¹⁵¹ The yields obtained were moderate (40 – 73%) for click reactions.

Next, the reactions with propiolic alkyne **2.9** were carried out using the same procedure, as they were also shown to be reactive in the absence of NaAsc (Scheme 2.18A).¹⁵³

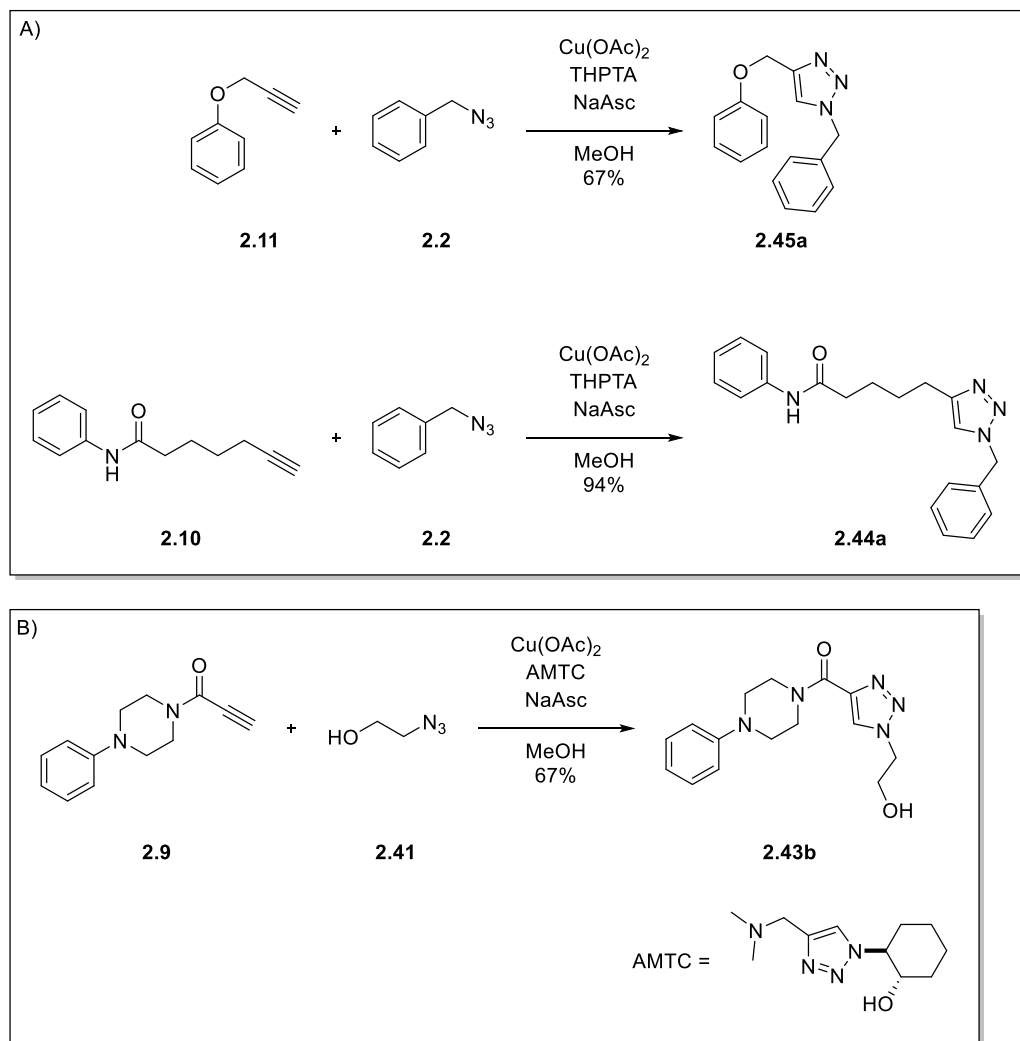
The rest of the triazoles (except **2.44a**) were synthesised with the addition of 1 equivalent of NaAsc and yields ranged from 20% to 67%, which again are low for CuAAC reactions (Scheme 2.18B).



Scheme 2.18. (A) Synthesis of **2.3a – c** and **2.43a – c**. Conditions: **2.1** or **2.9** (1 equiv), **2.3, 2.41** or **2.42** (1.1 equiv), Cu(OAc)₂ (0.1 equiv), rt, overnight. (B) Synthesis of **2.44a – c** and **2.45a – c**. Conditions: **2.10** or **2.11** (1 equiv), **2.3, 2.41** or **2.42** (1.1 equiv), Cu(OAc)₂ (0.1 equiv), NaAsc (1 equiv), rt, overnight.

Due to the low yields, the influence of Cu-chelating ligands on triazole formation was explored. The addition of THPTA improved the yield of **2.45a** from 20% to 67% and triazole **2.44a** was obtained in 94% yield (Scheme 2.19A). A cheaper alternative ligand for THPTA is AMTC, which is easily synthesised.²¹² The reaction to form **2.43b** was repeated with the addition of AMTC and the yield increased from 32% to 67%.

Improved Synthesis with CuAAC Ligands:



Scheme 2.19. (A) Improved synthesis of **2.44a** and **2.45a** using THPTA. *Conditions:* **2.10** or **2.11** (1 equiv), **2.2** (1.1 equiv), Cu(OAc)₂ (0.05 equiv), THPTA (0.1 equiv) NaAsc (0.1 equiv). (B) Improved synthesis of **2.43b** using AMTC. *Conditions:* **2.9** (1 equiv), **2.41** (1.1 equiv), Cu(OAc)₂ (0.05 equiv), AMTC (0.1 equiv), NaAsc (0.1 equiv), rt, overnight.

Next, conditions were explored to optimize the formation of triazole **2.3** in the presence of a Cu(II) source and GSH (Figure 2.15). Conditions such as GSH concentration (1 – 6.5 mM), copper sources (CuI and Cu(OAc)₂), copper concentration (200 – 400 μ M) and benzyl azide

2.2 concentration (200 – 800 μM) were explored (Experimental Table 2.3). High GSH concentrations inhibited the reaction completely, but conversion was observed at 1 mM GSH. By increasing copper (to 350 μM) and azide concentration (to 500 μM) the reaction was optimised to reach full conversion within 2 h (Figure 2.15).

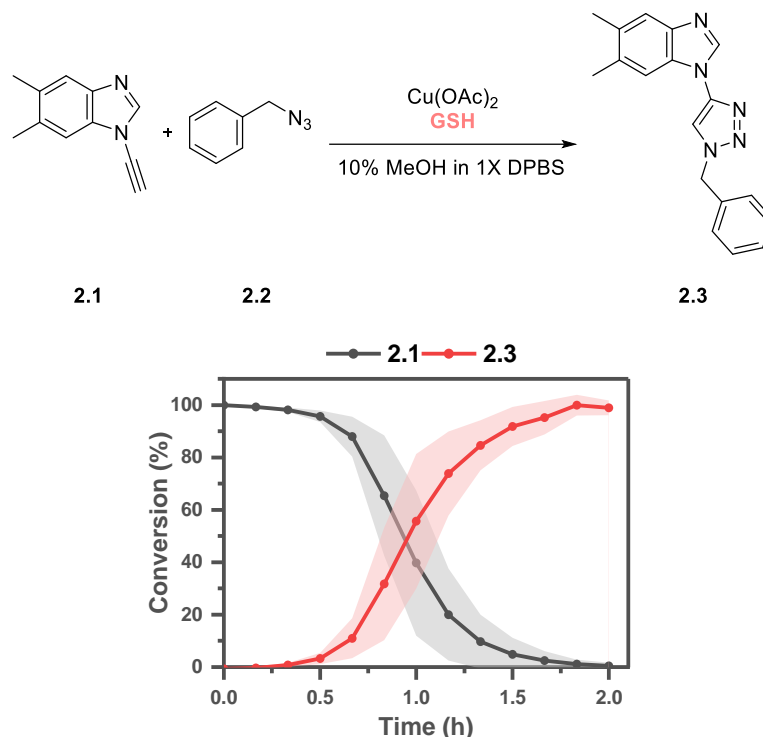


Figure 2.15. Reaction profile for the optimised reaction of **2.1** with benzyl azide (**2.2**) in the presence of a Cu(II) source and GSH (1 mM). *Conditions:* **2.1** (200 μM), $\text{Cu}(\text{OAc})_2$ (350 μM), **2.2** (500 μM), GSH (1 mM), 10% MeOH in 1X DPBS, rt, 2 h. Buffer pH = 7.4. Shaded areas represent the standard deviation calculated from three experiments.

With the optimised conditions in hand, the reactivity of the synthesised alkyne panel (**2.1**, **2.9** – **2.11**) with the different azides (**2.2**, **2.41** and **2.42**) was analysed.

However, when alkynes **2.9** – **2.11** were incubated with benzyl azide (**2.2**) using the optimal conditions, no conversion for alkynes **2.9** and **2.10** was observed after 24 h (Experimental Table 2.4). This could be caused by the absence of a reductant as the CuAAC reaction is exclusively catalysed by Cu(I).

The optimised conditions do not include such a reductant with the assumption that GSH acts as a reductant. In control experiments (in the absence of GSH), no conversion was observed for alkynes **2.9** – **2.11** (after 24 h) unless 1 mM NaAsc was added (Experimental Table 2.5). This afforded full conversion for alkynes **2.9** – **2.11** in under 8 h (Experimental Table 2.6).

Therefore, the following experiments were repeated using the optimal condition and 1 mM NaAsc.

Under these conditions, the overall alkyne reactivity followed the trend: **2.1** > **2.9** > **2.11** > **2.10** and the overall azide reactivity followed the trend: picolyl azide (**2.42**) > benzyl azide (**2.2**) > azido-ethanol (**2.41**) (Figure 2.16A-C). The conversion for ynamine **2.1** decreased over time and a precipitate formed during the reaction in the HPLC vials, which was assumed to be triazole product **2.3**. This precipitate also formed when triazole **2.3** (200 μ M) was prepared in a HPLC vial separately, strengthening this hypothesis.

In detail, **2.1** was more reactive than the other alkynes, reaching full conversion in under 5 h (except for the reaction with azido-ethanol). In comparison, none of the other alkynes reached full conversion with benzyl azide or azido-ethanol in 24 h.

In terms of azide reactivity, full conversion for all alkynes in under 14 h is only observed with picolyl azide **2.42** (Figure 2.16C). This effect was especially pronounced for the aliphatic alkyne (**2.9**), going from <20% conversion (with benzyl azide **2.2**, Figure 2.16A) after 24 h to 100% (with picolyl azide **2.42**, Figure 2.16C) in under 15 h.

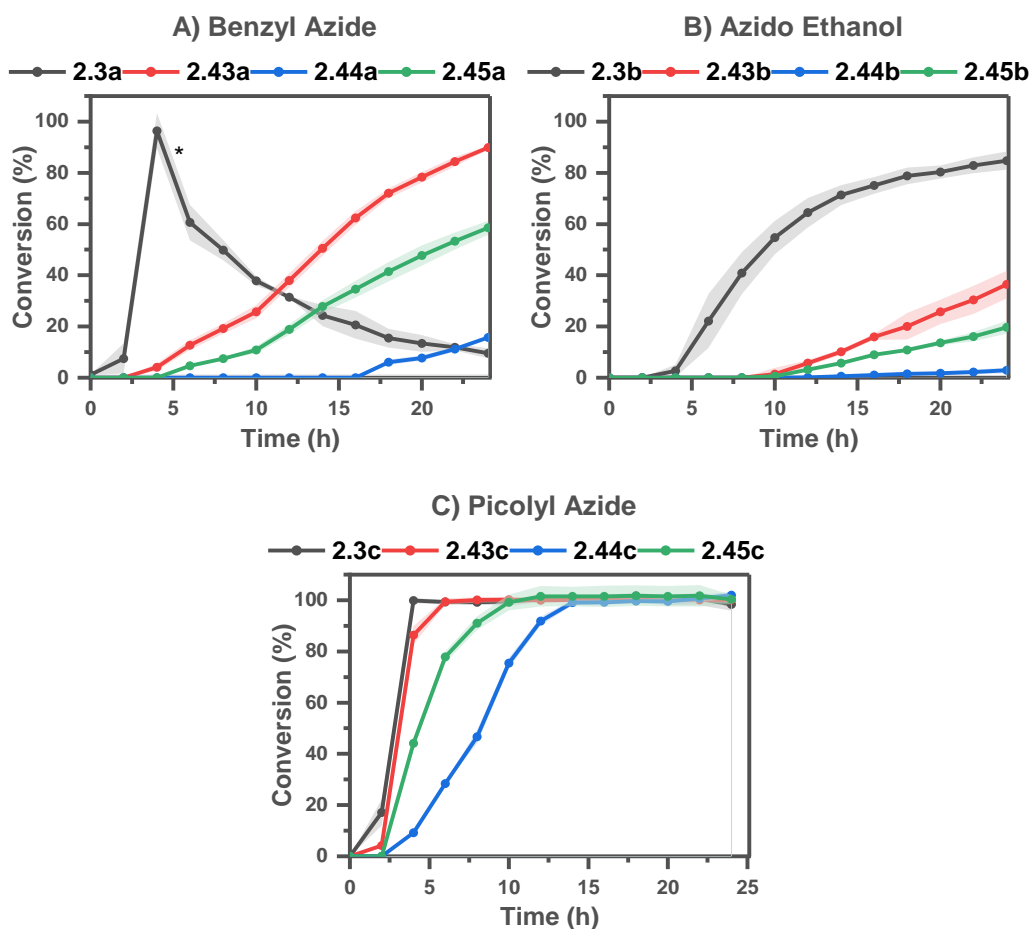
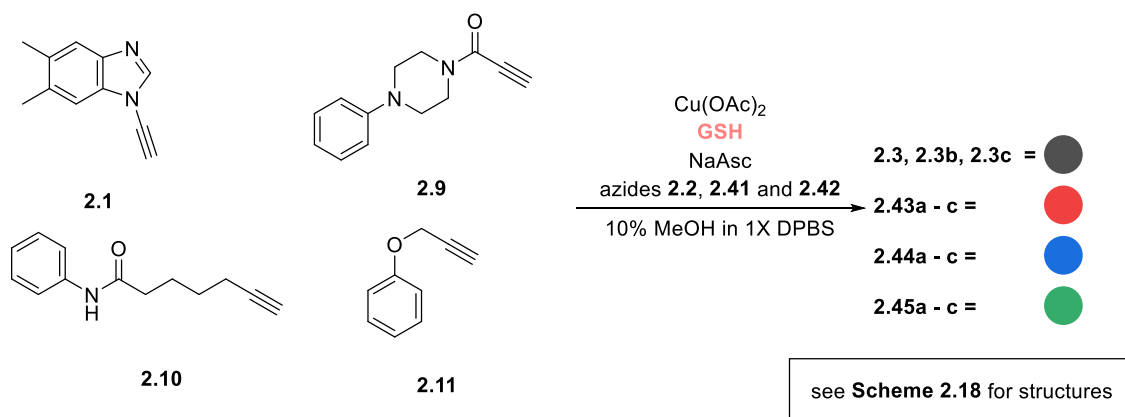


Figure 2.16. (A) Alkyne reactivity (**2.1**, **2.9** – **2.11**) with benzyl azide (**2.2**) in the presence of GSH (1 mM). *Conditions:* **2.1**, **2.9** – **2.11** (200 μM), Cu(OAc)_2 (350 μM), **2.2** (500 μM), GSH (1 mM), NaAsc (1 mM), 10% MeOH in 1X DPBS, rt, 24 h. *Conversion decreased due to precipitation of **2.3**. (B) Alkyne reactivity (**2.1**, **2.9** – **2.11**) with azido-ethanol (**2.41**) in the presence of GSH (1 mM). *Conditions:* **2.1**, **2.9** – **2.11** (200 μM), Cu(OAc)_2 (350 μM), **2.41** (500 μM), GSH (1 mM), NaAsc (1 mM), 10% MeOH in 1X DPBS, rt, 24 h. (C) Alkyne reactivity (**2.1**, **2.9** – **2.11**) with picolyl azide (**2.42**) in the presence of GSH (1 mM). *Conditions:* **2.1**, **2.9** – **2.11** (200 μM), Cu(OAc)_2 (350 μM), **2.42** (500 μM), GSH (1 mM), NaAsc (1 mM), 10% MeOH in 1X DPBS, rt, 24 h. Buffer pH = 7.4. Shaded areas represent the standard deviation calculated from three experiments.

The observed alkyne reactivity follows the expected pattern of propiolic > propargylic > aliphatic which matches with literature reports^{153,198} and the copper chelating effect of picolyl azide (**2.42**)⁷⁸ minimised the reactivity difference across the alkyne series. For the ynamine **2.1**, the difference between benzyl azide (**2.2**) and picolyl azide (**2.42**) was only minimal. This highlights the already high reactivity of the ynamine, which is only increased slightly by copper chelating azides such as **2.42**.

The reactivity for all alkynes was the lowest with azido-ethanol (**2.41**), which is readily soluble in water. The difference in reactivity might be explained by the “on-water” effect, which was observed for multiple cycloadditions.^{213–215} It is thought that aggregation of hydrophobic molecules in aqueous environments increases the effective local concentration which then increases reaction speed.^{216,217} The observation that azido-ethanol (**2.41**) is the least reactive azide could be explained by this effect.

In summary, the addition of GSH lengthened reaction times for all alkynes (**2.1**, **2.9** – **2.11**) with benzyl azide to reach full conversion in under 6 h to more than 24 h (in case of **2.9** – **2.11**). Ynamine **2.1** was least affected by the addition of GSH and retained superior reactivity compared with other alkynes which were also unreactive unless NaAsc was added. Picolyl azide (**2.42**) markedly increased reaction rates while the water-soluble azido-ethanol led to slower reaction rates.

2.4.7 Influence of Glutathione on SPAAC/IEDDA Cycloadditions

Reagents **2.12** and **2.13** (200 μ M each) were reacted with benzyl azide **2.2** (500 μ M) (Figure 2.17A), whereas cyclopropene **2.15** (200 μ M) was reacted with tetrazine **2.14** (500 μ M) (Figure 2.17B) first in the absence and then in the presence of GSH (1 mM). The addition of 1 mM GSH did not affect the SPAAC and IEDDA cycloadditions (Figure 2.17C and D). DBCO **2.12** reached full conversion in under 2 h in both experiments, cyclopropene **2.15** ~95% after 24 h, while cyclooctyne **2.13** reached a maximum conversion of ~80% (conversion decreased due to precipitation).

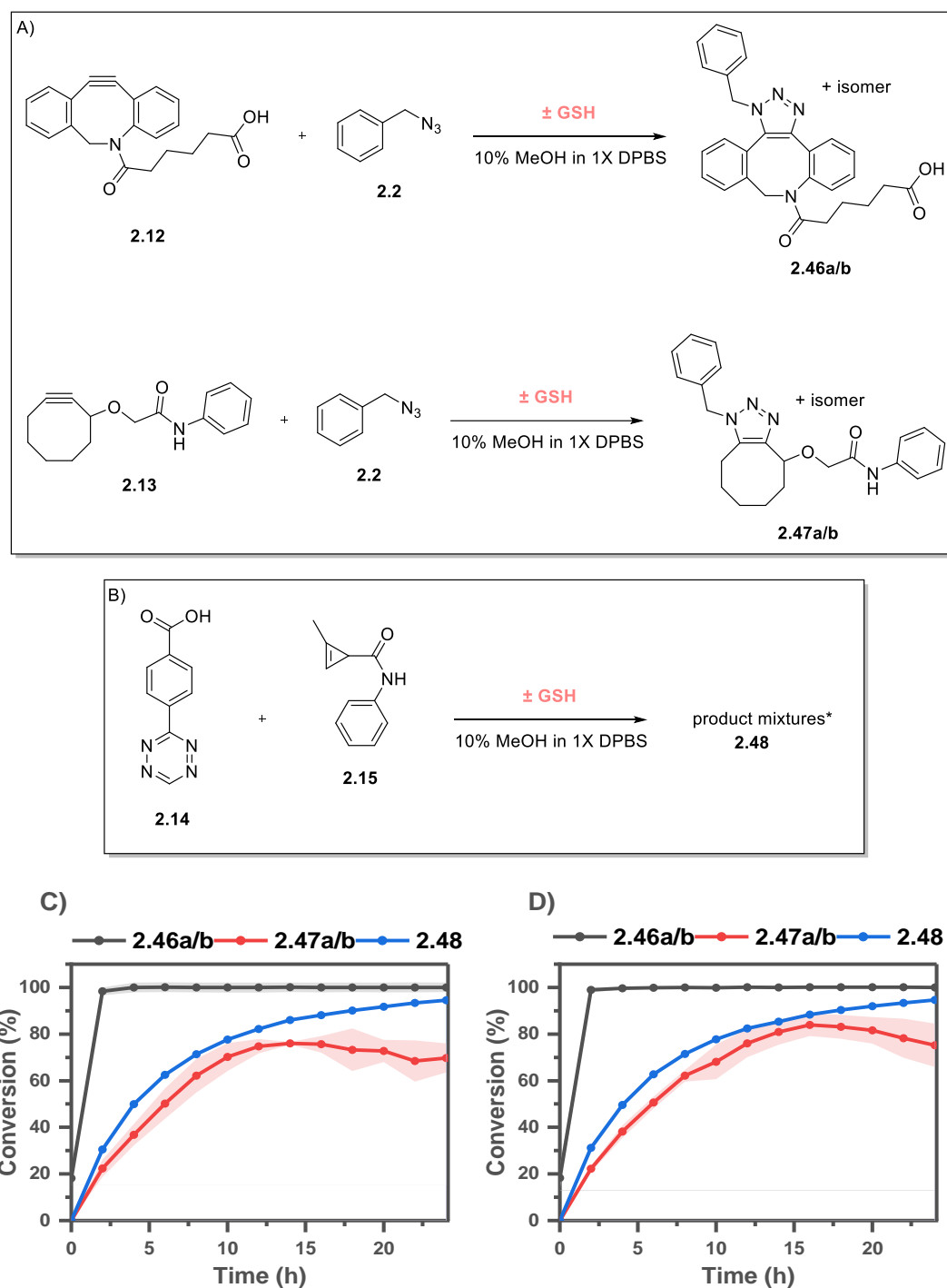


Figure 2.17. (A) Scheme for reaction of **2.12** and **2.13** with benzyl azide (**2.2**) in the presence and absence of GSH (1 mM). (B) Scheme for reaction of **2.15** with tetrazine (**2.14**) in the presence and absence of GSH (1 mM). (C) Reaction profiles for reactions A – B in the absence of GSH. *Conditions:* **2.12** or **2.13** (200 μ M), **2.2** (500 μ M), GSH (\pm 1 mM), 10% MeOH in 1X DPBS, rt, 24 h. (D) Reaction profiles for reactions A – B in the presence of GSH (1 mM). *Conditions:* **2.15** (200 μ M), **2.14** (500 μ M), GSH (\pm 1 mM), 10% MeOH in 1X DPBS, rt, 24 h. *Conversion of **2.15** to **2.48** calculated based on consumption of starting material, as multiple IEDDA products were formed. Buffer pH = 7.4. Shaded areas represent the standard deviation calculated from three experiments.

These experiments highlight the significant differences in reactivities among copper-free click reagents. For the SPAAC reaction, DBCO **2.12** outclasses cyclooctyne **2.12** in terms of reaction rate. Driven by commercial availability and superior reactivity, DBCO has become the reagent of choice for SPAAC reactions.^{200,218} Similar observations apply to cyclopropene **2.15**. Full conversion was not reached in 24 h, whereas reactions with other IEDDA reagents (*i.e.*, TCO or BCN) with tetrazines are known to reach full conversion within minutes.^{126,219}

2.5 Summary of Chapter 2

An HPLC assay was developed to investigate the influence of biologically relevant GSH concentrations of common bio-orthogonal reagents, with particular focus on exploring the reactivity of ynamine **2.1**. All reagents displayed good stability (> 75%) after 24 h in the presence of the highest physiologically relevant GSH concentration (10 mM). The susceptibility of **2.1** to form GSH adducts was influenced by the type of buffer and the presence of a Cu(II) source. It is proposed that the Z-alkene GSH adduct (**2.30**) could be formed by a radical-mediated reaction whereas the geminal isomer (**2.31**) could be formed through a nucleophilic addition. However, further experiments will be carried out in the future to confirm this hypothesis.

Whilst high concentrations of GSH (> 1 mM) inhibited the CuAAC reaction of ynamine **2.1** with benzyl azide (**2.2**), full conversion was achieved in under 4 h at a GSH concentration of 1 mM. When the CuAAC reactivity of other alkynes (**2.9** – **2.11**) with several azides (**2.2**, **2.40** and **2.41**) was compared under the same conditions, it revealed ynamine reactivity was superior under all circumstances.

Unlike CuAAC reagents, the reactivity of SPAAC or IEDDA was unaffected by the presence of GSH, which highlights their advantage for *in vivo* bioconjugation. However, the solubilities of copper-free click reagents in aqueous media can be poor, which hampers biological applications. Furthermore, both SPAAC and IEDDA produce ranges of products and not a single isomer as the CuAAC reaction. SPAAC reagents also tend to be bulky, expensive, and difficult to synthesise. The ynamine was shown to be more reactive than conventional alkynes in the presence of GSH and on par with copper-free reagents.

2.6 Experimental

2.6.1 General Experimental Techniques and Procedures

2.6.1.1 Reagents and Solvents

All reagents and solvents were used as supplied from commercial sources without further purification unless otherwise stated. Thin layer chromatography (TLC) was carried out using Merck silica plates coated with fluorescent indicator UV254. TLC plates were analysed under 254 nm UV light or developed using potassium permanganate solution.

2.6.1.2 Column Chromatography

Normal-phase flash chromatography was carried out using ZEOprep 60 HYD 40-63 μm silica gel.

2.6.1.3 NMR Spectroscopy

NMR spectroscopy was carried out using either a Bruker 400 UltraShield™ B-ACS 60 spectrometer, Bruker AV500 spectrometer at 500 MHz (^1H) and 126 Hz (^{13}C) or Bruker AV600 spectrometer at 156 Hz (^{13}C). All chemical shifts (δ) in CDCl_3 were referenced at 7.26 (^1H) and 77.06 ppm (^{13}C), in $\text{DMSO}-d_6$ at 2.50 (^1H) and 39.52 (^{13}C), in D_2O at 4.79 ppm (^1H) and in CD_3OD at 3.31 (^1H) and 49.0 ppm (^{13}C) and reported in parts per million (ppm). Coupling constants are quoted in hertz (Hz). Abbreviations for splitting patterns are s (singlet), br. s (broad singlet), d (doublet), dd (doublet of doublets), ddd (doublet of doublets of doublets), t (triplet), td (triplet of doublets), app. t (apparent triplet), q (quartet) and m (multiplet). All NMR data were processed using Mestrenova 11.0 software. Proton and carbon chemical shifts were assigned using proton (^1H), carbon (^{13}C), Heteronuclear Single Quantum Coherence (HSQC), Heteronuclear Multiple-Bond Correlation Spectroscopy (HMBC), Correlation Spectroscopy (COSY) and Nuclear Overhauser Effect Spectroscopy (NOESY) whenever possible (see Appendix for assigned protons/carbons).

2.6.1.4 High Resolution Mass Spectrometry

High-resolution mass spectra were recorded on an LTQ Orbitrap XL 1 mass spectrometer at the EPSRC UK National Mass Spectrometry Facility (Swansea), a Thermo Exactive Orbitrap mass spectrometer at the University of St Andrews and a Bruker Micro TOF II at the university of Edinburgh.

2.6.1.5 IR Spectroscopy

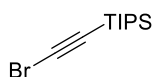
IR data were collected on either an Agilent or Shimadzu FTIR spectrometer and the data processed using the proprietary software. Only major absorbances were reported.

2.6.2 Liquid Chromatography-Mass Spectrometry (LC-MS) and Ultra-Performance-Mass-Spectrometry (UPLC-MS)

LC-MS was carried out on an Agilent HPLC instrument in conjunction with an Agilent Quadrupole mass detector on an Agilent Poroshell 120 C18 column (75 mm × 4.6 mm, 2.7 μm). UPLC-MS was carried out on an AVANT UPLC with an Advion Expression CMS L attached for mass detection on a Phenomenex Kinetex C18 column (30 mm × 2.1 mm, 2.7 μm). Electrospray ionization (ESI) was used in all cases.

2.6.3 Synthetic Procedures

(bromoethynyl)triisopropylsilane (**2.6**)¹⁹⁶



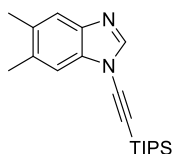
A mixture of *N*-bromosuccinimide (7.52 g, 42.2 mmol), TIPS acetylene (7.7 g, 41.6 mmol) and silver nitrate (650 mg, 3.82 mmol) in acetone (37 ml) was covered in foil and stirred overnight at room temperature. The reaction mixture was filtered through a celite pad and concentrated under vacuum to give a yellow oil. The residue was dissolved in petroleum ether and filtered through silica and eluted with petroleum ether. The solvents were removed under vacuum and the desired product was obtained as a clear liquid (10.49 g, 96%).

¹H NMR (500 MHz, CDCl₃) δ 1.11 – 1.06 (m, 21H).

¹³C NMR (126 MHz, CDCl₃) δ 83.5, 61.8, 18.5, 11.4.

NMR spectra in accordance with literature values.²²⁰

5,6-dimethyl-1-((triisopropylsilyl)ethynyl)-1H-benzo[d]imidazole (**2.8**)¹⁹⁷



5,6-Dimethyl-1H-benzo[d]imidazole (100 mg, 0.68 mmol), caesium carbonate (266 mg, 0.82 mmol), copper iodide (6.5 mg, 3.4 μmol) and PEG 400 (27 mg, 6.8 μmol) were dissolved in dry dioxane (2.2 mL). The mixture was degassed under vacuum three times (20 min, 10 min, 5 min) and (bromoethynyl)triisopropylsilane (195 mg, 0.75 mmol) was added. The reaction

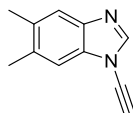
mixture was heated to reflux (110 °C) for 40 h under an argon atmosphere. The reaction was allowed to reach room temperature and the diluted with diethyl ether (20 mL). The mixture was washed with sat. EDTA solution (pH 3, 20 mL) and brine (20 mL) and then dried over Na₂SO₄. The organic phase was concentrated under vacuum and purified by flash column chromatography (0 – 10% ethyl acetate in petroleum ether) to give the desired compound as a colourless oil (176 mg, 80%).

¹H NMR (500 MHz, CDCl₃) δ 7.97 (s, 1H), 7.55 (s, 1H), 7.29 (s, 1H), 2.41 (s, 3H), 2.38 (s, 3H), 1.19 – 1.14 (m, 21H).

¹³C NMR (126 MHz, CDCl₃) δ 143.0, 140.3, 134.2, 133.0, 133.0, 120.8, 111.2, 90.6, 72.4, 20.6, 20.3, 18.7, 11.3.

NMR spectra in accordance with literature values.¹⁵³

*1-ethynyl-5,6-dimethyl-1H-benzo[d]imidazole (2.1)*¹⁹⁷



5,6-Dimethyl-1-((triisopropylsilyl)ethynyl)-1H-benzo[d]imidazole (4.0 g, 12.5 mmol) was dissolved in acetonitrile (62 mL), fluoride on polymer (415 mg, 12.5 mmol) was added and the reaction was stirred at room temperature overnight. Then the reaction mixture was filtered, and the filtrate was concentrated under vacuum. The residue was purified by flash column chromatography (0 – 20% ethyl acetate in petroleum ether) and the desired product was obtained as a white solid (1.99 g, 94%).

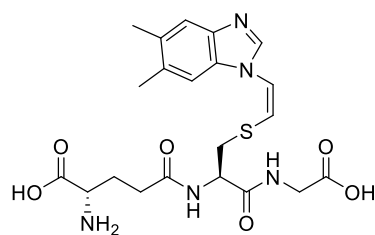
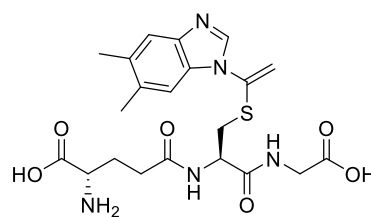
¹H NMR (500 MHz, CDCl₃) δ 7.98 (s, 1H), 7.56 (s, 1H), 7.35 (s, 1H), 3.26 (s, 1H), 2.41 (s, 3H), 2.38 (s, 3H).

¹³C NMR (126 MHz, CDCl₃) δ 144.0, 143.6, 143.1, 128.2, 114.4, 111.3, 105.7, 90.6, 72.4, 18.7, 11.3.

IR (ν_{max}): 3195 (sp C-H), 3107 (ar. C-H), 2148 (C≡C), 1492 (ar. C=C), 1460 (ar. C=C) cm⁻¹.

NMR spectra in accordance with literature values.¹⁹⁷

N5-((R)-1-((carboxymethyl)amino)-3-(((Z)-2-(5,6-dimethyl-1H-benzo[d]imidazol-1-yl)vinyl)thio)-1-oxopropan-2-yl)-L-glutamine (2.30) and N5-((R)-1-((carboxymethyl)amino)-3-((1-(5,6-dimethyl-1H-benzo[d]imidazol-1-yl)vinyl)thio)-1-oxopropan-2-yl)-L-glutamine (2.31)

**2.30****2.31**

1-Ethynyl-5,6-dimethyl-1H-benzodimidazole (20 mg, 0.12 mmol) and glutathione (370 mg, 1.2 mmol) were dissolved in a mixture of acetonitrile and 0.2 M sodium phosphate buffer. The reaction was stirred at room temperature for 2 weeks. Then water and diethyl ether were added, and phases separated. The aqueous layer was washed again with diethyl ether, then water was evaporated under vacuum, and the residue purified by semi-preparative HPLC to yield **2.30** (6 mg, 10%) and **2.31** (1 mg, 2%) as a white solid.

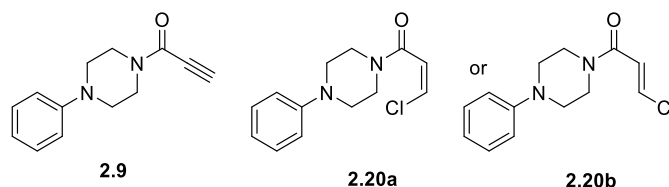
Compound **2.30**: $^1\text{H NMR}$ (500 MHz, D_2O) δ 9.24 (s, 1H), 7.63 (s, 1H), 7.52 (s, 1H), 7.19 (d, $J = 7.6$ Hz, 1H), 6.98 (d, $J = 7.6$ Hz, 1H), 4.66 (dd, $J = 8.3, 5.5$ Hz, 1H), 3.94 (s, 2H), 3.79 (t, $J = 6.5$ Hz, 1H), 3.43 (dd, $J = 14.5, 5.5$ Hz, 1H), 3.23 (dd, $J = 14.5, 8.3$ Hz, 1H), 2.47 – 2.41 (m, 8H), 2.03 (dd, $J = 14.3, 7.3$ Hz, 2H).

$^{13}\text{C NMR}$ (151 MHz, D_2O) δ 174.4, 173.1, 171.7, 138.0, 137.7, 129.0, 118.1, 114.2, 113.0, 112.4, 53.5, 41.4, 35.3, 31.3, 25.9, 19.7, 19.5. (2 quat. C not observed).

HR-MS (ESI): $\text{C}_{21}\text{H}_{26}\text{N}_5\text{O}_6\text{S}$ (M-H) $^-$ calculated 476.1609, found 476.1611.

Compound **2.31**: $^1\text{H NMR}$ (500 MHz, D_2O) δ 9.39 (s, 1H), 7.85 (s, 1H), 7.70 (s, 1H), 6.14 (d, $J = 2.4$ Hz, 1H), 6.07 (d, $J = 2.4$ Hz, 1H), 4.61 – 4.54 (m, 1H), 3.92 (s, 2H), 3.83 (d, $J = 6.5$ Hz, 1H), 3.16 (dd, $J = 14.7, 5.5$ Hz, 1H), 2.99 (dd, $J = 14.7, 8.1$ Hz, 1H), 2.53 – 2.44 (m, 9H), 2.22 – 2.08 (m, 2H).

1-(4-phenylpiperazin-1-yl)prop-2-yn-1-one (**2.9**)



Propiolic acid (500 mg, 7.14 mmol) was dissolved in MTBE (10 mL) under an argon atmosphere and oxalyl chloride (1.09 g, 8.57 mmol) was added dropwise followed by 2 drops of DMF. The reaction was left stirring for 1.5 hours and then added dropwise to a mixture of 1-phenylpiperazine (1.39 g, 8.57 mmol) and DIPEA (4.61 g, 35.7 mmol) in MTBE (5 mL).

The reaction was stirred for 1.5 hours and then quenched with sat. NaHCO_3 (30 mL). The phases were separated, and the aqueous phase was extracted with ethyl acetate (20 mL), the organic phases combined and washed with water (2×30 mL) and brine (30 mL) and then dried over Na_2SO_4 . The solvents were removed under vacuum and the residue purified by column chromatography (25 – 30% ethyl acetate in petroleum ether) to give the desired product as a brown solid (271 mg, 18%).

^1H NMR (500 MHz, CDCl_3) δ 7.29 (dd, $J = 8.7, 7.2$ Hz, 2H), 6.97 – 6.89 (m, 3H), 3.93 (app. t, $J = 5.0$ Hz, 2H), 3.81 (app. t, $J = 5.0$ Hz, 2H), 3.22 (app. t, $J = 5.2$ Hz, 2H), 3.17 (app. t, $J = 5.2$ Hz, 2H), 3.15 (s, 1H).

^{13}C NMR (126 MHz, CDCl_3) δ 151.8, 150.8, 129.3, 120.9, 117.0, 79.5, 75.3, 50.0, 49.3, 46.9, 41.4.

IR (ν_{max}): 3205 (ar C-H), 2917 (C-H), 2103 ($\text{C}\equiv\text{C}$), 1622 ($\text{C}=\text{O}$) cm^{-1} .

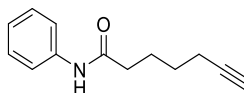
HR-MS (ESI): $\text{C}_{13}\text{H}_{14}\text{N}_2\text{OH}^+$ calculated 215.1179, found 215.1179.

Side product (**2.20a** or **2.20b**):

^1H NMR (500 MHz, CDCl_3) δ 7.32 (d, $J = 12.9$ Hz, 1H), 7.31 – 7.27 (m, 2H), 6.96 – 6.89 (m, 3H), 6.73 (d, $J = 12.9$ Hz, 1H), 3.83 (s, 2H), 3.69 (s, 2H), 3.20 (t, $J = 5.1$ Hz, 4H).

^{13}C NMR (126 MHz, CDCl_3) δ 162.7, 150.7, 135.6, 129.3, 123.4, 120.8, 116.8, 49.9, 49.4, 45.8, 41.9.

N-phenylhept-6-ynamide (**2.10**)²²¹



Hept-6-ynoic acid (200 mg, 1.58 mmol), aniline (162 mg, 1.74 mmol) and 4-dimethylaminopyridine (20 mg, 0.16 mmol) were dissolved in dichloromethane (10 mL). DCC (326 mg, 1.58 mmol) was dissolved in dichloromethane (10 mL) and slowly added to the stirred solution. After 4 h the suspension was cooled in an ice bath and filtered. The filtrate was collected and washed with 5 % wt HCl (2×20 mL), saturated NaHCO_3 (20 mL) and brine (20 mL), then dried over anhydrous Na_2SO_4 . The solvent was removed under vacuum and the residue purified by column chromatography (0 – 20% ethyl acetate in petroleum ether) to give the desired compound as a white solid (292 mg, 92%).

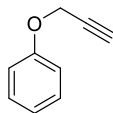
^1H NMR (500 MHz, CDCl_3) δ 7.51 (d, $J = 7.9$ Hz, 2H), 7.36 – 7.27 (m, 3H), 7.10 (t, $J = 7.4$ Hz, 1H), 2.39 (t, $J = 7.5$ Hz, 2H), 2.28 – 2.20 (m, 2H), 1.97 (t, $J = 2.6$ Hz, 1H), 1.91 – 1.80 (m, 2H), 1.67 – 1.57 (m, 2H).

^{13}C NMR (126 MHz, CDCl_3) δ 170.9, 137.9, 129.0, 124.3, 119.8, 84.0, 68.7, 37.1, 27.8, 24.6, 18.2.

IR (ν_{max}): 3271 (sp C-H), 2951 (C-H), 2163 ($\text{C}\equiv\text{C}$), 1657 ($\text{C}=\text{O}$) cm^{-1} .

NMR spectra in accordance with literature values.²²²

(*prop-2-yn-1-yloxy*)benzene (**2.11**)²²³



Phenol (500 mg, 5.31 mmol), propargyl bromide (790 mg, 5.31 mmol) and potassium carbonate (734 mg, 5.31 mmol) were dissolved in acetone and stirred overnight under reflux. The solution was filtered, and the solvent evaporated under vacuum. A ^1H -NMR spectrum of crude product still showed phenol, so the crude product was dissolved in diethyl ether and washed with 5% wt NaOH (20 mL), brine (20 mL) and then dried over anhydrous Na_2SO_4 . The solvent was evaporated under vacuum, and the desired compound was obtained as a yellow liquid without the need for further purification (426 mg, 61%).

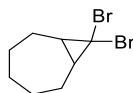
^1H NMR (500 MHz, CDCl_3) δ 7.35 – 7.27 (m, 2H), 7.04 – 6.95 (m, 3H), 4.70 (d, J = 2.4 Hz, 2H), 2.52 (t, J = 2.4 Hz, 1H).

^{13}C NMR (126 MHz, CDCl_3) δ 157.6, 129.5, 121.6, 114.9, 78.6, 75.4, 55.8.

IR (ν_{max}): 3291 (sp C-H), 2080 ($\text{C}\equiv\text{C}$), 1600 ($\text{C}=\text{C}$) cm^{-1} .

NMR spectra in accordance with literature values.²²⁴

8,8-dibromobicyclo[5.1.0]octane (**2.22**)²⁰²



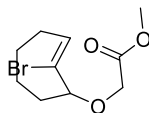
Cycloheptane (3 g, 31 mmol) and potassium tert-butoxide (8.7 g, 77.5 mmol) were dissolved in petroleum ether 40 – 60 °C (10 mL). The resulting suspension was cooled to –10 °C and bromoform (11.8 g, 46.5 mmol) in petroleum ether 40 – 60 °C (5 mL) was added dropwise over 1 hour. Upon completion of the addition, the temperature was slowly raised to 20 °C and the reaction was left to stir for 2 days. The organic phase was washed with aq. 5 % HCl (2 × 50 mL), then brine (50 mL) and dried over anhydrous Na_2SO_4 . The solvent was removed under vacuum and the residue purified by column chromatography (100% petroleum ether) to afford the desired compound as a colourless oil (2.28 g, 28%).

^1H NMR (500 MHz, CDCl_3) δ 2.30 – 2.21 (m, 2H), 1.95 – 1.84 (m, 1H), 1.87 – 1.77 (m, 2H), 1.76 – 1.65 (m, 2H), 1.45 – 1.30 (m, 2H), 1.26 – 1.10 (m, 3H).

^{13}C NMR (126 MHz, CDCl_3) δ 40.7, 34.7, 32.3, 28.9, 28.0.

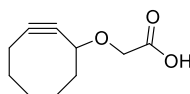
NMR spectra in accordance with literature values.²⁰²

*methyl 2-((2-bromocyclohept-2-en-1-yl)oxy)acetate (2.23)*²⁰²



8,8-dibromobicyclo[5.1.0]octane (2.28 g, 8.5 mmol) was dissolved in DCM (20 mL). Methyl glycolate (6.89 g, 76.5 mmol) was added and the reaction flask was covered in tin foil. Then silver perchlorate (3.52 g, 17 mmol) was added in one portion and the reaction was stirred for 3 hours. The reaction was quenched with saturated sodium hydrogen carbonate solution (50 mL) and brine (50 mL). The precipitated solid was filtered off and washed with MTBE (then discarded). The combined filtrate was separated, and the organic phase was washed with water (2×50 mL) and then dried over anhydrous Na_2SO_4 . The solvents were removed under vacuum to give crude product as a brown oil (2.15g, 96% mass recovery) and was used directly in the next step.

*2-(cyclooct-2-yn-1-yloxy)acetic acid (2.24)*²⁰²

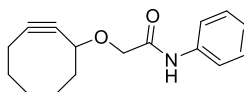


Crude methyl 2-((2-bromocyclohept-2-en-1-yl)oxy)acetate (8.5 mmol, assumed) was dissolved in DMSO (12 mL) and sodium methoxide (30 % in methanol, 10.4 g, 57.8 mmol) was added. The suspension was stirred overnight, then water (50 mL) and DCM (50 mL) were added. The phases were separated, and the aqueous layer was washed with DCM (2×50 mL). The aqueous layer was acidified and then extracted with MTBE (2×50 mL). The organic phases were combined and washed with water (2×50 mL), brine (50 mL) and then dried over anhydrous Na_2SO_4 . The solvents were removed under vacuum to obtain the crude product as a beige solid (786 mg, 50%).

^1H NMR (500 MHz, CDCl_3) δ 4.42 – 4.35 (m, 1H), 4.24 (d, $J = 16.7$ Hz, 1H), 4.09 (d, $J = 16.7$ Hz, 1H), 2.32 – 2.23 (m, 1H), 2.22 – 2.11 (m, 2H), 2.09 – 2.00 (m, 1H), 1.98 – 1.75 (m, 3H), 1.70 – 1.62 (m, 2H), 1.55 – 1.41 (m, 1H). NMR sample was left in deuterated chloroform for several hours before measuring, therefore the COOH proton is not observed due to deuterium exchange.

^{13}C NMR (126 MHz, CDCl_3) δ 172.9, 102.3, 90.8, 73.2, 65.7, 42.2, 34.2, 29.6, 26.2, 20.7.

NMR spectra in accordance with literature values.²⁰²

2-(cyclooct-2-yn-1-yloxy)-N-phenylacetamide (2.13)

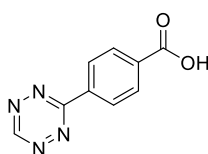
Crude 2-(cyclooct-2-yn-1-yloxy)acetic acid (500 mg, 2.74 mmol), DMAP (67 mg, 0.5 mmol) and EDC.HCl (579 mg, 3 mmol) were dissolved in DCM (2 mL) and cooled to 0 °C. Then aniline (383 mg, 4.1 mmol) was added dropwise, and the reaction stirred overnight. Ethyl acetate (20 mL) and saturated sodium hydrogen carbonate (20 mL) were added. The phases were separated, and the organic phase washed with brine (20 mL) and the dried over Na₂SO₄. The solvents were removed under vacuum to obtain crude product as a yellow solid which was purified by column chromatography (10 – 20% ethyl acetate in petroleum ether) to obtain the product as a yellow solid (365 mg, 52%).

¹H NMR (500 MHz, CDCl₃) δ 8.23 (br. s, 1H), 7.59 – 7.53 (m, 2H), 7.37 – 7.27 (m, 2H), 7.12 (tt, *J* = 7.5, 1.2 Hz, 1H), 4.36 – 4.27 (m, 1H), 4.16 (d, *J* = 15.2 Hz, 1H), 4.01 (d, *J* = 15.2 Hz, 1H), 2.34 – 2.22 (m, 1H), 2.26 – 2.13 (m, 2H), 2.14 – 2.01 (m, 1H), 2.02 – 1.89 (m, 1H), 1.94 – 1.78 (m, 2H), 1.78 – 1.58 (m, 2H), 1.59 – 1.45 (m, 1H).

¹³C NMR (126 MHz, CDCl₃) δ 167.7, 137.3, 129.1, 124.6, 120.0, 102.3, 91.0, 73.6, 68.6, 42.4, 34.4, 29.7, 26.4, 20.8.

IR (ν_{\max}): 3376 (N-H), 3057 (ar. C-H), 2933 (C-H), 2208 (very weak, C≡C), 1695 (C=O) cm⁻¹.

HR-MS (ESI): C₁₆H₁₉NO₂H⁺ calculated 258.1489, found 258.1487.

*4-(1,2,4,5-tetrazin-3-yl)benzoic acid (2.14)*²⁰³

4-cyanobenzoic acid (294 mg, 2 mmol), DCM (340 mg, 4 mmol) and sulfur (128 mg, 4 mmol) were suspended in ethanol (2 mL). Hydrazine hydrate (64% solution, 512.8 mg, 16 mmol) was added slowly and the reaction heated to 50 °C for 24 hours. Then DCM and sodium nitrite (1.4 g) in water (20 mL) were added, followed by the slow and careful addition of acetic acid (7.5 ml). After the completion of the addition, ethyl acetate (40 mL) and water (40 mL) were added, the layers separated, and the aqueous phase extracted with ethyl acetate (4 × 20 mL) until colourless. The organic phases were combined and washed with brine (40 mL), then dried over anhydrous Na₂SO₄. The solvents were removed under vacuum and the resulting pink solid

purified by column chromatography (5 – 10% methanol in DCM) to give the desired compound as a pink solid (30 mg, 7%).

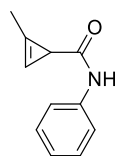
¹H NMR (500 MHz, DMSO) δ 13.36 (br. s, 1H), 10.66 (s, 1H), 8.65 – 8.59 (m, 2H), 8.25 – 8.19 (m, 2H).

¹³C NMR (101 MHz, DMSO) δ 166.7, 165.1, 158.2, 135.7, 134.4, 130.2, 128.0.

IR (ν_{\max}): 2816 (very broad, COOH), 1676 (C=O) cm^{-1} .

NMR spectra in accordance with literature values.²⁰³

2-methyl-N-phenylcycloprop-2-ene-1-carboxamide (2.15)



trimethyl(prop-1-yn-1-yl)silane (673 mg, 6 mmol) and $\text{Rh}(\text{OAc})_2$ (88 mg, 0.2 mmol) were dissolved in DCM (10 mL) and ethyl diazoacetate (13% in DCM, 250 mg, 2 mmol) was added slowly over 1 hour. After the addition, the reaction was stirred for an additional hour, then filtered through Celite® (eluted with DCM) and the solvent was removed under vacuum to give a brown oil. The residue was then passed through a silica column (5% ethyl acetate in petroleum ether) to give impure a mixture of products. This mixture was then dissolved in methanol (10 mL), 10% KOH (10 mL) was added and the reaction stirred overnight. Then water (20 mL) was added, and the aqueous layer was washed once with ethyl acetate (30 mL, discarded) and then acidified with 5% HCl, followed by extraction with ethyl acetate (2 \times 50 mL). The organic layers were combined, washed with brine (40 mL) and then dried over anhydrous Na_2SO_4 . The solvents were removed under vacuum and the residue was dissolved in MTBE (10 mL) and put under an argon atmosphere. Oxalyl chloride (254 mg, 2 mmol) was added dropwise, followed by 3 drops of DMF. The mixture was stirred for 1 hour, then aniline (931 mg, 10 mmol) was added slowly. The reaction was stirred for another 1 hour, then MTBE (10 mL) was added, and the mixture washed with 5% HCl (3 \times 20 mL), saturated NaHCO_3 (20 mL), brine (20 mL) and then dried over anhydrous Na_2SO_4 . The solvents were removed under vacuum and the residue was purified by column chromatography (20 – 40% ethyl acetate in petroleum ether) to give the desired product as a beige solid (110 mg, 32%).

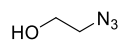
¹H NMR (500 MHz, CDCl_3) δ 7.52 (d, J = 8.0 Hz, 2H), 7.30 (app. t, J = 8.0 Hz, 2H), 7.20 (br. s, 1H), 7.07 (t, J = 7.4 Hz, 1H), 6.51 (s, 1H), 2.22 (s, 3H), 2.14 (s, 1H).

¹³C NMR (126 MHz, CDCl_3) δ 174.3, 138.2, 128.9, 123.8, 119.4, 114.1, 96.1, 23.6, 10.8.

IR (ν_{\max}): 3288 (N-H), 1650 (C=O), 1438 (C=C) cm^{-1} .

HR-MS (ESI): $C_{11}H_{11}NOH^+$ calculated 174.0913, found 174.0910.

2-azidoethan-1-ol (2.41)



Bromoethanol (6.2 g, 50 mmol) was dissolved in water (20 mL) and sodium azide (3.9 g, 60 mmol) was added. The reaction was heated to 50 °C for 21 hours and then cooled to rt. Sodium chloride was added to saturate the aqueous solution which was then extracted with diethyl ether (3 × 50 mL). The combined organic phases were washed with brine (50 mL) and the solvent was removed under a stream of air to give the desired compound as a colourless oil (3.1 g, 72%).

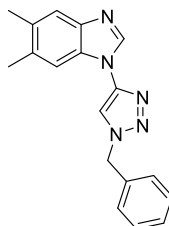
¹H NMR (500 MHz, $CDCl_3$) δ 3.82 – 3.75 (m, 2H), 3.45 (t, J = 5.0 Hz, 2H), 1.74 (t, J = 5.9 Hz, 1H).

¹³C NMR (126 MHz, $CDCl_3$) δ 61.6, 53.6.

IR (ν_{max}): 3361 (broad, O-H), 2097 (N_3) cm^{-1} .

NMR spectra in accordance with literature values.²²⁵

1-(1-benzyl-1H-1,2,3-triazol-4-yl)-5,6-dimethyl-1H-benzo[d]imidazole (2.3a)



1-ethynyl-5,6-dimethyl-1H-benzo[d]imidazole (200 mg, 1.17 mmol), $Cu(OAc)_2 \cdot H_2O$ (24 mg, 0.12 mmol) and benzyl azide (160 mg, 1.20 mmol) were dissolved in methanol (2 mL). The reaction was stirred at room temperature for 24 h, then ethyl acetate was added. The mixture was washed with sat. EDTA (pH 3, 2 × 30 mL), followed by brine (30 mL) and then dried over anhydrous Na_2SO_4 . The solvents were removed under vacuum and the residue was purified by column chromatography (80% ethyl acetate in petroleum ether) to give the desired compound as a light yellow solid (230 mg, 64%).

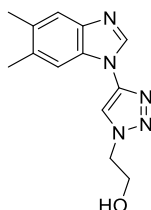
¹H NMR (500 MHz, DMSO) δ 8.80 (s, 1H), 8.52 (s, 1H), 7.66 (s, 1H), 7.53 (s, 1H), 7.45 – 7.40 (m, 4H), 7.40 – 7.34 (m, 1H), 5.73 (s, 2H), 2.36 (s, 3H), 2.33 (s, 3H).

¹³C NMR (126 MHz, DMSO) δ 142.1, 141.9, 141.1, 135.5, 132.7, 131.3, 130.7, 128.9, 128.3, 128.0, 119.9, 115.7, 111.7, 53.8, 20.1, 19.8.

IR (ν_{max}): 3090 (ar C-H), 2958 (C-H), 1584 (C=C), 1495 (C=C), 1459 (C=C) cm^{-1} .

HR-MS (ESI): $C_{18}H_{17}N_5H^+$ calculated 304.1557, found 304.1558.

2-(4-(5,6-dimethyl-1H-benzo[d]imidazol-1-yl)-1H-imidazol-1-yl)ethan-1-ol (2.3b)



1-ethynyl-5,6-dimethyl-1H-benzo[d]imidazole (20 mg, 0.12 mmol) was dissolved in MeOH (2 mL). Then $Cu(OAc)_2 \cdot H_2O$ (2 mg, 0.01 mmol) was added, followed by 2-azidoethan-1-ol (12 mg, 0.14 mmol) and the reaction was stirred at room temperature overnight. Sat. EDTA solution (pH 3, 20 mL) and ethyl acetate (20 mL) were added, and the phases were separated. The aqueous phase was extracted with ethyl acetate (20 mL) and then the combined organic layers were washed with brine (30 mL) and dried over anhydrous Na_2SO_4 . The solvents were removed under vacuum and the residue was purified by column chromatography (3 – 10% MeOH in DCM) to give the desired compound as a white solid (12 mg, 40%).

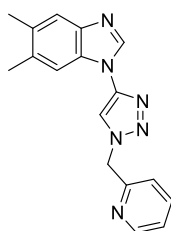
1H NMR (500 MHz, DMSO) δ 8.69 (s, 1H), 8.52 (s, 1H), 7.66 (s, 1H), 7.54 (s, 1H), 5.13 (t, J = 5.4 Hz, 1H), 4.52 (t, J = 5.4 Hz, 2H), 3.88 (q, J = 5.4 Hz, 2H), 2.37 (s, 3H), 2.35 (s, 3H).

^{13}C NMR (126 MHz, DMSO) δ 142.4, 142.1, 141.6, 133.1, 131.8, 131.2, 120.4, 116.6, 112.2, 60.2, 53.7, 20.6, 20.3.

IR (ν_{max}): 3218 (broad O-H), 3088 (ar. C-H), 2926 (C-H), 1600 (C=C) cm^{-1} .

HR-MS (ESI): $C_{13}H_{15}N_5OH^+$ calculated 258.1349, found 258.1340.

5,6-dimethyl-1-(1-(pyridin-2-ylmethyl)-1H-1,2,3-triazol-4-yl)-1H-benzo[d]imidazole (2.3c)



1-ethynyl-5,6-dimethyl-1H-benzo[d]imidazole (20 mg, 0.12 mmol) was dissolved in MeOH (2 mL). Then $Cu(OAc)_2 \cdot H_2O$ (2 mg, 0.01 mmol) was added, followed by picolyl azide (12 mg, 0.14 mmol) and the reaction was stirred at room temperature overnight. Sat. EDTA solution (pH 3, 20 mL) and ethyl acetate (10 mL) were added, and the phases were separated. The aqueous phase was extracted with ethyl acetate (20 mL) and then the combined organic layers were washed with brine (30 mL) and dried over anhydrous Na_2SO_4 . The solvent was

removed under vacuum and the residue was purified by column chromatography (5 - 10% MeOH in DCM) to give the desired product as a brown oil (26 mg, 73%).

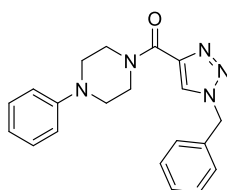
¹H NMR (500 MHz, DMSO) δ 8.84 (s, 1H), 8.70 (s, 1H), 8.61 – 8.55 (m, 1H), 7.88 (td, J = 7.7, 1.8 Hz, 1H), 7.70 (s, 1H), 7.56 (s, 1H), 7.44 (d, J = 7.6 Hz, 1H), 7.40 (ddd, J = 7.6, 4.8, 1.1 Hz, 1H), 5.85 (s, 2H), 2.37 (s, 3H), 2.35 (s, 3H).

¹³C NMR (126 MHz, DMSO) δ 154.4, 149.5, 141.8, 141.1, 140.6, 137.5, 133.1, 131.9, 130.5, 123.5, 122.4, 119.4, 116.7, 111.9, 55.2, 20.1, 19.8.

IR (ν_{\max}): 3107 (ar. C-H), 2923 (C-H), 1587 (C=C) cm^{-1} .

HR-MS (ESI): $\text{C}_{17}\text{H}_{16}\text{N}_6\text{H}^+$ calculated 305.1509, found 305.1508.

(1-benzyl-1H-1,2,3-triazol-4-yl)(4-phenylpiperazin-1-yl)methanone (**2.43a**)



1-(4-phenylpiperazin-1-yl)prop-2-yn-1-one (20 mg, 93 μmol), $\text{Cu}(\text{OAc})_2 \cdot \text{H}_2\text{O}$ (1.8 mg, 9 μmol) and benzyl azide (13.6 mg, 102 μmol) were dissolved in methanol (2 mL). The reaction was stirred at room temperature for 24 h, then ethyl acetate (20 mL) was added. The mixture was washed with sat. EDTA (pH 3, 2×20 mL) solution, followed by brine (20 mL) and then dried over anhydrous Na_2SO_4 . The solvent was removed under vacuum and the residue was purified by column chromatography (50% ethyl acetate in petroleum ether with 1% triethylamine) to give the desired compound as a beige solid (18 mg, 56%).

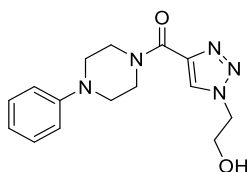
¹H NMR (500 MHz, CDCl_3) δ 8.03 (s, 1H), 7.41 – 7.33 (m, 3H), 7.32 – 7.23 (m, 4H), 6.97 (d, J = 8.0 Hz, 2H), 6.90 (t, J = 7.3 Hz, 1H), 5.53 (s, 2H), 4.49 (s, 2H), 3.95 – 3.89 (m, 2H), 3.29 – 3.22 (m, 4H).

¹³C NMR (126 MHz, CDCl_3) δ 159.7, 150.7, 144.6, 133.8, 129.3, 129.3, 129.1, 128.4, 128.4, 120.7, 116.8, 54.4, 50.2, 49.7, 46.4, 42.6.

IR (ν_{\max}): 3120 (ar C-H), 2802 (C-H), 1603 (C=C) cm^{-1} .

HR-MS (ESI): $\text{C}_{20}\text{H}_{21}\text{N}_5\text{OH}^+$ calculated 348.1819, found 348.1822.

(1-(2-hydroxyethyl)-1H-1,2,3-triazol-4-yl)(4-phenylpiperazin-1-yl)methanone (**2.43b**)



1-(4-phenylpiperazin-1-yl)prop-2-yn-1-one (40 mg, 0.19 mmol) and 2-azidoethanol (18 mg, 0.21 mmol) were dissolved in MeOH (2 mL). Then $\text{Cu}(\text{OAc})_2 \cdot \text{H}_2\text{O}$ (2 mg, 0.01 mmol) was added and AMTC (4.2 mg, 0.02 mmol) and NaAsc (3.7 mg, 0.02 mmol) were dissolved in the minimum amount of water and then added dropwise. The reaction was stirred at room temperature for 2 hours and then sat. EDTA solution (pH 3, 20 mL) and ethyl acetate (20 mL) were added, and the phases were separated. The aqueous phase was extracted with ethyl acetate (20 mL) and then the combined organic layers were washed with brine (30 mL) and dried over anhydrous Na_2SO_4 . The solvents were removed under vacuum and the residue was purified by column chromatography (60% ethanol/ethyl acetate (1:3) in petroleum ether) to give the desired compound as a brown solid (38 mg, 67%).

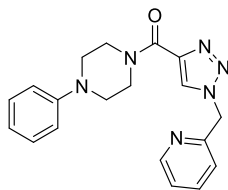
^1H NMR (500 MHz, CDCl_3) δ 8.27 (s, 1H), 7.32 – 7.25 (m, 2H), 6.95 (d, J = 8.2 Hz, 2H), 6.90 (t, J = 7.3 Hz, 1H), 4.53 (app. t, J = 4.9 Hz, 2H), 4.45 (app. t, J = 5.1 Hz, 2H), 4.06 (app. t, J = 5.1 Hz, 2H), 3.91 (app. t, J = 5.2 Hz, 2H), 3.27 (app. t, J = 5.1 Hz, 4H).

^{13}C NMR (126 MHz, CDCl_3) δ 160.0, 150.9, 143.8, 129.5, 129.3, 120.5, 116.6, 60.9, 52.8, 50.0, 49.4, 46.6, 42.7.

IR (ν_{max}): 3408 (broad, O-H), 3117 (ar. C-H), 2923 (C-H), 1619 (C=O) cm^{-1} .

HR-MS (ESI): $\text{C}_{15}\text{H}_{19}\text{N}_5\text{O}_2\text{H}^+$ calculated 302.1612, found 302.1606.

(4-phenylpiperazin-1-yl)(1-(pyridin-2-ylmethyl)-1H-1,2,3-triazol-4-yl)methanone (**2.43c**)



1-(4-phenylpiperazin-1-yl)prop-2-yn-1-one (40 mg, 0.19 mmol) was dissolved in MeOH (2 mL). Then $\text{Cu}(\text{OAc})_2 \cdot \text{H}_2\text{O}$ (4 mg, 0.02 mmol) was added, followed by picolyl azide (28 mg, 0.21 mmol) and the reaction was stirred at room temperature overnight. Sat. EDTA solution (pH 3, 20 mL) and ethyl acetate (20 mL) were added, and the phases were separated. The aqueous phase was extracted with ethyl acetate (20 mL) and then the combined organic layers were washed with brine (20 mL) and dried over anhydrous Na_2SO_4 . The solvent was removed under vacuum and the residue was purified by column chromatography (60% ethanol/ethyl acetate (1:3) in petroleum ether) to give the desired compound as a brown solid (9 mg, 13%).

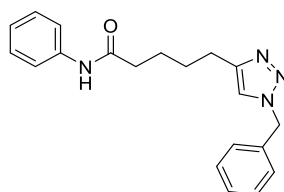
¹H NMR (500 MHz, CDCl₃) δ 8.63 – 8.58 (m, 1H), 8.26 (s, 1H), 7.70 (td, *J* = 7.7, 1.8 Hz, 1H), 7.32 – 7.21 (m, 4H), 6.96 (d, *J* = 8.1 Hz, 2H), 6.90 (t, *J* = 7.3 Hz, 1H), 5.68 (s, 2H), 4.48 (app. t, *J* = 5.0 Hz, 2H), 3.94 (app. t, *J* = 5.1 Hz, 2H), 3.27 (app. t, *J* = 5.3 Hz, 4H).

¹³C NMR (126 MHz, CDCl₃) δ 159.7, 153.6, 150.9, 150.0, 144.6, 137.4, 129.3, 129.0, 123.7, 122.6, 120.6, 116.7, 55.7, 50.2, 49.6, 46.5, 42.6.

IR (ν_{\max}): 3123 (ar. C-H), 2793 (C-H), 1609 (C=O) cm⁻¹.

HR-MS (ESI): C₁₉H₂₀N₆OH⁺ calculated 349.1771, found 349.1769.

5-(1-benzyl-1H-1,2,3-triazol-4-yl)-N-phenylpentanamide (2.44a)



N-phenylhept-6-ynamide (20 mg, 99 μmol), Cu(OAc)₂•H₂O (1 mg, 5 μmol), benzyl azide (15 mg, 110 μmol) and THPTA (5 mg, 10 μmol) were dissolved in methanol (2 mL). Sodium ascorbate (2 mg, 10 μmol) was dissolved in the minimum amount of water and the solution was added dropwise to the reaction which was stirred at room temperature for 24 h, then dichloromethane (20 mL) was added. The mixture was washed with sat. EDTA (pH 3, 2 × 20 mL) solution, followed by brine (20 mL) and then dried over anhydrous Na₂SO₄. The solvent was removed under vacuum and the residue was purified by column chromatography (80% ethyl acetate in petroleum ether) to give the desired compound as a white solid (31 mg, 94%).

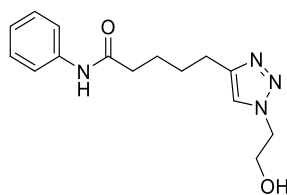
¹H NMR (500 MHz, CDCl₃) δ 7.84 (s, 1H), 7.58 (d, *J* = 8.0 Hz, 2H), 7.40 – 7.34 (m, 2H), 7.30 (t, *J* = 7.9 Hz, 2H), 7.29 – 7.23 (m, 4H), 7.08 (t, *J* = 7.4 Hz, 1H), 5.49 (s, 2H), 2.77 (app. t, *J* = 6.6 Hz, 2H), 2.41 (app. t, *J* = 6.9 Hz, 2H), 1.80 – 1.74 (m, 4H).

¹³C NMR (126 MHz, CDCl₃) δ 171.3, 147.7, 138.3, 134.4, 129.2, 129.0, 128.9, 128.2, 124.0, 121.3, 119.8, 54.5, 37.0, 28.4, 24.8, 24.7.

IR (ν_{\max}): 3297 (N-H), 3112 (ar. C-H), 3066 (C-H), 2936 (C-H), 1654 (C=C), 1603 (C=O) cm⁻¹.

HR-MS (ESI): C₂₀H₂₂N₄OH⁺ calculated 335.1866, found 335.1869.

5-(1-(2-hydroxyethyl)-1H-1,2,3-triazol-4-yl)-N-phenylpentanamide (2.44b)



N-phenylhept-6-ynamide (40 mg, 0.2 mmol) was dissolved in MeOH (2 mL). $\text{Cu}(\text{OAc})_2 \cdot \text{H}_2\text{O}$ (4 mg, 0.02 mmol) was added, followed by 2-azidoethan-1-ol (19 mg, 0.22 mmol) and sodium ascorbate (39 mg, 0.2 mmol), then the reaction was stirred at room temperature overnight. Sat. EDTA solution (pH 3, 20 mL) and ethyl acetate (20 mL) were added, and the phases were separated. The aqueous phase was extracted with ethyl acetate (2×20 mL) and then the combined organic layers were washed with brine and dried over anhydrous Na_2SO_4 . The solvent was removed under vacuum and the residue was purified by column chromatography (60% ethanol/ethyl acetate (1:3) in petroleum ether) to give the desired compound as a clear oil (24 mg, 42%).

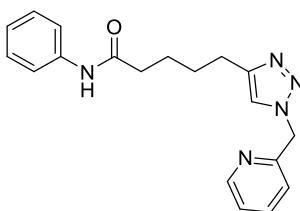
^1H NMR (500 MHz, DMSO) δ 9.85 (s, 1H), 7.80 (s, 1H), 7.58 (d, $J = 7.9$ Hz, 2H), 7.27 (app. t, $J = 7.7$ Hz, 2H), 7.01 (t, $J = 7.4$ Hz, 1H), 4.98 (br. s, 1H), 4.33 (app. t, $J = 5.5$ Hz, 2H), 3.75 (app. t, $J = 5.5$ Hz, 2H), 2.67 – 2.60 (m, 2H), 2.37 – 2.30 (m, 2H), 1.66 – 1.61 (m, 4H).

^{13}C NMR (126 MHz, DMSO) δ 171.6, 146.8, 139.8, 129.1, 123.4, 122.6, 119.5, 60.4, 52.4, 36.6, 29.1, 25.3, 25.2.

IR (ν_{max}): 3268 (N-H), 3063 (ar. C-H), 2933 (C-H), 1651 (C=O) cm^{-1} , O-H observed but not reported, overlaps with N-H.

HR-MS (ESI): $\text{C}_{15}\text{H}_{20}\text{N}_4\text{O}_2\text{H}^+$ calculated 289.1659, found 289.1651.

N-phenyl-5-(1-(pyridin-2-ylmethyl)-1H-1,2,3-triazol-4-yl)pentanamide (**2.44c**)



N-phenylhept-6-ynamide (40 mg, 0.2 mmol) was dissolved in MeOH (2 mL). $\text{Cu}(\text{OAc})_2 \cdot \text{H}_2\text{O}$ (4 mg, 0.02 mmol) was added, followed by picolyl azide (29 mg, 0.22 mmol) and sodium ascorbate (39 mg, 0.2 mmol), then reaction was stirred at room temperature overnight. Sat. EDTA solution (pH 3, 20 mL) and ethyl acetate (20 mL) were added, and the phases were separated. The aqueous phase was extracted with ethyl acetate (20 mL) and then the combined organic layers were washed with brine and dried over anhydrous Na_2SO_4 . The solvent was removed under vacuum and the residue was purified by column chromatography (70%

ethanol/ethyl acetate (1:3) in petroleum ether) to give the desired compound as a clear oil which crystallized upon cooling (39 mg, 67%).

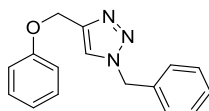
¹H NMR (500 MHz, DMSO) δ 9.85 (s, 1H), 8.56 – 8.51 (m, 1H), 7.92 (s, 1H), 7.80 (td, J = 7.7, 1.8 Hz, 1H), 7.57 (d, J = 7.7 Hz, 2H), 7.37 – 7.30 (m, 1H), 7.31 – 7.22 (m, 2H), 7.20 (d, J = 7.9 Hz, 1H), 7.01 (t, J = 7.4 Hz, 1H), 5.64 (s, 2H), 2.69 – 2.62 (m, 2H), 2.37 – 2.29 (m, 2H), 1.68 – 1.59 (m, 4H).

¹³C NMR (126 MHz, DMSO) δ 171.6, 155.8, 149.8, 147.3, 139.8, 137.8, 129.1, 123.6, 123.4, 123.1, 122.5, 119.5, 54.8, 36.6, 29.1, 25.3, 25.2.

IR (ν_{\max}): 3275 (N-H), 3136 (ar. C-H), 2955 (C-H), 1691 (C=O) cm^{-1} .

HR-MS (ESI): $\text{C}_{19}\text{H}_{21}\text{N}_5\text{OH}^+$ calculated 336.1819, found 336.1812.

1-benzyl-4-(phenoxymethyl)-1H-1,2,3-triazole (2.45a)



(prop-2-yn-1-yloxy)benzene (20 mg, 151 μmol), $\text{Cu}(\text{OAc})_2 \cdot \text{H}_2\text{O}$ (1.6 mg, 8 μmol), benzyl azide (22 mg, 166 μmol) and THPTA (8 mg, 15 μmol) were dissolved in methanol (2 mL). Sodium ascorbate (3 mg, 15 μmol) was dissolved in the minimum amount of water and added dropwise to the reaction which was stirred at room temperature for 24 h, then dichloromethane (20 mL) was added. The mixture was washed with sat. EDTA solution (pH 3, 2×20 mL), followed by brine (20 mL) and then dried over anhydrous Na_2SO_4 . The solvent was removed under vacuum and the residue purified by column chromatography (30% ethyl acetate in petroleum ether) to give the desired compound as a white solid (25 mg, 62%).

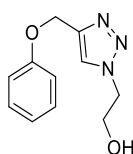
¹H NMR (500 MHz, CDCl_3) δ 7.53 (s, 1H), 7.42 – 7.32 (m, 3H), 7.32 – 7.24 (m, 4H), 7.00 – 6.93 (m, 3H), 5.53 (s, 2H), 5.19 (s, 2H).

¹³C NMR (126 MHz, CDCl_3) δ 158.2, 144.7, 134.4, 129.6, 129.2, 128.9, 128.2, 122.6, 121.3, 114.8, 62.1, 54.4.

IR (ν_{\max}): 3133 (ar. C-H), 2924 (C-H), 1600 (C=C), 1486 (CH_2) cm^{-1}

HR-MS (ESI): $\text{C}_{16}\text{H}_{15}\text{N}_3\text{OH}^+$ calculated 266.1288, found 266.1291.

2-(4-(phenoxymethyl)-1H-1,2,3-triazol-1-yl)ethan-1-ol (2.45b)



(prop-2-yn-1-yloxy)benzene (40 mg, 0.3 mmol) was dissolved in MeOH (2 mL). Cu(OAc)₂•H₂O (6 mg, 0.03 mmol) was added, followed by 2-azidoethan-1-ol (29 mg, 0.3 mmol) and sodium ascorbate (60 mg, 0.3 mmol), then reaction was stirred at room temperature overnight. Sat. EDTA solution (pH 3, 20 mL) and diethyl ether (20 mL) were added, and the phases were separated. The aqueous phase was extracted with diethyl ether (20 mL) and then the combined organic layers were washed with brine (30 mL) and dried over anhydrous Na₂SO₄. The solvents were removed under vacuum and the residue was purified by column chromatography (80% ethyl acetate in petroleum ether) to give the desired product as a clear oil (13 mg, 20%).

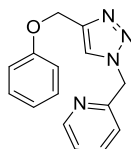
¹H NMR (500 MHz, CDCl₃) δ 7.73 (s, 1H), 7.32 – 7.26 (m, 2H), 7.00 – 6.96 (m, 3H), 5.19 (s, 2H), 4.48 (app. t, *J* = 5.0 Hz, 2H), 4.07 (app. t, *J* = 5.1 Hz, 2H), 2.23 (br. s, 1H).

¹³C NMR (126 MHz, CDCl₃) δ 158.2, 144.1, 129.6, 123.9, 121.3, 114.8, 61.9, 61.1, 52.7.

IR (ν_{max}): 3283 (O-H), 3146 (ar. C-H), 2974 (C-H), 1599 (C=C), 1495 (C=C), 1212 (C-O) cm⁻¹.

HR-MS (ESI): C₁₁H₁₃N₃O₂H⁺ calculated 220.1081, found 220.1076.

2-((4-(phenoxymethyl)-1H-1,2,3-triazol-1-yl)methyl)pyridine (2.45c)



(prop-2-yn-1-yloxy)benzene (40 mg, 0.3 mmol) was dissolved in MeOH (2 mL). Cu(OAc)₂•H₂O (6 mg, 0.03 mmol) was added, followed by picolyl azide (45 mg, 0.3 mmol) and sodium ascorbate (60 mg, 0.3 mmol), then reaction was stirred at room temperature overnight. Sat. EDTA solution (pH 3, 20 mL) and diethyl ether (20 mL) were added, and the phases were separated. The aqueous phase was extracted with diethyl ether (20 mL) and then the combined organic layers were washed with brine (30 mL) and dried over anhydrous Na₂SO₄. The solvents were removed under vacuum and the residue purified by column chromatography (70% ethyl acetate in petroleum ether) to give the desired compound as a clear oil (41 mg, 51%).

¹H NMR (500 MHz, CDCl₃) δ 8.62 – 8.57 (m, 1H), 7.79 (s, 1H), 7.69 (td, *J* = 7.7, 1.8 Hz, 1H), 7.31 – 7.26 (m, 3H), 7.20 (d, *J* = 7.8 Hz, 1H), 7.00 – 6.93 (m, 3H), 5.66 (s, 2H), 5.22 (s, 2H).

¹³C NMR (126 MHz, CDCl₃) δ 158.2, 154.3, 149.8, 144.7, 137.4, 129.5, 123.5, 123.3, 122.5, 121.3, 114.8, 62.1, 55.7.

IR (ν_{max}): 3132 (ar. C-H), 2926 (C-H), 1603 (C=C) cm^{-1}

HR-MS (ESI): $\text{C}_{15}\text{H}_{14}\text{N}_4\text{O}_1\text{H}^+$ calculated 267.1240, found 267.1253.

2.6.4 HPLC Assay

2.6.4.1 Procedure

Stock solutions of reagents were prepared each day. Reagents (~1 – 20 mg) were measured out on a microbalance.

Stock solutions:

[Alkyne] = 6 mM in organic solvent (*i.e.*, MeOH)

[Azide] = 30 mM in organic solvent (*i.e.*, MeOH)

[GSH] = 30 mM in 1X DPBS

[Cu(OAc)₂] = 10 mM in H₂O

[NaAsc] = 30 mM in 1X DPBS

Appropriate amounts of the stock solutions were added to reach specified concentrations to an HPLC vial and made up with MeOH and 1X DPBS buffer to a final volume of 1.5 mL. The addition order was as follows: MeOH, alkyne, benzyl azide, buffer, GSH, Cu(OAc)₂. The vials were then placed in the autosampler (not capable of temperature control) and sampled for the specified time.

2.6.4.2 Instrument, Method and Quantification

HPLC was carried out on a Shimadzu Prominence LC system.

Typical HPLC conditions are described below:

Column Specifications: Phenomenex Kinetex C18, 50 × 4.6 mm, 2.6 μm

Column Temperature: 40 °C

Mobile Phase A: 0.1 % v/v TFA in water

Mobile Phase B: 0.1 % v/v TFA in MeCN

Flow rate 1.5 mL/min

Injection Volume: 10 μL

Gradient Profile:

Time (min)	B%
0 – 5	5 – 60
5 – 5.1	60 – 95
5.1 – 7.2	95
7.2 – 7.3	95 – 5
7.3 – 9.5	5

UV detection signal was recorded at 254 nm. Conversions for the ynamine (**2.1**) and the corresponding triazole (**2.3**), were calculated using calibration curves (Figure 2.18).

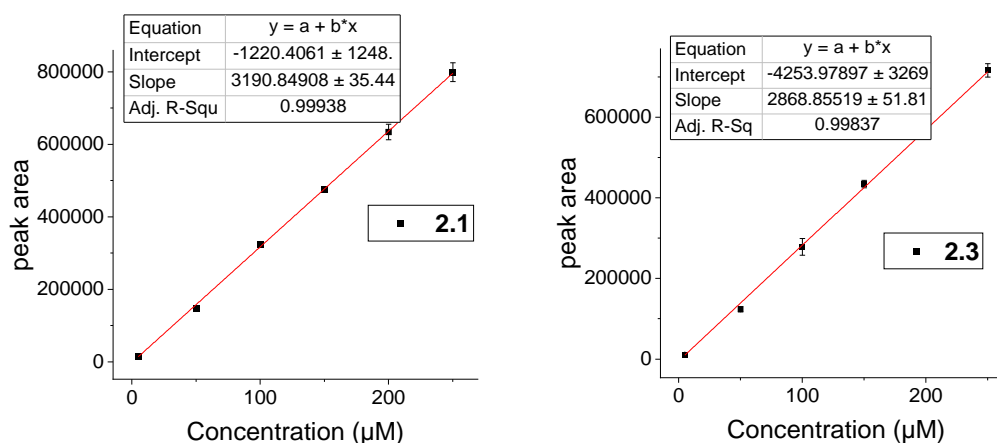


Figure 2.18. Each calibration curve was measured in triplicate. The averaged peak area for each concentration was used to construct the calibration curves. (A) Calibration curve for ynamine **2.1**. (B) Calibration curve for triazole **2.3**.

To determine the remaining percentage of reagents (**2.9** – **2.15**) in Figure 2.12 and Figure 2.13 the peak area at $t = 24$ h was divided by the peak area at $t = 0$ h.

To determine the conversion in Figure 2.16A and B, peak area of the product was divided by the peak area of the starting material and the product at each timepoint. For conversions in Figure 2.16C, the peak area of the product at each timepoint was divided by the average peak area after reaching full conversion (for **2.3c** average peak area of $t = 4 - 24$ h, for **2.43c** average peak area of $t = 6 - 24$ h, for **2.44c** average peak area of $t = 14 - 24$ h, for **2.45c** average peak area of $t = 10 - 24$ h).

To determine the conversion in Figure 2.17, the combined peak areas of the regio-isomer products (*i.e.*, **2.47a/b** or **2.48a/b**) were divided by the sum of the peak area of the starting material (*i.e.*, **2.12** or **2.13**) and products (*i.e.*, **2.47a/b** or **2.48a/b**). For **2.48**, the conversion was calculated by starting material (**2.15**) consumption.

Variability of Autosampler:

To analyse the variability of the autosampler injections, the data in Figure 2.16C was analysed. As all reactions reached full conversion any changes in peak area after reaching full conversion should only be caused by the inaccuracy of the HPLC system.

Therefore, the standard deviation of the obtained peak areas after reaching full conversion (**2.3c** = $4 - 24$ h, **2.43c** = $6 - 24$ h, **2.44c** = $16 - 24$ h, **2.45c** = $10 - 24$ h) was calculated for each individual experiment and then average for each set of triplicate experiments. This resulted in an average standard deviation of 1.5% (**2.3c**), 0.2% (**2.43c**), 1.3% (**2.44c**) and 0.7%

(**2.45c**), giving an overall standard deviation of 0.9%. This deviation is a good estimate of the accuracy of the autosampler.

2.6.4.3 Buffer Composition

Table 2.2. Buffer composition and salt concentration of 0.1 M phosphate buffer and 10X DPBS; 10X = 0.1 M. Salt concentration doubles for 0.2 M phosphate buffer and reduces 10-fold for 1X DPBS. The pH for each buffer was adjusted to 7.4.

0.1 M Phosphate Buffer	Salt Concentration (g/L)
NaH ₂ PO ₄	2.3
Na ₂ HPO ₄	11.5
10X DPBS	
Na ₂ HPO ₄	11.5
KH ₂ PO ₄	2.0
NaCl	80
KCl	2.0
MgCl ₂ ·6H ₂ O	1.0
CaCl ₂ ·2H ₂ O	1.3

2.6.4.4 Additional HPLC Data

Table 2.3. Reaction optimisation of ynamine **2.1** with benzyl azide **2.2**.

Entry	[GSH] (mM)	Copper source/[Cu] (μ M)	[2.2] (μ M)	Ligand (200 μ M)	Co- solvent (10% in 1X DPBS)	Conversion after 24 h (%)
1	6.5	Cu(CF ₃ SO ₃) ₂ /200	200		MeCN	Not detected
2	6.5	Cu(OAc) ₂ /200	200		MeCN	Not detected
3	6.5	Cu(OAc) ₂ /200	200	THPTA	MeCN	Not detected
4	6.5	Cu(OAc) ₂ /200	400		MeCN	<1
5	6.5	Cu(OAc) ₂ /400	200		MeCN	6
6	6.5	Cu(OAc) ₂ /400	400		MeCN	<1
7	1	CuI/200	200	THPTA	MeCN	41 (20h)
8	6.5	Cu(OAc) ₂ /200	200		MeOH	2
9	1	Cu(OAc) ₂ /200	200		MeOH	42 (8h)
10	2	Cu(OAc) ₂ /200	200		MeOH	6
11	1	Cu(OAc) ₂ /400	200		MeOH	49 (2h)
12	1	Cu(OAc) ₂ /200	400		MeOH	72 (8h)
13	1	Cu(OAc) ₂ /350	800		MeOH	99 (4h)

Conversion calculated by peak area; Single experiments; *Standard Conditions*: ynamine (**2.1**) (200 μ M), copper source (200 μ M), benzyl azide (**2.2**) (200 μ M), GSH (6.5 mM), 10% co-solvent in 1X DPBS, rt, 24 h.

Table 2.4. Reaction of alkynes **2.1**, **2.9** – **2.11** with benzyl azide **2.2** in the presence of GSH (no added NaAsc).

Entry	Alkyne (200 μ M)	Conversion (%)	Time (h)
1	2.1	89	4
2	2.9	4	24
3	2.10	0	24
4	2.11	65	4

Conversion calculated by peak area; Single experiments; *Conditions*: alkynes (**2.1**, **2.9** – **2.11**) (200 μ M), Cu(OAc)₂ (350 μ M), benzyl azide (**2.2**) (500 μ M), GSH (1 mM), 10% MeOH in 1X DPBS, rt, 24 h.

Table 2.5. Reaction of alkynes **2.1**, **2.9** – **2.11** with benzyl azide **2.1** without added GSH or NaAsc.

Entry	Alkyne (200 μ M)	Conversion after 24h (%)
1	2.1	63
2	2.9	5
3	2.10	0
4	2.11	0

Conversion calculated by peak area; Single experiments; *Conditions:* alkynes (**2.1**, **2.9** – **2.11**) (200 μ M), Cu(OAc)₂ (350 μ M), benzyl azide (**2.2**) (500 μ M), 10% MeOH in 1X DPBS, rt, 24 h.

Table 2.6. Reaction of alkynes **2.1**, **2.9** – **2.11** with benzyl azide **2.1** with added NaAsc (no GSH).

Entry	Alkyne (200 μ M)	Conversion (%)	Time (h)
1	2.1	97	8
2	2.9	100	4
3	2.10	100	8
4	2.11	100	4

Conversion calculated by peak area; Single experiments; *Conditions:* alkynes (**2.1**, **2.9** – **2.11**) (200 μ M), Cu(OAc)₂ (350 μ M), benzyl azide (**2.2**) (500 μ M), NaAsc (1 mM), 10% MeOH in 1X DPBS, rt, 24 h.

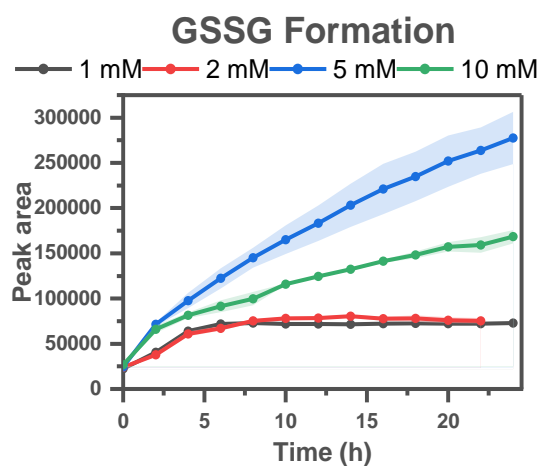


Figure 2.19. Formation of GSSG during the experiment testing the influence of Cu(OAc)₂ (350 μ M) addition on ynamine **2.1** reactivity with GSH (1, 2, 5 and 10 mM). *Conditions:* **2.1** (200 μ M), Cu(OAc)₂ (350 μ M), GSH (1, 2, 5 or 10 mM), 10% MeOH in 1X DPBS, rt, 24 h. Buffer pH = 7.4. Shaded areas represent the standard deviation calculated from three experiments.

Chapter 3

Influence of Glutathione on the Reactivity of the Ynamine-CuAAC Reaction

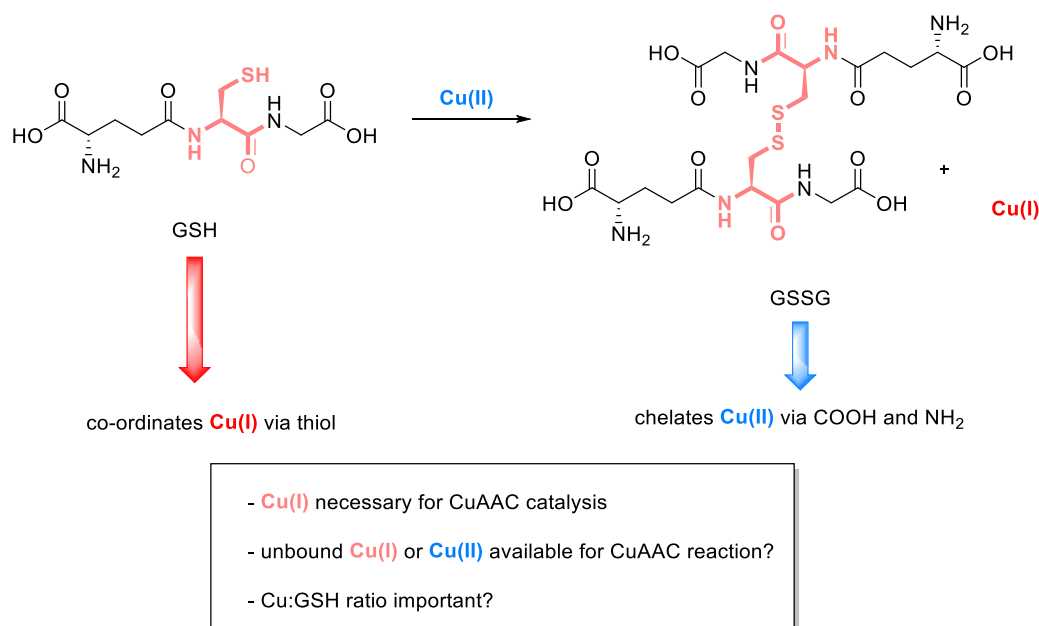
3.1 Introduction

As described in the previous chapter, GSH inhibited and reduced the conversion of the ynamine-CuAAC reaction. High GSH concentrations (≥ 6.5 mM) inhibited the reaction over a 24 h period. This chapter will explore the mechanistic determinants of how GSH influences the reaction kinetics.

3.1.1 *The Glutathione and Copper Interplay*

In cells, GSH acts as a redox buffer and prevents the build-up of transition metals which can facilitate the formation of reactive oxygen species (ROS).²²⁶ Apart from reducing the amount of ROS formed, GSH is also involved in cellular copper trafficking.⁶⁴ As such, this tripeptide has evolved a high affinity for copper ($K_D \sim 9 \times 10^{-12} \text{ M}^{-1}$)⁶⁴, especially Cu(I).¹⁶¹ Beyond Cu-co-ordination, GSH also reduces Cu(II) to Cu(I), producing GSSG.¹⁷¹ Although GSSG does not readily bind Cu(I), it is a good ligand for Cu(II).¹⁶⁵ Thus, there is a fine interplay between the oxidation state of Cu species with GSH. Speisky and co-workers proposed that for every equivalent of Cu(II) present, three equivalents of GSH are consumed, producing a Cu(I)-GSH complex and half a mole of GSSG.¹⁶⁵ Depending on the ratio of Cu(II) to GSH, partial or complete reduction of Cu(II) to Cu(I) results, creating GSSG, which in turn chelates Cu(II) (Scheme 3.1).

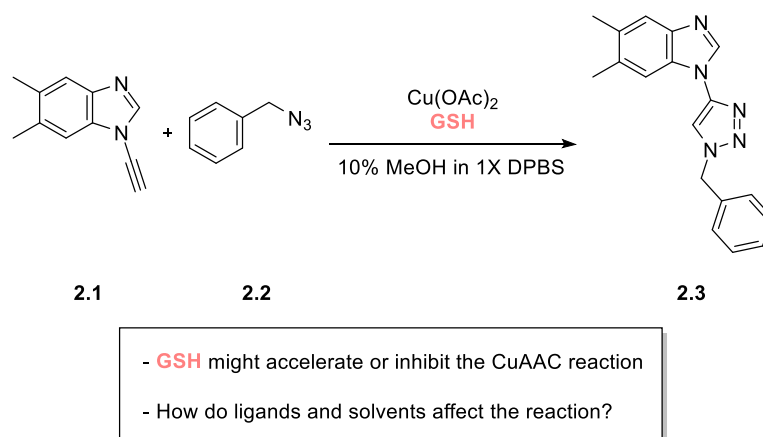
Perhaps the best insight into the consequences of such a system has been determined by experiments looking at copper induced oxidative damage to DNA.^{163,227} Ratios of >1:3 (Cu(II):GSH) prevented oxidative damage to DNA whereas smaller ratios accelerated the formation of oxidative DNA lesions.¹⁶⁴ In terms of the CuAAC reaction, this could translate into successful catalysis at ratios lower than 1:3.



Scheme 3.1. Overview of the redox buffering of Cu with GSH. Cu(I) is co-ordinated by the thiol in GSH, whereas GSSG likely chelates Cu(II) via carboxylates and amines.²²⁸

3.2 Hypothesis to be tested in this Chapter

The work reported in Chapter 2 focused on high GSH concentrations to mimic the CuAAC reaction under cellular conditions. However, GSH can both reduce and bind copper and therefore might act as both an accelerator as well as an inhibitor. The Cu:GSH ratio likely determines which role dominates. The working hypothesis to be tested in this chapter is that the Cu:GSH ratio determines the kinetics of ynamine-based CuAAC reaction. Additional factors, such as buffer, ligands and co-solvents might also influence the ynamine-CuAAC reaction in the presence of GSH (Scheme 3.2). To test the influences of these factors, the HPLC assay developed in Chapter 2 will be used and all reactions carried out in triplicate unless noted otherwise.



Scheme 3.2. Model reaction between ynamine **2.1** and benzyl azide (**2.2**) which will be used to explore the effect of Cu:GSH ratios as well as ligands and solvents on the reaction.

3.3 Aims of Chapter 3

The specific aims of this chapter are:

- Determine the influence of GSH on the reaction kinetics of the ynamine-CuAAC.
- Investigate the influence of co-solvents on the reactivities of ynamine and alkyne substrates in the CuAAC reaction.

3.4 Results & Discussion

3.4.1 Influence of Increasing Glutathione Concentrations on the Ynamine-CuAAC Reaction

To illustrate the impact of the GSH concentration on the CuAAC between ynamine **2.1** and benzyl azide (**2.2**), a series of experiments varying the GSH concentration (1 – 4 mM) was conducted while keeping copper and azide concentration constant. An increase from 1 mM to 2 mM GSH delayed reaction onset by 8 h (Figure 3.1). A further 1 mM (*i.e.*, from 2 mM to 3 mM) delayed reaction initiation by a further 8 h. Finally, 4 mM GSH resulted in the initiation of the reaction after 22 h. Maximum conversion (2 mM = 60%, 3 mM = 40%, 4 mM = 3%) decreased due to the formation of side product **2.30**. After reaching maximum conversion the triazole concentration decreased over time due to precipitation.

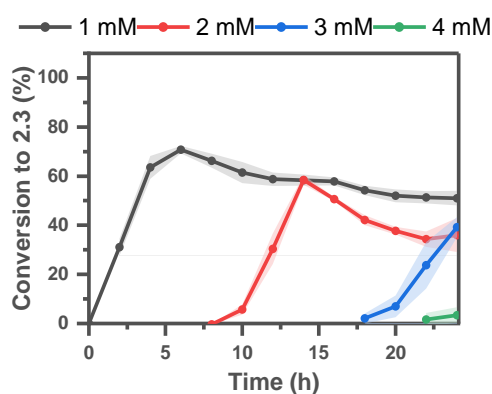
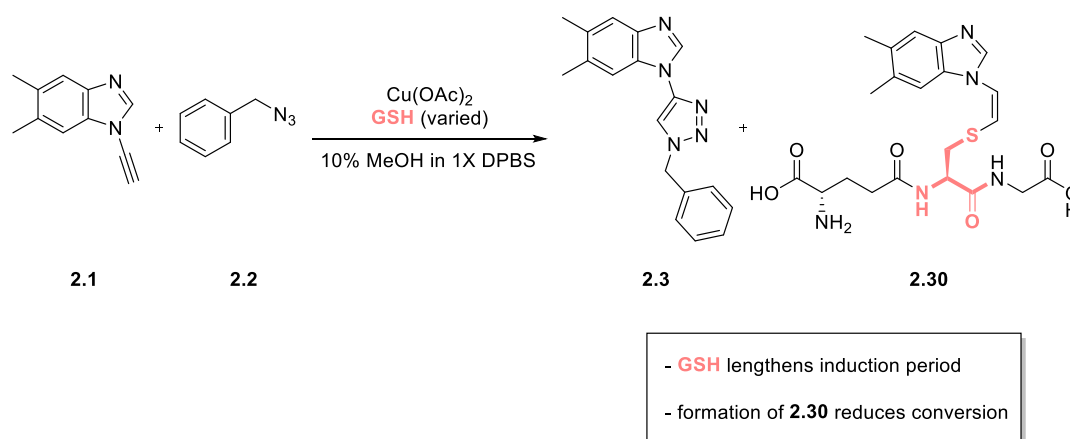
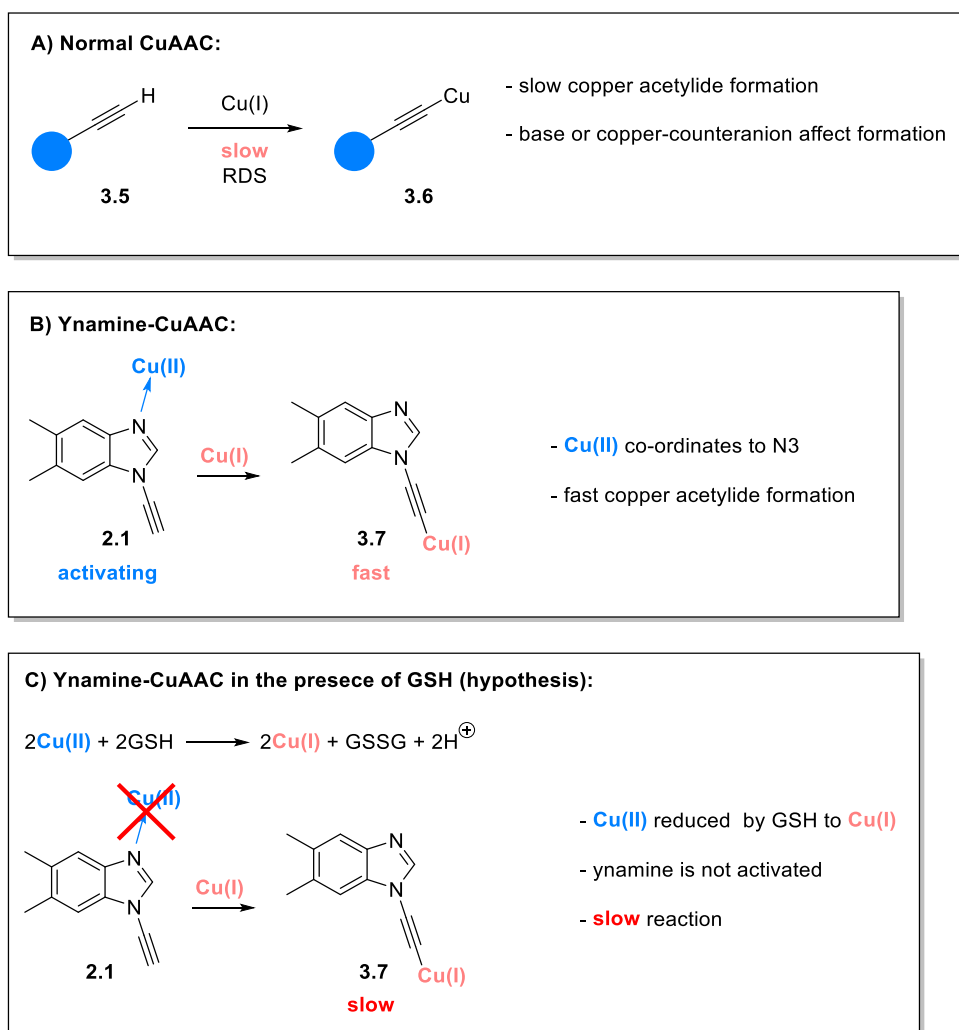


Figure 3.1. Effect of increasing GSH concentrations (1 – 4 mM) on the reaction of ynamine **2.1** with benzyl azide (**2.2**). Conditions: **2.1** (200 μ M), Cu(OAc)₂ (350 μ M), **2.2** (500 μ M), GSH (1 – 4 mM), 10% MeOH in 1X DPBS, rt, 24 h. Buffer pH = 7.4. Shaded areas represent the standard deviation calculated from three experiments.

The length of the induction period correlates with GSH concentration. An induction period for the CuAAC was also observed previously by Bertrand and co-workers who linked the induction period to formation of the copper acetylide **3.6** (Scheme 3.3A).⁵⁷ Slow deprotonation of the alkyne **3.5** causes the induction period which can be accelerated either by basic copper counter-anions or base addition.⁶² This step is also rate-determining. In contrast, the ynamine-CuAAC shifts the RDS to the azide insertion, presumably facilitated by co-ordination of Cu(II) to the N3 of **2.1** (Scheme 3.3B).¹⁵³ However, little Cu(II) remains at high concentrations of GSH and the deprotonation to form **3.7** likely becomes rate-limiting causing prolonged induction periods (Scheme 3.3C).



Scheme 3.3. A) Copper acetylide formation is the RDS of the conventional CuAAC reaction.⁵⁷ B) Cu(II) co-ordination to the ynamine **2.1** accelerates copper insertion. C) GSH reduces Cu(I) to Cu(II) and ynamine **2.1** is not activated leading to a slow reaction.

3.4.2 Comparison of the Ynamine-CuAAC in the Presence and Absence of Glutathione

The reaction between ynamine **2.1** and benzyl azide (**2.2**) was first performed in the absence of GSH and compared with the reaction in the presence of GSH. In the absence of GSH, triazole **2.3** was produced steadily and reached 35% conversion after 4 h (Figure 3.2A). In contrast, the reaction reached full conversion within 2 h in the presence of 1 mM GSH (Figure 3.2B).

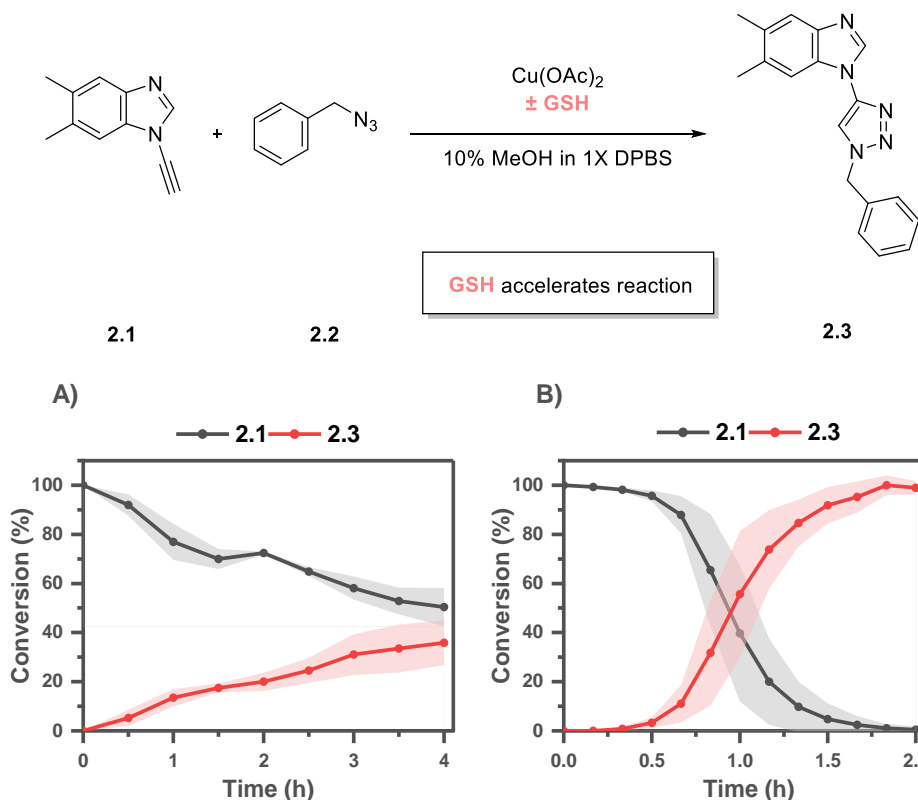
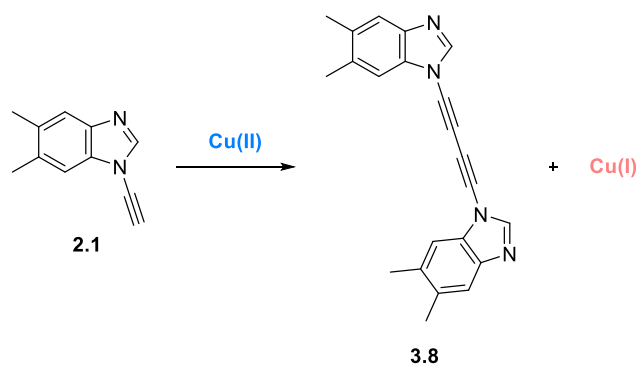


Figure 3.2. (A) Reaction of ynamine **2.1** with benzyl azide (**2.2**). Conditions: **2.1** (200 μM), $\text{Cu}(\text{OAc})_2$ (350 μM), **2.2** (500 μM), 10% MeOH in 1X DPBS, rt, 4 h. (B) Reaction of ynamine **2.1** with benzyl azide (**2.2**) in the presence of GSH (1 mM). Conditions: **2.1** (200 μM), $\text{Cu}(\text{OAc})_2$ (350 μM), **2.2** (500 μM), GSH (1 mM), 10% MeOH in 1X DPBS, rt, 2 h. Buffer pH = 7.4. Shaded areas represent the standard deviation calculated from three experiments.

Although 1.75 equivalents of $\text{Cu}(\text{OAc})_2$ were used, the reaction was sluggish in the absence of GSH. Without the addition of a reducing agent, Cu(I) can only be generated through the Glaser/Hay coupling (Scheme 3.4) or potentially through alcohol oxidation (only for primary and secondary alcohols).²²⁹ As the reaction was run under predominantly aqueous conditions, the Cu(II) reduction to Cu(I) is expected to be minimal leading to slow reaction rates; diyne **3.8** could also not be detected by HPLC.



Scheme 3.4. Diyne **3.8** and Cu(I) formation by the Glaser/Hay coupling of ynamine **2.1** with a Cu(II) source.

The increased reaction rate in the presence of GSH could be explained by the fast reduction of Cu(II) by GSH which bypasses the need for the slow Glaser/Hay coupling.²³⁰ However, GSH and the ynamine **2.1** likely compete for Cu(I) which could explain the observed induction period which lengthens with higher GSH concentrations.

3.4.3 Influence of Sodium Ascorbate on the Ynamine-CuAAC

To test whether the generation of Cu(I) was rate-limiting for the reaction of **2.1** with benzyl azide (**2.2**), the reactions were repeated with additional NaAsc (1 mM) both in the absence and presence of GSH. In the absence of GSH, the addition of NaAsc increased initial conversion considerably (20% compared with 0% without NaAsc, Figure 3.3A). After the initial burst, the conversion only increased slowly, reaching ~50% conversion after 3 h. After this timepoint, the conversion became unreliable due to product (**2.3**) precipitation. The addition of NaAsc to the reaction with GSH lengthened the induction period from ~0.5 h to ~1.5 h, but the time to reach full conversion only increased slightly to ~2.5 h (Figure 3.3B).

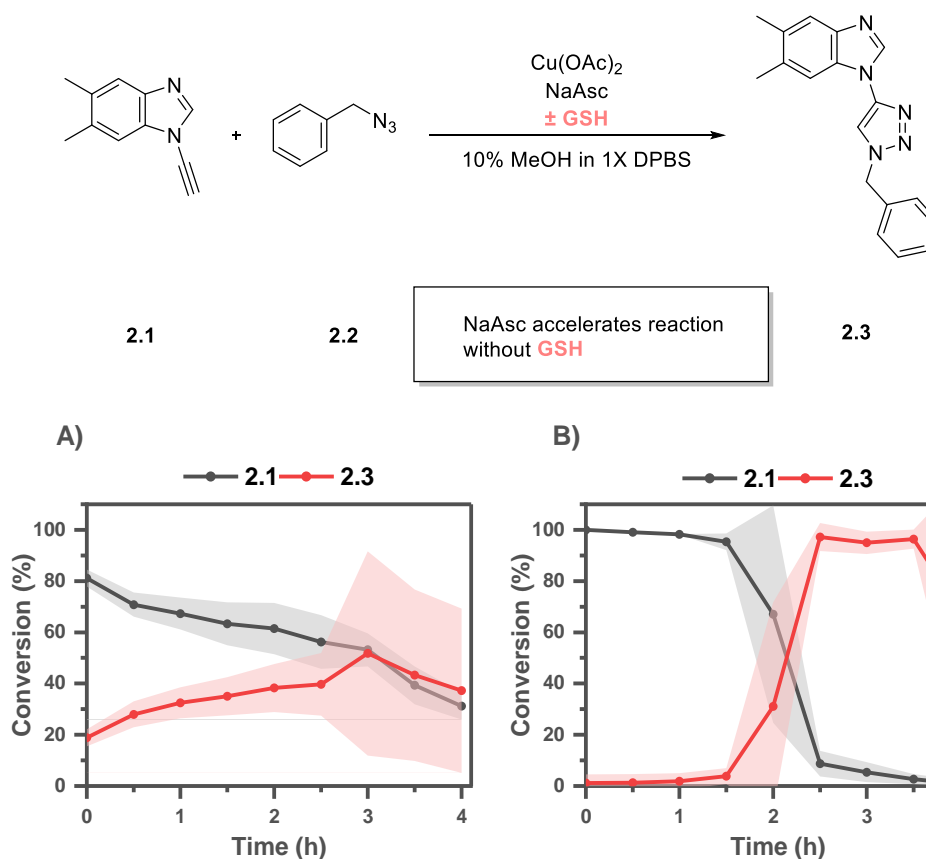


Figure 3.3. (A) Reaction of ynamine **2.1** with benzyl azide (**2.2**) with added NaAsc (1 mM). *Conditions:* **2.1** (200 μM), $\text{Cu}(\text{OAc})_2$ (350 μM), **2.2** (500 μM), NaAsc (1 mM), 10% MeOH in 1X DPBS, rt, 4 h. (B) Reaction of ynamine **2.1** with benzyl azide (**2.2**) with added NaAsc (1 mM) and GSH (1 mM). *Conditions:* **2.1** (200 μM), $\text{Cu}(\text{OAc})_2$ (350 μM), **2.2** (500 μM), GSH (1 mM), NaAsc (1 mM), 10% MeOH in 1X DPBS, rt, 4 h. Buffer pH = 7.4. Shaded areas represent the standard deviation calculated from three experiments.

The rapid initial conversion in the absence of GSH indicates that Cu(II) reduction was rate-limiting in the previous experiment. The slow reaction rate after the initial burst could signify the failure of NaAsc to keep Cu(I) in its oxidation state. This is a known issue in the absence of copper stabilising ligands as Cu(I) can either disproportionate²³¹ in aqueous solutions or be oxidised by dissolved oxygen.²³² The origin of the longer induction period in the presence of GSH could be due to the reduction of residual Cu(II) to Cu(I) by NaAsc. Since Cu(II) activates aromatic ynamines presumably by co-ordination with the N3 atom, as shown in Scheme 3.3B, one hypothesis is that in the absence of Cu(II), the formation times of the copper acetylide might be prolonged.

3.4.4 Influence of Ligand THPTA on the Ynamine-CuAAC

Copper-chelating ligands (such as THPTA) might be effective in shielding Cu(I) from GSH and positively influencing the reaction of ynamine **2.1** with benzyl azide **2.2** in the presence of GSH. The combination THPTA (350 μ M) and NaAsc (1 mM) was also tested and compared to the reaction without additives. Contrary to the expectation, the induction period lengthened when THPTA was added to the reaction (Figure 3.4).

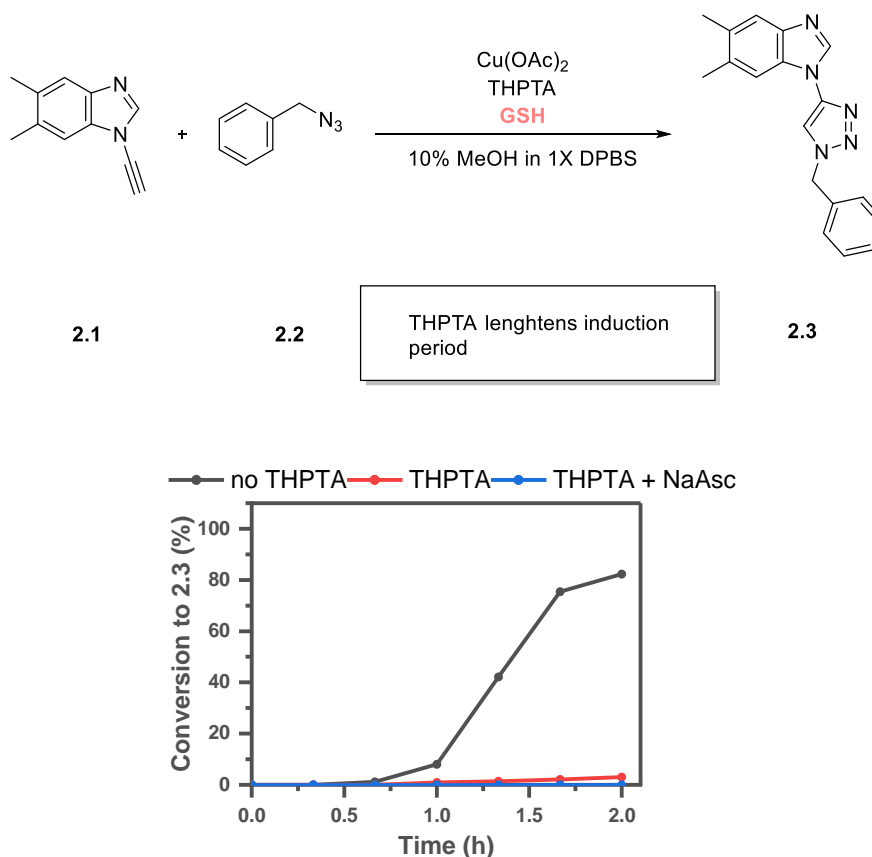


Figure 3.4. Influence of THPTA (1 equiv) on the reaction of ynamine **2.1** with benzyl azide (**2.2**) in the presence of GSH (1 mM). *Conditions (no THPTA):* **2.1** (200 μ M), Cu(OAc)₂ (350 μ M), **2.2** (500 μ M), GSH (1 mM), 10% MeOH in 1X DPBS, rt, 2 h. *Conditions (THPTA):* **2.1** (200 μ M), Cu(OAc)₂ (350 μ M), **2.2** (500 μ M), THPTA (350 μ M), GSH (1 mM), 10% MeOH in 1X DPBS, rt, 2 h. *Conditions (THPTA + NaAsc):* **2.1** (200 μ M), Cu(OAc)₂ (350 μ M), **2.2** (500 μ M), THPTA (350 μ M), NaAsc (1 mM), GSH (1 mM), 10% MeOH in 1X DPBS, rt, 2 h. Buffer pH = 7.4. All results from a single experiment.

3.4.5 The Ynamine-CuAAC Reaction in the Presence and Absence of Glutathione in Water

Next, the difference between water and buffer (1X DPBS) as a reaction medium was investigated. The reaction between ynamine **2.1** and benzyl azide (**2.2**) was performed in water in both the presence and absence of GSH and monitored over 4 h. In the absence of GSH, the reaction progress was comparable with the reaction in 1X DPBS, albeit only reaching 27% conversion after 4 h (vs 35% in 1X DPBS) (Figure 3.5A). No reaction in the presence of GSH was observed within 4 h (Figure 3.5B).

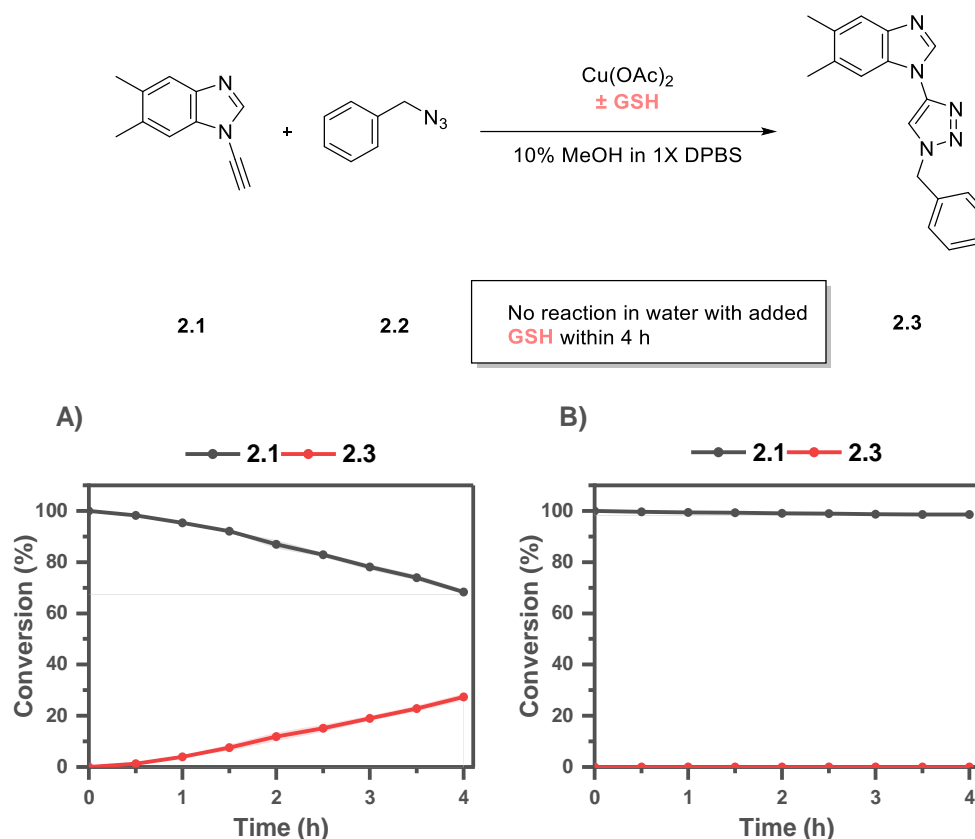


Figure 3.5. (A) Reaction of ynamine **2.1** with benzyl azide (**2.2**) in water. *Conditions:* **2.1** (200 μM), $\text{Cu}(\text{OAc})_2$ (350 μM), **2.2** (500 μM), 10% MeOH in water, rt, 4 h. (B) Reaction of ynamine **2.1** with benzyl azide (**2.2**) in water with added GSH (1 mM). *Conditions:* **2.1** (200 μM), $\text{Cu}(\text{OAc})_2$ (350 μM), **2.2** (500 μM), GSH (1 mM), 10% MeOH in water, rt, 4 h. Buffer pH = 7.4. Shaded areas represent the standard deviation calculated from three experiments.

The reason for the lack of reactivity when switching from 1X DPBS to water is unknown. A difference in pH (7.4 vs 7) is unlikely to account for the difference. But as the reaction in the absence of GSH is not affected, it stands to reason that the effect stems from GSH co-ordination to copper. Possibly, GSH binding to Cu(I) is weakened by the additional ions present in the buffer. However, this is purely speculative at this point.

The experiments performed so far demonstrate that GSH can either accelerate or prevent the reaction of ynamine **2.1** with benzyl azide (**2.2**). The induction period increased with higher GSH concentrations which points to competitive co-ordination for Cu(I) between the ynamine **2.1** and GSH. Attempts to shield Cu(I) from GSH by adding copper chelating ligands failed.

As GSH can be used to either accelerate or delay the ynamine-CuAAC, the Cu:GSH was explored in a more systematic approach utilising Design of Experiments (DoE).

3.4.6 Design of Experiment on the Ynamine-CuAAC Reaction in the Presence of Glutathione

Design of Experiments is a systematic approach for optimising reactions. The traditional one factor at a time approach usually applied to reaction optimisation is prone to missing key interactions between factors as the synergistic effects of changing two factors simultaneously are never explored (Figure 3.6A).²³³ The second aim of the DoE approach is to minimise the number of experiments needed for optimisation. This is achieved by picking experimental designs which maximise the covered reaction space.

The most basic DoE is a two-factor full factorial design (Figure 3.6B).²³⁴ Two factors (*i.e.*, reaction conditions such as time and temperature) are chosen at a low and high boundary (called levels) for each factor. Four experiments are then created by the combination of factors and levels (*i.e.*, low/low, low/high, high/low and high/high). This creates a square over the potential reaction surface giving valuable information about interactions between factors.

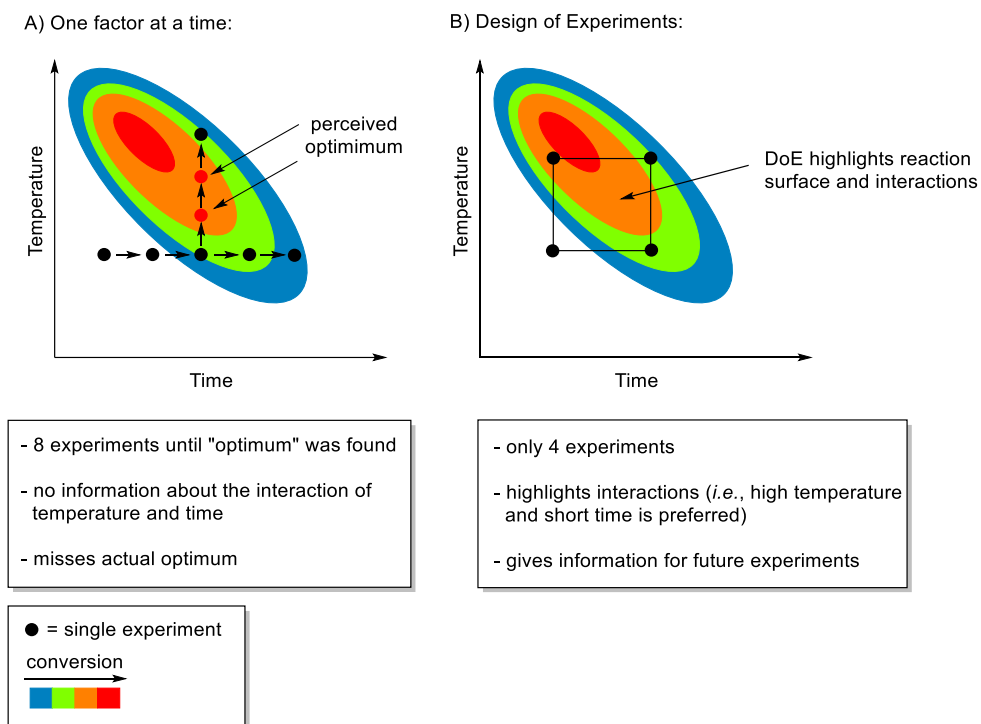


Figure 3.6. (A) One factor at a time approach to reaction optimisation. (B) DoE approach to reaction optimisation.

3.4.6.1 Design Choice for Ynamine-CuAAC in the Presence of Glutathione

The aim of this DoE was to elucidate the influence of the Cu:GSH ratio in more detail. A reactive surface map design is well suited for this task as it surveys the reaction space in a grid-like fashion. Previous experiments already explored the GSH and Cu(OAc)₂ relationship and indicated that conditions such as [GSH] = 1 mM and [Cu(OAc)₂] = 400 μM would be a suitable upper boundary of the design. As a lower boundary, it was envisioned that a GSH and Cu(OAc)₂ concentration of 100 μM would be suitable. These conditions were entered into MODDE® Design of Experiments Software to create a reactive surface map design consisting of 9 unique experiments (Table 3.1), which were performed in triplicate.

Table 3.1. Concentrations of Cu(OAc)₂ and GSH chosen for the DoE.

Experiment	[Cu(OAc) ₂] (μM)	[GSH] (μM)
1	100	100
2	100	550
3	100	1000
4	250	100
5	250	550
6	250	1000
7	400	100
8	400	550
9	400	1000

Conditions: **2.1** (200 μM), Cu(OAc)₂ (100 – 400 μM), **2.2** (500 μM), GSH (0.1 – 1 mM), 10% MeOH in 1X DPBS, rt, 2.5 h. Buffer pH = 7.4.

3.4.6.2 Results of the DoE

The results of the DoE were first plotted as reaction profiles to observe the conversion to triazole **2.3** over time (Figure 3.7). The reaction displayed no measurable induction period when Cu(OAc)₂ was used in equimolar amounts or in excess to GSH (Figure 3.7A). At 550 μM GSH (Figure 3.7B), the full effect of GSH on the CuAAC reaction was illustrated best. When Cu:GSH exceeds 1:3, no reaction was observed (100 μM, black line). When the ratio was ~1:2 (250 μM, red line), a short induction period (~ 30 min) was followed by a sudden increase in conversion which levelled off over time. When the Cu:GSH ratio was close to 1:1 (400 μM, blue line), no induction period was observed, and the reaction profile was similar to that of Figure 3.7A.

At a GSH concentration of 1 mM, conversion was only observed for a Cu(OAc)₂ concentration of 400 μM (Figure 3.7C), where an induction period of 1 h was followed by a burst of conversion to triazole **2.3**.

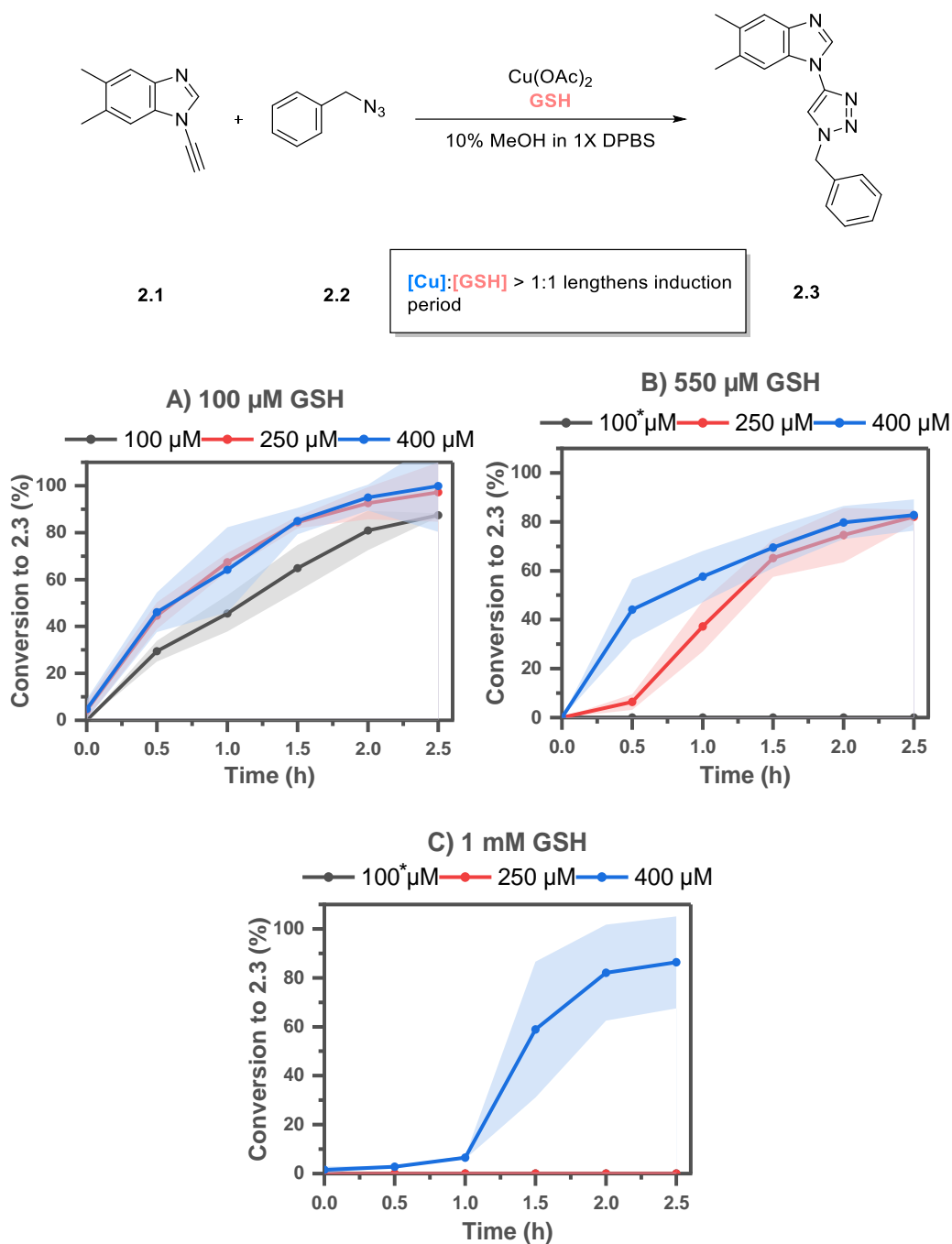


Figure 3.7. (A) Reaction of ynamine **2.1** with benzyl azide (**2.2**) using varied $\text{Cu}(\text{OAc})_2$ (100, 250 and 400 μM) concentration in the presence of GSH (100 μM). *Conditions:* **2.1** (200 μM), $\text{Cu}(\text{OAc})_2$ (100, 250 or 400 μM), **2.2** (500 μM), GSH (100 μM), 10% MeOH in 1X DPBS, rt, 2.5 h. (B) Reaction of ynamine **2.1** with benzyl azide (**2.2**) using varied $\text{Cu}(\text{OAc})_2$ (100, 250 and 400 μM) concentration in the presence of GSH (550 μM). *No conversion observed, overlaps with X-axis. *Conditions:* **2.1** (200 μM), $\text{Cu}(\text{OAc})_2$ (100, 250 or 400 μM), **2.2** (500 μM), GSH (550 μM), 10% MeOH in 1X DPBS, rt, 2.5 h. (C) Reaction of ynamine **2.1** with benzyl azide (**2.2**) using varied $\text{Cu}(\text{OAc})_2$ (100, 250 and 400 μM) concentration in the presence of GSH (1 mM). *No conversion observed, overlaps with X-axis. *Conditions:* **2.1** (200 μM), $\text{Cu}(\text{OAc})_2$ (100, 250 or 400 μM), **2.2** (500 μM), GSH (1 mM),

10% MeOH in 1X DPBS, rt, 2.5 h. Buffer pH = 7.4. Shaded areas represent the standard deviation calculated from three experiments.

The purpose of applying DoE was to construct a reactive surface map which could visualise the interplay between the stoichiometry of the Cu catalyst and GSH on the CuAAC reaction. Final conversions at 2.5 h were entered into MODDE® Design of Experiments Software to model the reaction and then used to construct a contour plot which illustrates the reaction surface (Figure 3.8). This plot demonstrates the dominant effect of GSH on the CuAAC reaction. For any given copper concentration, full conversion to triazole **2.3** was observed by simply adjusting the GSH concentration.

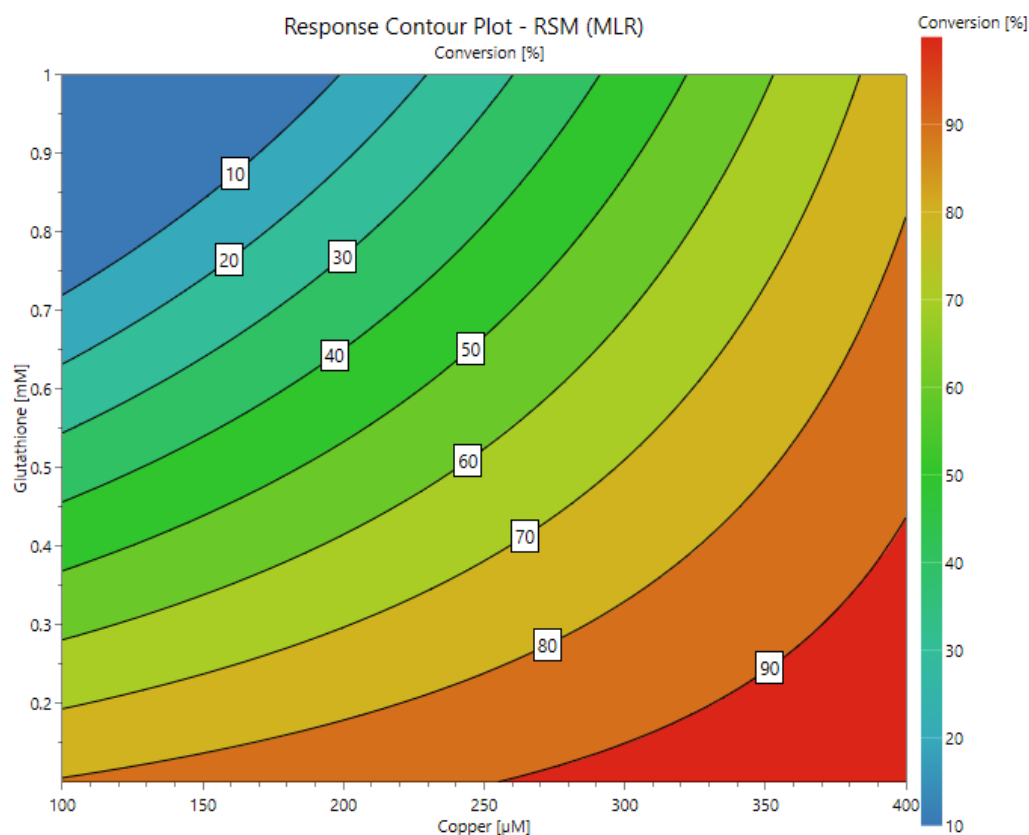


Figure 3.8. Reactive surface map for the reaction of ynamine **2.1** with benzyl azide (**2.2**) using varied Cu(OAc)₂ (100 – 400 μM) and GSH (0.1 – 1 mM) concentrations. Constructed from the conversion obtained from the DoE experiments after 2.5 h. Animated plot available in Appendix (RSM_animated.html).

To further illustrate the effect of the Cu:GSH ratio on the ynamine-CuAAC, the conversion to triazole **2.3** over time was plotted as a function of Cu:GSH ratio. Once the ratio exceeds 1:1, an induction period was observed which increased with higher ratios. This phenomenon seems

to be independent of the absolute reagent concentrations and only dependent on the ratio of Cu:GSH.

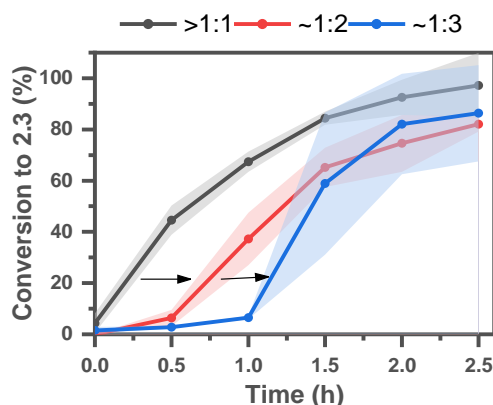


Figure 3.9. Plot showing the effect of the Cu/GSH ratio on the induction period on the reaction of ynamine **2.1** with benzyl azide (**2.2**). Constructed using the results from the DoE. *Conditions (>1:1):* **2.1** (200 μ M), Cu(OAc)₂ (250 μ M), **2.2** (500 μ M), GSH (100 μ M), 10% MeOH in 1X DPBS, rt, 2.5 h. *Conditions (~1:2):* **2.1** (200 μ M), Cu(OAc)₂ (250 μ M), **2.2** (500 μ M), GSH (550 μ M), 10% MeOH in 1X DPBS, rt, 2.5 h. *Conditions (~1:3):* **2.1** (200 μ M), Cu(OAc)₂ (400 μ M), **2.2** (500 μ M), GSH (1 mM), 10% MeOH in 1X DPBS, rt, 2.5 h. Buffer pH = 7.4. Shaded areas represent the standard deviation calculated from three experiments.

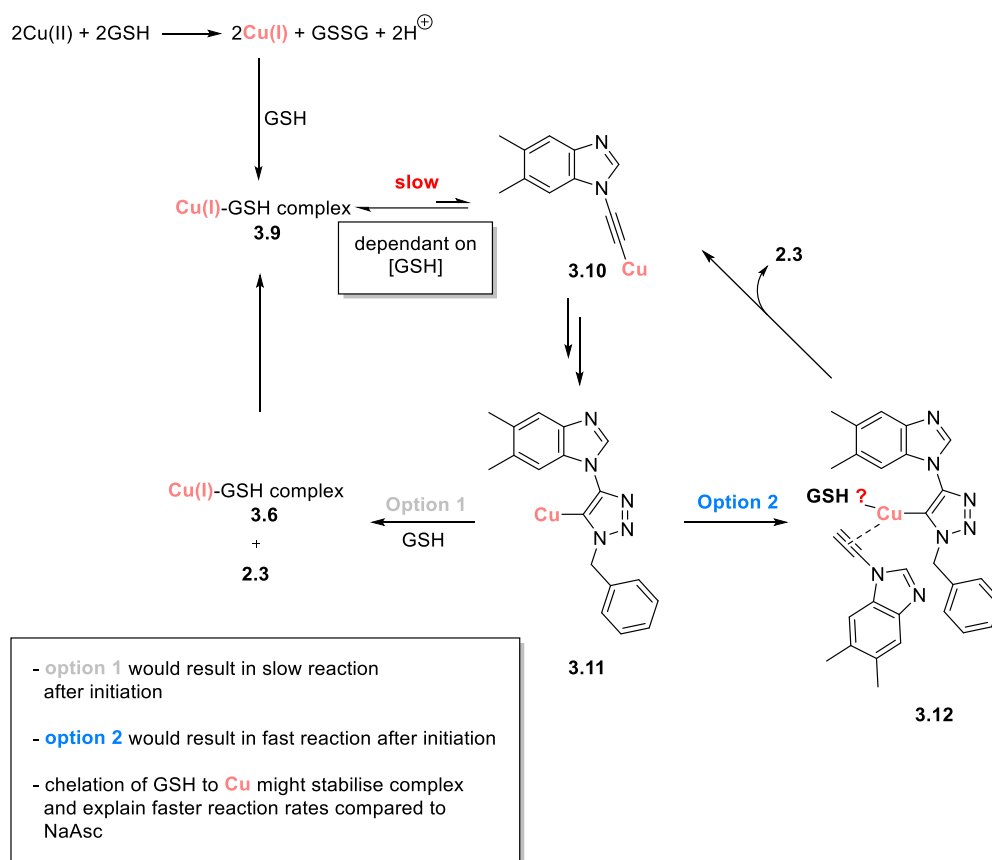
3.4.7 Hypothesis of the Ynamine-CuAAC in the Presence of Glutathione

The experiments performed so far demonstrated that the length of the induction period was related to the Cu:GSH ratio. In the context of the CuAAC reaction, an induction period is usually caused by slow formation of the copper-acetylide.⁵⁷ One hypothesis for this phenomenon was that there was competition for Cu(I) between the ynamine **2.1** and GSH to form acetylide **3.10** (Scheme 3.5). An excess of GSH would shift the equilibrium in favour of a Cu(I)-GSH complex (**3.9**), resulting in a longer induction period.

After azide insertion, intermediate **3.11** was formed. Two fates for intermediate **3.11** are conceivable, in option 1, protonation forms the triazole product **2.3** and GSH binds Cu(I) to form the Cu(I)-GSH complex (**3.9**). This complex would then re-enter the catalytic cycle. Consequently, formation of copper-acetylide **3.10** would remain the rate determining step and no reaction acceleration after the induction period would be observed. This is not observed experimentally.

In the second option, intermediate **3.11** would activate a further ynamine **2.1** molecule to form acetylide **3.10** and thereby release the triazole product **2.3**; a step that resembles autocatalysis, which has been observed for CuAAC reactions.²⁰⁵ This would exclude the slow step from the

cycle and lead to an increase in conversion after the induction period. This is observed experimentally and would explain the rapid conversion to product regardless of the GSH concentration or the length of the induction period once the reaction is initiated.



Scheme 3.5. Hypothesised influence of GSH on the ynamine-CuAAC reaction.

A further speculation is the involvement of GSH as a stabilising ligand in the CuAAC cycle. When comparing the results at the lowest copper and GSH concentration (100 μM each) of the DoE with the reaction using only 350 μM $\text{Cu}(\text{OAc})_2$ (no GSH) (Figure 3.2A) it is clear that the reaction was accelerated by the addition of GSH (~25% vs ~90% conversion after 2.5 h). In fact, GSH accelerated the reaction more effectively than NaAsc (Figure 3.3A). Using 1 mM NaAsc, the ynamine-CuAAC reaction was only accelerated initially and then proceeded in a steady manner. In contrast, GSH seems to be much better at maintaining the activity of the system. Potentially, GSH might act as a stabilising ligand (like THPTA) during catalysis (intermediate **3.12**, Scheme 3.5). This makes the system potentially attractive for bioconjugation and a viable alternative to the commonly used THPTA/NaAsc systems. GSH could serve as a ligand, reducing agent and scavenger of reactive oxygen species which might otherwise degrade biomolecules.

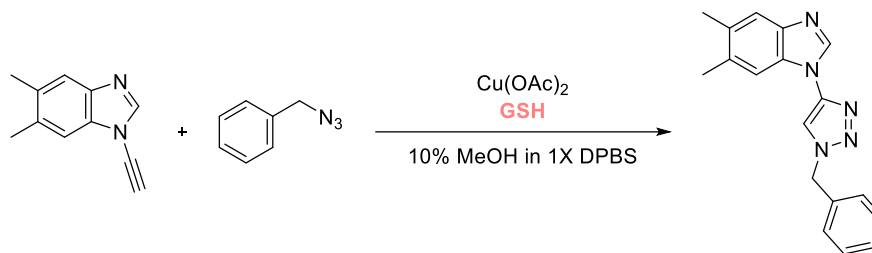
3.4.8 Kinetic Analysis of the Ynamine-CuAAC using Visual Time-Normalised Analysis

Visual time-normalised analysis (VTNA) is a novel tool to investigate reaction kinetics developed by Bures.^{235,236} It aims to deliver valuable kinetic information in the minimum number of experiments. By time-normalising change in concentration over time, experiments with different concentration of reagents can be compared (Equation 3.1).²³⁷ By plotting the concentration of reagents against normalised time, the order of each reagent can be elucidated by changing the order in reactant until the curves overlay. The curve overlay is determined by visual analysis (*i.e.*, judging by eye). If the correct order in all reactants has been found, the curve overlay becomes a straight line. The advantage of this method is that concentration data can be used to perform this analysis and no rate data or mathematical transformed data (*i.e.*, log) is required. In combination with visual data analysis, this makes this method suitable for noisy data.

$$\sum [B]^{\beta} \Delta t = \sum_{i=1}^n \left(\frac{[B]_i + [B]_{i-1}}{2} \right)^{\beta} (t_i - t_{i-1})$$

Equation 3.1. Equation to elucidate the reaction order (β) of reagent B using VNTA analysis.

The kinetic analysis of the ynamine-CuAAC would be complicated by the presence of an induction period. Therefore, it was decided to keep Cu(OAc)₂ concentration equal or in excess to GSH. In this manner, the order of each reactant (not GSH) can be investigated in just four experiments (Table 3.2). For accurate analysis, the concentration of copper should also be measured during the experiment. However, this is impossible by HPLC. Therefore, the concentration of the catalyst is assumed to be constant. If this approximation proved false, curve overlay would not be achieved.²³⁸

Table 3.2. Conditions for the reaction of ynamine **2.1** with benzyl azide (**2.2**) conducted for the VTNA analysis.

	2.1	2.2	2.3	
Entry	[2.1]	[2.2]	[GSH]	[Cu]
1	200 μM	400 μM	100 μM	100 μM
2	200 μM	400 μM	100 μM	250 μM
3	400 μM	400 μM	100 μM	100 μM
4	200 μM	600 μM	100 μM	100 μM

Conditions: **2.1** (200 – 400 μM), $\text{Cu}(\text{OAc})_2$ (100 – 250 μM), **2.2** (400 – 600 μM), GSH (100 μM), 10% MeOH in 1X DPBS, rt, 2.5 h. Buffer pH = 7.4.

Increasing either $\text{Cu}(\text{OAc})_2$ or benzyl azide (**2.2**) concentration led to a faster reaction rate (Figure 3.10A). Increasing the ynamine **2.1** concentration also slightly increased the reaction rate.

Next, the change of concentration over time was calculated and normalised against time according to the VTNA formula (Equation 3.1). The best overlay was achieved by setting the reaction order of the reagents as follows: ynamine = 0.4, $\text{Cu}(\text{OAc})_2$ = 0.6 and benzyl azide = 1 (Figure 3.10). The final data points diverge from the straight line. This is because the reaction is finished and conversions plateau in all cases except for excess ynamine.

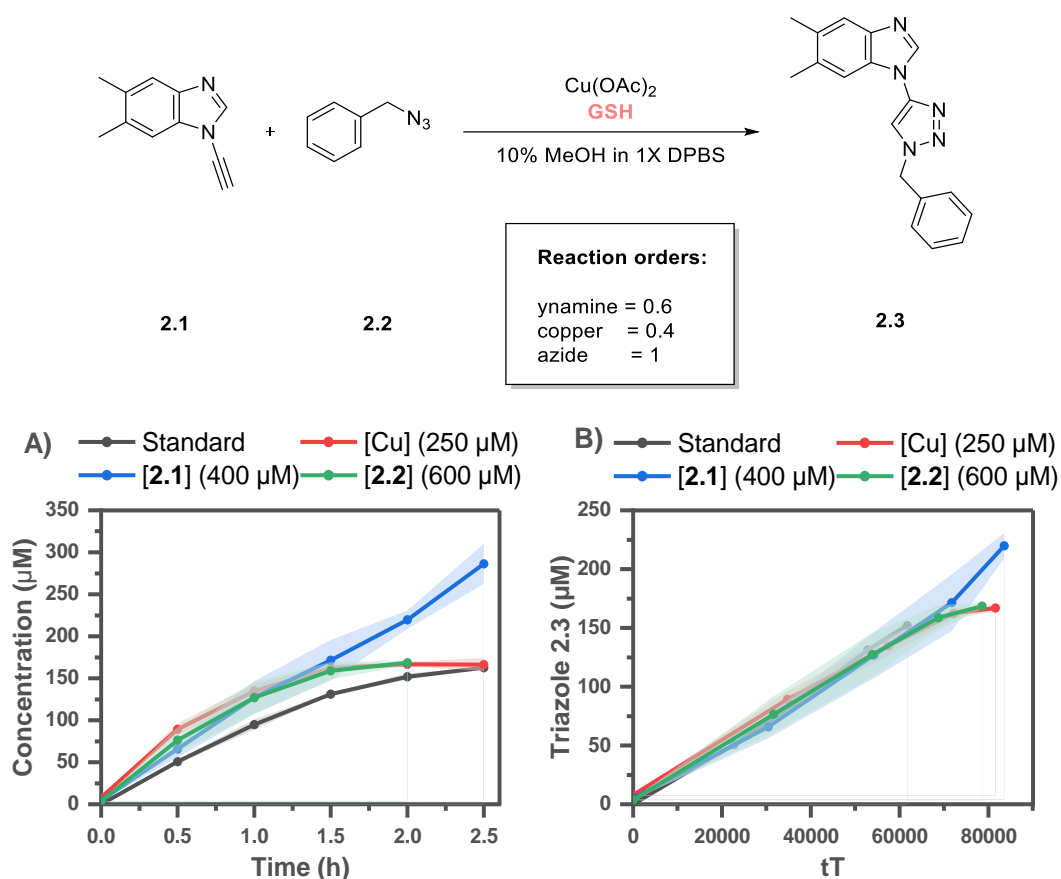


Figure 3.10. (A) Reaction of ynamine **2.1** and benzyl azide (**2.2**) using specified VTNA analysis. *Conditions (Standard):* **2.1** (200 μM), $\text{Cu}(\text{OAc})_2$ (100 μM), **2.2** (400 μM), GSH (100 μM), 10% MeOH in 1X DPBS, rt, 2.5 h. Legend indicates the changed concentration of each reactant. (B) Result of the VTNA analysis using the results for $t = 0$ to $t = 2$ h. Best overlay can be achieved by setting the following orders for each reagent: **2.1** = 0.6, $\text{Cu}(\text{OAc})_2$ = 0.4 and **2.2** = 1. Buffer pH = 7.4. Shaded areas represent the standard deviation calculated from three experiments.

The observed orders indicate that the azide is still part of the RDS of the ynamine-CuAAC as was previously observed.¹⁵³ The \sim half-order dependence on the ynamine and $\text{Cu}(\text{OAc})_2$ indicates that both reagents are also rate-limiting. This is likely due to the presence of GSH which will be in competition for $\text{Cu}(\text{I})$ with the ynamine.

3.4.9 Conventional Alkyne using the Optimal Reaction Conditions

To investigate whether the accelerating effect of GSH on the CuAAC reaction was unique to aromatic ynamines, a series of experiments with alkyne **2.10** were performed. 100 μM $\text{Cu}(\text{OAc})_2$ and GSH achieved the best conversion for ynamine **2.1** at the lowest copper concentration and were therefore chosen as the reaction conditions. NaAsc was added to the reaction, as conventional alkynes required NaAsc to be reactive as described in the previous

chapter. However, no conversion to the product **2.44a** was observed within 2 h. It was speculated that the copper concentration was not high enough to show conversion within 2 h.

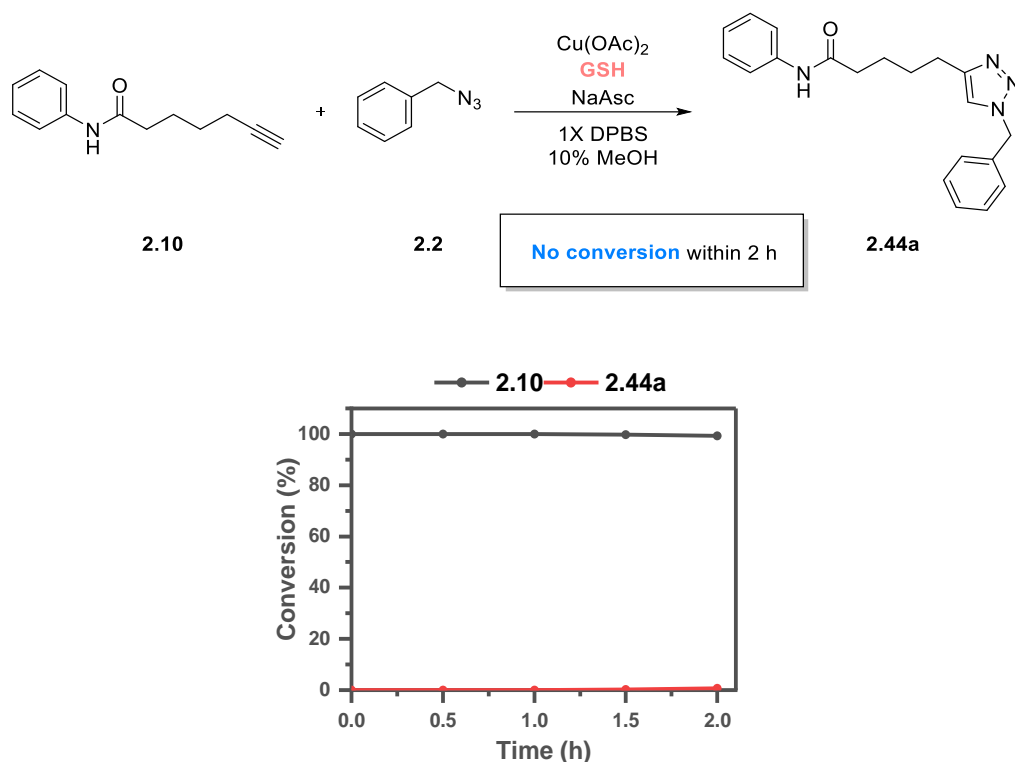


Figure 3.11. Reaction of alkyne **2.10** with benzyl azide **2.2** using the optimal ynamine-CuAAC conditions. *Conditions:* **2.10** (200 μM), $\text{Cu}(\text{OAc})_2$ (100 μM), **2.2** (500 μM), **GSH** (100 μM) in 10% MeOH in 1X DPBS, rt, 2 h. Buffer pH = 7.4. Shaded areas represent the standard deviation calculated from three experiments.

The $\text{Cu}(\text{OAc})_2$ concentration was then raised to 250 μM (resulting in a Cu:GSH ratio of 2.5:1) and the experiments were repeated both in the presence and absence of **GSH** as well as without NaAsc. The higher $\text{Cu}(\text{OAc})_2$ concentration increased the conversion in the presence of **GSH** to ~75% within 2 h (Figure 3.12). If NaAsc was omitted from the reaction, no conversion was observed within 2 h. If instead **GSH** was omitted, the conversion only reached ~60% and showed signs of plateauing. This again suggests that NaAsc alone was not able to keep Cu(I) reduced for the full duration of the experiment,¹⁷⁹ as observed previously in this chapter. In contrast, the combination of NaAsc and **GSH** was superior and showed no signs of plateauing and would likely have reached full conversion if monitored for longer.

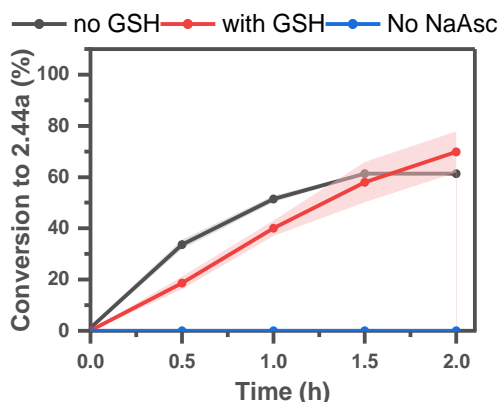
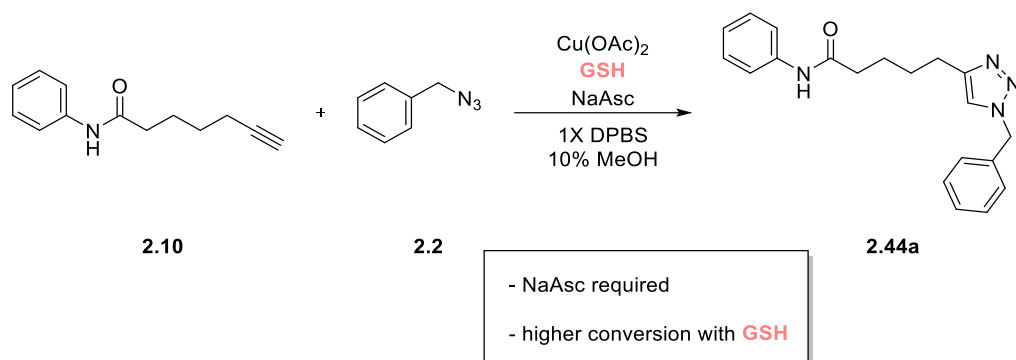
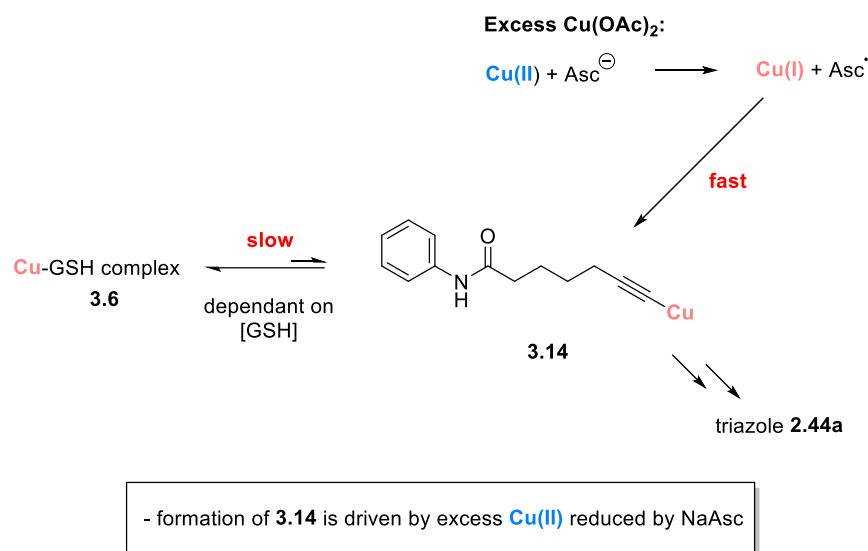


Figure 3.12. Reaction of alkyne **2.10** with benzyl azide **2.2** using increased Cu(OAc)_2 (250 μM) and with added NaAsc (1 mM) in the presence and absence of GSH (100 μM). Addition of NaAsc is crucial as otherwise no conversion is observed in the presence of GSH. *Conditions (no GSH):* **2.10** (200 μM), Cu(OAc)_2 (250 μM), **2.2** (500 μM), NaAsc (1 mM) in 10% MeOH in 1X DPBS, rt, 2 h. In duplicate *Conditions (with GSH):* **2.10** (200 μM), Cu(OAc)_2 (250 μM), **2.2** (500 μM), GSH (100 μM), NaAsc (1 mM) in 10% MeOH in 1X DPBS, rt, 2 h. Shaded areas represent the standard deviation calculated from three experiments. *Conditions (no NaAsc):* **2.10** (200 μM), Cu(OAc)_2 (250 μM), **2.2** (500 μM), GSH (100 μM) in 10% MeOH in 1X DPBS, rt, 2 h. Single experiment. Buffer pH = 7.4.

Although the combination of GSH and NaAsc performed better than NaAsc alone, NaAsc is essential for the reaction when conventional terminal alkynes are used as substrates. Unlike aromatic ynamines, conventional alkynes rely on Cu(I) formation by reductants (Scheme 3.6). The copper acetylide (**3.14**) formation remains the rate limiting step. In the presence of GSH, this step was extraordinarily slow if a $\text{Cu}:\text{GSH} \geq 1:1$ is used. Only an excess of Cu(II) eliminated the induction period which indicates that unbound Cu(I) is formed by the reduction of excess Cu(II) through NaAsc. The superiority of the combined NaAsc/GSH system again indicates that GSH might participate in the CuAAC as a stabilising ligand.



Scheme 3.6. Possible impact of GSH on the CuAAC of conventional alkynes.

3.4.10 Solvent Screen for the Ynamine-CuAAC using the Optimal Conditions

Finally, the influence of the co-solvent on the ynamine-CuAAC reaction in the presence of GSH was investigated. The reaction between ynamine **2.1** and benzyl azide **2.2** was screened with a selection of polar protic (MeOH, EtOH, IPA) and polar non-protic solvents (DMSO and MeCN) as well as two fluorinated solvents (TFE and HFIP) using 100 μM $\text{Cu}(\text{OAc})_2$ and GSH. The rationale for including fluorinated solvents is based on literature reports, which have described rate accelerations for cycloadditions when HFIP or TFE were used.^{239,240}

Out of the solvents tested MeCN displayed the slowest reaction rate, only reaching a conversion of ~37% after 2.5 h (Figure 3.13). Polar protic solvents displayed intermediate reactivity reaching ~60% (IPA), 75% (EtOH) and 85% (MeOH) conversion respectively. DMSO provides slightly faster reaction rates, reaching a conversion of ~95% after 2.5 h. However, all solvents were outclassed by the fluorinated solvents TFE and HFIP which provided full conversion in under 10 mins.

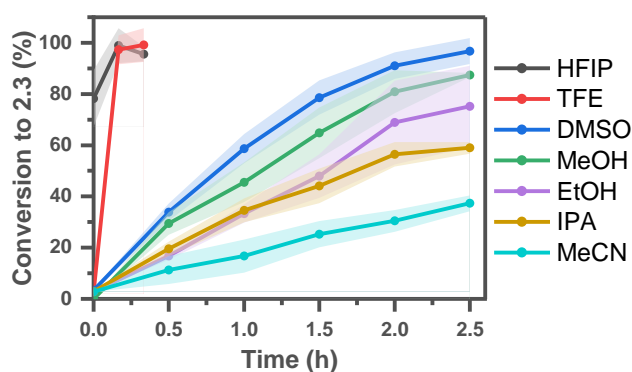
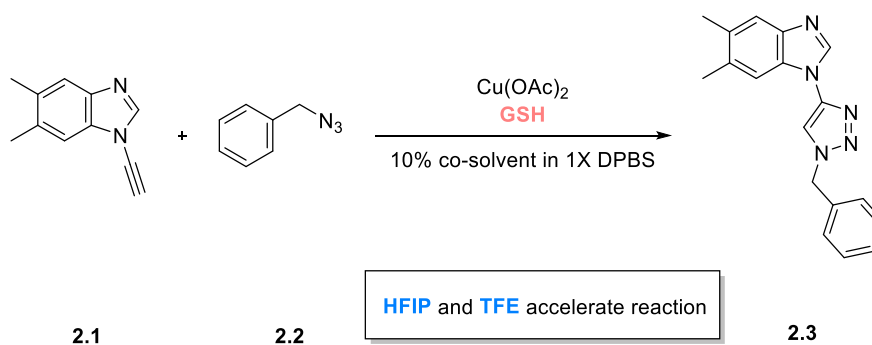


Figure 3.13. Solvent screen for the reaction of ynamine **2.1** with benzyl azide **2.2** using the optimal reaction conditions. *Conditions:* **2.1** (200 μM), $\text{Cu}(\text{OAc})_2$ (100 μM), **2.2** (500 μM), **GSH** (100 μM), 10% co-solvent in 1X DPBS, rt, 2.5 h. Buffer pH = 7.4. Shaded areas represent the standard deviation calculated from three experiments.

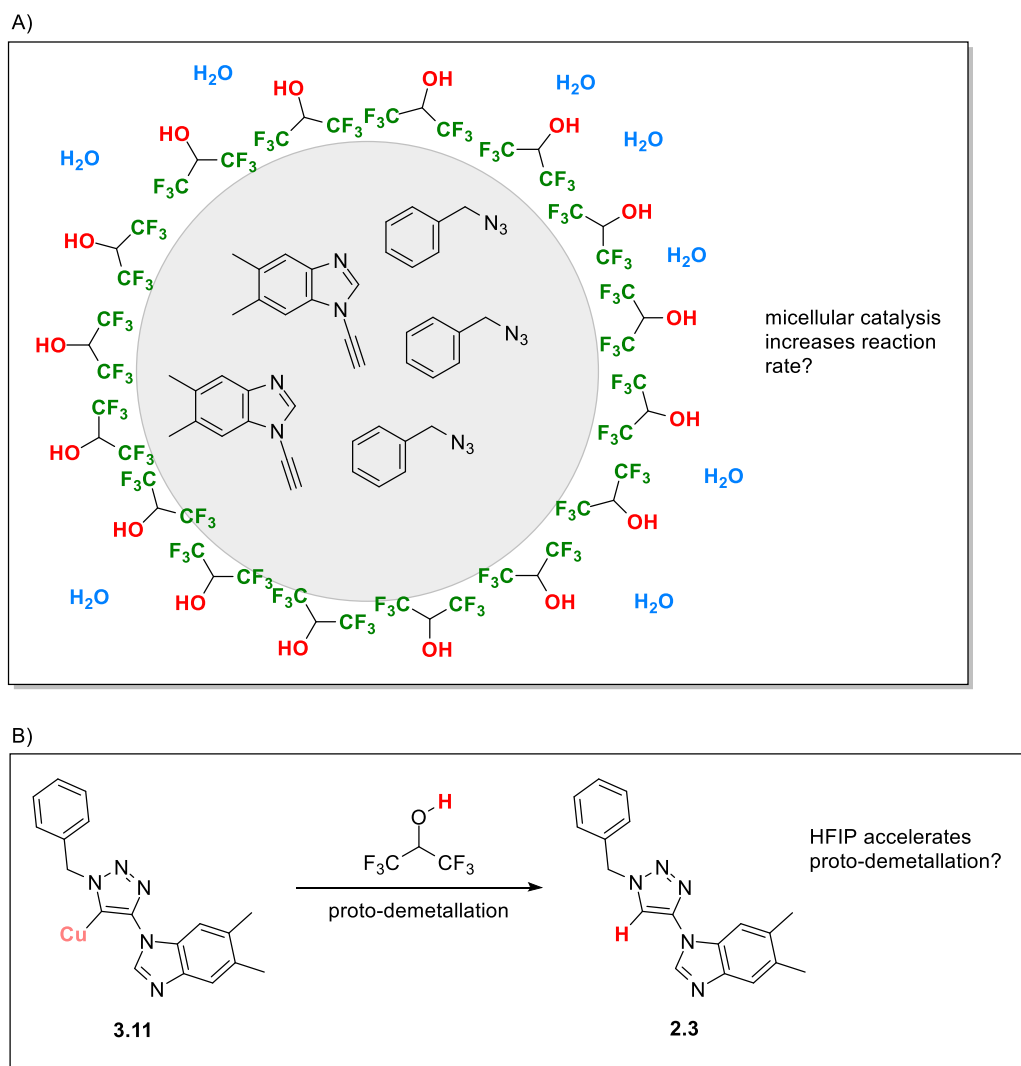
As a solvent HFIP has several unique properties. Due to the electron withdrawing nature of the CF_3 groups, HFIP features one of the most acidic hydroxyl groups ($\text{p}K_{\text{a}} \sim 9.3$) of common alcohols while also being the least nucleophilic.²⁴¹ Second, HFIP has enhanced hydrogen bonding abilities which can stabilise hydrogen bonding complexes by forming higher order aggregates of HFIP (usually trimers shaped into helices).²⁴² This hydrogen bond donating ability can be used to increase amine basicity or modulate secondary structures of peptides and proteins. In water/HFIP mixtures, the natural conformation of proteins is denatured and forced into alpha-helices.^{243,244} Additionally, HFIP features good redox stability and can stabilise cations efficiently.

Only one report utilised HFIP as a co-solvent for the CuAAC reaction¹⁸⁰ so far and the influence of HFIP on the CuAAC reaction is therefore subject to speculation. One possibility for the observed rate-enhancement is due to micellar catalysis. Binary HFIP/ H_2O mixture have been subject to extensive investigations by FTIR-ATC,²⁴⁵ molecular dynamics,²⁴⁶ X-ray scattering, neutron scattering, NMR and mass spectrometry.²⁴⁷ The aims of these studies were

to investigate the molecular structures and bulk properties. All techniques came to similar conclusions. At low HFIP concentrations (<10% v/v), the tetrahedral water structure remains undisturbed by HFIP. Disperse at first and highly hydrated, HFIP then increasingly forms micelles up to a concentration of ~30% (v/v). In these micelles, the CF₃ groups face each other, and the hydroxyl group participates in hydrogen-bonding with water. This concentration also denatures proteins and stabilises α -helixes most effectively. At higher HFIP concentrations, the micelles are broken up into solvated dimers and trimers and eventually form helixes.

The effect of such structures on reactions was investigated by Holl  czki *et al.* in 2013.²⁴⁸ The epoxidation of cyclooctene proceeded faster in HFIP/water mixtures. Through molecular dynamics simulations they uncovered a tight association of H₂O₂ with HFIP and the tendency of HFIP to form micelles. The addition of cyclooctene disturbed the hydrogen-bonding network and increased the H₂O₂-HFIP interactions. Furthermore, they observed the formation of a triphasic system. Cyclooctene molecules were surrounded by the CF₃-groups of HFIP with the hydroxyl groups pointed outwards and engaged in hydrogen-bonding with H₂O₂ and water.

In the case of the ynamine-CuAAC reaction, such a clustering would result in an increase of the effective concentrations of reagents and potentially lead to rate acceleration (Scheme 3.7A). However, it is unknown how GSH, copper or buffer-ions would influence the micelle formation. Additionally, at 10% HFIP the micelle concentration is not at its highest and other factors might be at play. To test this hypothesis, the ynamine-CuAAC should be performed at different HFIP percentages (*i.e.*, 10%, 20%, 30%, 50%, 80% and 100%). If the rate of the reaction were influenced, this potentially could point towards this mechanism. Another influence of HFIP could be through increased hydrogen-bonding and acidity. Hydrogen-bonding could stabilise the polar transition state while HFIP could increase the speed of the proto-demetalation (Scheme 3.7B).



Scheme 3.7. Possible influence of HFIP on the CuAAC reaction. A) Rate enhancement through micellar catalysis. B) Faster proto-demetallation.

TFE and HFIP might open unique opportunities for fast and efficient *in vitro* CuAAC bioconjugation as the toxicity of HFIP and TFE will likely prevent *in vivo* use. Combining the results from the DoE and solvent screen, the fastest ynamine-CuAAC reaction employs $\text{Cu}(\text{OAc})_2$, GSH (100 μM each) and fluorinated solvents. This combination promises interesting results for *in vitro* conjugation of biomolecules such as peptides or oligonucleotides which will be explored in the next chapter.

3.5 Summary & Future Work

This chapter explored the influence of GSH on the reaction of ynamine **2.1** with benzyl azide (**2.2**). The concentration of GSH could be used to tune the reaction from full conversion in 2.5 h to no reaction within 18 h. Additives such as NaAsc or THPTA did not increase the reaction rate in the presence of GSH. The reason for this substantial influence of GSH on the reaction is postulated to be the ratio of copper to GSH. GSH is an excellent ligand for Cu(I) which creates a competition for Cu(I) between GSH and the ynamine **2.1**. The resulting equilibrium can be influenced by the relative concentration of each reagent. Consequently, choosing the ratio of Cu:GSH is crucial.

A ratio of 1:1 leads to excellent reaction kinetics (full conversion in 2.5 h) while simultaneously limiting the amount of copper used, which is desired for bioconjugation. By changing the co-solvent to fluorinated solvents such as HFIP or TFE, full conversion can be achieved within 10 mins. The effect of HFIP on the reaction should be investigated in more detail in the future. The reaction could be performed at different HFIP percentages to uncover if micellar catalysis is at play. Potentially, this could then also be confirmed by performing a SPAAC reaction with HFIP as the co-solvent. If the same accelerating effect is observed, it could be concluded that HFIP might not accelerate the rate by interaction with GSH or copper. Alternatively, the reaction could also be investigated by NMR or IR/Raman spectroscopy. Shifts in NMR or IR/Raman spectroscopy could point towards changes in hydrogen bonding during the reaction.

Further questions remain on the exact nature of the interaction between copper and GSH at the different ratios used in the DoE. Potentially EPR and UV-spectrometer assays (using Cu(I) probes) could elucidate the exact nature of the copper oxidation states over the course of the reaction.

The discoveries in this chapter show promise for conjugation of biomolecules such as peptides or oligonucleotides. Limiting the amount of copper is crucial for bioconjugation to avoid oxidative damage. Unfortunately, this usually leads to extended reaction times and a balance between reactivity and oxidative damage must be found. The ynamine was found to be uniquely reactive in the presence of GSH. Using the optimal conditions described in this chapter (Cu(OAc)₂ (100 µM) and GSH (100 µM) as well as switching the co-solvent to a fluorinated co-solvent could create unique possibilities for the bioconjugation of peptides and oligonucleotides. This will be explored in the next chapter.

3.6 Experimental Procedures

3.6.1 HPLC Assay Procedures

Stock solutions of reagents were prepared each day. Reagents (~1 – 20 mg) were measured out on a microbalance.

Stock solutions:

[Alkyne] = 6 mM in organic solvent (*i.e.*, MeOH)

[Azide] = 30 mM in organic solvent (*i.e.*, MeOH)

[GSH] = 30 mM in 1X DPBS

[Cu(OAc)₂] = 10 mM in H₂O

[NaAsc] = 30 mM in 1X DPBS

Appropriate amounts of the stock solutions were added to reach specified concentrations to an HPLC vial and made up with MeOH and 1X DPBS buffer to a final volume of 1.5 mL. The addition order was as follows: MeOH, alkyne, benzyl azide, buffer, GSH, Cu(OAc)₂. The vials were then placed in the autosampler (not capable of temperature control) and sampled for the specified time.

3.6.2 Instruments and Methods

HPLC was carried out on a Shimadzu Prominence LC system.

Typical HPLC conditions are described below:

Column Specifications: Phenomenex Kinetex C18, 50 × 4.6 mm, 2.6 μm

Column Temperature: 40 °C

Mobile Phase A: 0.1 % v/v TFA in water

Mobile Phase B: 0.1 % v/v TFA in MeCN

Flow rate 1.5 mL/min

Injection Volume: 10 μL

Gradient Profile:

Time (min)	B% (MeCN, 1% TFA)
0 – 5	5 – 60
5 – 5.1	60 – 95
5.1 – 7.2	95
7.2 – 7.3	95 – 5
7.3 – 9.5	5

UV detection signal was recorded at 254 nm. Conversions for the ynamine (**2.1**) and the corresponding triazole (**2.3**), which were calculated using a calibration curve (Figure 3.14).

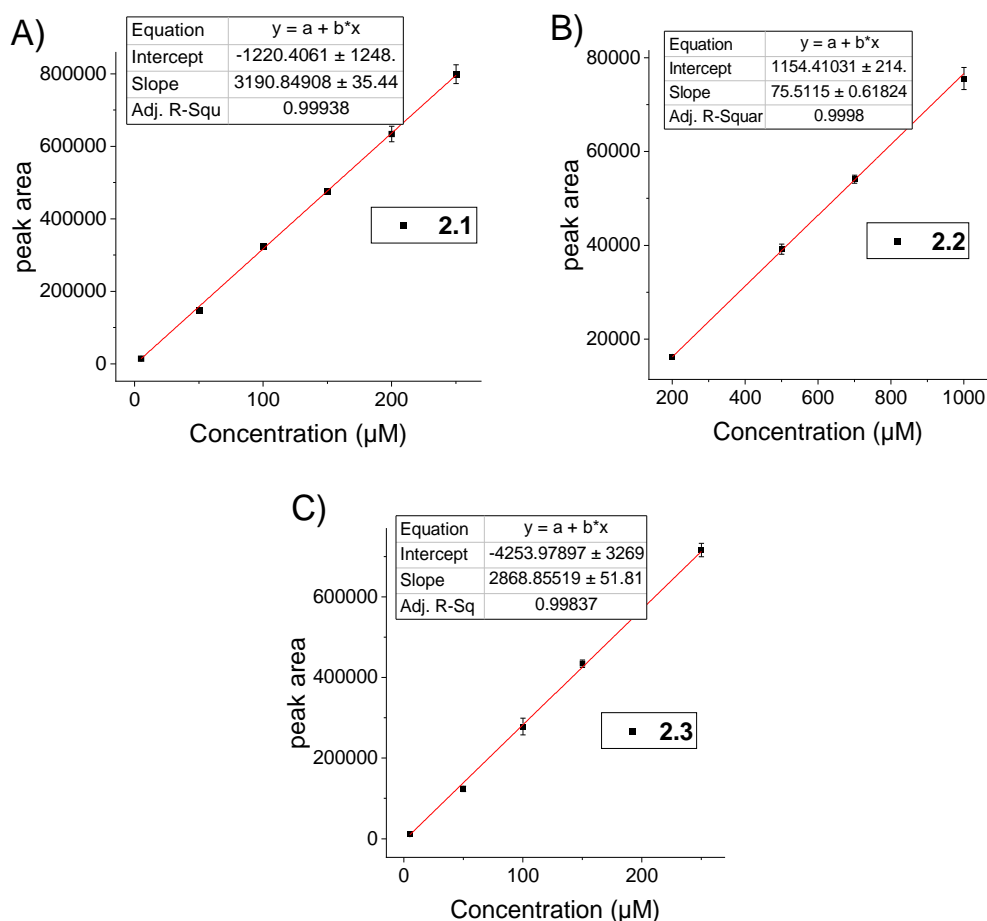


Figure 3.14. Each calibration curve was measured in triplicate. The averaged peak area for each concentration was used to construct the calibration curves. (A) Calibration curve for ynamine **2.1**. (B) Calibration curve for benzyl azide **2.2**. (C) Calibration curve for triazole **2.3**.

To determine the conversion in Figure 3.11 and Figure 3.12, peak area of the product (**2.44c**) was divided by the peak area of the starting material (**2.10**) and the product (**2.44c**) at each timepoint.

3.6.3 VTNA Analysis

Spreadsheet detailing VTNA available in the Appendix.

Chapter 4

Exploration of Using Ynamines as Bio-Orthogonal Reagents for the Preparation of Bioconjugates

4.1 Introduction

4.1.1 CuAAC for Bio-orthogonal Conjugation of Peptides and Oligonucleotides

The CuAAC is a popular tool for peptide and protein modifications and is used in a variety of applications, such as a key step in proteomic analysis (Figure 4.1A).²⁴⁹ The high reactivity and specificity of alkyne and azide substrates ensure high sensitivity of proteomic analysis, which is either performed after on-bead digestion of whole labelled proteins²⁵⁰ or after protein digestion and subsequent tagging via the CuAAC reaction. The later procedure exhibits better sensitivity compared to the former.²⁵¹

Another use of the CuAAC reaction in chemical biology is the modification of oligonucleotides to improve pharmacokinetic properties (Figure 4.1B).²⁵² One example are antisense oligonucleotides, which suffer from poor *in vivo* stability and are easily degraded by DNA or RNA digesting enzymes.²⁵³ Conjugation to peptides by CuAAC enhances cellular uptake.^{254,255}

The perhaps most common modification of peptides²⁵⁶ and oligonucleotides²⁵⁷ by the CuAAC reaction is the tagging with fluorescent reporters (Figure 4.1C). A variety of alkyne or azide modified fluorescent probes and commercially CuAAC kits are available which makes the use of the CuAAC reaction for fluorescent labelling widespread.

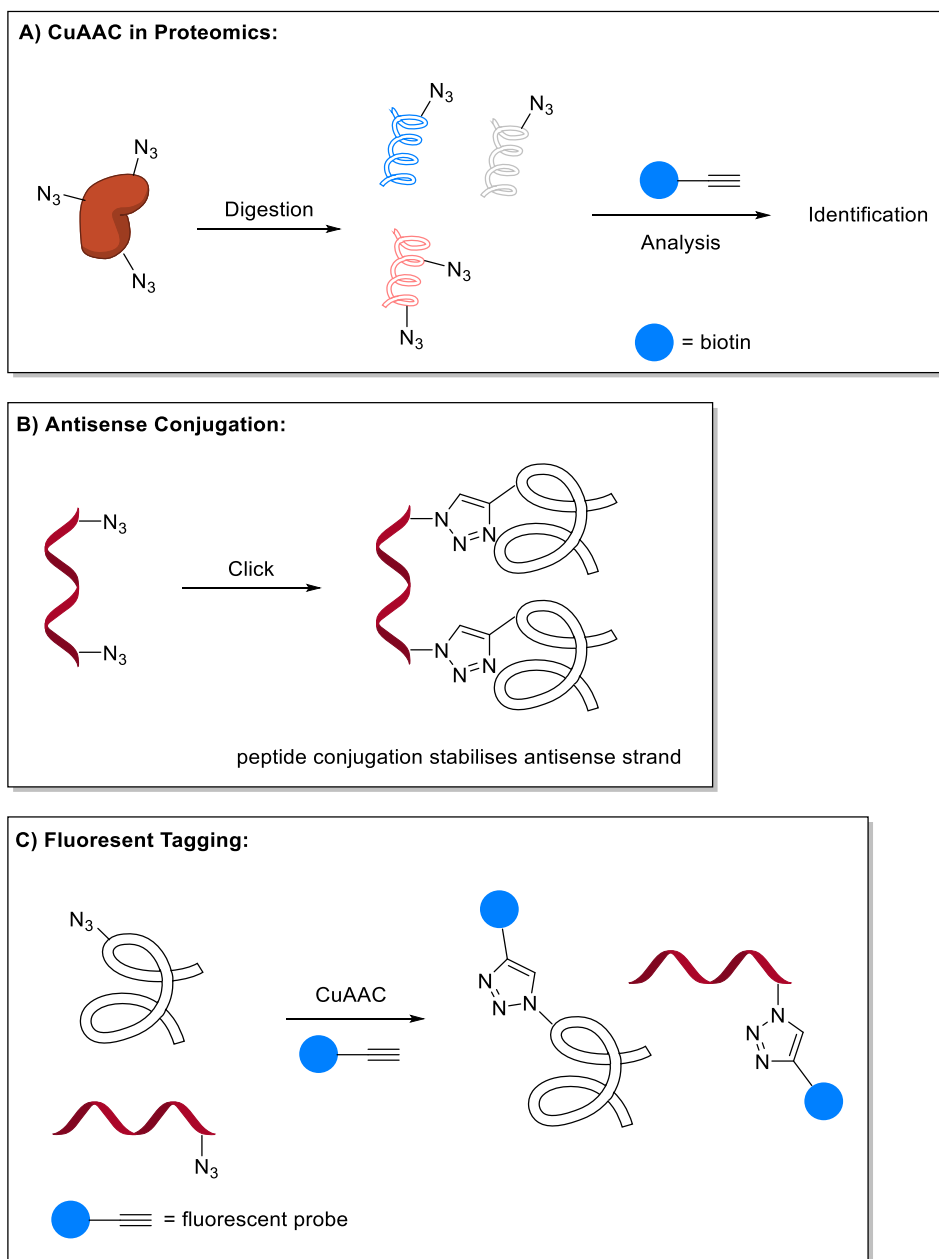


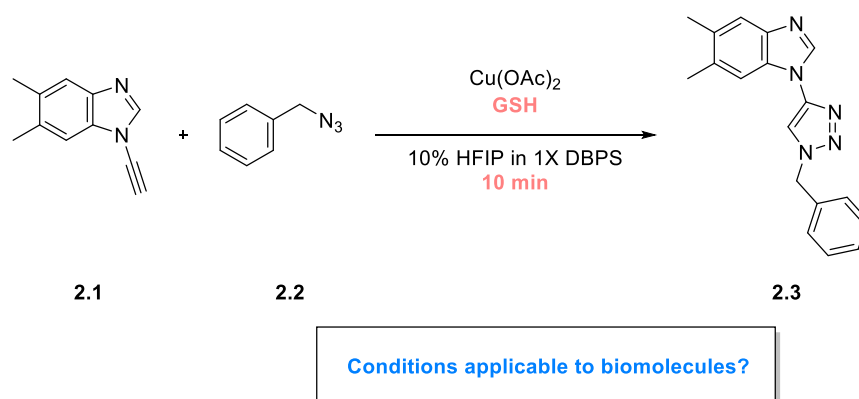
Figure 4.1. (A) CuAAC used to label azide modified proteins or peptides for proteomic analysis. (B) CuAAC used to conjugate peptides to oligonucleotides to improve pharmacokinetic properties. (C) CuAAC used to tag peptides/proteins and oligonucleotides with fluorescent labels.

There remains, however, one significant drawback of the CuAAC reaction for *in vivo* modifications of biomolecules. The abundance of chelating groups in biomolecules necessitates high copper catalyst loadings which can lead to biomolecule oxidation.⁹³ Histidine, cysteine, and methionine are especially prone to copper induced oxidation.¹⁰⁰ NaAsc, while usually benign, can also cause side reactions and toxicity at high NaAsc concentrations.⁹² Whilst Cu-chelating ligands such as THPTA and BTAA can counteract

some of this oxidative damage,²⁵⁸ the build-up of oxidative damage could lead to reagent degradation and cytotoxicity.

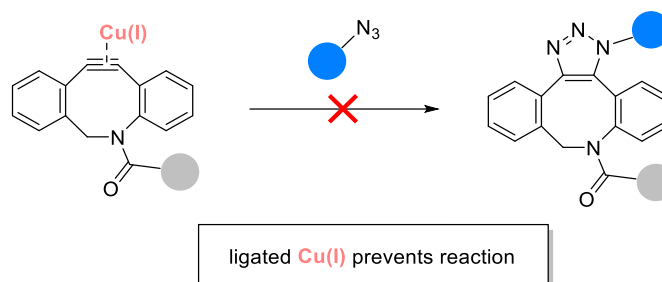
4.2 Hypothesis to be tested in this Chapter

The ynamine-CuAAC conjugation conditions identified in Chapter 3 resulted in full conversion of ynamine **2.1** with benzyl azide **2.2** in under 10 min utilising HFIP as a co-solvent and only 100 μM $\text{Cu}(\text{OAc})_2$ and GSH (Scheme 4.1). These conditions offer an alternative to conventional *in vitro* CuAAC conditions (*i.e.*, CuSO_4 , THPTA and NaAsc)^{255,257,259–261} commonly used for the conjugation of alkyne/azide-modified peptides or oligonucleotides with functional groups.



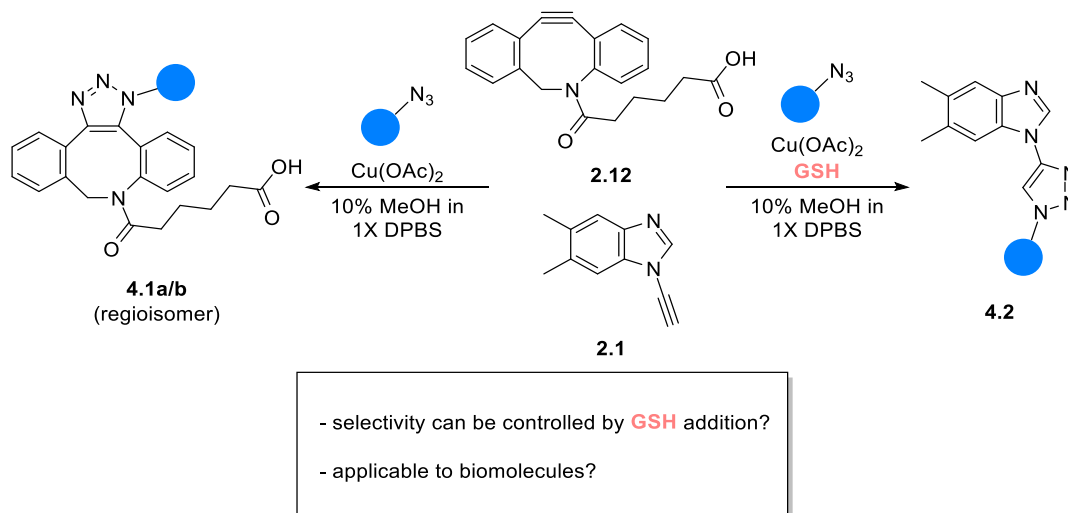
Scheme 4.1. Reaction of ynamine **2.1** with benzyl azide (**2.2**) using the optimised CuAAC conditions in 10% HFIP. Conditions: **2.1** (200 μM), $\text{Cu}(\text{OAc})_2$ (100 μM), **2.2** (500 μM), GSH (100 μM), 10% HFIP in 1X DPBS, rt, 10 mins.

Recently, dual^{262,263} or even triple^{264,265} modification of biomolecules using multiple bio-orthogonal reactions in tandem has become a powerful technique. For example, Yoshida *et al.* carried out a CuAAC reaction selectively in the presence of a strained alkyne.²⁶⁶ It was proposed that Cu(I) co-ordinates to the strained alkyne and acts as a transient protecting group (Scheme 4.2). By the addition of a copper scavenger (*e.g.*, EDTA), the strained alkyne could be deprotected and further functionalised.²⁶⁷



Scheme 4.2. Ligation of Cu(I) to alkyne prevents SPAAC reaction.

Potentially, this strategy could be employed for the ynamine-CuAAC and GSH used to modulate reactivity. In the presence of GSH, Cu(II) would be reduced to Cu(I) and protect the strained alkyne, leaving the ynamine free to react to form **4.2** (Scheme 4.3). Conversely, in the absence of GSH, the SPAAC reaction could proceed to form **4.1a/b**.



Scheme 4.3. Potential strategy to either form **4.1a/b** or **4.2** depending on GSH addition.

4.3 Aims of Chapter 4

The specific aims of this chapter are:

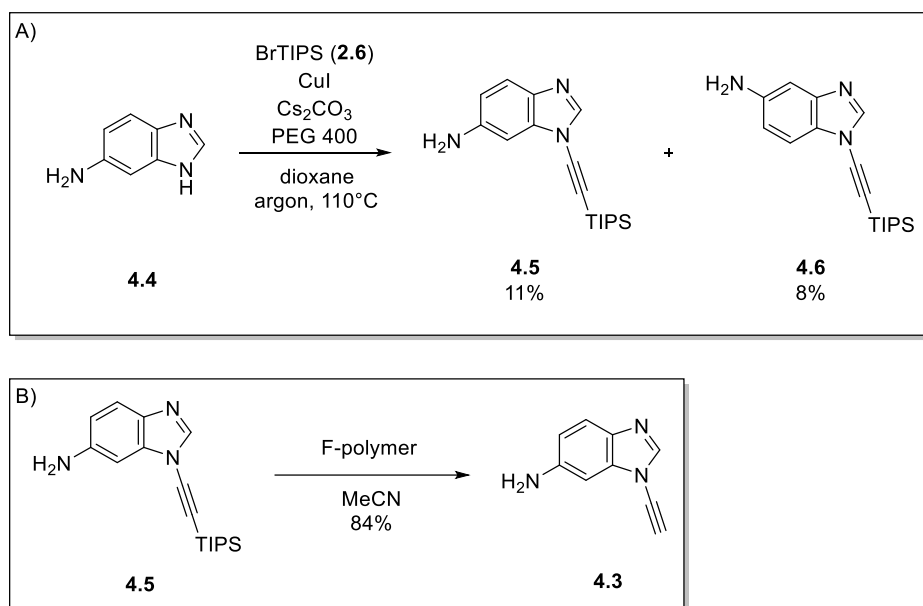
- (i) Synthesise azide modified peptides and test optimal ynamine-CuAAC conditions.
- (ii) Develop sequential CuAAC/SPAAC labelling protocol on small molecules and transfer to peptides.
- (iii) Explore the reactivity of an ynamine-modified oligonucleotide.

4.4 Results & Discussion

4.4.1 Synthesis of Reagents

All experiments performed so far used ynamine **2.1**, which does not offer any functional groups for further modification. To demonstrate the utility of ynamines as a tool for bioconjugation, the preparation of an ynamine with a functional handle (**4.3**) was explored. The TIPS-protected ynamine **4.5** was synthesised following the standard protocol¹⁹⁷ and obtained in 11% yield (Scheme 4.4A). Unfortunately, poor yields are usually obtained when a functional group is present on the benzimidazole. The poor yields are attributed to copper co-ordination which prevents catalysis.²⁶⁸ The yields are further reduced as both isomers (**4.5** and **4.6**) are formed in roughly equal amounts. The regio-isomers had previously been determined by other members of the group through NOESY interactions between the TIPS protons and the proton at the 7-position on the benzimidazole ring.

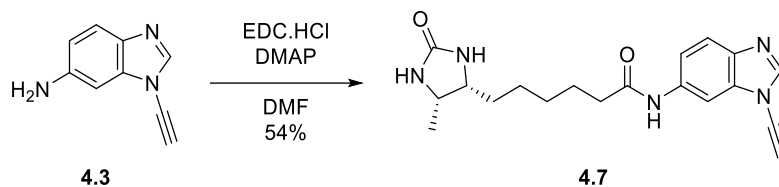
Deprotection of the TIPS group of **4.5** with fluoride on polymer yielded ynamine **4.3** in 84% (Scheme 4.4B).



Scheme 4.4. (A) Synthesis of **4.6**. Conditions: **4.4** (1 equiv), **2.6** (1.2 equiv), CuI (0.1 equiv), Cs₂CO₃ (1.1 equiv), PEG 400 (0.2 equiv), 110 °C, 2 days. (B) Synthesis of **4.3**. Conditions: **4.5** (1 equiv), fluoride on polymer (1.5 equiv), rt, overnight.

Amide coupling of **4.3** with *d*-desthiobiotin (a structural analogue of *d*-biotin) afforded **4.7** in 54% yield (Scheme 4.5). Biotin is commonly used as a functional handle for pulldown assays. Tagged biomolecules can easily be trapped on streptavidin beads and cellular debris be washed

off. The purified biomolecule can then be eluted from the column. Due to the femtomolar affinity of biotin for streptavidin,²⁶⁹ the release can be problematic. Desthiobiotin, a biotin analogue, exhibits a lower affinity for streptavidin and can be more readily eluted from the column (*e.g.*, *via* displacement with biotin).²⁷⁰



Scheme 4.5. Synthesis of **4.7**. Conditions: *d*-desthiobiotin (1 equiv), **4.3** (1.2 equiv), EDC.HCl (1.2 equiv), DMAP (0.2 equiv), rt, overnight.

Two cell penetrating peptides were chosen to demonstrate the suitability of the optimised ynamine-CuAAC protocol. The first, Penetratin,^{271,272} is a commonly used cell penetrating peptide, which is derived from the homodomain ANTENNAPEPEDIA, a transcription factor in *Drosophila*. Glycine and azido-lysine were attached to the C-terminus to give Penetratin-Az (Figure 4.2). The peptide was synthesised on a Protein Technologies Tribute automated synthesizer using Rink amide resin. Dithiothreitol (DTT) was added to the cleavage cocktail to prevent oxidation of the methionine residue. DTT can reduce the azide²⁷³ during the prolonged cleavage time (4 h) needed for Penetratin-Az (to remove all Pbf-protecting groups from the arginine residues). Fortunately, azide reduction was not observed in this case.

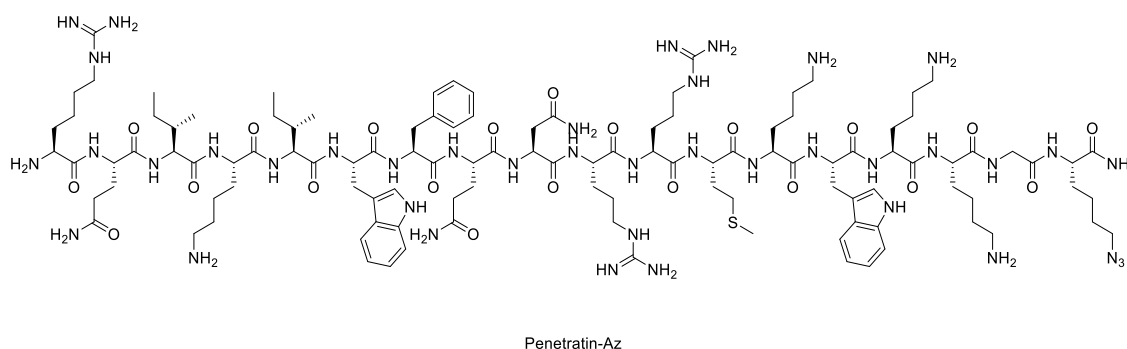


Figure 4.2. Structure of Penetratin-Az.

The second cell-penetratin peptide (TP2)²⁷⁴ is more lipophilic and includes fewer copper chelating moieties. An azido-lysine building block was attached to the C-terminus to give TP2-Az (Figure 4.3). The preparation of this peptide was achieved on Rink amide resin using the standard solid phase peptide coupling protocols.

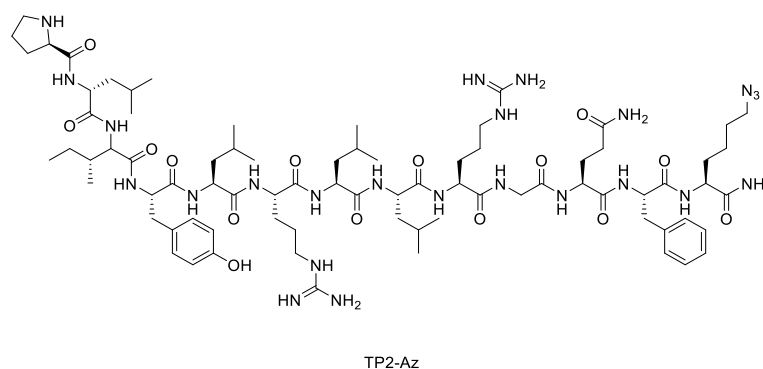


Figure 4.3. Structure of TP2-Az.

4.4.2 Optimization of the Solvent System used in the Ynamine-CuAAC Conjugation

With the synthesised reagents in hand, the influence of the co-solvent was tested first. The click reaction between ynamine **4.7** and Penetratin-Az was used as a model reaction. The reaction was performed using the previously optimised conditions (*i.e.*, GSH and Cu(OAc)₂, 100 μ M) in MeOH, TFE and HFIP as well as with the initial conditions reported in Chapter 2 (*i.e.*, Cu(OAc)₂ = 350 μ M and GSH = 1 mM, ratio = ~1:3) in HFIP for comparison. All reactions described in this chapter were performed according to the HPLC assay described in Chapter 2 and carried out in triplicate (unless stated otherwise).

As before, HFIP provided the fastest and highest conversions (~80% in 2 h) when compared with MeOH or TFE which only reached ~40% conversion after 4 h (Figure 4.4). The initial conditions (~1:3) displayed an induction period (~2 h) as was observed with small molecules. These results demonstrate that findings obtained for small molecules can generally be translated to peptides.

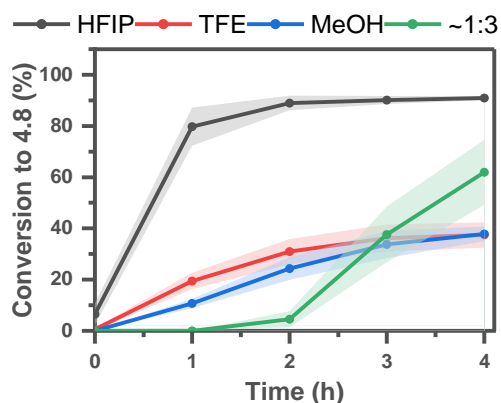
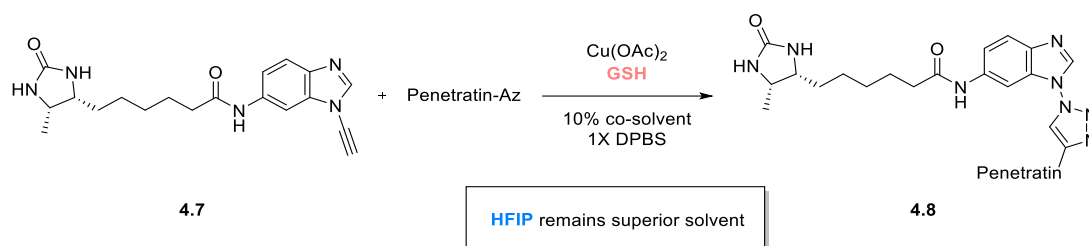


Figure 4.4. Solvent screen for the reaction of ynamine **4.7** and Penetratin-Az. *Conditions (HFIP, TFE and MeOH):* **4.7** (200 μ M), Penetratin-Az (200 μ M), Cu(OAc)₂ (100 μ M), GSH (100 μ M), 10% co-solvent in 1X DPBS, rt, 4 h. *Conditions (~1:3):* **4.7** (200 μ M), Penetratin-Az (200 μ M), Cu(OAc)₂ (350 μ M), GSH (1 mM), 10% HFIP in 1X DPBS, rt, 4 h. Buffer pH = 7.4. Shaded areas represent the standard deviation calculated from three experiments.

As HFIP was superior to both TFE and MeOH, the ligation of ynamine **4.7** with TP2-Az was only repeated in HFIP, and 90% conversion was achieved in under 1 h. The faster reaction rate could be due to the reduced numbers chelating moieties in TP2-Az. Alternatively, the increased lipophilicity could boost an “on water” effect and or a combination of both increase the rate of the reaction.

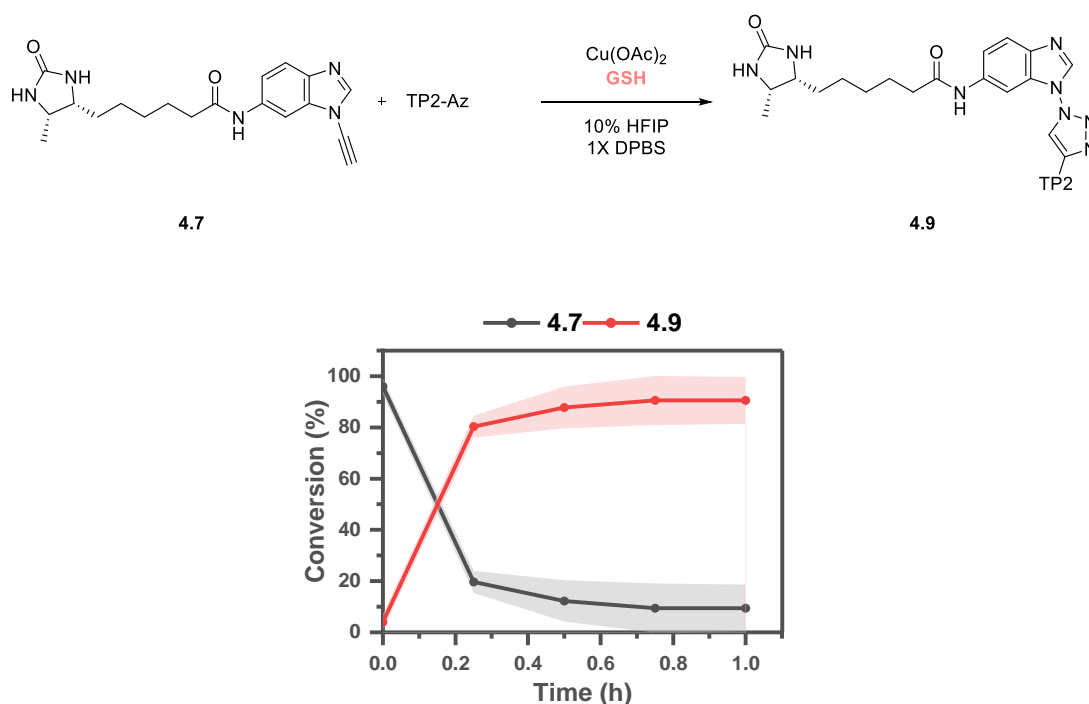


Figure 4.5. Reaction of ynamine **4.7** with TP2-Az using the optimised conditions. *Conditions:* **4.7** (200 μM), TP2-Az (200 μM), $\text{Cu}(\text{OAc})_2$ (100 μM), GSH (100 μM), 10% HFIP in 1X DPBS, rt, 1 h. Buffer pH = 7.4. Shaded areas represent the standard deviation calculated from three experiments.

4.4.3 The Ynamine-CuAAC Ligation is Modulated by Glutathione Addition

To explore the possibility of modulating CuAAC or SPAAC reactivity by the addition of GSH in competition reactions, equimolar amounts of ynamine **2.1** and DBCO **2.12** were incubated with one equivalent of picolyl azide (**2.42**) (200 μM each). The chelating azide should offset the reduction in reactivity when lowering the azide concentration from the previous small molecule standard conditions (500 μM). The reactions were performed using 350 μM $\text{Cu}(\text{OAc})_2$ and 1 mM GSH to ensure efficient protection of DBCO **2.12** by Cu(I).

In the absence of GSH, DBCO **2.12** reacted with picolyl azide **2.42** exclusively to give a mixture of regio-isomers (**4.10a/b**) and no ynamine-triazole (**2.3c**) formed (Figure 4.6A). In the presence of GSH, the reverse was observed (> 80% **2.3c** and < 5% DBCO triazoles) (Figure 4.6B). To confirm that the observed reactivity was due to Cu(I) co-ordination, DBCO **2.12** was reacted with picolyl azide (**2.42**) in the presence of CuI (350 μM) (Experimental Figure 4.15). Indeed, slow conversion (< 5%) was observed and the reaction profile matched the competition experiment in the presence of GSH (Figure 4.6B).

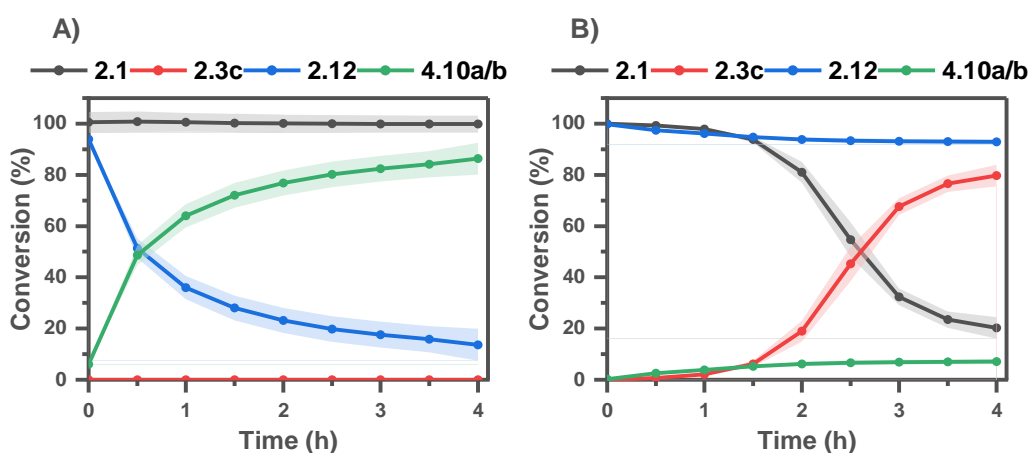
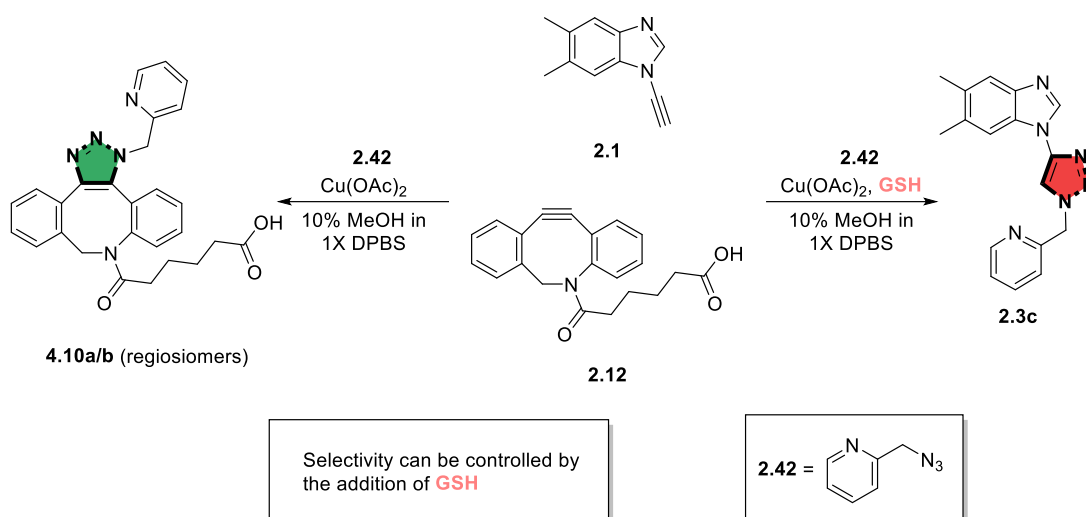


Figure 4.6. (A) Competition reaction between ynamine **2.1** and DBCO **2.12** without GSH. *Conditions:* **2.1** (200 μ M), **2.12** (200 μ M), Cu(OAc)₂ (350 μ M), **2.42** (200 μ M), 10% MeOH in 1X DPBS, rt, 4 h. (B) Competition reaction between ynamine **2.1** and DBCO **2.12** in the presence of GSH (1 mM). *Conditions:* **2.1** (200 μ M), **2.12** (200 μ M), Cu(OAc)₂ (350 μ M), **2.42** (200 μ M), GSH (1 mM), 10% MeOH in 1X DPBS, rt, 4 h. Buffer pH = 7.4. Shaded areas represent the standard deviation calculated from three experiments.

4.4.4 Chemoselective Ynamine Click Labelling of Azido Peptides

4.4.4.1 Optimisation on Mono-Azido-Peptides

One potential issue with the competition labelling protocol when using azido peptides is that the presence of Lewis basic sites in the peptides might inhibit the Cu(I) catalyst and weaken DBCO protection. This was explored using a reaction between DBCO **2.12** and TP2-Az with varying Cu:GSH ratios to observe the effect on DBCO inhibition. The conditions chosen were: control (no Cu or GSH), 1:1 (optimal CuAAC conditions, 500 μ M each), 1:2.5 (DoE conditions, 400 μ M Cu(OAc)₂ and 1 mM GSH) and 1:2.85 (optimal small molecule

conditions, 350 μM $\text{Cu}(\text{OAc})_2$ and 1 mM GSH). For the optimal CuAAC conditions, the concentration of copper and GSH was raised to 500 μM (from 100 μM) to ensure enough Cu(I) was present to co-ordinate to DBCO **2.12**.

In the absence of $\text{Cu}(\text{OAc})_2$ and GSH, the SPAAC reaction reached maximum conversion within 1 h, whereas the reactivity was reduced in the presence of $\text{Cu}(\text{OAc})_2$ and GSH. A Cu:GSH of 1:1 inhibited DBCO the best (only 25% conversion after 4 h), while a ratio of 2.5 and 2.85 still gave 40 – 50% conversion after 4 h.

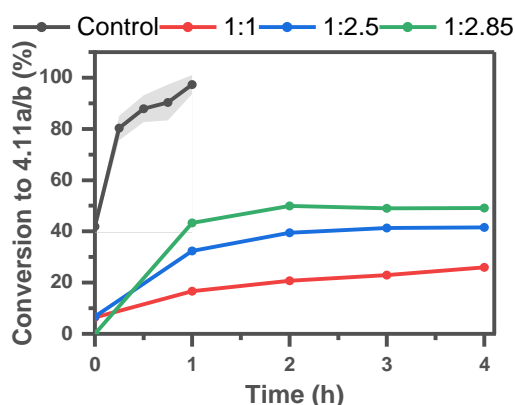
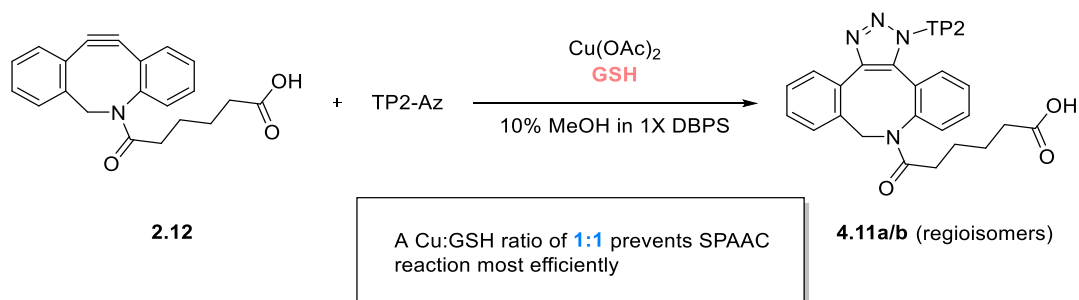


Figure 4.7. Ratio of Cu:GSH most effective at inhibiting the SPAAC reaction between DBCO **2.12** and TP2-Az. *Conditions (Control):* **2.12** (200 μM), TP2-Az (200 μM), 10% HFIP in 1X DPBS, rt, 4 h. Performed in duplicate. *Conditions (1:1):* **2.12** (200 μM), TP2-Az (200 μM), $\text{Cu}(\text{OAc})_2$ (500 μM), GSH (500 μM), 10% MeOH in 1X DPBS, rt, 4 h. Single experiment. *Conditions (1:2.5):* **2.12** (200 μM), TP2-Az (200 μM), $\text{Cu}(\text{OAc})_2$ (400 μM), GSH (1 mM), 10% MeOH in 1X DPBS, rt, 4 h. Single experiment. *Conditions (1:2.85):* **2.12** (200 μM), TP2-Az (200 μM), $\text{Cu}(\text{OAc})_2$ (350 μM), GSH (1 mM), 10% MeOH in 1X DPBS; Single experiment. Buffer pH = 7.4.

These results demonstrate that DBCO inhibition in the presence of peptides decreases when compared with the small molecule experiments. Potentially, chelating moieties within TP2-Az (two arginine residues) could bind copper and cause incomplete protection of the DBCO triple bond. The ratio of 1:1 performed best and was chosen for the future experiments. However, the effects of potential interference from the amide in ynamine **4.7** were unknown (vs di-methyl ynamine **2.1**).

4.4.4.2 Selective Click Labelling Penetratin-Az and TP2-Az with an Ynamine or DBCO

For selective click labelling of Penetratin-Az via either CuAAC or SPAAC reactions, HFIP was the co-solvent of choice to ensure complete conversion for the ynamine-CuAAC. In competition experiments without GSH, the SPAAC reached >90% conversion after 30 min and no CuAAC product **4.8** was observed (Figure 4.8A). The addition of GSH (500 μ M) inhibited the SPAAC reaction (< 10% conversion to **4.12a/b** after 1 h) and ~80% CuAAC-triazole **4.8** was formed after 4 h (Figure 4.8B).

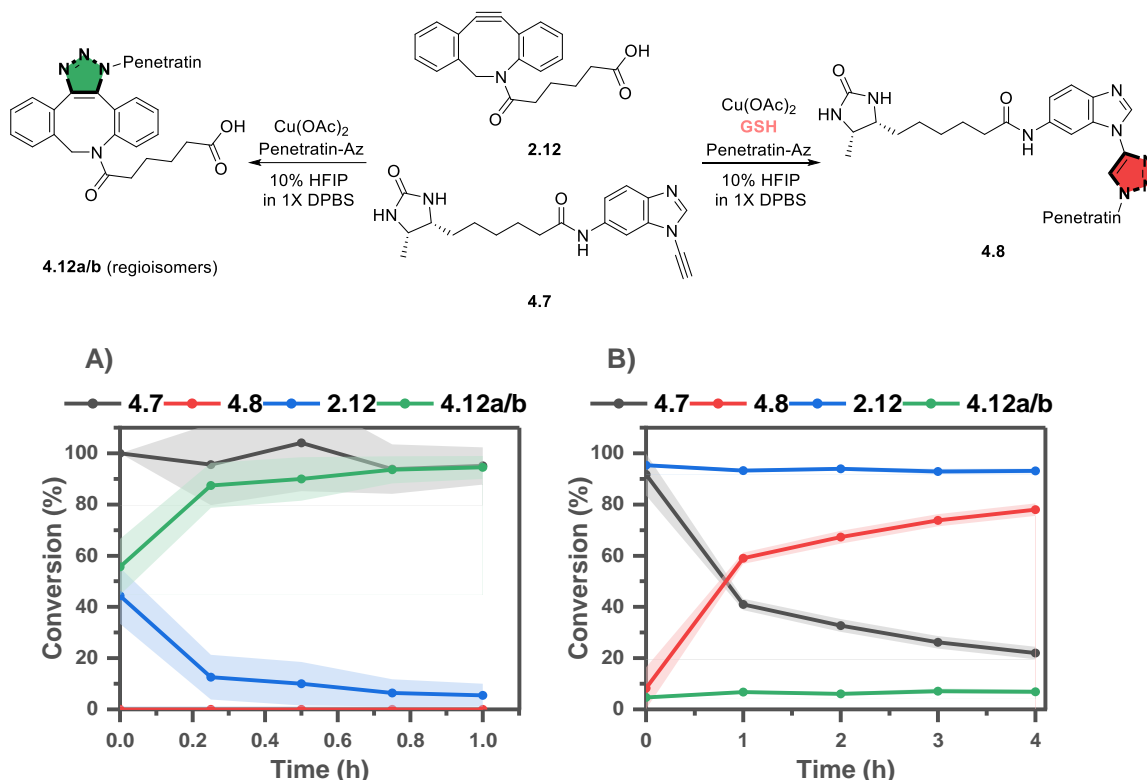


Figure 4.8. (A) Selective labelling of Penetratin-Az with DBCO **2.12** in the presence of ynamine **4.7**. *Conditions:* **4.7** (200 μ M), **2.12** (200 μ M), Penetratin-Az (200 μ M), Cu(OAc)₂ (500 μ M), 10% HFIP in 1X DPBS, rt, 1 h. (B) Selective labelling of Penetratin-Az with ynamine **4.7** in the presence of DBCO **2.12** facilitated by GSH. *Conditions:* **4.7** (200 μ M), **2.12** (200 μ M), Penetratin-Az (200 μ M), Cu(OAc)₂ (500 μ M), GSH (500 μ M), 10% HFIP in 1X DPBS, rt, 4 h. Buffer pH = 7.4. Shaded areas represent the standard deviation from calculated from three experiments.

The same series of experiments was repeated with TP2-Az. Unfortunately, both products (**4.9** and **4.11a/b**) precipitated in 10% HFIP/1X DPBS eventually but remained soluble for most of the analysis. Again, ynamine-triazole (**4.9**) only formed in the presence of GSH (Figure 4.9A)

and in the absence of GSH the DBCO-triazoles (**4.11a/b**) were the major products (Figure 4.9B).

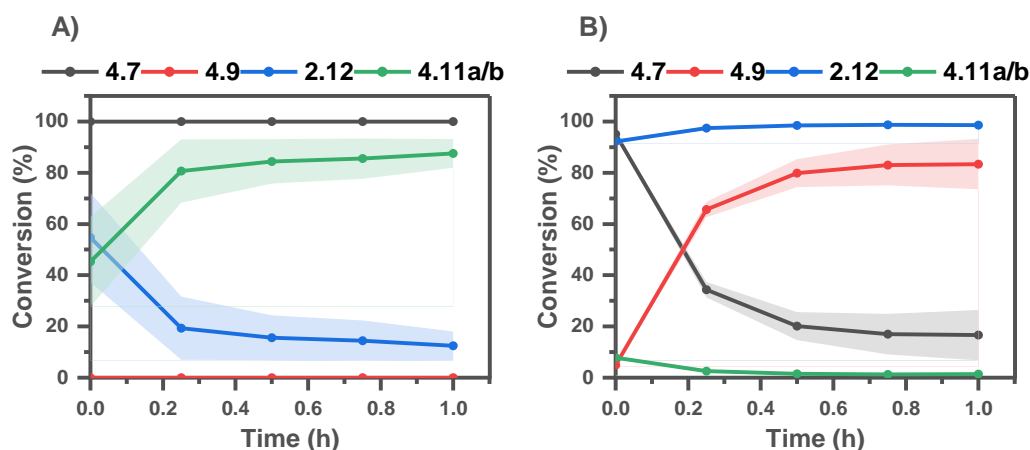
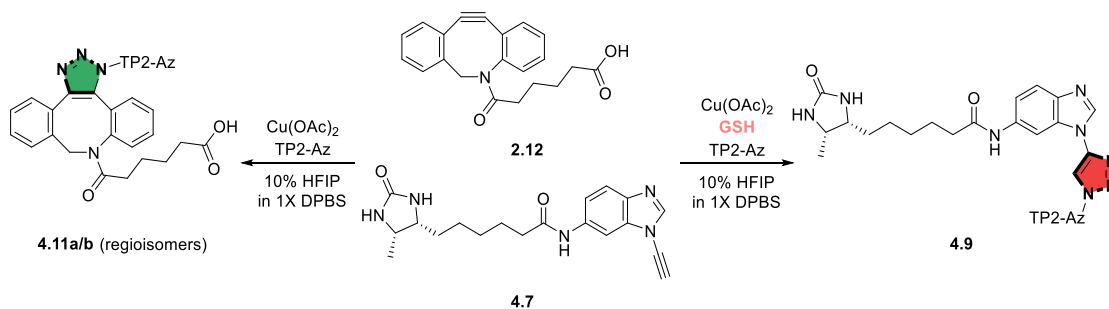


Figure 4.9. (A) Selective labelling of TP2-Az with DBCO **2.12** in the presence of ynamine **4.7**. Conditions: **4.7** (200 μM), **2.12** (200 μM), TP2-Az (200 μM), $\text{Cu}(\text{OAc})_2$ (500 μM), 10% HFIP in 1X DPBS, rt 1 h. (B) Selective labelling of TP2-Az with ynamine **4.7** in the presence of DBCO **2.12** facilitated by GSH. Conditions: **4.7** (200 μM), **2.12** (200 μM), TP2-Az (200 μM), $\text{Cu}(\text{OAc})_2$ (500 μM), GSH (500 μM), 10% HFIP in 1X DPBS. Buffer pH = 7.4. Shaded areas represent the standard deviation from calculated from three experiments.

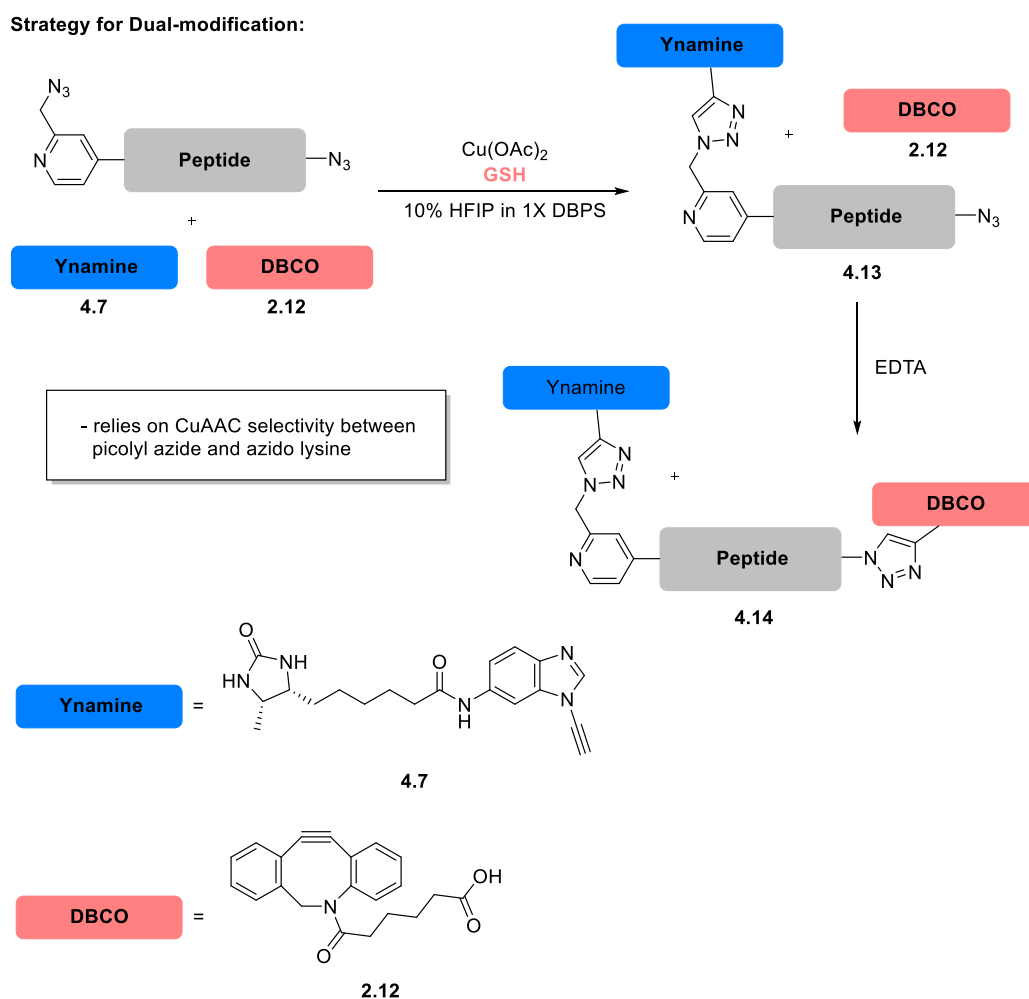
When comparing the SPAAC reaction on peptides (Figure 4.8 and Figure 4.9) with the reaction on small molecules (Figure 4.6), the peptide SPAAC reaction was faster. The competition reaction on small molecules was performed in MeOH and the peptide labelling in HFIP. This could indicate that HFIP might also accelerate the SPAAC reaction. This is an interesting observation and might warrant further investigation in the future.

Extending this strategy to the selective labelling of azides with ynamines (*e.g.*, **4.7**) and DBCO **2.12** in the same peptide would increase the power of this methodology.

4.4.5 Sequential Click Labelling of Dual Azide-Modified Peptides

4.4.5.1 Strategy for Sequential Labelling

A sequential labelling approach was then explored using a peptide outfitted with a Cu-chelating and non-chelating azide group. In this design, DBCO **2.12** or the ynamine **4.7** must react selectively with one azide first to avoid creating a mixture of regio-isomers. Ynamine **4.7** should preferentially react first with the picolyl azide over the aliphatic azide. The aliphatic azide would then be free to react with DBCO after the addition of a Cu(I) chelating agents such as EDTA (Scheme 4.6).



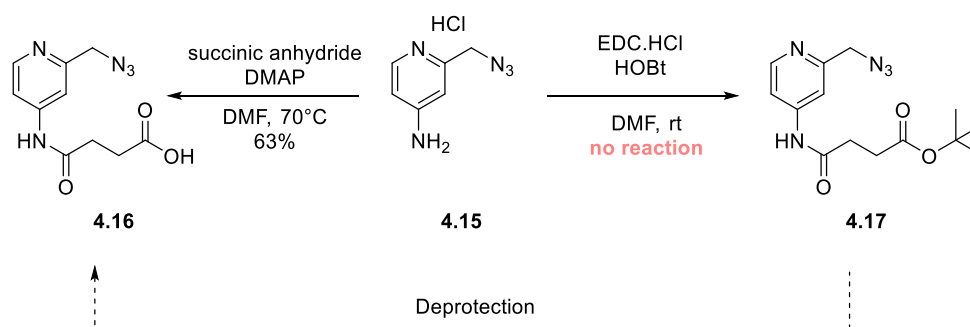
Scheme 4.6. Strategy for selective sequential labelling of peptides with an ynamine and DBCO.

4.4.5.2 Solid Phase Synthesis of a Dual Azide-Labelled Peptide (Pico-TP2-Az)

As Penetratin-Az and TP2-Az were already modified on the C-terminus, it was envisioned to modify the N-terminus with picolyl azide. Compound **4.15** was identified as a suitable starting

material for either an amide coupling with mono-protected succinic acid or a ring opening reaction with succinic anhydride (Scheme 4.7). The created picolyl azide acid (**4.16**) could then be coupled to the peptide.

The amide coupling to form picolyl azide **4.17** was unsuccessful and no conversion to product was observed. Possibly, the use of reagents as hydrogen chloride salts could lower the pH and prevent either acid activation or deactivate the aniline by protonation. Instead, ring opening of succinic anhydride with amine **4.15** led to full consumption of the starting material. Initially, the reaction was conducted at room temperature with 6 equiv of succinic anhydride. However, this complicated purification as succinic anhydride co-eluted with the product using RP-HPLC (**4.16**). Full consumption of the starting material was achieved with only 2 equiv of succinic anhydride and heating the reaction to 70 °C, but isolated yields remained poor (< 40%). Inspection of the aqueous phase by TLC revealed that **4.16** was still present after extraction. The aqueous work up was improved by adjusting the pH to ~ 4.1 and extracting with MeTHF. The final optimised procedure afforded the product **4.16** as a white solid in 63% yield. Electron-rich picolyl azide derivatives have been shown to be more reactive than their electron-poor analogues. In **4.15**, the lone pair of the amine is free donate electron density into the aromatic ring, whereas the amide in **4.17** will be a weaker electron donor (due to adjacent carbonyl). Potentially, this could reduce reactivity and could be solved by disconnecting the amide from the picolyl system *via* a short linker. However, the starting material **4.15** was readily available.



Scheme 4.7. Synthetic strategy to for picolyl azide **4.16**. Reaction using EDC.HCl and HOBT was not successful. Ring opening of succinic anhydride instead afforded the product **4.16**. *Conditions:* **4.15** (1 equiv), succinic anhydride (2 equiv), DMAP (1.1 equiv), 70°C, overnight.

With picolyl azide **4.16** in hand, conditions for the on-resin amide coupling to TP2-Az were explored. The use of HATU/DIPEA (3 equiv) led to minimal conversion to Pico-TP2-Az, while the combination of DIC/OxymaPure® (3 equiv) afforded higher but still incomplete conversion (~ 30%). After heating the reaction to 75 °C for 1 h in the microwave, TP2-Az was

fully consumed and Pico-TP2-Az could be isolated successfully after deprotection, cleavage and purification (Figure 4.10).

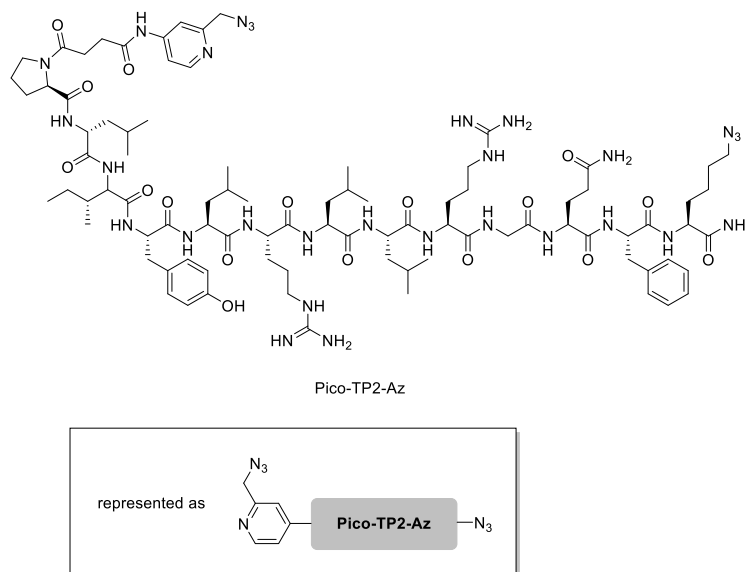
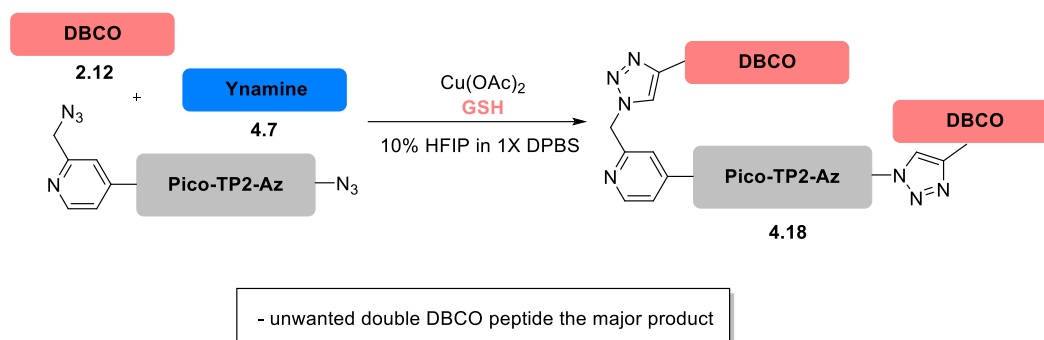


Figure 4.10. Structure of Pico-TP2-Az.

4.4.5.3 Exploration of the Chemoselective Dual-Labelling of Azide-Modified Peptide Pico-TP2-Az

With Pico-TP2-Az in hand, the dual labelling with DBCO **2.12** and ynamine **4.7** was tested. As a baseline, the original competition reaction conditions (350 μM $\text{Cu}(\text{OAc})_2$ and 1 mM GSH) were tested first in 10% HFIP. Unfortunately, the reaction could not be followed in the usual HPLC setup, as precipitation of the peptide and eventually ynamine **4.7** was observed. Instead, the reaction was performed in an Eppendorf tube quenched with EDTA after 4 h to stop the CuAAC reaction and the SPAAC reaction allowed to proceed for a further 2 h. Then the reaction solvent was removed, the residue was redissolved in 1:1 $\text{H}_2\text{O}/\text{MeCN}$ (0.1 % formic acid) and the analysed by UPLC-MS.

Unfortunately, these conditions furnished mostly double DBCO-labelled Pico-TP2-Az **4.18** (Scheme 4.8). This indicates that ynamine **4.7** was not reactive enough under these conditions and/or DBCO **2.12** was not inhibited.



Scheme 4.8. Attempted dual-labelling strategy mostly furnished double DBCO product **4.18**. *Conditions:* **4.7** (200 μ M), **2.12** (200 μ M), $\text{Cu}(\text{OAc})_2$ (350 μ M), GSH (1 mM), 10% HFIP in 1X DPBS, rt, 4 h, then EDTA addition (1 mM), further 2 h. Buffer pH = 7.4.

4.4.5.4 Chemoselective Ynamines Labelling of Azide-Modified Peptides

Due to this result (Scheme 4.8), it was decided to perform control experiments to gain more insight into the reaction. The optimised peptide competition reaction conditions (500 μ M $\text{Cu}(\text{OAc})_2$ and 500 μ M GSH, Figure 4.7) were tested on Pico-TP2-Az in the absence of DBCO to elucidate the chemoselectivity of the ynamine **4.7** over the two azides. As the solubility of the products was limited in HFIP, this reaction was performed in MeOH and DMSO instead to enable monitoring via the standard HPLC setup.

In both solvents, the reaction showed a similar pattern (Figure 4.11A and B). First, mono-labelled Pico-TP2-Az (**4.19**) formed which then slowly converted into double-labelled Pico-TP2-Az (**4.20**). The temporary bias towards the mono-labelled peptide (**4.19**) makes selective dual-labelling challenging. However, in the solvent screen (see Section 3.4.10) DMSO afforded faster reaction rates than MeOH. If selectivity correlates with reactivity, then the reaction might be more selective in HFIP.

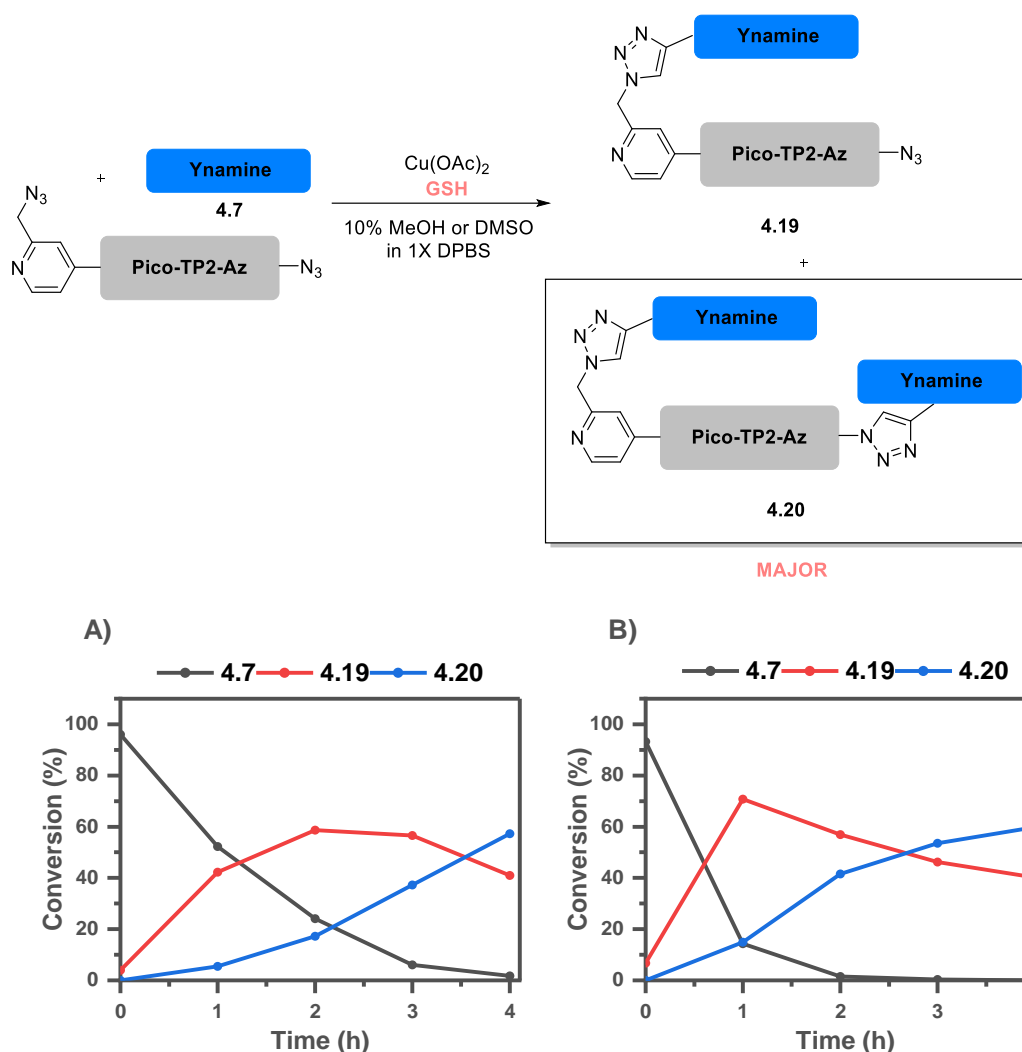


Figure 4.11. (A) Chemoselectivity of ynamine **4.7** over terminal picolyl azide or azido-lysine in MeOH. *Conditions:* **4.7** (200 μ M), Pico-TP2-Az (200 μ M), Cu(OAc)₂ (500 μ M), GSH (500 μ M), 10% MeOH in 1X DPBS, rt, 4 h. Single experiment. (B) Chemoselectivity of ynamine **4.7** over terminal picolyl azide or azido-lysine in DMSO. *Conditions:* **4.7** (200 μ M), Pico-TP2-Az (200 μ M), Cu(OAc)₂ (500 μ M), GSH (500 μ M), 10% DMSO in 1X DPBS, rt, 4 h. Single experiment. Buffer pH = 7.4

Consequently, the experiment was repeated in HFIP. Due to the precipitation issues, the reaction was performed using the above-mentioned procedure (see 4.4.5.3, reaction in Eppendorf tube, followed by work up and UPLC-MS analysis). Unfortunately, peak baseline resolution could not be achieved even after extensive gradient tuning, but the mass analysis allowed identification of the different species. After 30 mins, no ynamine **4.7** remained and mostly mono-labelled peptide (**4.19**) formed (presumably labelled via picolyl azide) (Figure 4.12). Unlike previous experiments, only minimal double labelled peptide **4.20** (~ 10%) was

observed. These results show that more selective dual modification of Pico-TP2-Az might be achieved under these conditions.

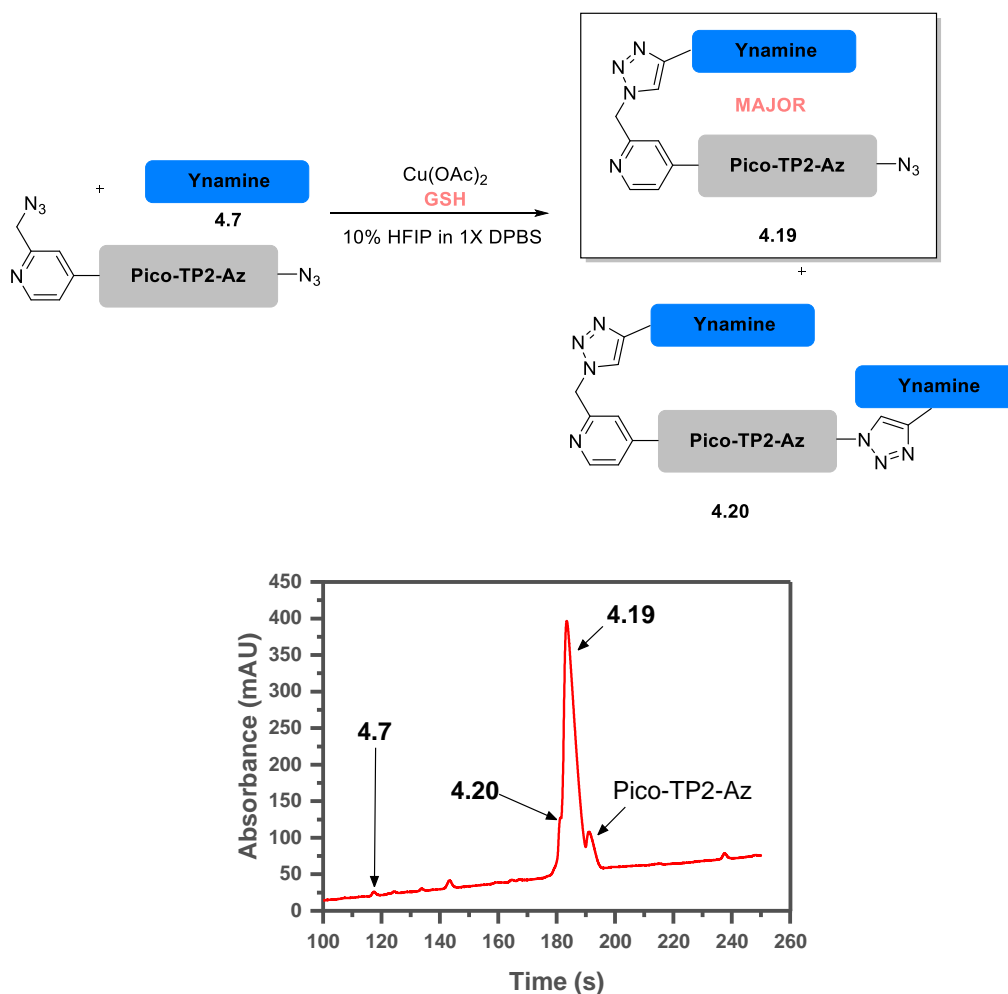


Figure 4.12. UV-UPLC-MS trace of labelling of Pico-TP2-Az with ynamine **4.7** (1 equiv) in HFIP. *Conditions:* **4.7** (200 μM), Pico-TP2-Az (200 μM), $\text{Cu}(\text{OAc})_2$ (500 μM), GSH (500 μM), 10% HFIP in 1X DPBS, rt, 30 min. Buffer pH = 7.4.

Therefore, this experiment was then repeated with the addition of DBCO (200 μM). The reaction was left for 2 h (to ensure full reaction of the ynamine **4.7**) before EDTA was added and left for a further 2 h before analysis. Unfortunately, all possible product configurations were obtained in a mixture (Figure 4.13).

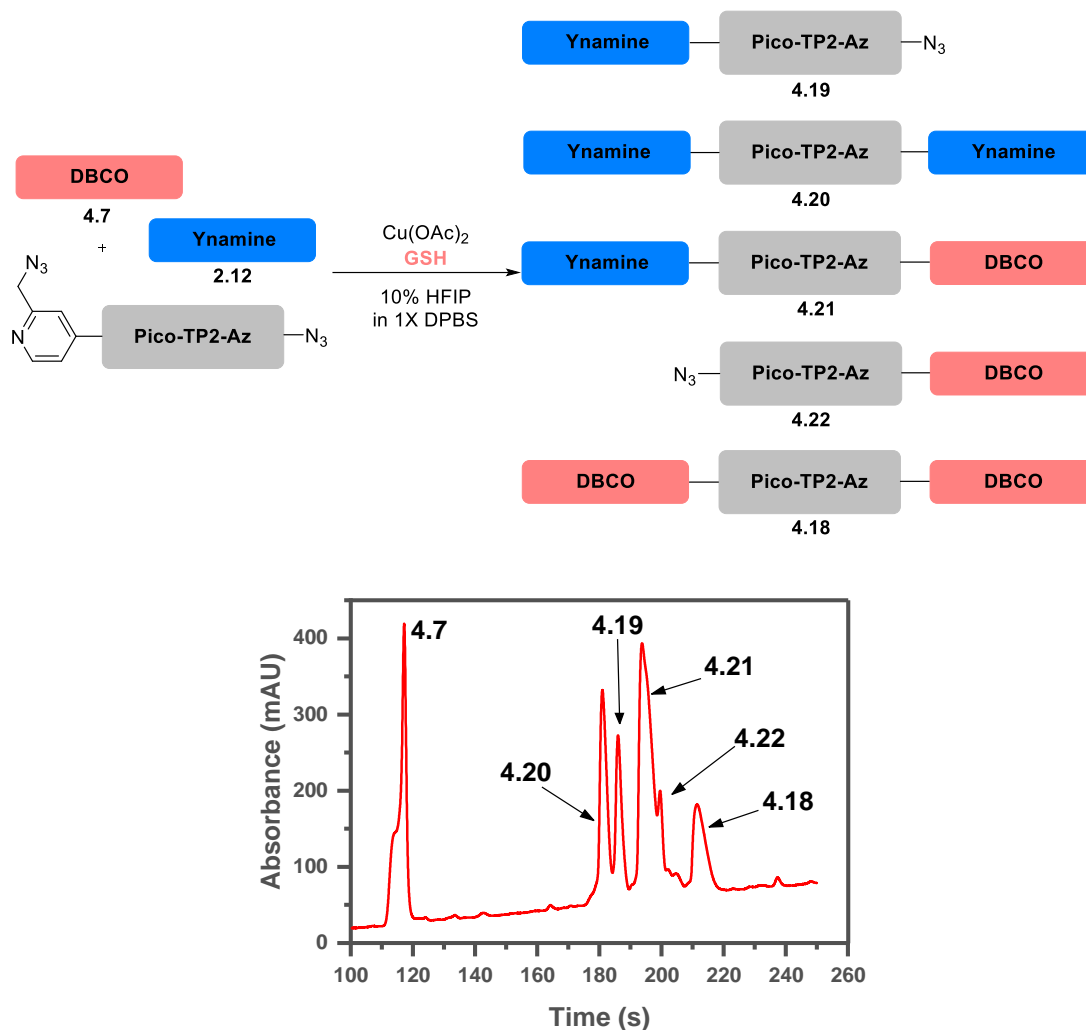


Figure 4.13. UV-UPLC-MS trace of attempted selective dual-labelling of Pico-TP2-Az with ynamine **4.7** and DBCO **2.12**. Conditions: **4.7** (200 μM), **2.12** (200 μM), $\text{Cu}(\text{OAc})_2$ (500 μM), GSH (500 μM), 10% HFIP in 1X DPBS, rt, 2 h, then EDTA (1 mM), further 2 h. Buffer pH = 7.4.

This result showed that further optimisation is needed. The formation of double ynamine-labelled (**4.20**) and DBCO-labelled peptide (**4.18**) indicate the challenges to achieve ultimate chemoselectivity in a dual azide-labelled peptide.

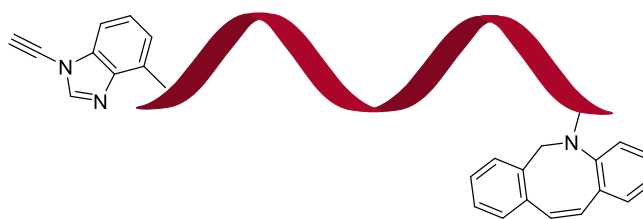
4.4.6 Synthesis of Ynamine-modified Oligonucleotides

Sequential labelling of a dual-azide modified peptide failed as the ynamine-CuAAC reaction was not selective for picolyl azide over an aliphatic azide. If the ynamine and DBCO were present in the peptide instead, the reaction might have succeeded. But presently, there is no

developed strategy for incorporation of an aromatic ynamine and/or DBCO in the same peptide.

However, a procedure has been developed in the group for incorporating aromatic ynamines into oligonucleotides. Commercial DBCO phosphoramidite building blocks for solid phase oligonucleotide synthesis are also available. Therefore, the synthesis of a dual modified oligonucleotide strand is tractable and would demonstrate the applicability of the sequential labelling protocol on a second class of biomolecules (Figure 4.14A). As such, the final aim of this chapter was to synthesise an ynamine-phosphoramidite **4.23** (Figure 4.14B) and incorporate it into a synthetic oligonucleotide.

A) Dual-modified Oligonucleotide



B) Ynamine-Phosphoramidite Building Block

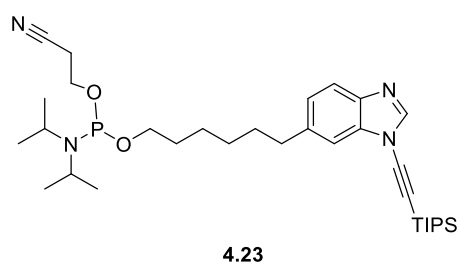
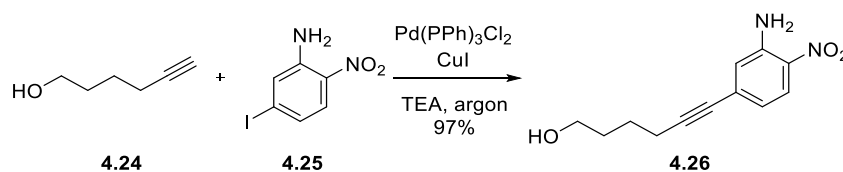


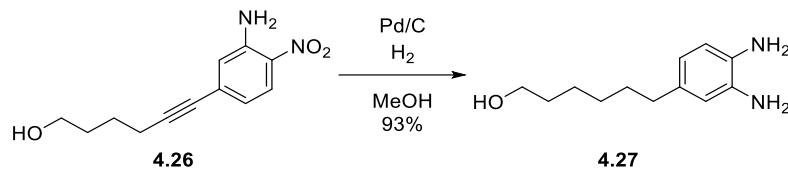
Figure 4.14. (A) Oligonucleotide modified with both an aromatic ynamine and DBCO. (B) Structure of ynamine-phosphoramidite **4.23**.

The synthesis of **4.23** starts with a Sonogashira reaction to couple the aliphatic hydroxyl tail **4.24** to 5-iodo-2-nitroaniline (**4.25**) (Scheme 4.9). The reaction proceeded in almost quantitative yield (97%) on a large scale (10 g). The product **4.26** was isolated after aqueous work up and precipitation.



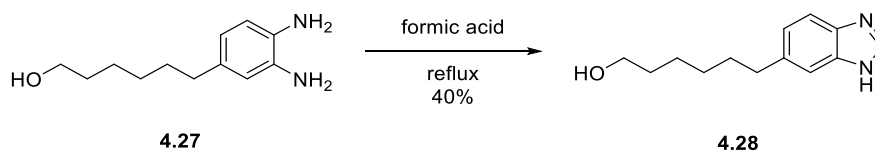
Scheme 4.9. Synthesis of **4.26**. Conditions: **4.25** (1 equiv), **4.24** (1.1 equiv), Pd(PPh)₃Cl₂ (0.1 equiv), CuI (0.08 equiv), rt, argon, 2 h.

Next the internal alkyne and the nitro group were reduced simultaneously in a Pd/C-catalysed hydrogenation (Scheme 4.10). Due to the large scale (10 g) the reaction took 2 days to reach full conversion and additional catalyst had to be added after the first day. Nevertheless, the reduced bis-aniline (**4.27**) could be obtained in 93% yield after removal of the catalyst.



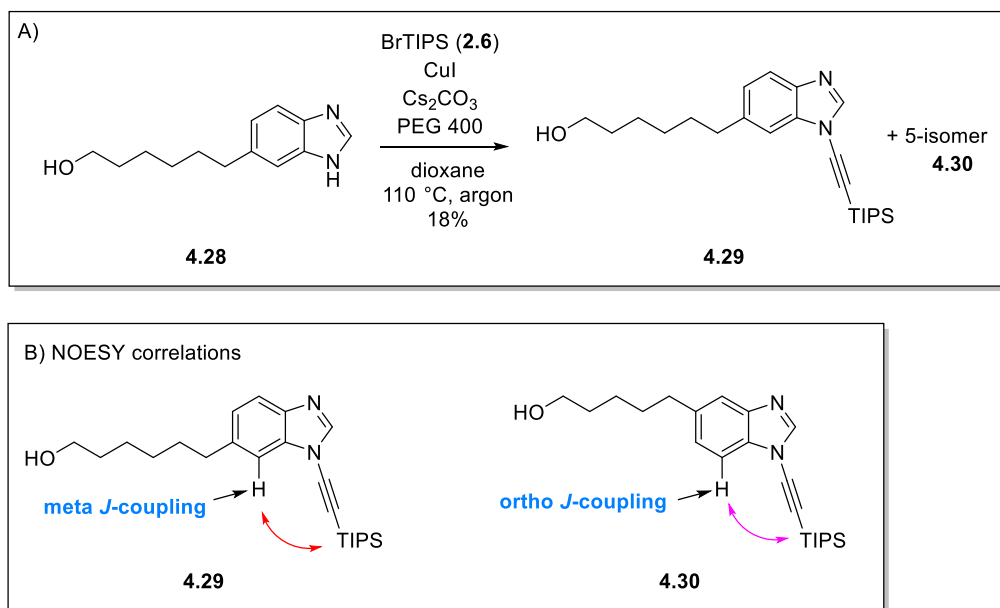
Scheme 4.10. Synthesis of **4.26**. Conditions: **4.27** (1 equiv), Pd/C, H₂ balloon, rt, 2 days.

Next the benzimidazole **4.28** was formed in a Phillips condensation with formic acid. The reaction gave a mediocre yield (40%) with several side products, none of which could be identified.



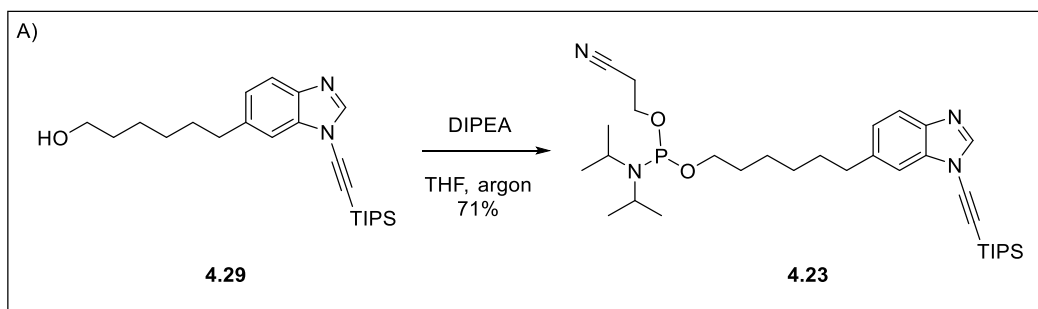
Scheme 4.11. Synthesis of **4.28**. Conditions: **4.27** (1 equiv), formic acid, reflux, overnight.

The benzimidazole **4.28** was coupled to bromo-TIPS-acetylene (**2.6**) using the standard reaction protocol (Scheme 4.12). As with the synthesis of **4.5**, the reaction performed poorly due to the presence of a functional group. The yield was further decreased as chromatographic separation was challenging and some co-elution of **4.28** and **4.29** was observed. Pure protected ynamine (**4.29**) could be isolated in 18% yield while the 5-isomer **4.30** could only be isolated as a mixture. The regio-isomers could be assigned due to the diagnostic NOSEY interaction of H-7 with the TIPS protons.

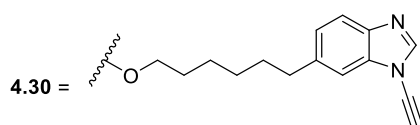
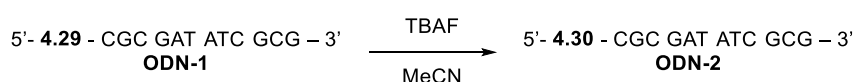


Scheme 4.12. (A) Synthesis of **4.29**. Conditions: **4.28** (1 equiv), **2.6** (1.6 equiv), CuI (0.05 equiv), Cs₂CO₃ (1.2 equiv), PEG 400 (0.1 equiv), 110 °C, argon, 2 days. (B) Diagnostic NOESY correlations enable identification of regio-isomers.

Finally, the phosphoramidite **4.23** was synthesised in 71% yield (Figure 4.13A) and then incorporated into a dodecamer by conventional phosphoramidite-based solid phase synthesis (**ODN-1**, Scheme 4.13B). The TIPS protecting group was removed successfully by passing TBAF over the solid phase column. Then the oligonucleotide was cleaved and purified by semi-preparative RP-HPLC to obtain **ODN-2**. This oligonucleotide will be used to test the optimal ynamine-CuAAC conditions in the future.



B) Oligonucleotide Synthesis:



Scheme 4.13. (A) Synthesis of **4.23**. *Conditions:* **4.29** (1 equiv), 2-Cyanoethyl *N,N*-diisopropylchlorophosphoramidite (3 equiv), DIPEA (9 equiv), rt, 1 h. B) ODN-1 synthesised by solid phase synthesis (for protocol see Experimental). Synthesis of ODN-2. *Conditions:* 1 M TBAF in THF (50 μ L) in dry MeCN (1.95 mL), rt, 3 min.

4.5 Conclusion & Future Work

In summary, two azide modified cell penetrating peptides (Penetratin-Az and TP2-Az) were successfully synthesised by solid phase synthesis. The optimised ynamine-CuAAC conditions performed well (> 90% conversion after 1 h) on the tested peptides when using HFIP as a co-solvent. The click reaction with TP2-Az was completed within 30 minutes while Penetratin-Az reached maximum conversion after 1 h. The difference in reactivity is likely due to the number of chelation moieties in the peptides. TP2-Az only has 2 arginine residues which could chelate copper, while Penetratin-Az has three arginine and four further lysine residues.

Then, a competition experiment between DBCO **2.12** and ynamine **2.1** with picolyl azide **2.42** was performed in the presence and absence of GSH. In the absence of GSH, the SPAAC triazoles (**4.10a/b**) formed exclusively, while in the presence of GSH the CuAAC triazole (**2.3c**) formed as the major product (> 90%). As dual functionalisation of peptides is highly desirable, it was attempted to translate these results into selective labelling of peptides.

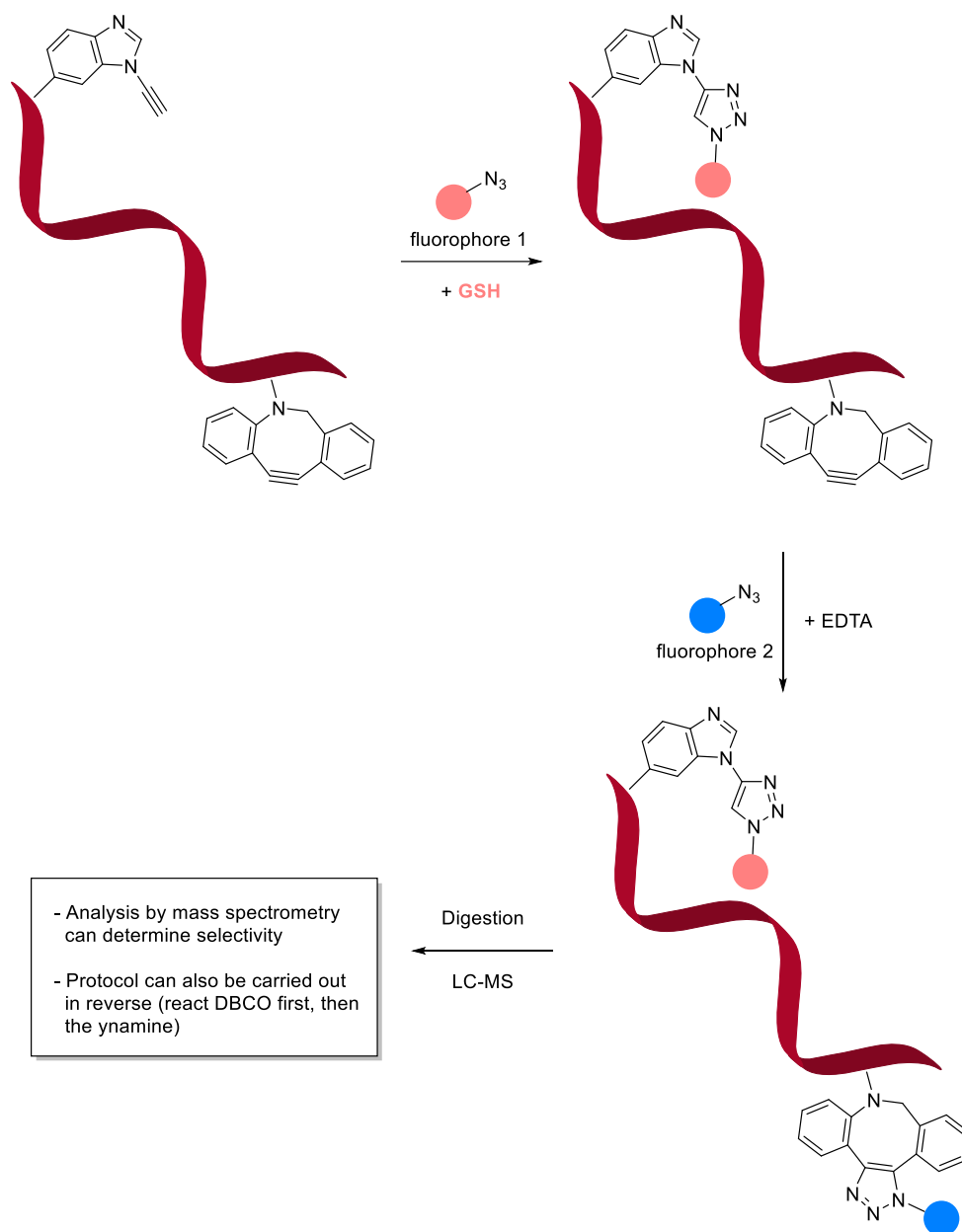
The conditions developed for small molecules ($\text{Cu}(\text{OAc})_2 = 350 \mu\text{M}$, $\text{GSH} = 1 \text{ mM}$) were not as effective for inhibiting the SPAAC reaction on peptides. Instead, the use of equimolar amounts of copper and GSH ($500 \mu\text{M}$ each) allowed the selective labelling of Penetratin-Az and TP2-Az by either CuAAC or SPAAC reaction which was controlled by GSH addition.

The selective dual modification of Pico-TP2-Az was attempted using the newly developed protocol. Unfortunately, a mixture of products was obtained which could not be improved by further optimisation. The most prominent side products were with double labelled ynamine **4.20** or double labelled DBCO peptide **4.18**, indicating poor selectivity of picolyl azide over an aliphatic azide.

Due to the poor chemoselectivity over azides, reversing the incorporation of functional groups (*i.e.*, both an aromatic ynamine and DBCO present in the same molecule) might circumvent the selectivity issue. To this end an ynamine-phosphoramidite (**4.23**) was synthesised and incorporated into an oligonucleotide. In the future, **ODN-2** will be used to test the optimal ynamine-CuAAC conditions ($100 \mu\text{M Cu}(\text{OAc})_2$ and $100 \mu\text{M GSH}$ in 10% HFIP). Due to the additional Cu-chelating functional groups present in oligonucleotides the reaction might require further optimisation. Consideration must also be given to the magnesium concentration of the buffer as Kollaschinski *et al.* showed that tuning the magnesium concentration was vital for successful CuAAC ligation.²⁷⁵

After the ligation conditions are optimised, an oligonucleotide strand containing both ynamine **4.30** and DBCO will be synthesised, and the sequential labelling protocol attempted with two

different azides. The selectivity of the protocol can be evaluated by mass spectrometry after oligonucleotide digestion (Scheme 4.14).



Scheme 4.14. Proposed workflow for the selective sequential labelling of oligonucleotides.

4.6 Experimental

4.6.1 General Experimental Techniques and Procedures

4.6.1.1 Reagents and Solvents

All reagents and solvents were used as supplied from commercial sources and used without further purification unless otherwise stated. Thin layer chromatography (TLC) was carried out using Merck silica plates coated with fluorescent indicator UV254. TLC plates were analysed under 254 nm UV light or developed using potassium permanganate solution.

4.6.1.2 Column Chromatography

Normal-phase flash chromatography was carried out using ZEOprep 60 HYD 40-63 μm silica gel.

4.6.1.3 NMR Spectroscopy

NMR spectroscopy was carried out using either a Bruker 400 UltraShield™ B-ACS 60 spectrometer, Bruker AV500 spectrometer at 500 MHz (^1H) and 126 Hz (^{13}C) or Bruker AV600 spectrometer at 156 Hz (^{13}C). All chemical shifts (δ) in CDCl_3 were referenced at 7.26 (^1H) and 77.06 ppm (^{13}C), in $\text{DMSO}-d_6$ at 2.50 (^1H) and 39.52 (^{13}C), in D_2O at 4.79 ppm (^1H) and in CD_3OD at 3.31 (^1H) and 49.0 ppm (^{13}C) and reported in parts per million (ppm). Coupling constants are quoted in hertz (Hz). Abbreviations for splitting patterns are s (singlet), br. s (broad singlet), d (doublet), dd (doublet of doublets), ddd (doublet of doublets of doublets), t (triplet), td (triplet of doublets), app. t (apparent triplet), q (quartet) and m (multiplet). All NMR data was processed using Mestrenova 11.0 software. Proton and carbon chemical shifts were assigned using proton (^1H), carbon (^{13}C), Heteronuclear Single Quantum Coherence (HSQC), Heteronuclear Multiple-Bond Correlation Spectroscopy (HMBC) and Correlation Spectroscopy (COSY) and Nuclear Overhauser Effect Spectroscopy (NOESY) whenever possible (see Appendix for assigned protons/carbons).

4.6.1.4 High Resolution Mass Spectrometry

High-resolution mass spectra were recorded on an LTQ Orbitrap XL 1 mass spectrometer at the EPSRC UK National Mass Spectrometry Facility (Swansea), a Thermo Exactive Orbitrap mass spectrometer at the University of St Andrews and a Bruker Micro TOF II at the university of Edinburgh.

4.6.1.5 IR Spectroscopy

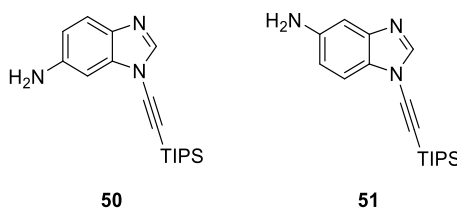
IR data were collected on either an Agilent or Shimadzu FTIR spectrometer and the data processed using the proprietary software. Only major absorbances were reported.

4.6.2 Liquid Chromatography-Mass Spectrometry (LC-MS) and Ultra-Performance-Mass-Spectrometry (UPLC-MS)

LC-MS was carried out on an Agilent HPLC instrument in conjunction with an Agilent Quadrupole mass detector on an Agilent Poroshell 120 C18 column (75 mm × 4.6 mm, 2.7 μm). UPLC-MS was carried out on an AVANT UPLC with an Advion Expression CMS L attached for mass detection on a Phenomenex Kinetex C18 column (30 mm × 2.1 mm, 2.7 μm). Electrospray ionization (ESI) was used in all cases.

4.6.3 Synthetic Procedures

1-((triisopropylsilyl)ethynyl)-1H-benzo[d]imidazol-5-amine (**4.5**) compound with 1-((triisopropylsilyl)ethynyl)-1H-benzo[d]imidazol-6-amine (**4.6**)



1H-benzo[d]imidazol-6-amine (2.0 g, 15 mmol), caesium carbonate (5.9 g, 18 mmol), copper iodide (143 mg, 0.75 mmol) and PEG 400 (1.2 g, 3.0 mmol) were dissolved in dry dioxane (100 mL). The mixture was degassed under vacuum three times (20 min, 10 min, 5 min) and (bromoethynyl)triisopropylsilane (4.7 g, 18 mmol) was added. The reaction mixture was heated to reflux (110 °C) for 42 hours under an argon atmosphere. The reaction was allowed to reach room temperature and the diluted with ethyl acetate (100 mL). The mixture was washed with sat. EDTA solution (pH 3, 100 mL) and brine (100 mL) and then dried over Na₂SO₄. The organic phase was concentrated under vacuum and purified by flash column chromatography (50 – 70% ethyl acetate in petroleum ether) to give the desired compounds as yellow solids (**50** 505 mg, 11% and **51** 376 mg, 8%).

Compound (**4.5**) ¹H NMR (500 MHz, CDCl₃) δ 7.88 (s, 1H), 7.55 (d, *J* = 8.5 Hz, 1H), 6.78 (d, *J* = 2.2 Hz, 1H), 6.72 (dd, *J* = 8.5, 2.2 Hz, 1H), 3.83 (s, 2H), 1.16 (s, 21H).

¹³C NMR (126 MHz, CDCl₃) δ 144.5, 141.8, 135.9, 135.1, 121.2, 113.5, 96.0, 90.5, 72.5, 18.7, 11.2.

IR (ν_{\max}): 3323 (N-H), 3210 (N-H), 2943 (C-H), 2865 (C-H), 2187 (C \equiv C), 1498 (ar. C=C) cm^{-1} .

HR-MS (ESI): $\text{C}_{18}\text{H}_{27}\text{N}_3\text{SiH}^+$ calculated 314.2047, found 314.2047.

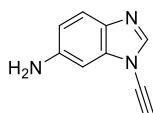
Compound (**4.6**) **^1H NMR** (500 MHz, CDCl_3) δ 7.97 (s, 1H), 7.31 (d, J = 8.5 Hz, 1H), 7.08 (d, J = 2.0 Hz, 1H), 6.81 (dd, J = 8.5, 2.0 Hz, 1H), 1.19 – 1.11 (m, 21H).

^{13}C NMR (126 MHz, CDCl_3) δ 144.0, 143.6, 143.1, 128.2, 114.4, 111.3, 105.7, 90.6, 72.4, 18.7, 11.3.

IR (ν_{\max}): 3326 (N-H), 3209 (N-H), 3069 (ar. C-H), 2946 (C-H), 2867 (C-H), 2183 (C \equiv C), 1486 (ar. C=C) cm^{-1} .

HR-MS (ESI): $\text{C}_{18}\text{H}_{27}\text{N}_3\text{SiH}^+$ calculated 314.2047, found 314.2049.

1-ethynyl-1H-benzo[d]imidazol-6-amine (4.3)



1-((triisopropylsilyl)ethynyl)-1H-benzo[d]imidazol-6-amine (359 mg, 1.15 mmol) was dissolved in acetonitrile (6 mL) and fluoride on polymer support 2 – 3 mmol/g loading (383 mg, 1.15 mmol) was added (Sigma catalogue number: 387789-10G). The reaction was stirred at room temperature overnight and then filtered and the solvent removed under vacuum. The residue was purified by flash column chromatography (0 – 60% in ethyl acetate in petroleum ether) and the desired product was obtained as a light brown solid (152 mg, 84 %).

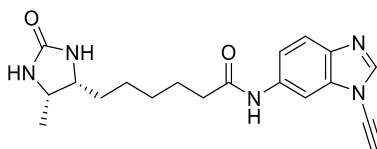
^1H NMR (500 MHz, CDCl_3) δ 7.87 (s, 1H), 7.55 (d, J = 8.6 Hz, 1H), 6.83 (d, J = 2.2 Hz, 1H), 6.72 (dd, J = 8.6, 2.2 Hz, 1H), 3.84 (s, 2H), 3.24 (s, 1H).

^{13}C NMR (126 MHz, CDCl_3) δ 144.9, 141.7, 135.9, 135.2, 121.5, 113.7, 96.0, 70.8, 61.9.

IR (ν_{\max}): 3409 (N-H), 3299 (N-H), 3180 (ar. C-H) 3116 (sp C-H), 2146 (C \equiv C), 1497 (ar. C=C) cm^{-1} .

HR-MS (ESI): $\text{C}_9\text{H}_7\text{N}_3\text{H}^+$ calculated 158.0713, found 158.0712.

N-(1-ethynyl-1H-benzo[d]imidazol-6-yl)-6-((4R,5S)-5-methyl-2-oxoimidazolidin-4-yl)hexanamide (4.7)



Desthiobiotin (40 mg, 0.18 mmol), DMAP (5 mg, 0.04 mmol) and then EDC.HCl (40 mg, 0.21 mmol) were dissolved in DMF (3 mL) and stirred for 30 minutes under argon atmosphere and cooled to 0 °C, then 1-ethynyl-1*H*-benzo[*d*]imidazol-6-amine (33 mg, 0.21 mmol) was added, and reaction stirred overnight. Dichloromethane (20 mL) was added, the organic phase was extracted with sat. NaHCO₃ (20 mL) and water (20 mL), then dried over Na₂SO₄. The solvent was removed under vacuum and the residue purified by column chromatography (7% methanol/ 1% TEA in dichloromethane) to give the desired compound as a white solid (36 mg, 54%).

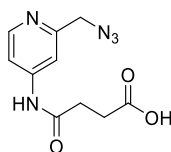
¹H NMR (400 MHz, DMSO) δ 10.12 (s, 1H), 8.54 (s, 1H), 8.26 (d, *J* = 2.0 Hz, 1H), 7.67 (d, *J* = 8.7 Hz, 1H), 7.33 (dd, *J* = 8.7, 2.0 Hz, 1H), 6.30 (s, 1H), 6.11 (s, 1H), 4.73 (s, 1H), 3.67 – 3.55 (m, 1H), 3.54 – 3.45 (m, 1H), 2.34 (t, *J* = 7.4 Hz, 2H), 1.67 – 1.55 (m, 2H), 1.46 – 1.19 (m, 6H), 0.96 (d, *J* = 6.4 Hz, 3H).

¹³C NMR (101 MHz, DMSO) δ 171.4, 162.8, 144.2, 137.0, 136.8, 134.3, 120.3, 116.0, 100.5, 70.2, 64.9, 55.0, 50.2, 36.4, 29.5, 28.7, 25.6, 25.0, 15.5.

IR (ν_{max}): 3256 (N-H), 3133 (ar. C-H), 2930 (C-H), 1707 (C=O), 1595 (C=O) cm⁻¹.

HR-MS (ESI): C₁₉H₂₃N₅O₂H⁺ calculated 354.1925, found 354.1935.

4-((2-(azidomethyl)pyridin-4-yl)amino)-4-oxobutanoic acid (4.16)



2-(azidomethyl)pyridin-4-amine (50 mg, 0.27 mmol), DMAP (40 mg, 0.32 mmol) and succinic anhydride (54 mg, 0.54 mmol) were dissolved in DMF (3 mL) and heated to 70 °C overnight. Then, 1% HCl (20 mL) was added, and the aqueous phase washed with chloroform (20 mL, layer discarded). The pH was adjusted to 4.1 and the aqueous phase was extracted with MeTHF (2 × 20 mL). The combined organic phases were washed with 5% LiCl (20 mL), brine (20 mL) and then dried over Na₂SO₄. The solvents were removed under vacuum and the residue purified by column chromatography (5 – 10% MeOH, 1% acetic acid in DCM) to give the desired compound as a white powder (42 mg, 63%).

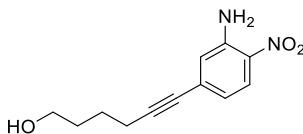
¹H NMR (500 MHz, MeOD) δ 8.71 (d, *J* = 2.3 Hz, 1H), 8.12 (dd, *J* = 8.4, 2.6 Hz, 1H), 7.42 (d, *J* = 8.4 Hz, 1H), 4.43 (s, 2H), 2.74 – 2.64 (m, 4H).

¹³C NMR (126 MHz, MeOD) δ 176.2, 173.3, 151.6, 141.7, 136.9, 129.3, 124.1, 55.8, 49.5, 49.3, 49.2, 49.0, 48.8, 48.7, 48.5, 32.2, 29.8.

IR (ν_{max}): 3327 (COOH), 21113 (N₃), 1685 (C=O) cm⁻¹.

UPLC-MS (ESI): C₁₀H₁₁N₅O₃H⁺ calculated 250.1, found 249.7.

6-(3-amino-4-nitrophenyl)hex-5-yn-1-ol (4.26)



4-Iodo-2-nitroaniline (11 g, 42 mmol), Pd(PPh)₃Cl₂ (3.2 g, 4.6 mmol) and CuI (634 mg, 3.3 mmol) were added to a flask which was put under vacuum and refilled with argon. Then triethylamine (200 mL) and hex-5-yn-1-ol (4.5 g, 46 mmol) were added and the reaction was stirred under argon atmosphere for 2 h. Diethyl ether (100 mL) was added and the suspension was filtered through celite and eluted with more diethyl ether (100 mL). The filtrate was concentrated under vacuum and washed with 5% HCl (70 mL), sat. NaHCO₃ (2 × 70 mL) and brine, then dried over Na₂SO₄. The solvents were removed under vacuum to give a brown solid, which was dissolved in ethyl acetate (50 mL) and heated to 40 °C. Hexane (200 mL) was added dropwise whereupon orange solid precipitated. The solid was filtered off, washed with hexane, and dried under vacuum to give the desired product as an orange solid (9.4 g, 97 %).

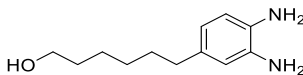
¹H NMR (500 MHz, CDCl₃) δ 8.16 (d, *J* = 2.0 Hz, 1H), 7.34 (dd, *J* = 8.6, 2.0 Hz, 1H), 6.72 (d, *J* = 8.6 Hz, 1H), 6.15 (br. s, 2H), 3.74 – 3.64 (m, 2H), 2.43 (t, *J* = 6.8 Hz, 2H), 1.79 – 1.57 (m, 4H), 1.40 (br. s, 1H).

¹³C NMR (126 MHz, CDCl₃) δ 144.0, 138.5, 131.8, 129.3, 118.8, 112.9, 89.2, 79.2, 62.6, 32.0, 25.1, 19.3.

IR (*v*_{max}): 3533 (N-H), 3444 (N-H), 3170 (ar. C-H), 2941 (C-H), 1636 (NO₂) cm⁻¹. Alkyne stretch very weak.

HR-MS (ESI): C₁₂H₁₄N₂O₃H⁺ calculated 235.1077, found 235.1091.

6-(3,4-diaminophenyl)hexan-1-ol (4.27)



6-(3-amino-4-nitrophenyl)hex-5-yn-1-ol (9.4 g, 402 mmol) was added to a two-neck 1 L round bottom flask, which was purged with argon three times. Palladium on carbon was added (10 spatula tips) and the flask was put under vacuum and refilled with argon. Dry methanol (400 mL) was added and the solution sparged with 1.5 balloons of hydrogen. The reaction was then kept under a hydrogen atmosphere overnight and stirred at room temperature. TLC analysis indicated incomplete conversion, therefore more catalyst (10 spatula tips) was added, the

reaction sparged with hydrogen and kept under a hydrogen atmosphere for another night. Then the reaction was filtered through celite and eluted with MeOH. The solvent was removed under vacuum to obtain the desired product as a purple solid (7.8 g, 93%).

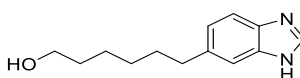
¹H NMR (400 MHz, CDCl₃) δ 6.62 (d, *J* = 7.4 Hz, 1H), 6.54 – 6.50 (m, 2H), 3.63 (t, *J* = 6.6 Hz, 2H), 3.27 (br. s, 4H), 2.52 – 2.42 (m, 2H), 1.63 – 1.50 (m, 4H), 1.44 – 1.23 (m, 4H).

¹³C NMR (101 MHz, CDCl₃) δ 135.2, 135.0, 132.3, 120.0, 117.1, 116.9, 63.2, 35.3, 32.9, 31.8, 29.2, 25.8.

IR (ν_{max}): 3375 (N-H), 3290 (broad, O-H), 2925 (C-H), 2852 (C-H), 1519 (C=C) cm⁻¹.

HR-MS (ESI): C₁₂H₂₀N₂OH⁺ calculated 209.1648, found 209.1649.

6-(1H-benzo[d]imidazol-6-yl)hexan-1-ol (4.28)



6-(3,4-diaminophenyl)hexan-1-ol (370 mg, 1.8 mmol) was dissolved in formic acid (5 mL) and heated to reflux overnight. The solvent was removed under vacuum and the residue was dissolved in ethyl acetate (30 mL). The organic phase was washed with 5% NaOH (wt) and brine (30 mL). The solvent was removed under vacuum and the residue purified by column chromatography (5 – 15% MeOH in DCM) to give the desired compound as a brown oil (157 mg, 40%).

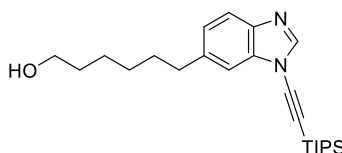
¹H NMR (400 MHz, MeOD) δ 8.12 (br. s, 1H), 7.52 (br. s, 1H), 7.41 (br. s, 1H), 7.07 (d, *J* = 8.0 Hz, 1H), 3.52 (t, *J* = 6.6 Hz, 2H), 2.69 (t, *J* = 7.6 Hz, 2H), 1.70 – 1.58 (m, 2H), 1.56 – 1.43 (m, 2H), 1.43 – 1.27 (m, 4H).

¹³C NMR (101 MHz, MeOD) δ 138.9, 124.8, 116.1, 115.0, 62.9, 49.6, 49.4, 48.4, 37.0, 33.6, 33.2, 30.1, 26.8.

IR (ν_{max}): 3195 (broad, O-H), 2925 (C-H), 2824 (C-H), 1603 (C=C) cm⁻¹.

HR-MS (ESI): C₁₃H₁₈N₂OH⁺ calculated 219.1492, found 219.1502.

6-(1-((triisopropylsilyl)ethynyl)-1H-benzo[d]imidazol-6-yl)hexan-1-ol (4.29)



6-(1H-benzo[d]imidazol-6-yl)hexan-1-ol (1.2 g, 5.4 mmol), CuI (51 mg, 0.27 mmol), caesium carbonate (2.1 g, 6.4 mmol) and PEG400 (214 mg, 0.54 mmol) were added to a flask and put under vacuum. Dry dioxane (50 mL) was added under argon atmosphere and the reaction

degassed under vacuum (3 ×). (Bromoethynyl)triisopropylsilane (2.2 g, 8.6 mmol) was added and the reaction heated to reflux for 2 days. The solvent was removed under vacuum and ethyl acetate (70 mL) and sat. EDTA solution (pH 3, 60 mL) were added and the phases were separated. The organic phase was washed with water (70 mL) and the combined aqueous phases extracted with ethyl acetate (70 mL). The organic phases were combined and washed with brine (70 mL) and then dried over Na₂SO₄. The solvent was removed under vacuum to give a brown oil, which was purified by column chromatography (10 – 50% ethyl acetate in hexane) to give the desired compound as a clear oil (383 mg, 18%).

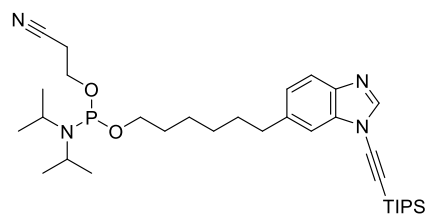
¹H NMR (500 MHz, CDCl₃) δ 8.02 (s, 1H), 7.69 (d, *J* = 8.2 Hz, 1H), 7.32 (d, *J* = 1.5 Hz, 1H), 7.18 (dd, *J* = 8.3, 1.5 Hz, 1H), 3.64 (t, *J* = 6.6 Hz, 2H), 2.78 (t, *J* = 7.7 Hz, 2H), 1.75 – 1.65 (m, 2H), 1.63 – 1.53 (m, 2H), 1.47 – 1.38 (m, 4H), 1.24 – 1.09 (m, 21H).

¹³C NMR (126 MHz, CDCl₃) δ 143.3, 140.2, 140.1, 134.9, 125.1, 120.4, 110.3, 90.5, 73.0, 63.1, 36.2, 32.9, 31.8, 29.1, 25.8, 18.8, 11.4.

IR (ν_{\max}): 3304 (broad, O-H), 2927 (C-H), 2803 (C-H), 2184 (C≡C), 1500 (C=C) cm⁻¹.

HR-MS (ESI): C₂₄H₃₈N₂OSiH⁺ calculated 399.2826, found 399.2824.

2-cyanoethyl (6-(1-((triisopropylsilyl)ethynyl)-1H-benzo[d]imidazol-6-yl)hexyl) diisopropylphosphoramidite (4.23)



6-(1-((triisopropylsilyl)ethynyl)-1H-benzo[d]imidazol-6-yl)hexan-1-ol (200 mg, 0.5 mmol) was dissolved in dry THF (4 mL) under argon in a vacuum-dried flask. Dry DIPEA (583 mg, 4.5 mmol) was added, followed by 2-cyanoethyl *N,N*-diisopropylchlorophosphoramidite (356 mg, 1.5 mmol) and the reaction was stirred at room temperature for 1 h. The solvent was removed under vacuum and the residue purified by column chromatography (5 – 20% ethyl acetate in hexane with 1% TEA) to give the desired compound as a colourless oil (208 mg, 71%).

¹H NMR (500 MHz, CDCl₃) δ 8.01 (s, 1H), 7.69 (d, *J* = 8.2 Hz, 1H), 7.32 (d, *J* = 1.5 Hz, 1H), 7.17 (dd, *J* = 8.2, 1.5 Hz, 1H), 3.89 – 3.75 (m, 2H), 3.69 – 3.52 (m, 4H), 2.77 (t, *J* = 7.6 Hz, 2H), 2.63 (t, *J* = 6.5 Hz, 3H), 1.75 – 1.56 (m, 5H), 1.47 – 1.35 (m, 4H), 1.26 – 1.12 (m, 32H).

¹³C NMR (126 MHz, CDCl₃) δ 143.4, 140.2, 134.9, 125.0, 120.5, 117.8, 110.3, 90.5, 72.9, 63.8 (d, *J* = 17.2 Hz), 58.4 (d, *J* = 18.8 Hz), 43.2 d, (*J* = 12.1 Hz), 36.3, 31.8, 31.3 (d, *J* = 7.3

Hz), 29.1, 26.0, 24.8 (d, $J = 7.3$ Hz), 24.7 (d, $J = 7.1$ Hz), 20.5 (d, $J = 6.9$ Hz), 18.8, 11.4. Not phosphorous decoupled.

^{31}P NMR (162 MHz, CDCl_3) δ 147.3

HR-MS (ESI): $\text{C}_{33}\text{H}_{56}\text{N}_4\text{O}_2\text{PSiH}^+$ calculated 599.3905, found 599.3898

4.6.4 General Peptide Synthesis Protocol

Solid-phase synthesis was performed using ChemMatrix® Rink amide resin (0.52 mmol/g) using a Protein Technologies Tribute automated synthesizer. Synthesis was performed using the standard Fmoc/tBu protected amino acids and were obtained from Merck without further purification.

The experimental protocol for automated synthesis was as follows:

The resin was swollen for 10 min in DCM (2 mL). Fmoc deprotection was achieved using 20% piperidine in DMF (3×5 min, 2 mL). Each amino acid (3.0 equiv) was activated with HATU (3.0 equiv) and DIPEA (0.5 M in DMF, 5 mL) for 5 min. The solution was then added to the resin and shaken for 1 h, then washed with further DMF (2 mL). Deprotection, coupling, and washing (DMF, 3×5 min, 2 mL) procedures were repeated until the final amino acid had been coupled to the peptide chain. The peptide was then cleaved from the resin, precipitated by addition of cold MTBE, and centrifuged at 4000 rpm for 5 min. The pellet was resuspended in cold MTBE, sonicated, and collected by centrifugation; this was repeated a total of three times. Peptides were then purified by RP-HPLC using a Dionex UltiMate 3000 HPLC equipped with a C18 column (Phenomenex Kinetex, 150×21.2 mm, $5 \mu\text{m}$, 15 mL/min). For purification HPLC method see individual peptide sections.

4.6.4.1 HPLC Method for Purity Analysis of Peptides

Conditions for peptide purity analysis:

Column Specifications: Phenomenex Aeris Widepore C18, 250×4.6 mm, $3.6 \mu\text{m}$

Column Temperature: 40°C

Mobile Phase A: 0.1% v/v TFA in water

Mobile Phase B: 0.1% v/v TFA in MeCN

Flow rate 1 mL/min

Injection Volume: 10 μL

Time (min)	B%
0 – 35	5 – 95
35 – 40	95
40 – 40.5	95 – 5
40.5 – 50	5

4.6.4.2 Penetratin-Az

Synthesis was performed using the general procedure given previously (100 mg resin, 50.0 μ mol). After the coupling the resin was split in half and one portion deprotected (2×5 min 20% piperidine in DMF, 3 mL), washed ($2 \times$ DCM, $2 \times$ DMF, 5 mL each) and then cleaved (90% TFA, 2.5% H₂O, 2.5% TIPS, 2.5% DTT, 2.5% Phenol, v/v/v/w/w, 3 mL total) for 4 h. The resin was filtered off and the peptide was precipitated with MTBE. The residue was purified by reverse phase semi-preparative chromatography. The relevant fractions were collected then pooled and the solvent removed by lyophilisation to give the target peptide as a colourless, amorphous solid.

HPLC purity (Rt = 11.36 min): 98% (254 nm), 97% (210 nm)

HR-MS (ESI):

C₁₁₂H₁₈₂N₄₀O₂₁S[4H⁺] calculated 614.8604, found 614.8603.

Gradient for HPLC purification:

Time (min)	B %
0 - 16	5 – 40
16 - 17	40 – 95
17 - 21	95
21 - 22	95 - 5
22 - 25	5

4.6.4.3 TP2-Az

Synthesis was performed using the general procedure (100 mg resin, 50.0 μ mol). After the coupling the resin was split in half and one portion deprotected (2×5 min 20% piperidine in DMF), washed ($2 \times$ DCM, $2 \times$ DMF, 5 mL each) and then cleaved (90% TFA, 5% H₂O, 2.5% TIS, 2.5% Phenol, v/v/v/w, 2 mL total) for 2 h. The resin was filtered off and the peptide precipitated with MTBE. The residue was purified by reverse phase semi-preparative chromatography. The relevant fractions were collected then pooled and the solvent removed by lyophilisation to give the target peptide as a colourless, amorphous solid.

HPLC purity (Rt = 15.59 min): 95 % (210 nm)

HR-MS (ESI):

C₇₈H₁₂₈N₂₄O₁₅[3H⁺] calculated 548.0070, found 548.0066.

Gradient for HPLC purification:

Time (min)	B %
------------	-----

0 – 11	5 – 50
11 – 12	50 – 95
12 – 15	95
15 – 16	95 – 5
16 - 19	5

4.6.4.4 Pico-TP2-Az

The second half of the TP2-Az resin was deprotected (2 x 5 min 20% piperidine in DMF) and washed (2 x DCM, 2 x DMF). 4-((2-(azidomethyl)pyridin-4-yl)amino)-4-oxobutanoic acid (19 mg, 75 μ mol) was preincubated with DIC (10 mg, 75 μ mol) and OxymaPure® (11 mg, 75 μ mol) for 1 h. The mixture was added to the resin and heated in the microwave to 75 °C for 1 h. The resin was washed (5 x DMF, 5 x DCM, 5 mL each) and then cleaved (90% TFA, 5% H₂O, 2.5% TIS, 2.5% Phenol v/v/v/w, 2 mL) for 2.5 h. The resin was filtered off and the peptide precipitated with MTBE. The residue was purified by reverse phase semi-preparative chromatography. The relevant fractions were collected then pooled and the solvent removed by lyophilisation to give the target peptide as a colourless, amorphous solid.

HPLC purity (R_t = 19.47 min): 100% (254 nm), 98% (210 nm)

HR-MS (ESI):

C₈₈H₁₃₇N₂₉O₁₇[3H⁺] calculated 625.0322, found 625.0322.

Gradient for HPLC purification:

Time (min)	B %
0 – 11	20 – 60
11 – 12	60 – 95
12 – 15	95
15 – 16	95 – 20
16 - 19	20

4.6.5 General Protocol for DNA Synthesis

ODN-1 was synthesized using standard solid phase oligonucleotide synthesis protocols on an ABI 394 synthesizer. Phosphoramidites and CPG supports loaded with standard nucleosides were purchased from LINK Technologies Ltd (Bellshill, UK). For the modified phosphoramidite **4.23** a longer coupling time of 5 min was used.

After the solid phase synthesis was finished the TIPS protecting group was removed on solid phase. TBAF (50 μ L, 1 M in THF) was mixed with 1.95 mL of acetonitrile and this mixture was taken up in a plastic syringe. The mixture was repeatedly passed over the column

containing the CPG support for 3 min. The CPG support was washed with MeCN (3×5 mL) and dried with air.

Ammonia (DNA grade, 1.5 ml/mmol) was added, and the suspension was shaken for 16 h at room temperature. (ATTENTION: Higher Temperatures led to degradation of the ynamine modifiers and need to be avoided!). The supernatant was removed, and the CPG support was then washed with water (2×1.5 mL). The combined aqueous phase was concentrated under reduced pressure to obtain crude ODN-2 as a white solid. Oligonucleotides were purified by reverse-phase HPLC on a Dionex UltiMate 3000 System (see following section for detail), lyophilised and then desalted using a NAP-25 Sephadex column.

MALDI-ToF mass spectra were recorded using a Shimadzu Biotech Axima CFR spectrometer, using 3-hydroxypicolinic acid (HPA) as the matrix. All mass spectra were recorded in negative mode. Analytical RP-HPLC was performed on a Dionex 3000 Ultimate HPLC System.

4.6.5.1 ODN-2

Synthesised using the standard protocol.

MALDI (ToF): $C_{131}H_{164}N_{48}O_{73}P_{12}[H^+]$ calculated 3949.75, found 3951.38.

HPLC purity (16.91 min): 96% (260 nm)

Purification on Dionex UltiMate 3000 Semi-prep HPLC System

Column: Phenomenex Clarity Oligo-RP, 250×10 mm, 5 μ m.

Mobile Phase A: 0.1 M TEAA in water (pH 7)

Mobile Phase B: 0.1 M TEAA, 80% MeCN in water (pH 7)

Flow rate 3 mL/min

Gradient:

Time (min)	B %
0 – 16	10 – 40
16 – 17	40 – 95
17 – 21	95
21 – 22	95 – 10
22 – 27	10

Purity analysis on Dionex 3000 Ultimate HPLC System

Column: Phenomenex Clarity Oligo-RP, 250×4.6 mm, 5 μ m.

Mobile Phase A: 0.1 M TEAA in water (pH 7)

Mobile Phase B: 0.1 M TEAA, 80% MeCN in water (pH 7)

Flow rate 0.8 mL/min

Injection Volume: 10 μ L

Gradient:

Time (min)	B %
0 – 21	10 – 40
21 – 22	40 – 95
22 – 25	95
25 – 26	95 – 10
26 – 45	10

4.6.6 HPLC Assay Procedure for Peptide Conjugation

4.6.6.1 Stock Solutions and Procedure

Stock solutions of reagents were prepared each day. Reagents (~1 – 20 mg) were measured out on a microbalance.

Stock solutions:

[Alkyne] = 8 mM in organic solvent (*i.e.*, HFIP)

[DBCO] = 8 mM in organic solvent (*i.e.*, HFIP)

[Peptide] = 2 mM (H₂O for Penetratin-Az, in organic/H₂O 1:1 for TP2-Az and Pico-TP2-Az)

[GSH] = 4 mM in 1X DPBS

[Cu(OAc)₂] = 4 mM in H₂O

Appropriate amounts of the stock solutions were added to reach specified concentrations to an HPLC vial (plastic V-shaped vial, 200 μ M capacity) and made up with MeOH (or other appropriate organic co-solvent) and 1X DPBS buffer to a final volume of 0.2 mL. The addition order was as follows: DBCO, alkyne, organic solvent, GSH, Cu(OAc)₂, buffer, and peptide. The vials were then placed in the autosampler (not capable of temperature control) and sampled for the specified time.

4.6.6.2 Instrument, Method and Quantification

HPLC was carried out on a Shimadzu Prominence LC system.

Typical HPLC conditions are described below:

Column Specifications: Phenomenex Luna Omega Polar C18, 100 \times 4.6 mm, 3.5 μ m

Column Temperature: 40 $^{\circ}$ C

Mobile Phase A: 0.1% v/v TFA in water

Mobile Phase B: 0.1% v/v TFA in MeCN

Flow rate 1.2 mL/min

Injection Volume: 10 μ L

Time (min)	B%
0 – 9	5 – 70
9 – 9.5	70 – 95
9.5 – 12	95
12 – 12.5	95 – 10
12.5 – 14.5	10

To determine the conversions in this chapter, peak area of the product was divided by the peak area of the starting material and the product at each timepoint. For DBCO products, the sum of the peak areas of each regio-isomer was used to calculate the total product area.

4.6.6.3 Additional HPLC Data

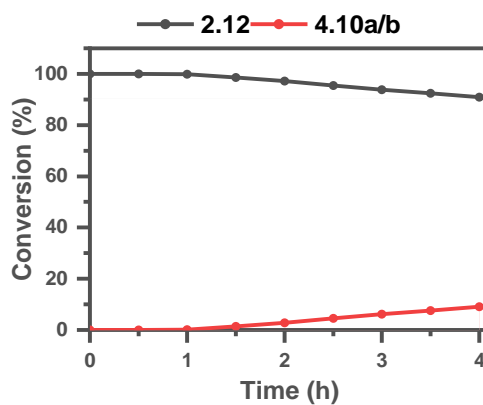


Figure 4.15. Reaction of DBCO **2.12** with picolyl azide (**2.42**) in the presence of CuI (350 μ M). *Conditions:* **2.12** (200 μ M), CuI (350 μ M), **2.42** (200 μ M), 10% MeOH in 1X DPBS, rt, 4 h. Buffer pH = 7.4.

Chapter 5

Exploration of the Bio-orthogonality of the Ynamine-CuAAC Reaction in Cell Lysate

5.1 Introduction

5.1.1 The Utility of the CuAAC Reaction for Live Cell Labelling

The toxicity of copper remains the main stumbling block for the CuAAC reaction for its wider use as a bio-orthogonal labelling tool in live cells. While copper is an important co-factor for enzyme catalysis,⁸⁶ it is only present in trace amounts inside cells (10 – 70 μM depending on the organism)^{276,65} and its homeostasis is tightly regulated (Figure 5.1).²⁷⁷ Virtually no unbound Cu(I) is present inside cells (less than one atom per cell inside yeasts.⁶⁵ Glutathione acts as the first line of defence against elevated cellular copper levels and can effectively buffer the transition metal as well as limit reactive oxygen species induced damage.²²⁶ By virtue of its high binding affinity for Cu, GSH is thought to deliver copper to chaperone proteins which regulate copper transport.¹⁶⁸ In order for the use of the CuAAC ligation strategy beyond *in vitro* applications, there is an inherent need to limit ROS damage, protect Cu(I) from competitive chelation and rely on reactive alkynes and azides to limit copper concentration needed to catalyse the CuAAC reaction.

Schematic of cellular copper homeostasis:

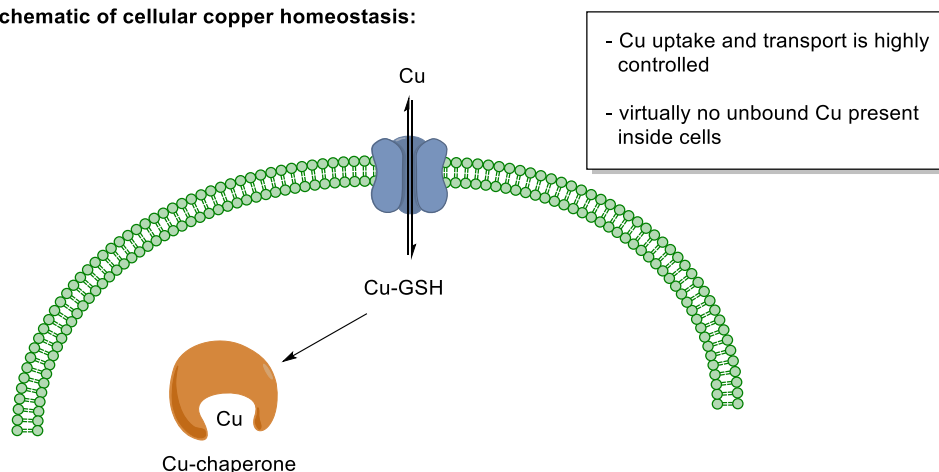


Figure 5.1. Schematic of copper uptake and transport inside cells.

The principal strategy to enable CuAAC has been the development of novel CuAAC ligands to improve copper uptake and reduce toxicity (Figure 5.2). The tripodal amine scaffold in TBTA⁶⁶ (first described CuAAC ligand) serves as the archetype for many water-soluble ligands, such as THPTA⁶⁸ and BTAA.⁹⁵ The later proved to be an excellent ligand and has been used extensively for bio-orthogonal chemistry.

While ligands are extremely effective at enhancing the catalytic activity of a Cu(I) species in the CuAAC reaction on the cell surface and preventing toxicity, they do not enhance the copper uptake significantly when compared to incubation with copper supplemented growth medium.

For example, while incubation of cells in copper supplemented media doubled the intracellular concentration, the addition of ligands did lead to greater copper uptake.⁸³ Additionally, the uptake of copper also varied between cell lines. A study of ligands and copper uptake in four different cell lines found no obvious correlation between the type of ligand and copper uptake.⁸⁹ Instead, they highlighted that copper uptake was dependant on the cell type and that toxicity did not correlate to copper uptake as some cell lines were more tolerant to higher copper concentrations than others.

Two strategies have successfully raised the intracellular copper concentration. The group of Cai conjugated the BTAA motif to a cell penetrating peptide.⁸³ This raised the intracellular Cu(I) concentration from $\sim 22 \mu\text{M}$ to $86 \mu\text{M}$. In combination with targeted GSH depletion, the intracellular CuAAC efficiency increased from $\sim 1\%$ to $\sim 15\%$ while toxicity was mitigated. In the second strategy, Miguel-Ávila *et al.* employed preformed complexes of $[\text{Cu}(\text{MeCN})_4]\text{PF}_6$ and BTTE to triple the intracellular copper concentrations and when compared to corresponding *in situ* complexes.²⁷⁸

The second purpose of ligands – preventing toxicity – was investigated by Kennedy *et al.* in 2011.⁸⁹ Out of a range of common ligands (TBTA and THPTA) histidine was uniquely effective in buffering copper toxicity while also maintaining good CuAAC efficiency. Cell surface alkynes were tagged using $50 \mu\text{M}$ copper and $50 \mu\text{M}$ histidine with no apparent toxicity observed even after 24 h.

Copper Ligands for *in vivo* catalysis:

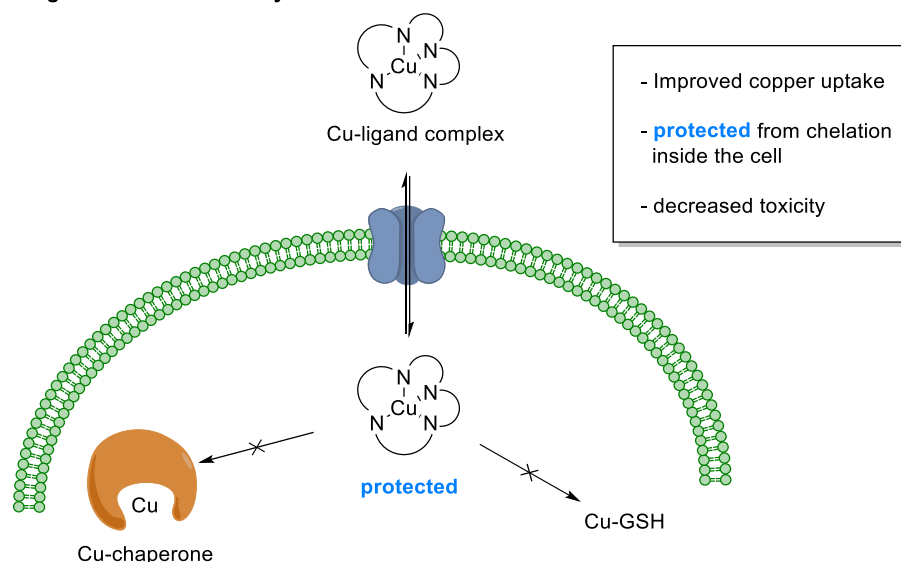


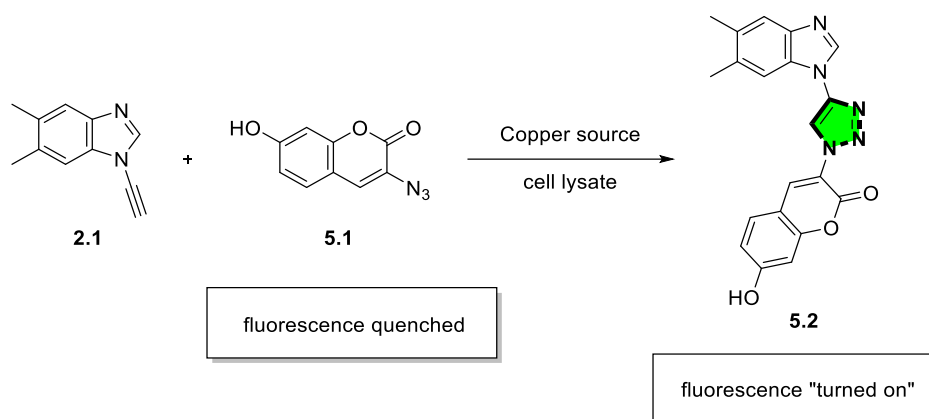
Figure 5.2. Copper-ligands increase copper uptake and prevent sequestering through cellular ligands.

The final strategy to enable *in vivo* CuAAC is the use of copper chelating azides. First introduced by Uttamapinant *et al.* in 2012,⁷⁸ they enabled efficient cellular tagging at a copper

concentration of 40 μM . Since then, Bevilacqua *et al.* further developed “all in one” chelating azides which were effective at 50 μM for *in vivo* labelling.⁸² An important outcome from all these studies is the tolerated copper concentration threshold that does not induce excessive toxicity. A concentration of 50 μM has been the sweet spot in terms of balancing reactivity and toxicity as above this threshold significant toxicity is observed.^{78,83,89,97,279}

5.2 Hypothesis to be tested in this Chapter

None of these approaches explored enhancing the reactivity of the alkyne functional group despite Cu-acetylide formation being the RDS. Ynamine **2.1** outcompeted a range of conventional alkynes in the presence of GSH which promises better *in vivo* reactivity at low copper concentrations (< 50 μM). The aromatic ynamine (*e.g.*, **2.1**) also has the advantage that it can potentially be combined with both ligands and copper chelating azides to boost reactivity even further. In the studies described above, testing of new research ideas is often carried out in cell lysate as a steppingstone for live cell experiments. Cell lysate experiments do not require incorporation of azides into cells and are operationally straightforward. A common approach to monitor reactivity in cell lysate has been to rely on a fluorescent “turn on” CuAAC reaction, using coumarin azides such as **5.1** (Scheme 5.1).^{83–85}



Scheme 5.1. Schematic for the proposed reaction conditions to be tested in this chapter. Reaction of ynamine **2.1** with coumarin azide (**5.1**) in cell lysate. Reaction monitored by increased fluorescence of triazole **5.2**.

5.3 Aims of Chapter 5

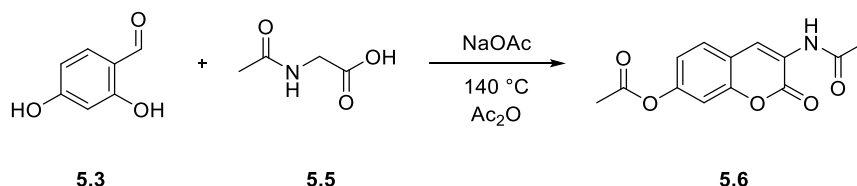
The specific aims of this chapter are:

- (i) Develop 96-well plate fluorescent assay to explore the CuAAC reactivity of ynamines relative to conventional alkynes in cell lysate.
- (ii) Compare ynamine reactivity in cell lysate relative to conventional alkynes.

5.4 Results & Discussion

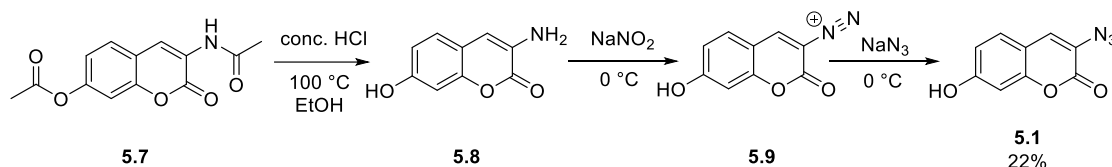
5.4.1 Synthesis of “Turn-on” Azide and Testing of Fluorescent Assay

3-azido-7-hydroxy-couamrin (**5.1**) was synthesized following the procedure from Sivakumar *et al.*²⁸⁰ 2,4-Dihydroxybenzaldehyde (**5.3**) was reacted with *N*-acetylglycine (**5.5**) in a condensation followed by ring closure to afford crude **5.6** after precipitation (Scheme 5.2).



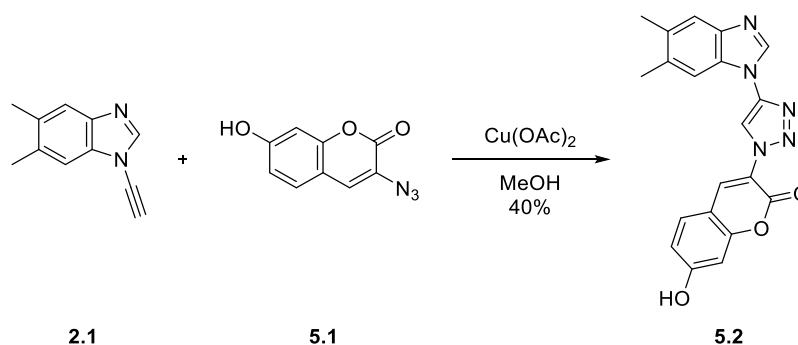
Scheme 5.2. Synthesis of **5.6**. Conditions: **5.3** (1 equiv), **5.5** (1 equiv), NaOAc (3 equiv), 140 °C, overnight.

The crude product **5.6** was then deacetylated under acidic conditions and the free amine functionalised as the diazonium salt (**5.9**) which was then displaced by sodium azide in a one pot reaction to afford the product **5.1** in 22% overall yield (starting from **5.3**) (Scheme 5.3).



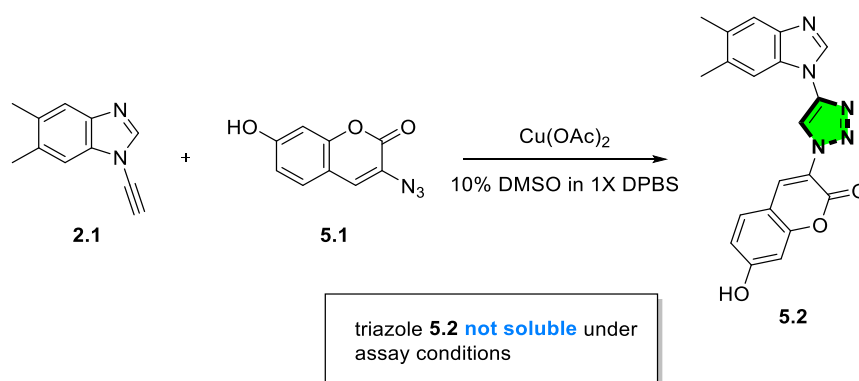
Scheme 5.3. Synthesis of **5.8**. Conditions: **5.7** (1 equiv), Conc. HCl/ EtOH (3:1), 100 °C, 1 h. Synthesis of **5.9**. Conditions: **5.8** (1 equiv), NaNO₂ (1 equiv), 0 °C, 20 min. Synthesis of **5.1**. Conditions: **5.9** (1 equiv), NaN₃ (1.5 equiv), 0 °C, 1 h.

The triazole of ynamine **2.1** was synthesised in 40% yield to serve as a standard in the fluorescence assay.



Scheme 5.4. Synthesis of **5.2**. Conditions: **2.1** (1 equiv), **5.1** (1 equiv), Cu(OAc)₂ (0.1 equiv), rt, overnight.

First, conditions based on an HPLC assay (Chapter 2) were tested (200 μM **2.1** and **5.1**, 350 μM $\text{Cu}(\text{OAc})_2$ in 10% MeOH/1X DPBS) in a 96-well plate format. Unfortunately, azide **5.1** was not soluble under these standard conditions. Switching to 10% DMSO solubilised the starting materials (Scheme 5.5), however, the concentrations of the reagents needed to be lowered to 50 μM as triazole **5.2** saturated the detector at higher concentrations. When the fluorescent signal of the calibration curve was monitored, it steadily decreased over 18 h (Experimental, Table 5.1). As triazole **5.2** was proving challenging to solubilise during synthesis and purification, it was assumed that precipitation caused the fluorescent signal to decrease. When triazole **5.2** (50 μM) was incubated in 100% DMSO no such decrease was observed, confirming that precipitation might cause this issue (Experimental Table 5.2).



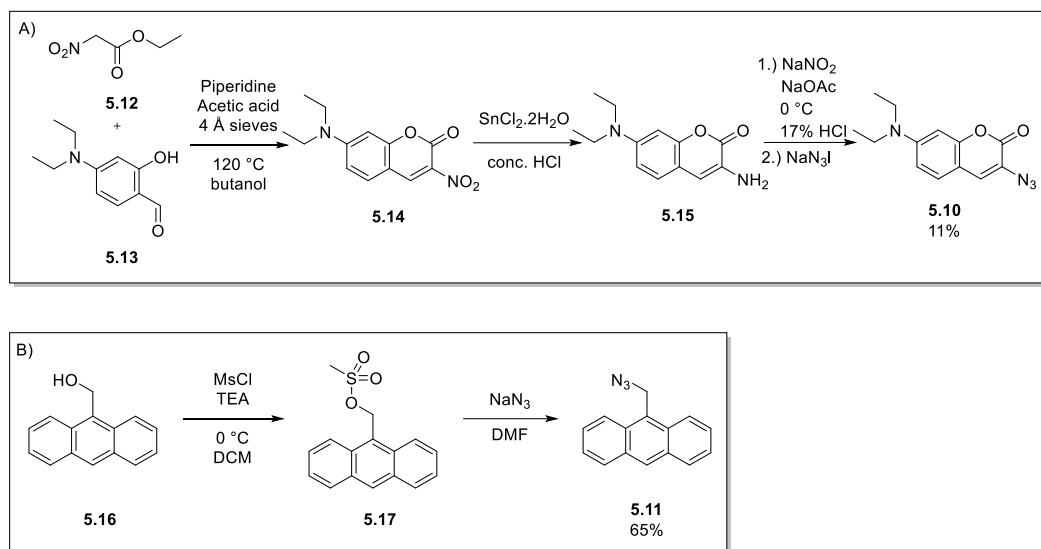
Scheme 5.5. Reaction of ynamine **2.1** with azide **5.1**. Product **5.2** not soluble under these conditions. *Conditions:* **2.1** (200 or 50 μM), $\text{Cu}(\text{OAc})_2$ (200 or 50 μM), **5.1** (200 or 50 μM), 10% DMSO in 1X DPBS, rt, 4 h. Buffer pH = 7.4.

To improve aqueous solubility of the triazole products, it was decided to synthesise two further “turn on” fluorescent azides as well as making modifications to the ynamine core to improve solubility.

5.4.2 Synthesis of further “Turn-on” Azides and Modified Ynamines

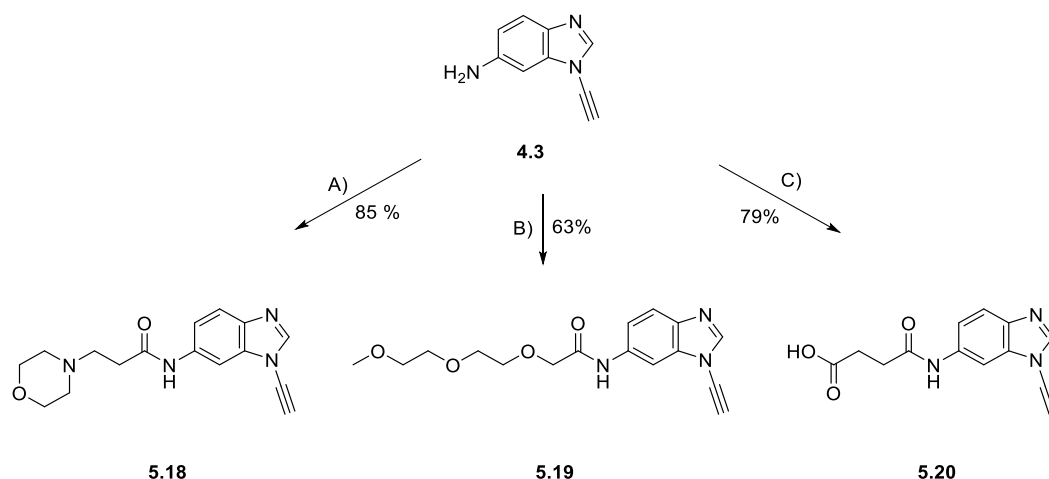
The two azides chosen were diethylamino-coumarin azide **5.10** (Scheme 5.6 A) and anthracene azide **5.11** (Scheme 5.6B). Azide **5.10** is a red-shifted variant of coumarin azide **5.1**.²⁸⁰ It was anticipated that the tertiary amine might improve solubility. Anthracene azide **5.11** was recently used for fluorescent CuAAC imaging by Miguel-Ávila *et al.* inside cells at 50 μM , because of its ease of synthesis and low background fluorescence of unreacted azide.²⁷⁸ They also remarked that they had experienced solubility problems with coumarin azides before switching to azide **5.11**.

After ring-closure and condensation, crude nitro-coumarin **5.14** was reduced with tin chloride to give the amine **5.15** which was diazotised and subsequently displaced by sodium azide to form the product **5.10** in 11% overall yield (Figure 5.5A).²⁸⁰ Anthracene azide **5.11** was synthesised in two steps from 9-(hydroxymethyl)anthracene **5.16** via mesylation (**5.17**) and subsequent displacement by sodium azide in 65% overall yield.²⁸¹



Scheme 5.6. (A) Synthesis of **5.14**. *Conditions:* **5.13** (1 equiv), **5.12** (1 equiv), 120 °C, overnight. Synthesis of **5.15**. *Conditions:* **5.14** (1 equiv), $\text{SnCl}_2 \cdot 2\text{H}_2\text{O}$ (7.5 equiv), rt, 5 hours. Synthesis of **5.10**. *Conditions:* **5.15** (1 equiv), NaNO_2 (1 equiv), 0 °C, 45 min, NaN_3 (2 equiv), rt, 4 hours. (B) Synthesis of **5.17**. *Conditions:* **5.16** (1 equiv), MsCl (1.1 equiv), TEA (2 equiv), 0 °C, 2 hours. Synthesis of **5.11**. *Conditions:* **5.17** (1 equiv), NaN_3 (1.5 equiv), DMF, rt, overnight.

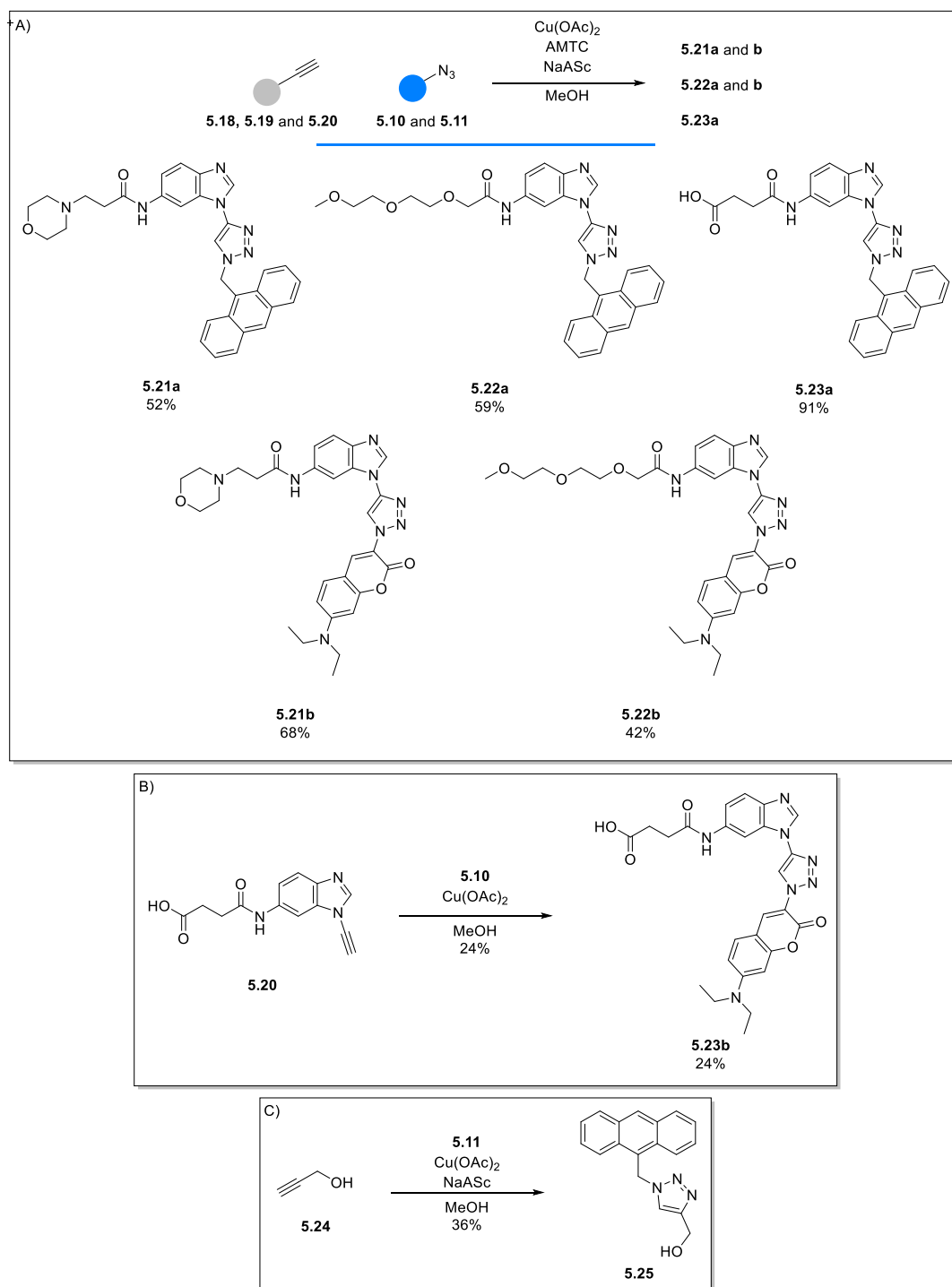
To improve the solubility of the aromatic ynamine, three distinct tails were coupled to ynamine **4.3**. A morpholino tail would provide access to a tertiary amine (**5.18**), a short PEG tail access to a neutral ynamine (**5.19**) and a short carboxylic acid tail access to a negatively charged ynamine (**5.20**) at physiological pH (Scheme 5.7). Ynamines **5.18** and **5.19** were obtained after an amide coupling in 85% and 63% yield respectively and ynamine **5.20** was obtained through a ring opening of succinic anhydride in 79% yield (Scheme 5.7).



Scheme 5.7. (A) Synthesis of **5.18**. *Conditions:* **4.3** (1 equiv), 3-morpholinopropanoic acid hydrochloride (1.2 equiv), EDC.HCl (1.2 equiv), DMAP (0.2 equiv), TEA (4 equiv), DCM, rt, 4 days, then 3-morpholinopropanoic acid hydrochloride (1.2 equiv), EDC.HCl (1.2 equiv), DMAP (0.2 equiv), 40 °C, 3 h. (B) Synthesis of **5.19**. *Conditions:* **4.3** (1 equiv), 2-(2-(2-methoxyethoxy)ethoxy)acetic acid (1.2 equiv), EDC.HCl (1.2 equiv), DMAP (0.2 equiv), DCM, rt, 5 hours. (C) Synthesis of **5.20**. *Conditions:* **4.3** (1 equiv), succinic anhydride (3 equiv), toluene, 100 °C, 7 hours.

The corresponding triazoles **5.21a/b** – **5.23a/b** as well as triazole **5.25** were then synthesised. Triazole **5.25** serves as a control as it was previously noted to be soluble up to concentrations of 50 μM .²⁷⁸ Using only $\text{Cu}(\text{OAc})_2$ led to a poor yield for triazole **5.23b** (24%), whereas the addition of AMTC and NaAsc led to higher yields for the rest of the ynamine triazoles (**5.21a/b**, **5.22a/b** and **5.23a**).

TLC analysis usually indicated full conversion, but product isolations were challenging, as most triazoles exhibited poor solubility and streaking during column chromatography, which led to significant losses during work up and purification. Compound **5.23a** (91% yield) exemplified this, as the product was isolated by precipitation in water and filtration.



Scheme 5.8. (A) Synthesis of **5.21a/b**, **5.22a/b** and **5.23a**. Conditions: **5.18**, **5.19** or **5.20** (1 equiv), **5.10** or **5.11** (1.1 equiv), Cu(OAc)_2 (0.05 equiv), AMTC (0.1 equiv), NaAsc (0.1 equiv), rt, overnight, MeOH. (B) Synthesis of **5.23b**. Conditions: **5.20** (1 equiv), **5.10** (1.1 equiv), Cu(OAc)_2 (0.05 equiv), rt, overnight MeOH. (C) Synthesis of **5.25**. Conditions: **5.24** (1 equiv), **5** (1 equiv), Cu(OAc)_2 (0.05 equiv), NaAsc (0.1 equiv), rt, overnight.

5.4.3 Testing the Solubility of Modified Ynamine Triazoles

With the panel of diverse triazoles in hand, the solubility under the fluorescent assay conditions were then tested. The triazoles were plated (50 μ M) in 10% DMSO in 1 X DPBS and the fluorescent intensity monitored over 4 h. Only ynamines carrying a negative charge (**5.23a/b**) and control triazole **5.25** were effectively solubilised over the duration of the experiment (Figure 5.3). As there was no difference between triazole **5.23a** and **5.23b**, it was decided to focus on the anthracene fluorogenic azide (**5.11**) due to its lower background fluorescence and ease of synthesis when compared with the coumarin azide **5.10**.

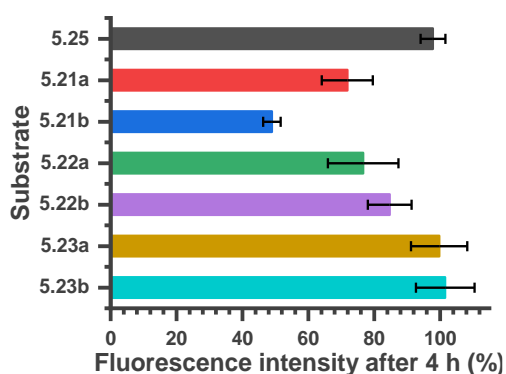


Figure 5.3. Percentage fluorescent intensity of triazoles **5.21a/b** – **5.23a/b** and **5.25** remaining after 4 h in 10% DMSO/1X DPBS. *Conditions:* **5.21a/b** – **5.23a/b** and **5.25** (50 μ M), 10% DMSO in 1X DPBS, 25 $^{\circ}$ C, 4 h. Buffer pH = 7.4. Error bars represent the standard deviation calculated from three experiments.

A parameter that had not been explored previously was the impact of Triton X-100 – commonly used to lysed cells – on solubility. Triton X-100 is a surfactant and might increase the solubility of the ynamine triazoles. Therefore triazole **5.21a** – **5.23a** and **5.25** were incubated at 50 μ M for 4 h in 10% DMSO/1X DPBS with an additional 1% Triton X-100. There was no decline in fluorescent intensity for all compounds over 4 h (Figure 5.4), indicating good solubility. The initial decrease after 15 minutes might be due to a measurement error as it was the same for all compounds. Therefore, the addition of 1% Triton solved the solubility issues and allows straightforward comparisons between buffer and cell lysate experiments.

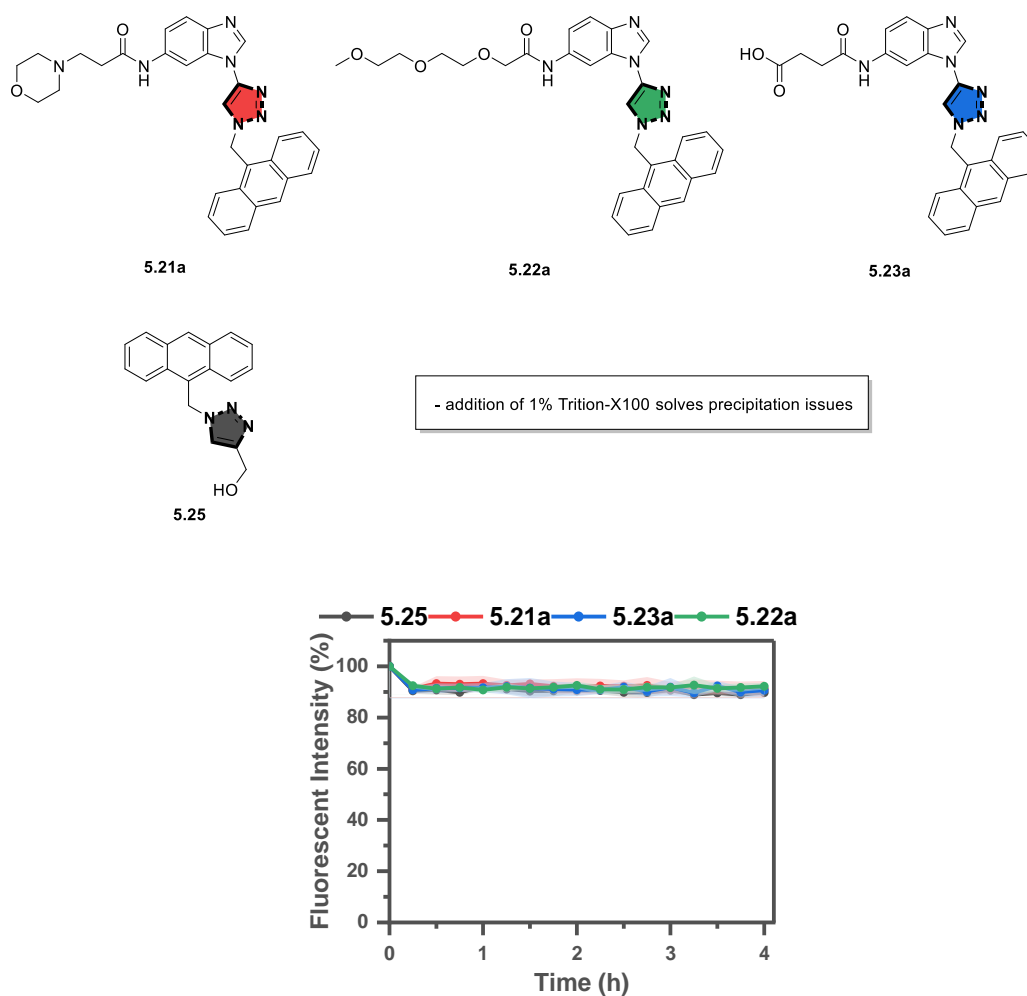


Figure 5.4. Fluorescent intensities of triazoles **5.21a** – **5.23a** and **5.25** over 4 h in 10% DMSO/1X DPBS with 1% added Triton X-100. *Conditions:* **5.21a** – **5.23a** and **5.25** (50 μ M), 1% Triton X-100/10% DMSO in 1X DPBS, 25 $^{\circ}$ C, 4 h. Buffer pH = 7.4. Shaded areas represent the standard deviation from calculated from three experiments.

5.4.4 Optimization of the Ynamine-CuAAC Ligation in Buffer

5.4.4.1 Screening of Reaction Conditions and Design of Experiments

The ynamine-CuAAC reaction was first tested in buffer to establish a baseline which then could be compared with cell lysate experiments. Traditionally, no ligand or NaAsc are needed to achieve fast reaction rates for the ynamine-CuAAC,^{151–153} but this might change in diluted aqueous conditions. Therefore, it was chosen to investigate a combination of factors: no NaAsc, just NaAsc, just BTAA and BTAA with NaAsc. Specifically, the reaction between ynamine **5.18** (50 μ M) and azide **5.11** (50 μ M) was conducted with NaAsc (1, 5 and 10 mM),

BTAA (50, 100 and 200 μM) and a combinations of NaAsc and BTAA as well as with only $\text{Cu}(\text{OAc})_2$ (50 μM).

No conversion was observed for reactions with using only $\text{Cu}(\text{OAc})_2$ as well as $\text{Cu}(\text{OAc})_2$ and BTAA (Experimental Table 5.3). A maximum conversion of 60 – 70% was reached after 1 h when NaAsc was added, and conversion decreased with higher NaAsc concentration (Figure 5.5A). The combination NaAsc and BTAA increased both reaction rate and maximum conversion (Figure 5.5B); higher NaAsc still decreased maximum conversion (for 2 and 4 equiv of BTAA see Experimental Figure 5.14A and B).

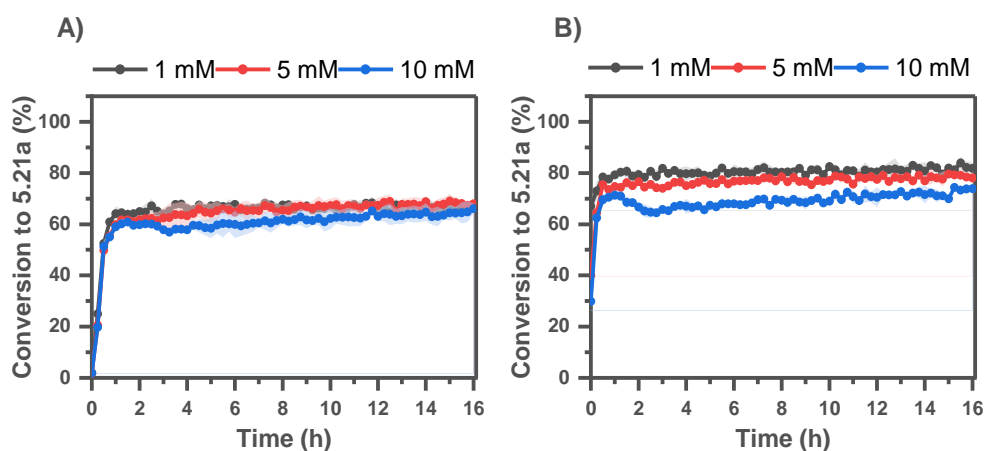
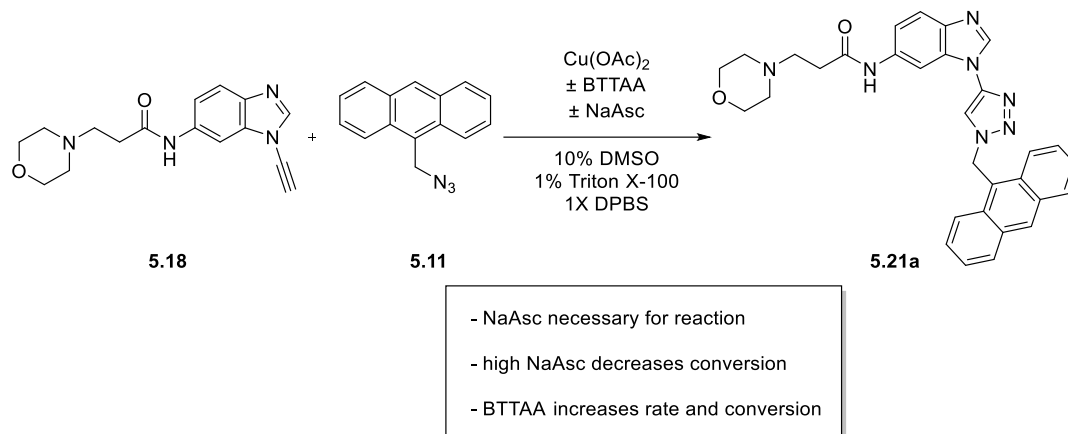


Figure 5.5. (A) Reaction of ynamine **5.18** with azide **5.11** with added NaAsc (1, 5 and 10 mM). *Conditions:* **5.18** (50 μM), **5.11** (50 μM), $\text{Cu}(\text{OAc})_2$ (50 μM), NaAsc (1, 5 or 10 mM), 1% Triton X-100/10% DMSO in 1X DPBS, 25 $^{\circ}\text{C}$, 16 h. (B) Reaction of ynamine **5.18** with azide **5.11** with added NaAsc (1, 5 and 10 mM) and BTAA (50 μM). *Conditions:* **5.18** (50 μM), **5.11** (50 μM), $\text{Cu}(\text{OAc})_2$ (50 μM), BTAA (50 μM), NaAsc (1, 5 and 10 mM), 1% Triton X-100/10% DMSO in 1X DPBS, 25 $^{\circ}\text{C}$, 16 h. Buffer pH = 7.4. Shaded areas represent the standard deviation from calculated from three experiments.

The ynamine **5.18** did not react in the absence of NaAsc which suggests that no $\text{Cu}(\text{I})$ was formed through the Glaser coupling. As expected, the addition of BTAA to the reaction with

NaAsc increased reaction rate and maximum conversion. Interestingly, higher NaAsc concentrations lower maximum conversion. This phenomenon is observed both with and without BTTTAA. The reason for this is not known, but NaAsc is known to generate side products in the presence of copper, which might react with the ynamine **5.18**.^{282,283}

The data for the NaAsc/BTTAA combination experiments were obtained in a DoE format (2-factor full factorial design) which was suitable for statistical analysis. The results were entered into MODDE[®] software and a contour plot was produced showing conversions at 2 h as a function of the stoichiometry of BTTAA (1 – 4 equivalents) relative to Cu(OAc)₂ and [NaAsc] (1 – 10 mM) (Figure 5.6). The plot illustrates that high NaAsc concentrations reduced conversion whereas a higher amounts of BTTAA (≥ 2.5) relative to a Cu(II) source were beneficial. The plot also indicated that the optimum reaction conditions had not been explored yet and potentially would lie between 2 – 4 equivalents of BTTAA and less than 1 mM NaAsc.

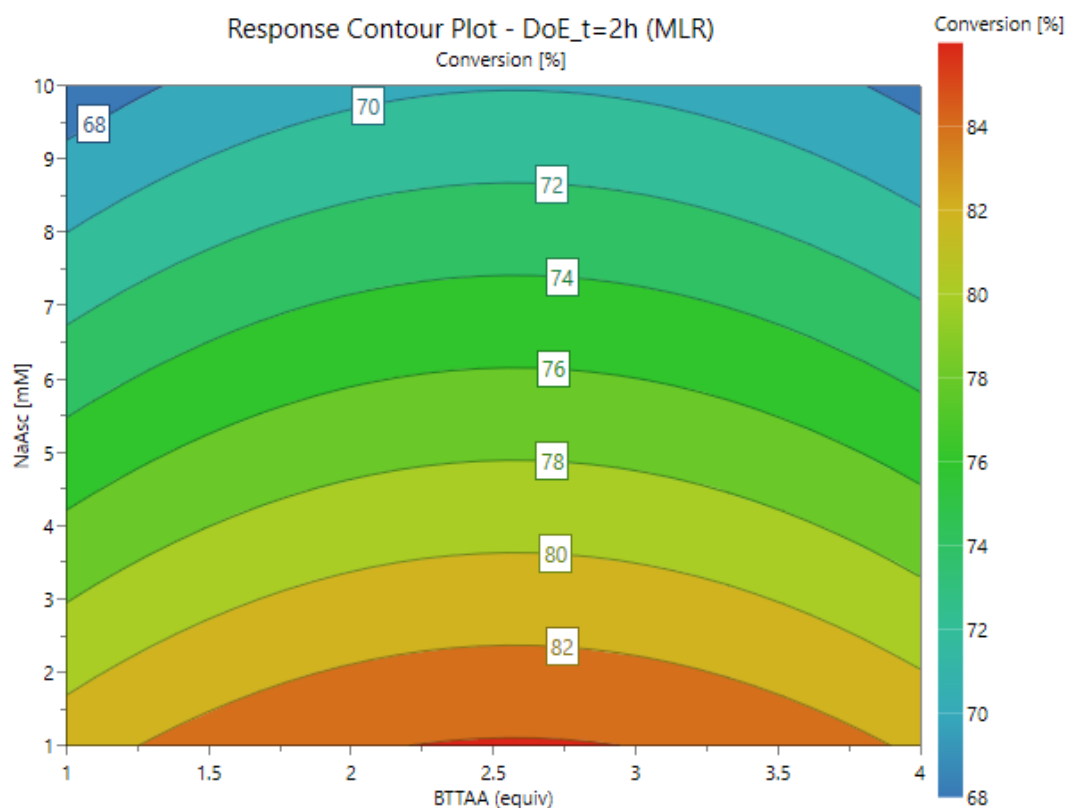


Figure 5.6. Response contour plot showing conversions to **5.21a** over a range of NaAsc concentrations (1 – 10 mM) and BTTAA equivalents (1 – 4), $t = 2$ h. Conditions: **5.18** (50 μ M), **5.11** (50 μ M), Cu(OAc)₂ (50 μ M), BTTAA (50, 100 and 200 μ M), NaAsc (1, 5 and 10 mM), 1% Triton X-100/10% DMSO in 1X DPBS, 25 $^{\circ}$ C, 16 h. Buffer pH = 7.4.

Therefore, a second DoE was devised to explore these conditions. The concentration of $\text{Cu}(\text{OAc})_2$ was kept at 50 μM and the boundaries of BTAA and NaAsc were set to 2 and 4 equivalents and to 0.1 and 1 mM respectively. The reactions were only monitored for 2 h as the previous experiments indicated maximum conversion at this point. From these experiments a response contour plot was constructed to illustrate the findings (Figure 5.7, for reaction profile plots see Experimental Figure 5.15A - C).

The plot revealed the reaction's strong dependence on NaAsc with the conversion falling sharply when going from 1 to 0.1 mM. The equivalents of BTAA affected the reaction less and both boundaries explored provided good conversion.

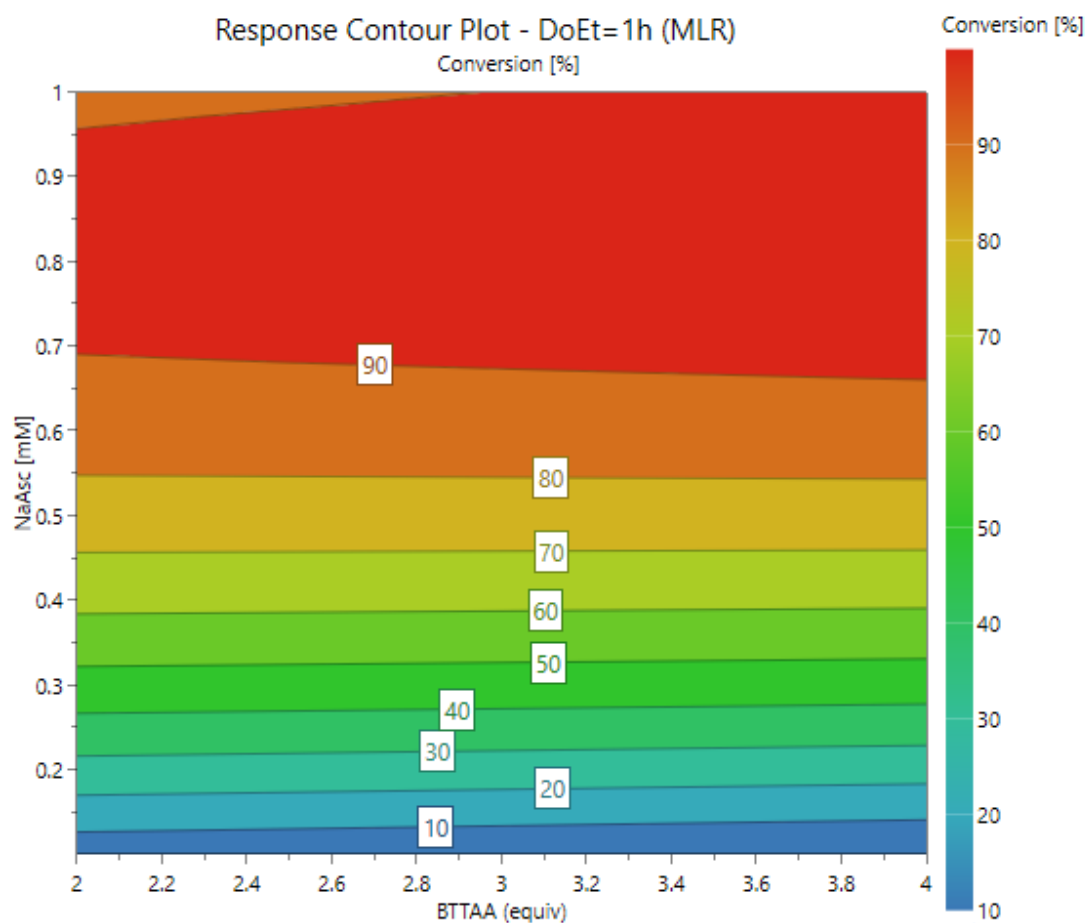


Figure 5.7. Response contour plot showing conversions to **5.21a** over a range of NaAsc concentrations (0.1 – 1 mM) and BTAA equivalents (2 – 4) at $t = 1$ h. Conditions: **5.18** (50 μM), **5.11** (50 μM), $\text{Cu}(\text{OAc})_2$ (50 μM), BTAA (100, 150 and 200 μM), NaAsc (0.1, 0.5 and 1 mM), 1% Triton X-100/10% DMSO in 1X DPBS, 25 $^{\circ}\text{C}$, 2 h. Buffer pH = 7.4.

Next, the dependence of the reaction rate on the copper concentration (0.1 – 5 μM) was explored. The concentration of NaAsc and BTAA was fixed to 1 mM and 50 μM respectively

and the reaction between ynamine **5.18** and azide (**5.11**) was monitored for 2 h (Figure 5.8). As expected, the conversion decreased with lower $\text{Cu}(\text{OAc})_2$ concentration and ranged from 80% at 30 min (5 μM) to ~30% after 2 h (0.1 μM).

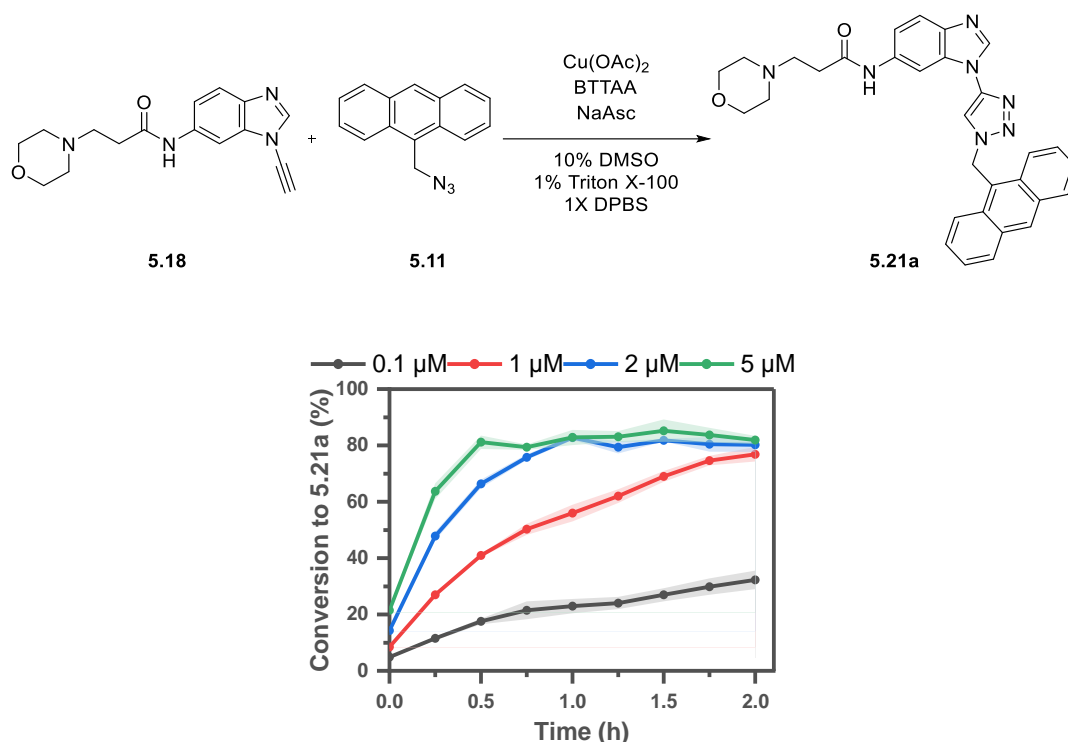


Figure 5.8. Reaction of ynamine **5.18** with azide **5.11** at varying $\text{Cu}(\text{OAc})_2$ concentrations using a fixed concentration of BTAA (50 μM) and NaAsc (1 mM). *Conditions:* **5.18** (50 μM), **5.11** (50 μM), $\text{Cu}(\text{OAc})_2$ (0.1, 1, 2 and 5 μM), BTAA (50 μM), NaAsc (1 mM), 1% Triton X-100/10% DMSO in 1X DPBS, 25 $^{\circ}\text{C}$, 2 h. Buffer pH = 7.4. Shaded areas represent the standard deviation from calculated from three experiments.

Finally, it was investigated whether NaAsc concentration could be scaled according to the copper concentration. Therefore, the experiments were repeated with 0.5, 1 and 2 μM $\text{Cu}(\text{OAc})_2$ and the NaAsc concentration either scaled (*i.e.*, 0.1, 0.2, 0.4 mM) or fixed to 1 mM. Almost no conversion was observed for the experiments with the scaled NaAsc concentration (Figure 5.9A), while the reaction using a fixed NaAsc concentration showed conversion (Figure 5.9B).

Furthermore, the results also demonstrate that a higher BTAA concentration was beneficial at low copper concentrations (< 2 μM). Only 30% conversion was observed at 1 μM $\text{Cu}(\text{Ac})_2$ when using 30 μM BTAA (Figure 5.9B), whereas ~80% conversion was achieved after 2 h with 50 μM BTAA (Figure 5.8).

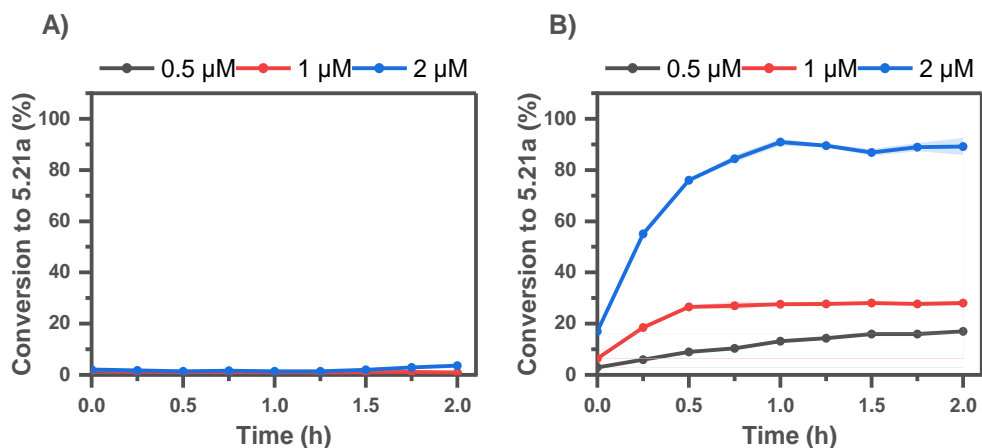
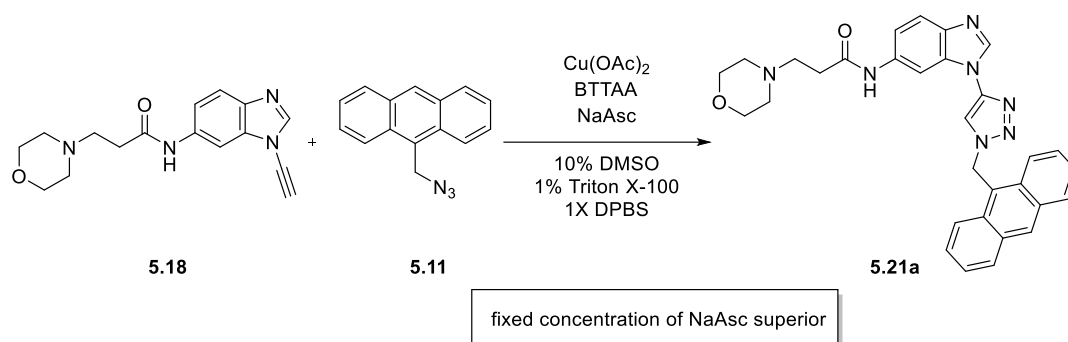


Figure 5.9. (A) Reaction of ynamine **5.18** with azide **5.11** at different $\text{Cu}(\text{OAc})_2$ concentrations. The NaAsc concentration was scaled according to $\text{Cu}(\text{OAc})_2$ concentration (200 equiv). *Conditions:* **5.18** (50 μM), **5.11** (50 μM), $\text{Cu}(\text{OAc})_2$ (0.5, 1 and 2 μM), BTAA (15, 30 and 60 μM), NaAsc (0.1, 0.2 and 0.4 mM), 1% Triton X-100/10% DMSO in 1X DPBS, 25 $^{\circ}\text{C}$, 2 h. (B) Reaction of ynamine **5.18** with azide **5.11** at different $\text{Cu}(\text{OAc})_2$ concentrations. The NaAsc concentration was fixed for all reactions (1 mM). *Conditions:* **5.18** (50 μM), **5.11** (50 μM), $\text{Cu}(\text{OAc})_2$ (0.5, 1 and 2 μM), BTAA (15, 30 and 60 μM), NaAsc (1 mM), 1% Triton X-100/10% DMSO in 1X DPBS, 25 $^{\circ}\text{C}$, 2 h. Buffer pH = 7.4. Shaded areas represent the standard deviation from calculated from three experiments.

In summary, the efficiency of the ynamine-azide click ligation performed in PBS is contingent on sufficient NaAsc being added to the reaction mixture. Concentrations of NaAsc lower than 500 μM decreased conversions significantly. Cu(I) can be oxidised in aqueous environments to $\text{Cu}(\text{II})$ ¹⁷⁹ and sufficient NaAsc must be present during the reaction to retain a catalytically active amount of $[\text{Cu}(\text{I})]$ species. The addition of BTAA both increased conversion and accelerated reaction rates; especially at lower copper concentrations. Therefore, the optimised concentrations for an ynamine-azide click ligation in a PBS buffer system are 50 μM BTAA and 1 mM NaAsc regardless of the $\text{Cu}(\text{OAc})_2$ concentration.

Direct comparisons with literature studies are difficult due to differing reaction conditions, but the ynamine-CuAAC reaction generally performs on par or better in terms of reaction rate at a given copper concentration. For example, studies evaluating novel ligands were usually performed with 50 – 75 μM CuSO_4 and only reaching maximum conversion in over ~30 – 60 mins.^{70,71,83} The performance of the ynamine (e.g., **5.18**) was more comparable to studies which evaluate copper chelating azides, where maximum conversion (60 – 100%) was achieved in 1 – 5 mins when using 10 – 20 μM CuSO_4 .^{78,82} In terms of ultralow copper concentration CuAAC (<1 μM) the ynamine performs comparably or slightly worse to specialist catalytic systems such as entrapped copper nanoparticles,⁸⁴ MOFs²⁸⁴ or short-chain organic nanoparticles.²⁸⁵

5.4.5 Exploration of Ynamine-CuAAC Ligations in Cell Lysate

After the first DoE, the reaction between ynamine **5.18** and azide **5.11** was performed using 5, 10 and 30 μM $\text{Cu}(\text{OAc})_2$ in HeLa cell lysate (Figure 5.10A). Full conversion was reached within 15 mins when using 30 μM $\text{Cu}(\text{OAc})_2$ and ~80% after 2 h when using 10 μM $\text{Cu}(\text{OAc})_2$. The reaction was repeated using ynamine **5.19** and showed that conversion to **5.22a** was comparable to that of **5.21a** (Figure 5.10B). Comparing these results to the reactions in buffer (Figure 5.8B), the reactivity was reduced considerably, especially at lower copper concentrations (5 and 10 μM). However, excellent reactivity was still achieved using 30 μM $\text{Cu}(\text{OAc})_2$.

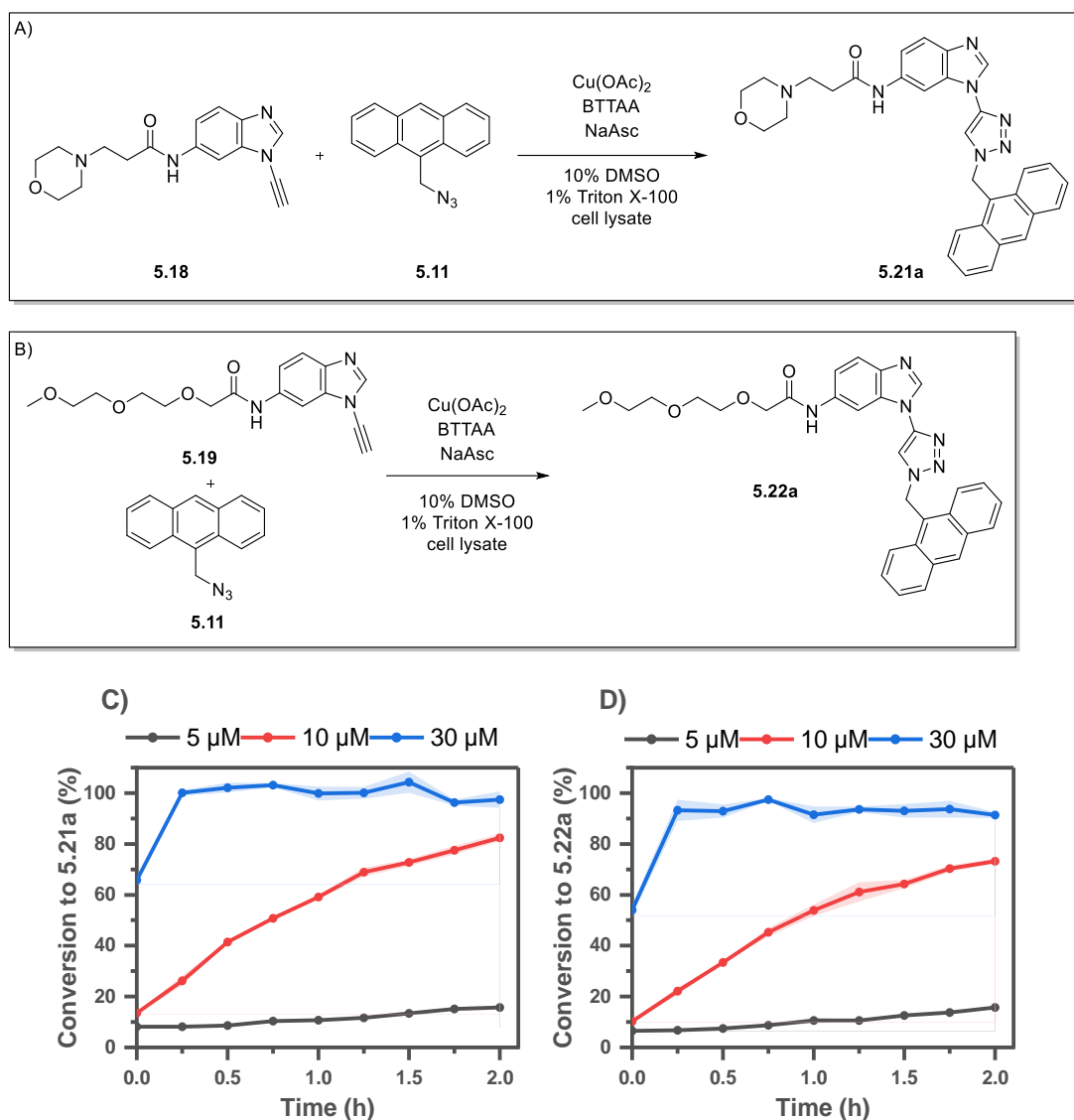


Figure 5.10. (A) Reaction of ynamine **5.18** with azide **5.11** in cell lysate. *Conditions:* **5.18** (50 μ M), **5.11** (50 μ M), $\text{Cu}(\text{OAc})_2$ (5, 10 and 30 μ M), BTAA (15, 30 and 90 μ M), NaAsc (1 mM), 1% Triton X-100/10% DMSO in cell lysate, 25 $^{\circ}\text{C}$, 2 h. (B) Reaction of ynamine **5.19** with azide **5.11** in cell lysate. *Conditions:* **5.19** (50 μ M), **5.11** (50 μ M), $\text{Cu}(\text{OAc})_2$ (5, 10 and 30 μ M), BTAA (15, 30 and 90 μ M), NaAsc (1 mM), 1% Triton X-100/10% DMSO in cell lysate, 25 $^{\circ}\text{C}$, 2 h. (C) Conversion to **5.21a** for reaction A in cell lysate. (D) Conversion to **5.22a** for reaction B in cell lysate. Buffer pH = 7.4. Shaded areas represent the standard deviation from calculated from three experiments.

Next, the reaction between propargyl alcohol **5.24** and azide **5.11** was carried out in buffer and cell lysate. In buffer, conversion was only observed for the highest copper concentration tested (30 μ M, ~30%) (Figure 5.11A). In cell lysate, no conversion to **5.25** was observed for all copper concentrations (Figure 5.11B). This shows the reactivity advantage of the aromatic ynamine (*e.g.*, **5.18**) relative to conventional alkynes.

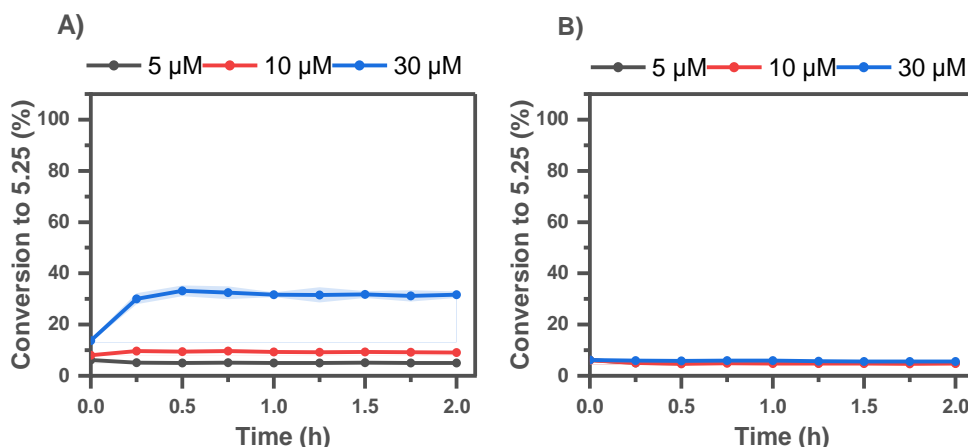
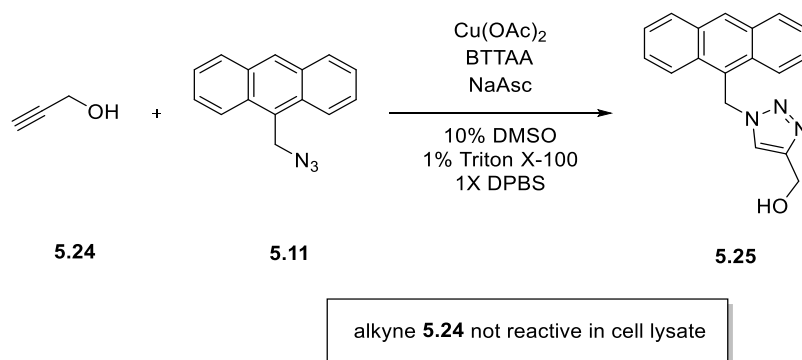


Figure 5.11. (A) Reaction of alkyne **5.24** with azide **5.11** in buffer. *Conditions:* **5.24** (50 μM), **5.11** (50 μM), Cu(OAc)₂ (5, 10 and 30 μM), BTAA (15, 30 and 90 μM), NaAsc (1 mM), 1% Triton X-100/10% DMSO in 1X DPBS, 25 °C. 2 h. (B) Reaction of alkyne **5.24** with azide **5.11** in cell lysate. *Conditions:* **5.24** (50 μM), **5.11** (50 μM), Cu(OAc)₂ (5, 10 and 30 μM), BTAA (15, 30 and 90 μM), NaAsc (1 mM), 1% Triton X-100/10% DMSO in cell lysate, 25 °C, 2 h. Buffer pH = 7.4. Shaded areas represent the standard deviation from calculated from three experiments.

Finally, the reactions between ynamine **5.18** and azide **5.11** as well as between alkyne **5.24** and azide **5.11** were then repeated using the optimal conditions (50 μM BTAA and 1 mM NaAsc) at different copper concentrations in cell lysate. For ynamine **5.18**, an increased BTAA concentration (50 vs 15 μM) again resulted in higher conversions to **5.21a** (60 vs 15% when using 5 μM Cu(OAc)₂, Figure 5.12A vs Figure 5.10A). The conversion was unaffected when 30 μM Cu(OAc)₂ was used, while no conversion was observed for the lowest Cu(OAc)₂ concentration (0.1 μM). As before, alkyne **5.24** remained unreactive in cell lysate for any Cu(OAc)₂ concentration used (Figure 5.12B).

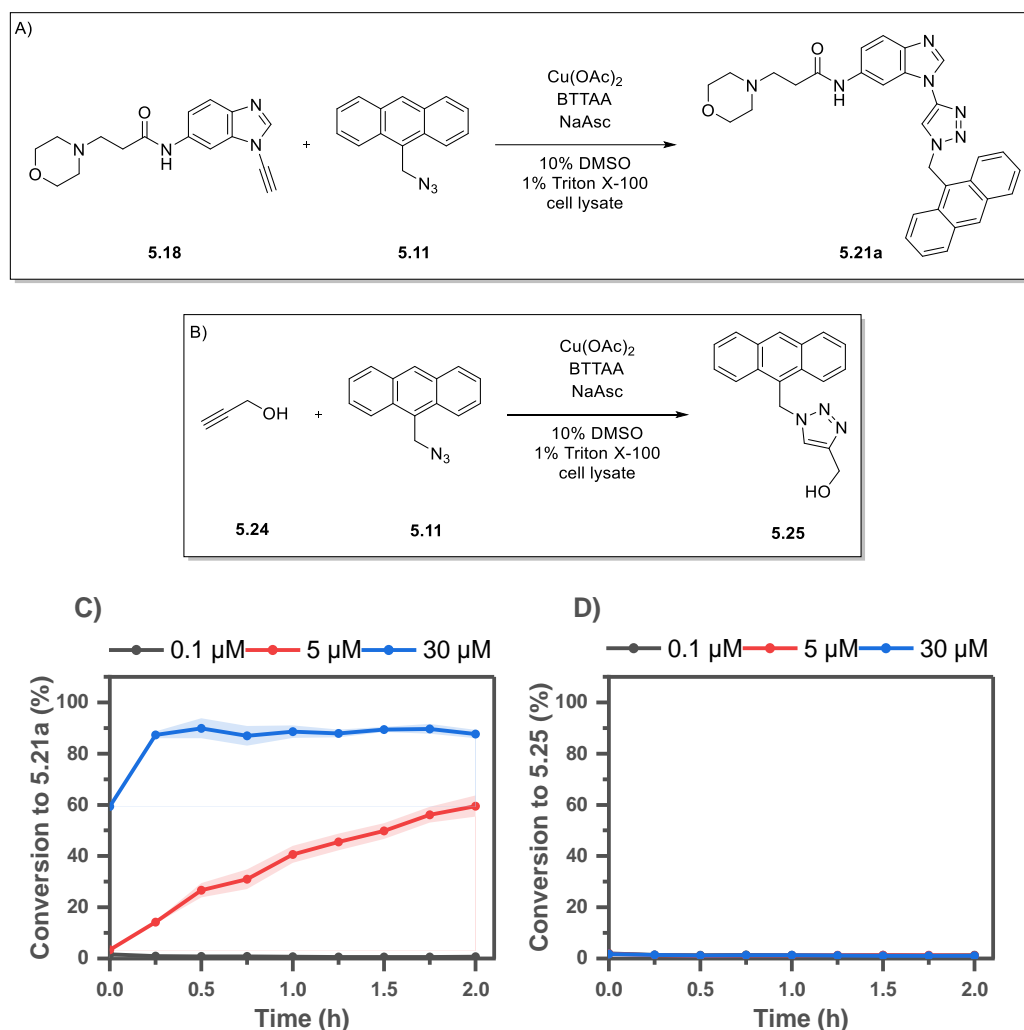


Figure 5.12. (A) Reaction ynamine **5.18** with azide **5.11** in cell lysate using the optimal conditions. *Conditions:* **5.18** (50 μ M), **5.11** (50 μ M), Cu(OAc)₂ (0.1, 5 and 30 μ M), BTAA (50 μ M), NaAsc (1 mM), 1% Triton X-100/10% DMSO in cell lysate, 25 $^{\circ}$ C, 2 h. (B) Reaction of alkyne **16** with azide **5** in cell lysate using the optimal conditions. *Conditions:* **5.18** (50 μ M), **5.11** (50 μ M), Cu(OAc)₂ (0.1, 5 and 30 μ M), BTAA (50 μ M), NaAsc (1 mM), 1% Triton X-100/10% DMSO in cell lysate, 25 $^{\circ}$ C, 2 h. (D) Conversion to **5.21a** for reaction A in cell lysate. (D) Conversion to **5.25** for reaction B in cell lysate. Buffer pH = 7.4. Shaded areas represent the standard deviation from calculated from three experiments.

These experiments demonstrate that aromatic ynamines (*e.g.*, **5.18**) are more reactive than conventional alkynes in cell lysate. It is believed that the superior reactivity will also translate to *in vivo* experiments.

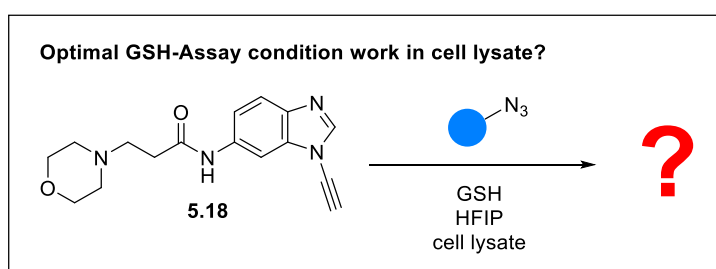
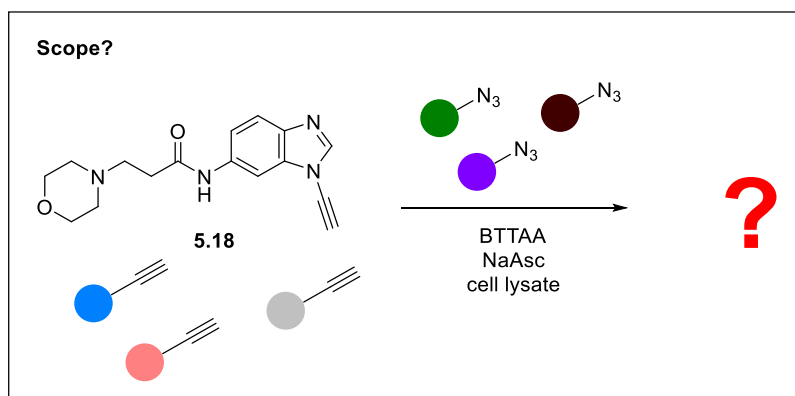
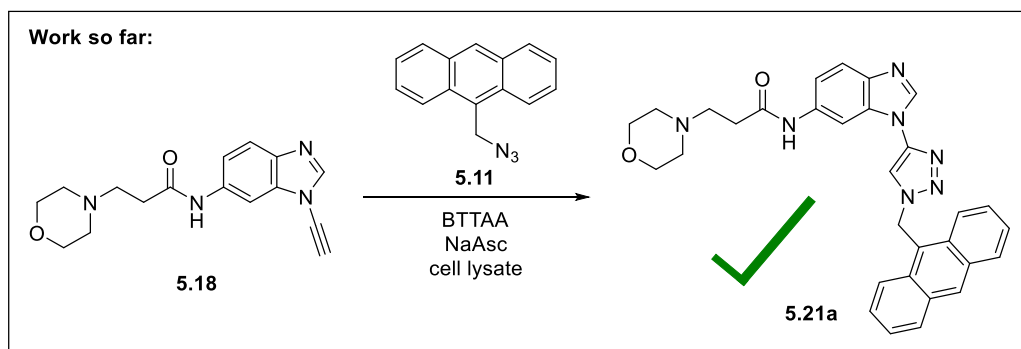
Another important point to investigate in the future is the potential influence of Triton X-100, which improved the SPAAC reaction through micellar catalysis.¹¹⁷ If the ynamine-CuAAC reaction were also accelerated by micellar catalysis in cell lysate, the reactivity in *in vivo* experiments would be reduced as no Triton X-100 would be present.

5.5 Summary & Future Directions

In summary, a fluorescent 96-well plate assay was developed to test the ynamine-CuAAC reactivity in cell lysate. The reaction between ynamine **5.18** and azide **5.25** was first optimised in buffer, and it was found that the addition of NaAsc was critical for reactivity. While high concentrations led to slightly lower conversions, low concentrations failed to initiate the reaction. A concentration of 1 mM NaAsc proved to be the most versatile and was used for most experiments. The addition of BTAA to the reaction increased conversions and a wide spectrum of BTAA equivalents was tolerated. The BTAA concentration was only critical when the reactions were performed at low copper concentrations ($<5\ \mu\text{M}$).

These conditions translated into cell lysate and full conversion in under 15 mins was observed for $\text{Cu}(\text{OAc})_2 > 30\ \mu\text{M}$. The reaction slowed considerably at low copper concentrations in cell lysate but still achieved ~60% conversion with $5\ \mu\text{M}$ copper. In comparison, the alkyne **5.24** was unreactive in cell lysate under the same conditions and showed only modest conversion in buffer with $30\ \mu\text{M}$ $\text{Cu}(\text{OAc})_2$.

Several open questions remain (Scheme 5.9). First, the scope of the ynamine-CuAAC should be supplemented with further fluorogenic azides to test the robustness of the system. Both coumarin azides (**5.1** and **5.10**) would be good substrates and should be soluble through the addition of Triton X-100. The optimal ynamine-CuAAC conditions with GSH have not been tested in the fluorescent assay as they were developed after the cell lysate experiments; they would be interesting to explore.



Scheme 5.9. (A) Only reactivity of ynamine **5.18** with azide **5.11** has been explored thoroughly so far. (B) Exploration of the reactivity of a range of ynamines and alkynes in cell lysate. (C) Exploration of optimal HPLC assay ($\text{Cu}(\text{OAc})_2$, 100 μM), GSH, 100 μM , in 10% HFIP) conditions in cell lysate.

Looking further into the future, the ynamine-CuAAC reaction will be explored *in vivo*. Incorporation of azide moieties into cell surface sugars,²⁸⁶ proteins,²⁸⁶ cellular lipids²⁸⁷ and DNA²⁸⁸ can be achieved (Figure 5.13). Modification of these azides with a fluorogenic ynamine would demonstrate the applicability of the ynamine-CuAAC *in vivo*. It would be interesting to see whether BTAA can be replaced with either histidine or GSH as a CuAAC ligand.

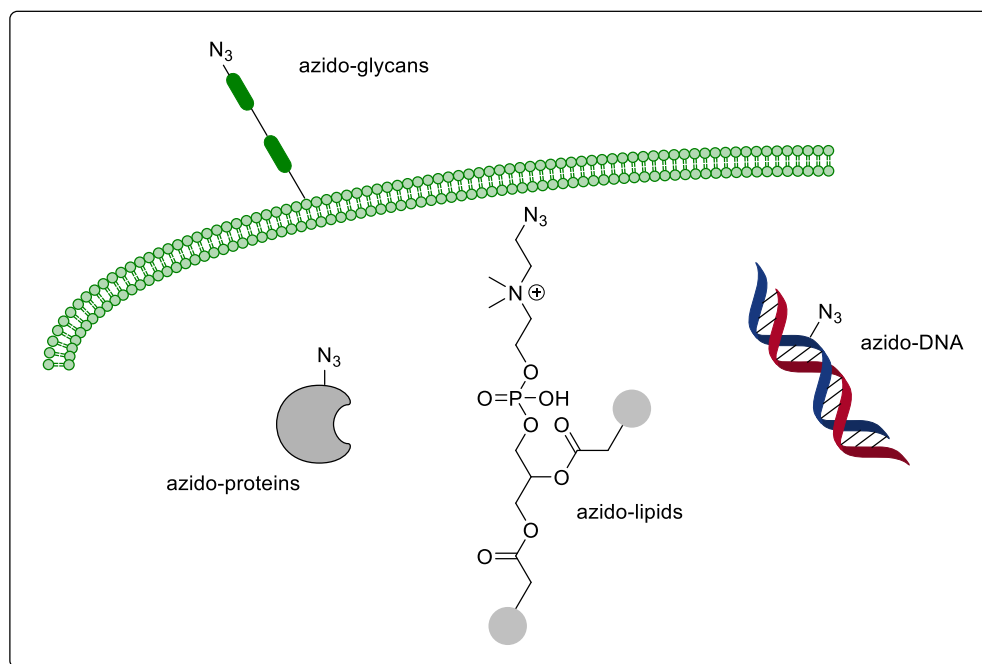


Figure 5.13. Azide functionalities can be incorporated into every major class of biomolecules. Tagging of these functionalities would demonstrate the in vivo applicability of the ynamine-CuAAC.

5.6 Experimental Procedures

5.6.1 General Experimental Techniques and Procedures

5.6.1.1 Reagents and Solvents

All reagents and solvents were used as supplied from commercial sources and used without further purification unless otherwise stated. Thin layer chromatography (TLC) was carried out using Merck silica plates coated with fluorescent indicator UV254. TLC plates were analysed under 254 nm UV light or developed using potassium permanganate solution.

5.6.1.2 Column Chromatography

Normal-phase flash chromatography was carried out using ZEOprep 60 HYD 40-63 μm silica gel.

5.6.1.3 NMR Spectroscopy

NMR spectroscopy was carried out using either a Bruker AV500 spectrometer at 500 MHz (^1H) and 126 Hz (^{13}C) or Bruker AV600 spectrometer at 156 Hz (^{13}C). All chemical shifts (δ) in CDCl_3 were referenced at 7.26 (^1H) and 77.06 ppm (^{13}C), in DMSO-d_6 at 2.50 (^1H) and 39.52 (^{13}C), in D_2O at 4.79 ppm (^1H) and in CD_3OD at 3.31 (^1H) and 49.0 ppm (^{13}C) and reported in parts per million (ppm). Coupling constants are quoted in hertz (Hz). Abbreviations for splitting patterns are s (singlet), d (doublet), t (triplet), q (quartet) and m (multiplet). All NMR data was processed using Mestrenova 11.0 software. Proton and carbon chemical shifts were assigned using proton (^1H), carbon (^{13}C), Heteronuclear Single Quantum Coherence (HSQC), Heteronuclear Multiple-Bond Correlation Spectroscopy (HMBC), Correlation Spectroscopy (COSY) and Nuclear Overhauser Effect Spectroscopy (NOESY) whenever possible (see Appendix for assigned protons/carbons).

5.6.1.4 High Resolution Mass Spectrometry

High-resolution mass spectra were recorded on an LTQ Orbitrap XL 1 mass spectrometer at the EPSRC UK National Mass Spectrometry Facility (Swansea), a Thermo Exactive Orbitrap mass spectrometer at the University of St Andrews and a Bruker Micro TOF II at the university of Edinburgh.

5.6.1.5 IR Spectroscopy

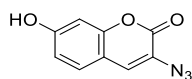
IR data were collected on either an Agilent or Shimadzu FTIR spectrometer and the data processed using the proprietary software. Only major absorbances were reported.

5.6.2 Liquid Chromatography-Mass Spectrometry (LC-MS) and Ultra-Performance-Mass-Spectrometry (UPLC-MS)

LC-MS was carried out on an Agilent HPLC instrument in conjunction with an Agilent Quadrupole mass detector on an Agilent Poroshell 120 C18 column (75 mm × 4.6 mm, 2.7 μm). UPLC-MS was carried out on an AVANT UPLC with an Advion Expression CMS L attached for mass detection on a Phenomenex Kinetex C18 column (30 mm × 2.1 mm, 2.7 μm). Electrospray ionization (ESI) was used in all cases.

5.6.3 Synthetic Procedures

3-azido-7-hydroxy-2H-chromen-2-one (**5.1**)²⁸⁰



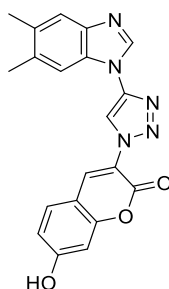
2,4-Dihydroxybenzaldehyde (2.8 g, 20 mmol) was dissolved in acetic anhydride (50 mL). Then N-acetylglycine (2.3 g, 20 mmol) and anhydrous NaOAc (4.9 g, 60 mmol) was added, and the reaction was heated to 140 °C. After 16 hours of stirring the reaction was allowed to reach room temperature and cooled to 0 °C and water (75 mL) was added. The precipitate was filtered off and the filter cakes washed with water (3 ×). The beige solid was dissolved in a mixture of conc. HCl and EtOH (3:1, 30 mL) and heated to 100 °C for 1 h, then cooled with an ice bath and water (40 mL) was added, followed by sodium nitrite (2.8 g, 40 mmol). After 20 minutes sodium azide (3.9 g, 60 mmol in 15 mL water) was added SLOWLY dropwise over 30 minutes. The reaction was left to stir for an additional 30 minutes before the precipitate was filtered off and washed with water (3 ×) to give the desired product as a brown solid (876 mg, 22%).

¹H NMR (500 MHz, DMSO) δ 10.52 (br. s, 1H), 7.59 (s, 1H), 7.48 (d, *J* = 8.5 Hz, 1H), 6.81 (dd, *J* = 8.5, 2.3 Hz, 1H), 6.76 (d, *J* = 2.3 Hz, 1H).

IR (ν_{max}): 3205 (broad, O-H), 2113 (N₃), 1701 (C=O) cm⁻¹.

NMR spectrum in accordance with literature values.²⁸⁰

3-(4-(5,6-dimethyl-1H-benzo[d]imidazol-1-yl)-1H-1,2,3-triazol-1-yl)-7-hydroxy-2H-chromen-2-one (**5.2**).



1-ethynyl-5,6-dimethyl-1H-benzo[d]imidazole (100 mg, 0.59 mmol) was dissolved in MeOH (10 mL) and 3-azido-7-hydroxy-2H-chromen-2-one (120 mg, 0.59 mmol) was added followed by $\text{Cu}(\text{OAc})_2 \cdot \text{H}_2\text{O}$ (11.7 mg, 0.59 mmol). The reaction was stirred for seven days, then the precipitated solid was filtered off and washed with sat. EDTA solution (pH 3, 20 mL), then triturated in diethyl ether to give the desired product (90 mg, 41%). A small amount of product was recrystallized from isopropanol for analysis.

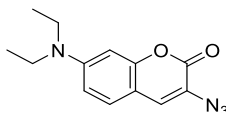
^1H NMR (500 MHz, DMSO) δ 10.99 (br. s, 1H), 9.15 (s, 1H), 8.73 (s, 1H), 8.64 (s, 1H), 7.80 (d, $J = 8.6$ Hz, 1H), 7.71 (s, 1H), 7.57 (s, 1H), 6.95 (dd, $J = 8.6, 2.2$ Hz, 1H), 6.90 (d, $J = 2.2$ Hz, 1H), 2.38 (s, 3H), 2.36 (s, 3H).

^{13}C NMR (126 MHz, DMSO) δ 163.4, 156.7, 155.4, 142.4, 142.4, 141.8, 138.1, 133.3, 132.0, 131.7, 131.3, 120.5, 119.6, 117.3, 114.9, 112.2, 110.7, 102.8, 20.6, 20.3.

IR (ν_{max}): 3133 (broad, O-H), 2958 (C-H), 1707 (C=O), 1246 (C-O) cm^{-1} .

HR-MS (ESI): $\text{C}_{20}\text{H}_{15}\text{N}_5\text{O}_3\text{H}^+$ calculated 374.1248, found 374.1246.

3-azido-7-(diethylamino)-2H-chromen-2-one (**5.10**)²⁸⁰



4-diethylamino salicylaldehyde (5.00 g, 25.8 mmol) was dissolved in n-butanol (60 mL). Then ethyl nitroacetate (3.44 g, 25.8 mmol) and molecular sieves (4 Å, 360 mg) were added, followed by piperidine (360 μL) and acetic acid (720 μL). The mixture was heated to 120 °C and heated overnight. The solid was filtered off, dissolved in DMF (40 mL) and heated to 80 °C. The hot solution was filtered to remove the molecular sieves. Ice water was added to the filtered solution and the precipitate filtered off, washed with ice water and dried under vacuum to give a red solid (4.40 g, 65%). $\text{SnCl}_2 \cdot 2\text{H}_2\text{O}$ was dissolved in 37% HCl (80 mL) and the crude material (4.40 g, 16.7 mmol) was added in portions. The reaction was stirred for 5 hours and then poured onto ice and made alkaline using 40% KOH (150 mL). The suspension was extracted with DCM (4 \times 100 mL) and the combined organic phases washed with water (150 mL) and brine (100 mL), then dried over Na_2SO_4 . The solvents were removed under vacuum

to give a red solid (2.1 g, 54%). Part of that red solid (1.85 g, 7.97 mmol) was dissolved in 17% HCl (80 mL) and cooled to 0 °C. Sodium nitrite (549 mg, 7.97 mmol) was dissolved in water (2 mL) and added dropwise to the reaction. After 45 minutes anhydrous NaOAc (38 g) was added to raise the pH to 4 and then sodium azide (1.04 g, 15.9 mmol) was dissolved in water (5 mL) and added dropwise to the reaction which was stirred at room temperature for 4 hours. The suspension was filtered, the filter cake washed with water and the solid dried under vacuum to give the desired compound as a grey/greenish solid (754 mg, 37%, 11% overall).

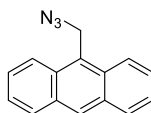
¹H NMR (500 MHz, CDCl₃) δ 7.19 (d, *J* = 8.8 Hz, 1H), 7.10 (s, 1H), 6.59 (dd, *J* = 8.8, 2.5 Hz, 1H), 6.51 (d, *J* = 2.5 Hz, 1H), 3.41 (q, *J* = 7.1 Hz, 4H), 1.21 (t, *J* = 7.1 Hz, 6H).

IR (*ν*_{max}): 2974 (C-H), 2110 (N₃), 1709 (C=O) cm⁻¹.

LC-MS: C₁₃H₁₄N₄O₂H⁺ calculated 259.1, found 259.3.

NMR spectrum in accordance to literature values.²⁸⁰

9-(azidomethyl)anthracene (**5.11**)



Anthracen-9-ylmethanol (200 mg, 0.96 mmol) was dissolved in DCM (4 mL) and cooled to 0 °C. Then triethylamine (194 mg, 1.92 mmol) and mesyl chloride (121 mg, 1.0 mmol) were added and the reaction was stirred at 0 °C for three hours. Then DCM was removed under a stream of air, DMF (4 mL) and NaN₃ (93 mg, 1.44 mmol) were added, and the reaction stirred overnight. Then ethyl acetate (30 mL) and water (30 mL) were added, and the phases separated. The organic phase was washed with water (30 mL) and brine (30 mL), then dried over Na₂SO₄. The solvents were removed under vacuum and the residue purified by column chromatography (20% ethyl acetate in petroleum ether) to give the desired compound as a yellow solid (146 mg, 65%).

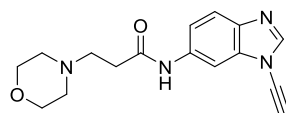
¹H NMR (500 MHz, CDCl₃) δ 8.50 (s, 1H), 8.29 (d, *J* = 9.1 Hz, 2H), 8.05 (d, *J* = 8.4 Hz, 2H), 7.64 – 7.56 (m, 2H), 7.55 – 7.48 (m, 2H), 5.33 (s, 2H).

¹³C NMR (126 MHz, CDCl₃) δ 131.4, 130.7, 129.3, 129.0, 126.9, 125.8, 125.2, 123.5, 46.4.

IR (*ν*_{max}): 3057 (ar. C-H), 2926 (C-H), 2100 (N₃) cm⁻¹

NMR spectra according to literature.²⁸⁹

N-(1-ethynyl-1*H*-benzo[*d*]imidazol-6-yl)-3-morpholinopropanamide (**5.18**)



3-(Morpholin-4-yl)propanoic acid hydrochloride (125 mg, 0.60 mmol), EDC.HCl (114 mg, 0.6 mmol), DMAP (12 mg, 0.1 mmol) and TEA (150 μ L) were dissolved in DCM (3 mL). 1-ethynyl-1*H*-benzo[d]imidazol-6-amine (78 mg, 0.5 mmol) was dissolved in DCM (2 mL) and added dropwise to reaction, which was stirred for 4 days. Due to incomplete conversion further 3-(Morpholin-4-yl)propanoic acid hydrochloride (125 mg, 0.60 mmol), EDC.HCl (114 mg, 0.6 mmol) and DMAP (12 mg, 0.1 mmol) were added and the reaction was heated to 40°C. After 3 hours the starting material was consumed, and the reaction diluted with DCM (20 mL) and water (20 mL). The aqueous phase was extracted with DCM (20 mL), the organic phases were combined, washed with brine (20 mL) and dried over Na₂SO₄. The solvent was removed under vacuum and the residue was purified by column chromatography (80% ethanol/ethyl acetate (1:3)/ 1% triethylamine in petroleum ether) to give the desired compound as a brown solid (126 mg, 85%).

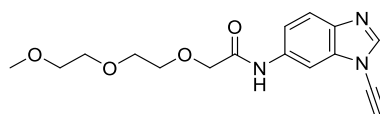
¹H NMR (500 MHz, CDCl₃) δ 11.01 (br. s, 1H), 8.32 (d, J = 2.0 Hz, 1H), 8.02 (s, 1H), 7.69 (d, J = 8.6 Hz, 1H), 7.07 (dd, J = 8.6, 2.0 Hz, 1H), 3.84 (t, J = 4.7 Hz, 4H), 3.29 (s, 1H), 2.77 (dd, J = 6.6, 5.2 Hz, 2H), 2.64 (br. s, 4H), 2.58 (dd, J = 6.6, 5.2 Hz, 2H).

¹³C NMR (126 MHz, CDCl₃) δ 170.3, 143.5, 138.0, 136.2, 135.0, 120.9, 116.3, 102.3, 70.1, 67.1, 62.5, 54.2, 52.8, 32.3.

IR (ν_{\max}): 3200 (sp C-H), 3087 (ar. C-H) 2826 (C-H), 2152 (C \equiv C), 1608 (C=O), 1489 (ar. C=C) cm⁻¹.

HR-MS (ESI): C₁₆H₁₈N₄O₂H⁺ calculated 299.1503, found 299.1502.

N-(1-ethynyl-1*H*-benzo[d]imidazol-6-yl)-2-(2-(2-methoxyethoxy)ethoxy)acetamide (**5.19**)



2-(2-(2-methoxyethoxy)ethoxy)acetic acid (136 mg, 0.76 mmol), EDC.HCl (146 mg, 0.76 mmol) and DMAP (15 mg, 0.13 mmol) were dissolved in DCM (4 mL). After 10 minutes 1-ethynyl-1*H*-benzo[d]imidazol-6-amine (100 mg, 0.64 mmol) was added, and the reaction was stirred for 5 hours. The mixture was diluted with DCM (20 mL) and water (20 mL). The phases were separated, and the organic phase was washed with brine (20 mL) and dried over Na₂SO₄. The solvent was removed under vacuum and the residue purified by column chromatography

(50 – 60% ethanol/ethyl acetate (1:3) in petroleum ether) to give the desired compound as a dark oil (126 mg, 63%).

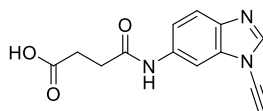
¹H NMR (500 MHz, CDCl₃) δ 8.97 (br. s, 1H), 8.27 (d, *J* = 2.0 Hz, 1H), 8.03 (s, 1H), 7.70 (d, *J* = 8.6 Hz, 1H), 7.29 (dd, *J* = 8.6, 2.0 Hz, 1H), 4.14 (s, 2H), 3.81 – 3.75 (m, 2H), 3.76 – 3.69 (m, 4H), 3.60 – 3.54 (m, 2H), 3.33 (s, 3H), 3.29 (s, 1H).

¹³C NMR (126 MHz, CDCl₃) δ 168.3, 143.7, 138.5, 135.0, 134.8, 120.8, 117.2, 102.8, 71.8, 71.3, 70.7, 70.5, 70.2, 70.1, 62.5, 59.0.

IR (ν_{\max}): 3228 (sp C-H), 3124 (ar. C-H) 2908 (C-H), 2154 (C≡C), 1690 (C=O), 1487 (ar. C=C) cm⁻¹.

HR-MS (ESI): C₁₆H₁₉N₃O₄H⁺ calculated 318.1448, found 318.1448.

4-((1-ethynyl-1H-benzo[d]imidazol-6-yl)amino)-4-oxobutanoic acid (5.20)



1-Ethynyl-1H-benzo[d]imidazol-6-amine (100 mg, 0.64 mmol) was dissolved in toluene (6 mL) and succinic anhydride (70 mg, 0.7 mmol) was added. Then, the reaction was heated to 100 °C for seven hours. The resulting suspension was filtered, and the precipitate kept. The filtrate was diluted with water (30 mL) and ethyl acetate (20 mL). The phases were separated, and the aqueous phase was extracted with ethyl acetate (20 mL). The combined organic phases were washed with brine (20 mL) and dried over Na₂SO₄. The solvent was removed under vacuum and the residue combined with the precipitate. The mixture was purified by column chromatography (10 – 40% ethanol/ethyl acetate (1:3) in petroleum ether) to give the desired compound as a light brown solid (129 mg, 79%).

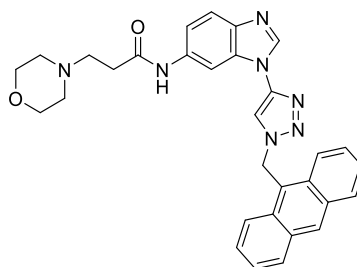
¹H NMR (500 MHz, DMSO) δ 12.17 (br. s, 1H), 10.23 (s, 1H), 8.54 (s, 1H), 8.25 (d, *J* = 2.0 Hz, 1H), 7.68 (d, *J* = 8.7 Hz, 1H), 7.32 (dd, *J* = 8.7, 2.0 Hz, 1H), 4.72 (s, 1H), 2.61 – 2.58 (m, 2H), 2.56 – 2.53 (m, 2H).

¹³C NMR (126 MHz, DMSO) δ 174.3, 170.8, 144.7, 137.5, 137.3, 134.8, 120.8, 116.4, 100.9, 70.7, 65.4, 31.6, 29.2.

IR (ν_{\max}): 3263 (sp C-H), 3200 (broad, COOH) 3128 (ar. C-H) 2936 (C-H), 2163 (C≡C), 1750 (C=O), 1608 (C=O), 1504 (ar. C=C) cm⁻¹.

HR-MS (ESI): C₁₃H₁₁N₃O₃H⁺ calculated 258.0873, found 258.0873.

N-(1-(1-(anthracen-9-ylmethyl)-1H-1,2,3-triazol-4-yl)-1H-benzo[d]imidazol-6-yl)-3-morpholinopropanamide (5.21a)



N-(1-ethynyl-1*H*-benzo[*d*]imidazol-6-yl)-3-morpholinopropanamide (30 mg, 0.1 mmol) and anthracene azide (26 mg, 0.11 mmol) were dissolved in MeOH (2 mL) followed by Cu(OAc)₂•H₂O (1.0 mg, 0.005 mmol). AMTC (2.3 mg, 0.01 mmol) and NaAsc (2.0 mg, 0.01 mmol) were dissolved in the minimum amount of water and then added dropwise. The reaction was stirred at room temperature overnight. Then sat. EDTA solution (pH 3, 20 mL) and DCM (30 mL) were added, and the phases were separated. The organic phase was washed with brine (20 mL) and dried over Na₂SO₄. The solvents were removed under vacuum and the residue purified by column chromatography (6% MeOH in DCM) to give the desired compound as a yellow solid (28 mg, 52%).

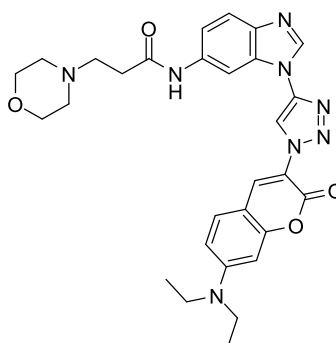
¹H NMR (500 MHz, CDCl₃) δ 10.78 (s, 1H), 8.58 (s, 1H), 8.40 (d, *J* = 8.9 Hz, 2H), 8.21 (s, 1H), 8.07 (d, *J* = 8.4 Hz, 2H), 8.01 (s, 1H), 7.70 – 7.62 (m, 3H), 7.53 (t, *J* = 7.5 Hz, 2H), 7.49 (s, 1H), 7.08 (dd, *J* = 8.5, 2.0 Hz, 1H), 6.62 (s, 2H), 3.81 (t, *J* = 4.6 Hz, 4H), 2.78 – 2.72 (m, 2H), 2.62 (br. s, 4H), 2.58 – 2.52 (m, 2H).

¹³C NMR (126 MHz, CDCl₃) δ 170.1, 142.2, 141.4, 140.0, 135.3, 133.2, 131.4, 130.8, 130.3, 129.6, 128.0, 125.5, 123.1, 122.8, 120.6, 115.8, 114.4, 102.5, 67.0, 54.2, 52.8, 47.4, 32.3.

IR (ν_{max}): 2908 (C-H), 1690 (C=O), 1504 (ar. C=C) cm⁻¹.

HR-MS (ESI): C₃₁H₂₉N₇O₂H⁺ calculated 532.2456, found 532.2451.

N-(1-(1-(7-(diethylamino)-2-oxo-2*H*-chromen-3-yl)-1*H*-1,2,3-triazol-4-yl)-1*H*-benzo[*d*]imidazol-6-yl)-3-morpholinopropanamide (**5.21b**)



N-(1-ethynyl-1*H*-benzo[*d*]imidazol-6-yl)-3-morpholinopropanamide (30 mg, 0.10 mmol) and anthracene azide (29 mg, 0.11 mmol) were dissolved in MeOH (2 mL). Then Cu(OAc)₂•H₂O

(1.0 mg, 0.005 mmol) was added. AMTC (2.2 mg, 0.01 mmol) and NaAsc (2.0 mg, 0.01 mmol) were dissolved in the minimum amount of water and then added dropwise. The reaction was stirred at room temperature overnight. Then sat. EDTA solution (pH 3, 20 mL) and DCM (20 mL) were added, and the phases were separated. The aqueous phase was extracted again with DCM (20 mL), the organic phases were combined and washed with brine (20 mL) and dried over Na₂SO₄. The solvents were removed under vacuum and the residue purified by column chromatography (5% MeOH in DCM) to give the desired compound as a yellow solid (38 mg, 68%).

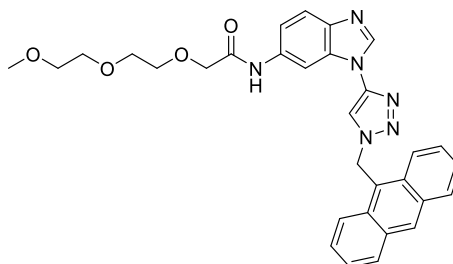
¹H NMR (400 MHz, CDCl₃) δ 10.92 (s, 1H), 8.87 (s, 1H), 8.47 (s, 1H), 8.38 (s, 1H), 8.32 (d, J = 2.0 Hz, 1H), 7.78 (d, J = 8.6 Hz, 1H), 7.46 (d, J = 9.0 Hz, 1H), 7.21 (dd, J = 8.6, 2.0 Hz, 1H), 6.71 (dd, J = 9.0, 2.5 Hz, 1H), 6.58 (d, J = 2.5 Hz, 1H), 3.86 (t, J = 4.6 Hz, 4H), 3.48 (q, J = 7.1 Hz, 4H), 2.77 (dd, J = 6.6, 5.0 Hz, 2H), 2.65 (br. s, 4H), 2.57 (dd, J = 6.6, 5.0 Hz, 2H), 1.27 (t, J = 7.1 Hz, 6H).

¹³C NMR (126 MHz, CDCl₃) δ 170.2, 156.8, 156.1, 151.9, 141.8, 141.5, 140.2, 135.5, 135.3, 133.1, 130.3, 120.8, 116.5, 115.9, 115.5, 110.3, 106.9, 102.3, 97.1, 67.1, 54.3, 52.9, 45.1, 32.3, 12.5.

IR (ν_{\max}): 3275 (N-H), 3139 (ar. C-H), 1716 (C=O), 1584 (C=C) cm⁻¹.

HR-MS (ESI): C₂₉H₃₂N₈O₄H⁺ calculated 557.2619, found 557.2618.

N-(1-(1-(anthracen-9-ylmethyl)-1H-1,2,3-triazol-4-yl)-1H-benzo[d]imidazol-6-yl)-2-(2-(2-methoxyethoxy)ethoxy)acetamide (**5.22a**)



N-(1-ethynyl-1H-benzo[d]imidazol-6-yl)-2-(2-(2-methoxyethoxy)ethoxy)acetamide (57 mg, 0.18 mmol) and anthracene azide (46 mg, 0.2 mmol) were dissolved in MeOH (2 mL). Then Cu(OAc)₂•H₂O (1.8 mg, 0.009 mmol) was added. AMTC (4.0 mg, 0.02 mmol) and NaAsc (3.6 mg, 0.02 mmol) were dissolved in the minimum amount of water and then added dropwise. The reaction was stirred at room temperature overnight. Then sat. EDTA solution (pH 3, 20 mL) and ethyl acetate (20 mL) were added, and the phases were separated. Additional ethyl acetate (40 mL) was added to the organic phase which was washed with brine (20 mL) and dried over Na₂SO₄. The solvents were removed under vacuum and the residue

purified by column chromatography (70% ethanol/ethyl acetate (1:3) in petroleum ether) to give the desired compound as a green solid (58 mg, 59%).

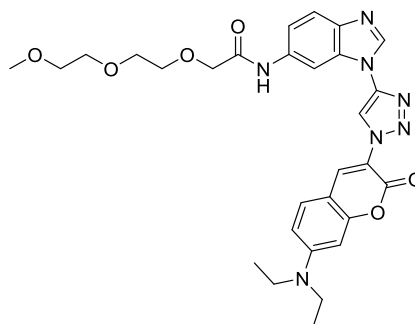
¹H NMR (500 MHz, CDCl₃) δ 8.87 (s, 1H), 8.59 (s, 1H), 8.39 (d, *J* = 8.9 Hz, 2H), 8.15 – 8.01 (m, 4H), 7.71 – 7.63 (m, 3H), 7.54 (t, *J* = 7.5 Hz, 2H), 7.47 (s, 1H), 7.32 (dd, *J* = 8.6, 2.0 Hz, 1H), 6.63 (s, 2H), 4.11 (s, 2H), 3.82 – 3.63 (m, 6H), 3.54 – 3.48 (m, 2H), 3.26 (s, 3H).

¹³C NMR (126 MHz, CDCl₃) δ 168.1, 142.2, 141.5, 140.5, 134.2, 132.9, 131.5, 130.8, 130.3, 129.6, 128.1, 125.5, 123.0, 122.7, 120.5, 116.7, 114.3, 103.1, 71.8, 71.3, 70.7, 70.5, 70.2, 58.9, 47.4.

IR (ν_{\max}): 3221 (N-H), 1663 (C=O), 1590 (C=C), 1103 (C-O) cm⁻¹.

HR-MS (ESI): C₃₁H₃₀N₆O₄H⁺ calculated 551.2401, found 551.2393.

N-(1-(1-(7-(diethylamino)-2-oxo-2H-chromen-3-yl)-1H-1,2,3-triazol-4-yl)-1H-benzo[d]imidazol-6-yl)-2-(2-(2-methoxyethoxy)ethoxy)acetamide (**5.22b**)



N-(1-ethynyl-1H-benzo[d]imidazol-6-yl)-2-(2-(2-methoxyethoxy)ethoxy)acetamide (56 mg, 0.18 mmol) and 3-azido-7-(diethylamino)-2H-chromen-2-one (50 mg, 0.19 mmol) were dissolved in MeOH (2 mL), followed by Cu(OAc)₂•H₂O (1.8 mg, 0.009 mmol). AMTC (4.0 mg, 0.02 mmol) and NaAsc (3.5 mg, 0.02 mmol) were dissolved in the minimum amount of water and then added dropwise. The reaction was stirred at room temperature overnight. Then sat. EDTA solution (pH 3, 20 mL) and ethyl acetate (20 mL) were added, and the phases were separated. The organic phase was washed with brine (20 mL) and dried over Na₂SO₄. The solvents were removed under vacuum and the residue purified by column chromatography (70% ethanol/ethyl acetate (1:3) in petroleum ether) to give the desired compound as a yellow solid (43 mg, 42%).

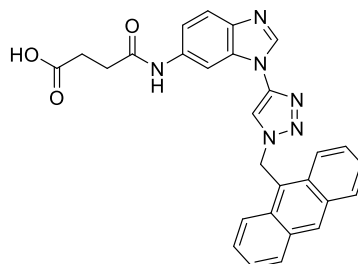
¹H NMR (500 MHz, CDCl₃) δ 8.96 (s, 1H), 8.88 (s, 1H), 8.46 (s, 1H), 8.40 (br. s, 1H), 8.31 (s, 1H), 7.80 (d, *J* = 8.6 Hz, 1H), 7.46 (d, *J* = 8.9 Hz, 1H), 7.40 (dd, *J* = 8.6, 1.9 Hz, 1H), 6.71 (dd, *J* = 9.0, 2.4 Hz, 1H), 6.58 (d, *J* = 2.4 Hz, 1H), 4.14 (s, 2H), 3.83 – 3.77 (m, 2H), 3.78 – 3.71 (m, 4H), 3.61 – 3.56 (m, 2H), 3.48 (q, *J* = 7.1 Hz, 4H), 3.32 (s, 3H), 1.26 (t, *J* = 6.9 Hz, 6H).

^{13}C NMR (126 MHz, CDCl_3) δ 168.3, 156.8, 156.1, 152.0, 141.8, 141.7, 140.7, 135.3, 134.4, 133.0, 130.3, 120.7, 116.7, 116.5, 115.6, 110.3, 106.9, 103.0, 97.1, 71.9, 71.3, 70.8, 70.5, 70.2, 59.0, 45.1, 12.4.

IR (ν_{max}): 3284 (N-H), 3142 (ar. C-H), 1714 (C=O), 1587 (C=C), 1128 (C-O) cm^{-1} .

HR-MS (ESI): $\text{C}_{29}\text{H}_{33}\text{N}_7\text{O}_6\text{H}^+$ calculated 576.2565, found 576.2561.

4-((1-(1-(anthracen-9-ylmethyl)-1H-1,2,3-triazol-4-yl)-1H-benzo[d]imidazol-6-yl)amino)-4-oxobutanoic acid (**5.23a**)



4-((1-ethynyl-1H-benzo[d]imidazol-6-yl)amino)-4-oxobutanoic acid (30 mg, 0.12 mmol) and anthracene azide (29.9 mg, 0.13 mmol) were dissolved in MeOH (2 mL), followed by $\text{Cu}(\text{OAc})_2 \cdot \text{H}_2\text{O}$ (1.2 mg, 0.006 mmol). AMTC (2.6 mg, 0.01 mmol) and NaAsc (2.3 mg, 0.01 mmol) were dissolved in the minimum amount of water and then added dropwise. The reaction was stirred at room temperature overnight. Then sat. EDTA solution (pH 3, 20 mL) and ethyl acetate (20 mL) were added, and the phases were separated. The organic phase was washed with brine (20 mL). The precipitate in the organic layer was filtered off and washed with ethyl acetate to give the desired compound as a yellow solid (52 mg, 91%).

^1H NMR (400 MHz, DMSO) δ 12.14 (br. s, 1H), 10.10 (br. s, 1H), 8.77 (s, 1H), 8.65 (d, J = 8.9 Hz, 2H), 8.57 (s, 1H), 8.49 (br. s, 2H), 8.18 (d, J = 8.4 Hz, 2H), 7.73 – 7.56 (m, 5H), 7.35 (br. s, 1H), 6.79 (s, 2H), 2.65 – 2.55 (m, 4H).

^{13}C NMR (101 MHz, DMSO) δ 170.0, 142.1, 135.9, 131.1, 130.5, 129.4, 129.1, 127.3, 125.4, 125.0, 123.9, 119.9, 116.2, 115.2, 102.4, 46.6, 31.1. 5 carbons not observed.

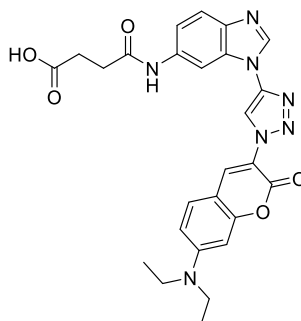
Observed benzimidazole and succinate tail peaks in the proton and correlating peaks in the carbon NMR were very broad. As the compound was not purified by column chromatography residual copper might be present (although crude was washed with EDTA) which broadens the signal and could explain the missing carbon signals.²⁹⁰ Increasing the relaxation time, number of scans or temperature (up to 80 °C) did not make a difference. Due to the limited solubility, the concentration of the sample also could not be increased.

IR (ν_{max}): 3303 (N-H), 2971 (COO-H), 1739 (C=O), 1616 (C=C), 1591 (C=C) cm^{-1} .

LC-MS (ESI): $\text{C}_{28}\text{H}_{22}\text{N}_6\text{O}_3\text{H}^+$ calculated 491.2, found 491.2.

HR-MS (ESI): $C_{28}H_{22}N_6O_3H^+$ calculated 491.1826, found 491.1807.

4-((1-(1-(7-(diethylamino)-2-oxo-2H-chromen-3-yl)-1H-1,2,3-triazol-4-yl)-1H-benzo[d]imidazol-6-yl)amino)-4-oxobutanoic acid (**5.23b**)



4-((1-ethynyl-1H-benzo[d]imidazol-6-yl)amino)-4-oxobutanoic acid (30 mg, 0.12 mmol) and 3-azido-7-(diethylamino)-2H-chromen-2-one (33 mg, 0.13 mmol) were dissolved in MeOH (2 mL). Then $Cu(OAc)_2 \cdot H_2O$ (1.2 mg, 0.006 mmol) was added and the reaction was stirred at room temperature overnight. Then sat. EDTA solution (pH 3, 20 mL) and DCM (20 mL) were added, and the phases were separated. The aqueous phase was extracted with DCM (2×20 mL). Yellow precipitate remained in the aqueous layer which was filtered off and washed with DCM to give the desired compound as a yellow solid (15 mg, 24%).

1H NMR (500 MHz, DMSO) δ 11.85 (br. s, 1H), 9.96 (s, 1H), 9.01 (s, 1H), 8.68 (br. s, 1H), 8.57 (s, 1H), 8.37 (br. s, 1H), 7.70 (br. ffs, 1H), 7.66 (d, $J = 8.9$ Hz, 1H), 7.49 – 7.44 (m, 1H), 6.86 (dd, $J = 9.0, 2.5$ Hz, 1H), 6.69 (d, $J = 2.4$ Hz, 1H), 3.51 (q, $J = 7.0$ Hz, 4H), 2.62 (s, 4H), 1.19 (t, $J = 7.0$ Hz, 6H).

^{13}C NMR (126 MHz, DMSO) δ 169.7, 156.2, 155.6, 151.7, 141.4, 137.3, 135.8, 130.4, 119.5, 117.0, 115.7, 115.4, 110.0, 106.2, 102.1, 96.3, 44.0, 12.0. 6 carbons not observed

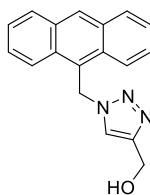
As with compound **5.23a**, the observed benzimidazole and succinate tail peaks in the proton and correlating peaks in the carbon NMR were very broad. As the compound was not purified by column chromatography residual copper might be present (although crude was washed with EDTA) which broadens the signal and could explain the missing carbon signals.²⁹⁰ Increasing the relaxation time, number of scans or temperature (up to 80 °C) did not make a difference. Due to the limited solubility, the concentration of the sample also could not be increased.

IR (ν_{max}): 3284 (N-H), 2980 (COO-H), 1717 (C=O), 1587 (C=C) cm^{-1} .

LC-MS: $C_{26}H_{25}N_7O_5H^+$ calculated 516.2, found 516.3.

HR-MS (ESI): $C_{26}H_{25}N_7O_5H^+$ calculated 516.1990, found 516.1990.

(1-(anthracen-9-ylmethyl)-1H-1,2,3-triazol-4-yl)methanol (**5.25**)



Propargyl alcohol (40 mg, 0.71 mmol) and 9-(azidomethyl)anthracene (166 mg, 0.71 mmol) were dissolved in MeOH (2 mL) and Cu(OAc)₂•H₂O (7 mg, 0.04 mmol) was added. NaAsc was dissolved in the minimum amount of water and added dropwise to the reaction, which was stirred overnight. Then DCM (20 mL) and water (20 mL) were added, and the phases separated. The phases were separated, and the organic phase washed with sat. EDTA solution (pH 3, 20 mL). Then, the combined aqueous phases were extracted with DCM (2 × 20 mL) and the combined organic phases washed with brine and dried over Na₂SO₄. The solvent was removed under vacuum and the residue purified by column chromatography (40% ethanol/ethyl acetate (1:3) in petroleum ether) to give the desired compound as a yellow solid (74 mg, 36%).

¹H NMR (500 MHz, DMSO) δ 8.74 (s, 1H), 8.61 (d, *J* = 8.9 Hz, 2H), 8.17 (d, *J* = 8.5 Hz, 2H), 7.72 (s, 1H), 7.69 – 7.62 (m, 2H), 7.61 – 7.54 (m, 2H), 6.62 (s, 2H), 5.00 (t, *J* = 5.7 Hz, 1H), 4.39 (d, *J* = 5.7 Hz, 2H).

IR (ν_{\max}): 3243 (broad, O-H) cm⁻¹.

NMR spectrum in accordance to literature values.²⁹¹

5.6.4 Fluorescent Plate Assay

HeLa cells were kindly provided by Dr. Inga Kruse (Strathclyde Institute of Pharmacy and Biomedical Sciences, University of Strathclyde, Glasgow). Cells were suspended in 1X DPBS and lysed by the addition of Triton X-100 (1% (v/v) final concentration) to give a concentration of ~8000 cells/ mL. Fluorescent measurements were carried out on a Hidex Sense Microplate reader.

Stock solutions:

[Alkyne] = 1 mM in DMSO

[Azide] = 1 mM in DMSO

[BTTAA] = 10 mM in H₂O

[Cu(OAc)₂] = 1 mM in H₂O

[NaAsc] = 10 mM in H₂O

From the stock solutions, two solutions were prepared containing either alkyne and azide or $\text{Cu}(\text{OAc})_2$, BTAA and NaAsc (total volume 1000 μL each, made up with buffer or lysate to reach the volume, double the final concentration intended for the 96-well plate).

To the 96-well plate was added 50 μL of each solution to reach a final volume of 100 μL /well and the final specified concentration.

5.6.5 Coumarin Azide Solubility Data

Table 5.1. Percentage of fluorescence of **5.1** remaining after 18 h.

Entry	5.1 [μM]	% initial fluorescence remaining after 18 h
1	100	~2
2	75	~2
3	50	~2
4	25	~2

Conditions: **5.1** (100, 75, 50 and 25 μM), 10% DMSO in 1X DPBS, 25 °C, 18 h.

Table 5.2. Percentage of fluorescence of **5.1** remaining after 3.5 h in 100% DMSO.

Entry	5.1 [μM]	% initial fluorescence remaining after 3.5 h
1	50	90 \pm 9

Conditions: **5.1** (50 μM), 100% DMSO, 25 °C, 3.5 h.

5.6.6 DoE 1 Additional Data

Table 5.3. Reaction of ynamine **5.18** with azide **5.11** using just $\text{Cu}(\text{OAc})_2$ or $\text{Cu}(\text{OAc})_2$ and BTAA.

Entry	[$\text{Cu}(\text{OAc})_2$] (μM)	[BTAA] (μM)	Conversion after 16 h (%)
1	50		>3
2	100		>3
3	150		>3
4	200		>3
5	50	50	>3
6	50	100	>3
7	50	200	>3

Conditions: **5.18** (50 μM), **5.11** (50 μM), $\text{Cu}(\text{OAc})_2$ (50, 100, 150 or 200 μM), BTAA (50, 100 or 200 μM), 1% Triton X-100/10% DMSO in 1X DPBS, 25 °C, 16 h.

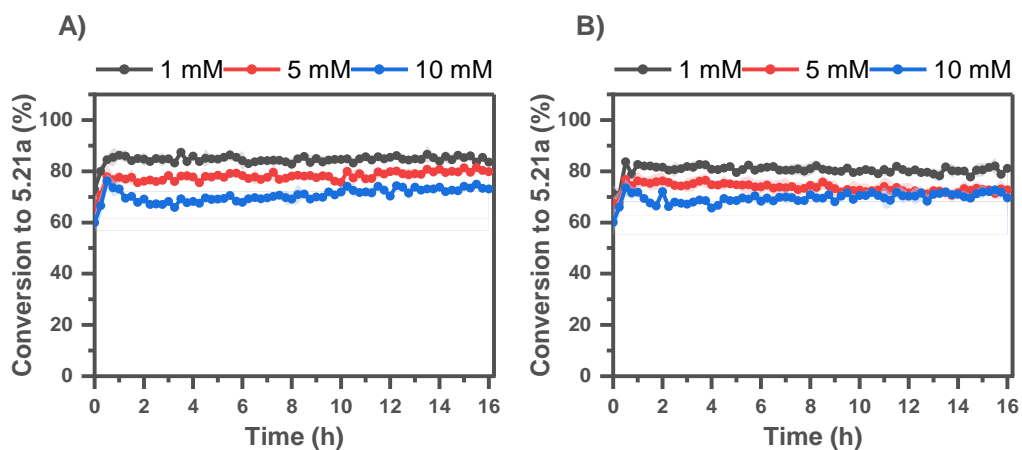


Figure 5.14. (A) Reaction of ynamine **5.18** with azide **5.11** with added NaAsc (1, 5 and 10 mM) and BTAA (2 equiv). *Conditions:* **5.18** (50 μ M), **5.11** (50 μ M), Cu(OAc)₂ (50 μ M), BTAA (100 μ M), NaAsc (1, 5 or 10 mM), 1% Triton X-100/10% DMSO in 1X DPBS, 25 $^{\circ}$ C, 16 h. (B) Reaction of ynamine **5.18** with azide **5.11** with added NaAsc (1, 5 and 10 mM) and BTAA (50 μ M). *Conditions:* **5.18** (50 μ M), **5.11** (50 μ M), Cu(OAc)₂ (200 μ M), BTAA (50 μ M), NaAsc (1, 5 and 10 mM), 1% Triton X-100/10% DMSO in 1X DPBS, 25 $^{\circ}$ C, 16 h. Buffer pH = 7.4.

5.6.7 DoE 2 Additional Data

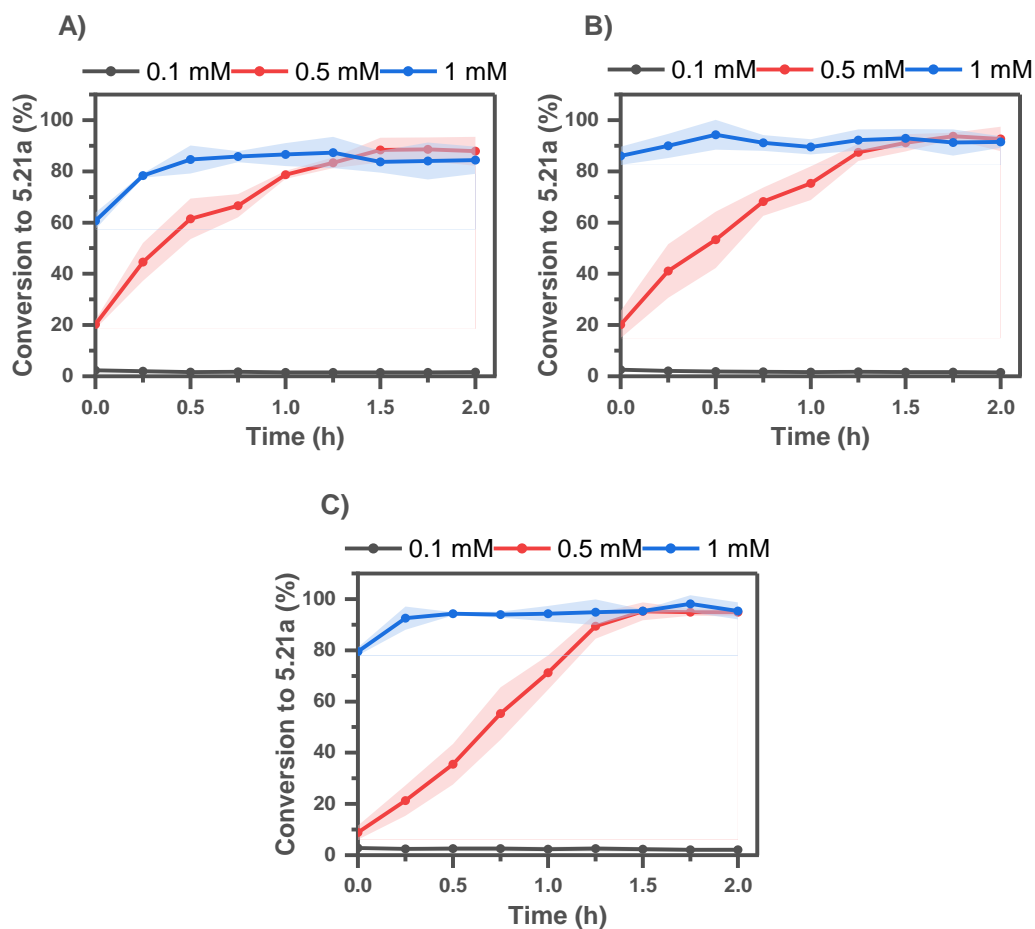


Figure 5.15. (A) Reaction of ynamine **5.18** with azide **5.11** with added BTAA (2 equiv). *Conditions:* **5.18** (50 μ M), **5.11** (50 μ M), Cu(OAc)₂ (50 μ M), BTAA (100 μ M), NaAsc (0.1, 0.5 or 1 mM), 1% Triton X-100/10% DMSO in 1X DPBS, 25 $^{\circ}$ C, 16 h. (B) Reaction of ynamine **5.18** with azide **5.11** with added BTAA (3 equiv). *Conditions:* **5.18** (50 μ M), **5.11** (50 μ M), Cu(OAc)₂ (50 μ M), BTAA (150 μ M), NaAsc (0.1, 0.5 or 1 mM), 1% Triton X-100/10% DMSO in 1X DPBS, 25 $^{\circ}$ C, 16 h. (C) Reaction of ynamine **5.18** with azide **5.11** with added BTAA (4 equiv). *Conditions:* **5.18** (50 μ M), **5.11** (50 μ M), Cu(OAc)₂ (50 μ M), BTAA (200 μ M), NaAsc (0.1, 0.5 or 1 mM), 1% Triton X-100/10% DMSO in 1X DPBS, 25 $^{\circ}$ C, 16 h. Buffer pH = 7.4.

Chapter 6

Conclusions and Future Directions

6.1 Conclusions and Future Directions

The aim of this thesis was to investigate the suitability of the ynamine-CuAAC for bioconjugation, first in *in vitro* assays and then moving towards *in vivo* applications. Glutathione was identified as a suitable surrogate to test *in vivo* reactivity. The tripeptide is the predominant detoxification reagent inside cells and acts as a nucleophile and transition metal chelator and could impact the ynamine-CuAAC reaction either by reagent degradation or catalyst sequestering.¹⁵⁶

First, the influence of GSH on aromatic ynamine (**2.1**) stability was explored. In sodium phosphate buffer, major degradation (> 75%) was observed after 24 h, whereas only minimal degradation (< 25%) was observed in phosphate buffered saline. Two degradation products could be isolated (Z- (**2.30**) and geminal (**2.31**) GSH-ynamine adduct) pointing towards nucleophilic and radical mediated degradation. The ratio of degradation products was dependant on reaction conditions (buffer type, GSH concentration) and was shifted exclusively towards the Z-isomer (**2.30**) when copper was added to the reaction. Changing the pH of the reaction did not affect rate of degradation nor the degradation product ratio. Copper-free click reagents (SPAAC and IEDDA) displayed similar stability (> 80%) in the presence of GSH after 24 h.

Next, conditions were developed for the CuAAC reaction at the highest concentration of GSH possible. Under these conditions, the ynamine **2.1** afforded full conversion with benzyl azide **2.2** in around 2 h. The rate of conversion for other alkynes (**2.9** – **2.11**) was slower under the same conditions, indicating that the ynamine had a significant reactivity advantage. In contrast, copper-free SPAAC and IEDDA reagents (**2.12** – **2.15**) were not affected by the presence of GSH.

The preliminary CuAAC experiments indicated that the GSH concentration determined reaction outcome, with higher concentrations either causing an induction period or completely inhibiting the reaction. This phenomenon was explored further in the second chapter. It was discovered that reaction rate could be fully tuned by the copper:GSH ratio. Ratios of 1:1 accelerated the reaction and increasing this ratio caused and prolonged an induction period. Visual time normalised analysis indicated the reaction was first order with respect to azide, ~0.5 order in ynamine and ~0.5 order in copper under these conditions. The reaction could be accelerated to reach full conversion in under 10 minutes by switching the co-solvent to fluorinated solvents such as HFIP or TFE.

These new conditions were promising to achieve conjugation of biomolecules at low copper catalyst loadings and were applied to two cell penetrating peptides (Penetratin-Az and TP2-Az). Using these conditions over 80% conversion was achieved after 1 h using only 100 μM copper.

Modifying biomolecules by two orthogonal reactions is an important tool for bioconjugation.²⁶³ As the SPAAC reaction using DBCO (**2.12**) is inhibited by Cu(I) – and the CuAAC reaction requires Cu(I) – it was attempted to develop a sequential labelling protocol using DBCO (**2.12**) and the aromatic ynamine (**2.1**). Trials on small molecules showed that either DBCO (**2.12**) or the ynamine (**2.1**) could be selectively reacted with an azide – only controlled by the addition of GSH. This concept was extended to Penetratin-Az and TP2-Az and in the presence of GSH, only the ynamine (**4.7**) reacted whereas only DBCO (**2.12**) reacted in the absence. It was attempted to apply this strategy to a dual-azide modified peptide, but sufficient selectivity could not be achieved.

Finally, as a further step towards *in vivo* bioconjugation using aromatic ynamines (**5.18** and **5.19**), the reactivity was analysed in cell lysate via a fluorescent assay. The conditions were optimised in buffer first and highlighted that good conversions (~80%) could be achieved within 2 h using only 1 μM Cu(OAc)₂ and that tuning the ligand (BTAA) and NaAsc concentration was crucial for conversion. In cell lysate, diminished reactivity was observed but good conversion could still be achieved. A conventional alkyne (**5.24**) was not reactive under the same conditions in cell lysate. These promising results are good starting points for *in vivo* bioconjugation.

A number of experiments can be proposed to expand on the findings presented in this thesis:

- (i) *Investigation of GSH mediated Ynamine degradation* – The mechanistic investigation of the ynamine (**2.1**) degradation by GSH was limited in this thesis. Preliminary experiments indicate a radical mediated degradation pathway under certain conditions but are not conclusive. So far, a radical scavenger (TEMPO) has only been added to the reactions containing copper. No inhibition was observed, but TEMPO is known to react with superoxide which is produced by GSH and copper. Therefore, repeating the experiment but without copper could allow TEMPO to intercept GSH radicals and reduce degradation. Furthermore,

EPR spectroscopy could be used to study the degradation. If radicals are formed during the reactions, they should be identified by EPR. Lastly, the significant difference in degradation between the sodium phosphate buffer and 1X DPBS warrants further investigation. Adding additional salts such as magnesium or calcium to the phosphate buffer could potentially elucidate the roles of the additives. Further understanding would potentially open the door for the ynamine to be used as a thiol tagging reagent.

- (ii) *Rate-accelerating effect of HFIP* – The addition of HFIP to the ynamine-CuAAC reaction enhanced the rate greatly. The origin of this effect is unknown but could potentially be caused by micellar catalysis. Investigating the reaction by DLS or DOSY NMR experiments could detect the presence of micelles. Furthermore, the use of HFIP in other cycloadditions (*i.e.*, SPAAC, IEDDA, conventional CuAAC) needs also to be explored further. If these reactions are also accelerated by HFIP, the solvent can be used as a further lever to accelerate bio-orthogonal reactions that is independent of the reagents.
- (iii) *Extension of bioconjugation protocol to further biomolecules* – The optimal ynamine-CuAAC protocol has only been applied to short peptides thus far. If further biomolecules such as oligonucleotides and proteins could be efficiently labelled under the same conditions, the general applicability of the protocol would be demonstrated. Furthermore, the dual labelling of peptides by ynamine-CuAAC and SPAAC failed due to insufficient selectivity between azides. However, both ynamines and DBCO can be incorporated into oligonucleotides which would remove this limitation and potentially allow the sequential labelling of ynamines and DBCO controlled by GSH in a one-pot reaction.
- (iv) *Move into in vivo experiments* – The superiority of the ynamine (**5.18**) over conventional alkynes (**5.24**) has been demonstrated in buffer and cell lysate. It is assumed that this would extend into live cell experiments but has not been demonstrated. Incorporation of azides into all major classes of biomolecules (DNA, proteins and lipids) is routinely achieved. Labelling of these classes by ynamine-CuAAC and comparing it with conventional alkynes would demonstrate the superiority of ynamines over alkynes in bioconjugation and potentially lead to more widespread adoption.

List of References

- 1 O. Shimomura, F. H. Johnson and Y. Saiga, *J. Cell. Comp. Physiol.*, 1962, **59**, 223–239.
- 2 R. Y. Tsien, *Annu. Rev. Biochem.*, 1998, **67**, 509–544.
- 3 M. Andresen, R. Schmitz-Salue and S. Jakobs, *Mol. Biol. Cell*, 2004, **15**, 5616–5622.
- 4 C. S. Lisenbee, S. K. Karnik and R. N. Trelease, *Traffic*, 2003, **4**, 491–501.
- 5 F. Yang, L. G. Moss and G. N. Phillips, *Nat. Biotechnol.*, 1996, **14**, 1246–1251.
- 6 J. A. Prescher and C. R. Bertozzi, *Nat. Chem. Biol.*, 2005, **1**, 13–21.
- 7 P. Shieh and C. R. Bertozzi, *Org. Biomol. Chem.*, 2014, **12**, 9307–9320.
- 8 E. M. Sletten and C. R. Bertozzi, *Angew. Chemie Int. Ed.*, 2009, **48**, 6974–6998.
- 9 C. S. McKay and M. G. Finn, *Chem. Biol.*, 2014, **21**, 1075–1101.
- 10 B. L. Oliveira, Z. Guo and G. J. L. Bernardes, *Chem. Soc. Rev.*, 2017, **46**, 4895–4950.
- 11 Y. Zhang, K.-Y. Park, K. F. Suazo and M. D. Distefano, *Chem. Soc. Rev.*, 2018, **47**, 9106–9136.
- 12 S. K. Mazmanian, G. Liu, H. Ton-That and O. Schneewind, *Science*, 1999, **285**, 760–763.
- 13 R. Parthasarathy, S. Subramanian and E. T. Boder, *Bioconjug. Chem.*, 2007, **18**, 469–476.
- 14 M. Rashidian, J. K. Dozier and M. D. Distefano, *Bioconjug. Chem.*, 2013, **24**, 1277–1294.
- 15 M. Sunbul and J. Yin, *Org. Biomol. Chem.*, 2009, **7**, 3361.
- 16 C. W. Lin and A. Y. Ting, *J. Am. Chem. Soc.*, 2006, **128**, 4542–4543.
- 17 J. S. Rush and C. R. Bertozzi, *J. Am. Chem. Soc.*, 2008, **130**, 12240–12241.
- 18 P. Wu, W. Shui, B. L. Carlson, N. Hu, D. Rabuka, J. Lee and C. R. Bertozzi, *Proc. Natl. Acad. Sci.*, 2009, **106**, 3000–3005.
- 19 I. Chen, M. Howarth, W. Lin and A. Y. Ting, *Nat. Methods*, 2005, **2**, 99–104.
- 20 S. A. Slavoff, I. Chen, Y. A. Choi and A. Y. Ting, *J. Am. Chem. Soc.*, 2008, **130**, 1160–1162.
- 21 A. Keppler, S. Gendreizig, T. Gronemeyer, H. Pick, H. Vogel and K. Johnsson, *Nat. Biotechnol.*, 2003, **21**, 86–89.
- 22 A. B. Foraker, S. M. Camus, T. M. Evans, S. R. Majeed, C. Y. Chen, S. B. Taner, I. R. Corrêa, S. J. Doxsey and F. M. Brodsky, *J. Cell Biol.*, 2012, **198**, 591–605.
- 23 K. Bojkowska, F. Santoni De Sio, I. Barde, S. Offner, S. Verp, C. Heinis, K. Johnsson and D. Trono, *Chem. Biol.*, 2011, **18**, 805–815.

- 24 A. a Hoskins, L. J. Friedman, S. S. Gallagher, D. J. Crawford, E. G. Anderson, R. Wombacher, N. Ramirez, V. W. Cornish, J. Gelles and M. J. Moore, *Science*, 2011, **331**, 1289–1296.
- 25 O. Koniev and A. Wagner, *Chem. Soc. Rev.*, 2015, **44**, 5495–5551.
- 26 G. W. Anderson, J. E. Zimmerman and F. M. Callahan, *J. Am. Chem. Soc.*, 1964, **86**, 1839–1842.
- 27 G. R. Grimsley, J. M. Scholtz and C. N. Pace, *Protein Sci.*, 2009, **18**, 247–251.
- 28 P. Cuatrecasas and I. Parikh, *Biochemistry*, 1972, **11**, 2291–2299.
- 29 A. J. Lomant and G. Fairbanks, *J. Mol. Biol.*, 1976, **104**, 243–261.
- 30 S. Kalkhof and A. Sinz, *Anal. Bioanal. Chem.*, 2008, **392**, 305–312.
- 31 S. Mädler, C. Bich, D. Touboul and R. Zenobi, *J. Mass Spectrom.*, 2009, **44**, 694–706.
- 32 J. M. J. M. Ravasco, H. Faustino, A. Trindade and P. M. P. Gois, *Chem. - A Eur. J.*, 2018, 1–18.
- 33 D. Gilis, S. Massar, N. J. Cerf and M. Rooman, *Genome Biol.*, 2001, **2**, 1–12.
- 34 S. D. Fontaine, R. Reid, L. Robinson, G. W. Ashley and D. V. Santi, *Bioconjug. Chem.*, 2015, **26**, 145–152.
- 35 A. D. Baldwin and K. L. Kiick, *Bioconjug. Chem.*, 2011, **22**, 1946–1953.
- 36 L. M. Tedaldi, M. E. B. Smith, R. I. Nathani and J. R. Baker, *Chem. Commun.*, 2009, 6583–6585.
- 37 M. E. B. Smith, F. F. Schumacher, C. P. Ryan, L. M. Tedaldi, D. Papaioannou, G. Waksman, S. Caddick and J. R. Baker, *J. Am. Chem. Soc.*, 2010, **132**, 1960–1965.
- 38 V. Chudasama, M. E. B. Smith, F. F. Schumacher, D. Papaioannou, G. Waksman, J. R. Baker and S. Caddick, *Chem. Commun.*, 2011, **47**, 8781–8783.
- 39 V. Chudasama, A. Maruani and S. Caddick, *Nat. Chem.*, 2016, **8**, 114–119.
- 40 E. Robinson, J. P. M. Nunes, V. Vassileva, A. Maruani, J. C. F. Nogueira, M. E. B. Smith, R. B. Pedley, S. Caddick, J. R. Baker and V. Chudasama, *RSC Adv.*, 2017, **7**, 9073–9077.
- 41 M. Morais, J. P. M. Nunes, K. Karu, N. Forte, I. Benni, M. E. B. Smith, S. Caddick, V. Chudasama and J. R. Baker, *Org. Biomol. Chem.*, 2017, **15**, 2947–2952.
- 42 N. Forte, M. Livanos, E. Miranda, M. Morais, X. Yang, V. S. Rajkumar, K. A. Chester, V. Chudasama and J. R. Baker, *Bioconjug. Chem.*, 2018, **28**, 486–492.
- 43 M. Staudinger, H. Jules, *Helv. Chim. Acta*, 1919, **2**, 635–646.
- 44 E. Saxon and C. R. Bertozzi, *Science*, 2000, **287**, 2007–2010.
- 45 F. L. Lin, H. M. Hoyt, H. Van Halbeek, R. G. Bergman and C. R. Bertozzi, *J. Am.*

- Chem. Soc.*, 2005, **127**, 2686–2695.
- 46 B. L. Nilsson, L. L. Kiessling and R. T. Raines, *Org. Lett.*, 2000, **2**, 1939–1941.
- 47 B. L. Nilsson, L. L. Kiessling and R. T. Raines, *Org. Lett.*, 2001, **3**, 9–12.
- 48 M. B. Soellner, B. L. Nilsson and R. T. Raines, *J. Am. Chem. Soc.*, 2006, **128**, 8820–8828.
- 49 L. Shah, S. T. Laughlin and I. S. Carrico, *J. Am. Chem. Soc.*, 2016, **138**, 5186–5189.
- 50 P. Hu, T. Feng, C. C. Yeung, C. K. Koo, K. C. Lau and M. H. W. Lam, *Chem. - A Eur. J.*, 2016, **22**, 11537–11542.
- 51 P. Hu, K. Berning, Y. W. Lam, I. H. M. Ng, C. C. Yeung and M. H. W. Lam, *J. Org. Chem.*, 2018, **83**, 12998–13010.
- 52 R. Huisgen, *Angew. Chemie Int. Ed.*, 1963, **2**, 565–598.
- 53 C. W. Tornøe, C. Christensen and M. Meldal, *J. Org. Chem.*, 2002, **67**, 3057–3064.
- 54 V. V. Rostovtsev, L. G. Green, V. V. Fokin and K. B. Sharpless, *Angew. Chemie Int. Ed.*, 2002, **41**, 2596–2599.
- 55 H. C. Kolb, M. G. Finn and K. B. Sharpless, *Angew. Chemie Int. Ed.*, 2001, **40**, 2004–2021.
- 56 B. F. Straub, *Chem. Commun.*, 2007, 3868–3870.
- 57 L. Jin, D. R. Tolentino, M. Melaimi and G. Bertrand, *Sci. Adv.*, 2015, **1**, e1500304.
- 58 C. Iacobucci, S. Reale, J. F. Gal and F. De Angelis, *Angew. Chemie Int. Ed.*, 2015, **54**, 3065–3068.
- 59 V. O. Rodionov, V. V. Fokin and M. G. Finn, *Angew. Chemie Int. Ed.*, 2005, **44**, 2210–2215.
- 60 B. T. Worrell, J. a. Malik and V. V. Fokin, *Science*, 2013, **340**, 457–460.
- 61 C. Nolte, P. Mayer and B. F. Straub, *Angew. Chemie Int. Ed.*, 2007, **46**, 2101–2103.
- 62 L. Jin, E. A. Romero, M. Melaimi and G. Bertrand, *J. Am. Chem. Soc.*, 2015, **137**, 15696–15698.
- 63 M. Meldal and F. Diness, *Trends Chem.*, 2020, 1–16.
- 64 L. Banci, I. Bertini, S. Ciofi-Baffoni, T. Kozyreva, K. Zovo and P. Palumaa, *Nature*, 2010, **465**, 645–648.
- 65 T. D. Rae, *Science*, 1999, **284**, 805–808.
- 66 T. R. Chan, R. Hilgraf, K. B. Sharpless and V. V. Fokin, *Org. Lett.*, 2004, **6**, 2853–2855.
- 67 V. O. Rodionov, S. I. Presolski, S. Gardinier, Y.-H. Lim and M. G. Finn, *J. Am. Chem. Soc.*, 2007, **129**, 12696–12704.

- 68 S. I. Presolski, V. Hong, S. H. Cho and M. G. Finn, *J. Am. Chem. Soc.*, 2010, **132**, 14570–14576.
- 69 V. Hong, S. I. Presolski, C. Ma and M. G. Finn, *Angew. Chemie Int. Ed.*, 2009, **48**, 9879–9883.
- 70 A. C. Yan, H. Jiang, D. Soriano del Amo, P. Wu, Y. Liu, M. Levy, W. Wang, C. Besanceney and F. L. Marlow, *J. Am. Chem. Soc.*, 2010, **132**, 16893–16899.
- 71 C. Besanceney-Webler, H. Jiang, T. Zheng, L. Feng, D. Soriano Del Amo, W. Wang, L. M. Klivansky, F. L. Marlow, Y. Liu and P. Wu, *Angew. Chemie Int. Ed.*, 2011, **50**, 8051–8056.
- 72 C. Gaulier, A. Hospital, B. Legeret, A. F. Delmas, V. Aucagne, F. Cisnetti and A. Gautier, *Chem. Commun.*, 2012, **48**, 4005–4007.
- 73 P.-Y. Liu, N. Jiang, J. Zhang, X. Wei, H.-H. Lin and X.-Q. Yu, *Chem. Biodivers.*, 2006, **3**, 958–966.
- 74 J. Miguel-Ávila, M. Tomás-Gamasa, A. Olmos, P. J. Pérez and J. L. Mascareñas, *Chem. Sci.*, 2018, **9**, 1947–1952.
- 75 Y. Bai, X. Feng, H. Xing, Y. Xu, B. K. Kim, N. Baig, T. Zhou, A. A. Gewirth, Y. Lu, E. Oldfield and S. C. Zimmerman, *J. Am. Chem. Soc.*, 2016, **138**, 11077–11080.
- 76 J. Chen, J. Wang, Y. Bai, K. Li, E. S. Garcia, A. L. Ferguson and S. C. Zimmerman, *J. Am. Chem. Soc.*, 2018, **140**, 13695–13702.
- 77 W. S. Brotherton, H. A. Michaels, J. T. Simmons, R. J. Clark, N. S. Dalal and L. Zhu, *Org. Lett.*, 2009, **11**, 4954–4957.
- 78 C. Uttamapinant, A. Tangpeerachaikul, S. Grecian, S. Clarke, U. Singh, P. Slade, K. R. Gee and A. Y. Ting, *Angew. Chemie Int. Ed.*, 2012, **51**, 5852–5856.
- 79 N. Inoue, A. Onoda and T. Hayashi, *Bioconjug. Chem.*, 2019, **30**, 2427–2434.
- 80 T. Machida and N. Winssinger, *ChemBioChem*, 2016, **17**, 811–815.
- 81 Y. Yang, S. Lin, W. Lin and P. R. Chen, *ChemBioChem*, 2014, **15**, 1738–1743.
- 82 V. Bevilacqua, M. King, M. Chaumontet, M. Nothisen, S. Gabillet, D. Buisson, C. Puente, A. Wagner and F. Taran, *Angew. Chemie Int. Ed.*, 2014, **53**, 5872–5876.
- 83 S. Li, L. Wang, F. Yu, Z. Zhu, D. Shobaki, H. Chen, M. Wang, J. Wang, G. Qin, U. J. Erasquin, L. Ren, Y. Wang and C. Cai, *Chem. Sci.*, 2017, **8**, 2107–2114.
- 84 J. Clavadetscher, S. Hoffmann, A. Lilienkamp, L. Mackay, R. M. Yusop, S. A. Rider, J. J. Mullins and M. Bradley, *Angew. Chemie Int. Ed.*, 2016, **55**, 15662–15666.
- 85 X. Qu, F. Wang, Y. Zhang, Z. Du, J. Ren, Z. Liu and L. Zhang, *Angew. Chemie Int. Ed.*, 2019, 1–7.

- 86 R. Uauy, M. Olivares and M. Gonzalez, *Am. J. Clin. Nutr.*, 1998, **67**, 952S-959S.
- 87 T. D. Rae, *Science*, 1999, **284**, 805–808.
- 88 L. Yang, R. McRae, M. M. Henary, R. Patel, B. Lai, S. Vogt and C. J. Fahrni, *Proc. Natl. Acad. Sci. U. S. A.*, 2005, **102**, 11179–11184.
- 89 D. C. Kennedy, C. S. McKay, M. C. B. Legault, D. C. Danielson, J. A. Blake, A. F. Pegoraro, A. Stelow, Z. Mester and J. P. Pezacki, *J. Am. Chem. Soc.*, 2011, **133**, 17993–18001.
- 90 M. Dizdaroglu and P. Jaruga, *Free Radic. Res.*, 2012, **46**, 382–419.
- 91 G. R. Abel, Z. A. Calabrese, J. Ayco, J. E. Hein and T. Ye, *Bioconjug. Chem.*, 2016, **27**, 698–704.
- 92 S. Li, H. Cai, J. He, H. Chen, S. Lam, T. Cai, Z. Zhu, S. J. Bark and C. Cai, *Bioconjug. Chem.*, 2016, **27**, 2315–2322.
- 93 N. W. Nairn, P. A. Bariola, T. J. Graddis, M. P. VanBrunt, A. Wang, G. Li and K. Grabstein, *Bioconjug. Chem.*, 2015, **26**, 2070–2075.
- 94 Y. Su, L. Li, H. Wang, X. Wang and Z. Zhang, *Chem. Commun.*, 2016, **52**, 2185–2188.
- 95 C. Besanceney-Webler, H. Jiang, T. Zheng, L. Feng, D. Soriano Del Amo, W. Wang, L. M. Klivansky, F. L. Marlow, Y. Liu and P. Wu, *Angew. Chemie Int. Ed.*, 2011, **50**, 8051–8056.
- 96 V. O. Rodionov, S. I. Presolski, S. Gardinier, Y.-H. Lim and M. G. Finn, *J. Am. Chem. Soc.*, 2007, **129**, 12696–12704.
- 97 V. Hong, N. F. Steinmetz, M. Manchester and M. G. Finn, *Bioconjug. Chem.*, 2010, **21**, 1912–1916.
- 98 D. Soriano Del Amo, W. Wang, H. Jiang, C. Besanceney, A. C. Yan, M. Levy, Y. Liu, F. L. Marlow and P. Wu, *J. Am. Chem. Soc.*, 2010, **132**, 16893–16899.
- 99 V. Hong, S. I. Presolski, C. Ma and M. G. Finn, *Angew. Chemie Int. Ed.*, 2009, **48**, 9879–9883.
- 100 S. Li, H. Cai, J. He, H. Chen, S. Lam, T. Cai, Z. Zhu, S. J. Bark and C. Cai, *Bioconjug. Chem.*, 2016, **27**, 2315–2322.
- 101 Z. Zhu, H. Chen, S. Li, X. Yang, E. Bittner and C. Cai, *Catal. Sci. Technol.*, 2017, **7**, 2474–2485.
- 102 A. Kumar, K. Li and C. Cai, *Chem. Commun.*, 2011, **47**, 3186–3188.
- 103 N. J. Agard, J. A. Prescher and C. R. Bertozzi, *J. Am. Chem. Soc.*, 2004, **126**, 15046–15047.
- 104 N. J. Agard, J. M. Baskin, J. A. Prescher, A. Lo and C. R. Bertozzi, *ACS Chem. Biol.*,

- 2006, **1**, 644–648.
- 105 J. M. Baskin, J. A. Prescher, S. T. Laughlin, N. J. Agard, P. V. Chang, I. A. Miller, A. Lo, J. A. Codelli and C. R. Bertozzi, *Proc. Natl. Acad. Sci. U. S. A.*, 2007, **104**, 16793–16797.
- 106 S. T. Laughlin, J. M. Baskin, S. L. Amacher and C. R. Bertozzi, *Science*, 2008, **320**, 664–667.
- 107 X. Ning, J. Guo, M. A. Wolfert and G. J. Boons, *Angew. Chemie Int. Ed.*, 2008, **47**, 2253–2255.
- 108 M. F. Debets, S. S. Van Berkel, S. Schoffelen, F. P. J. T. Rutjes, J. C. M. Van Hest and F. L. Van Delft, *Chem. Commun.*, 2010, **46**, 97–99.
- 109 J. C. Jewett, E. M. Sletten and C. R. Bertozzi, *J. Am. Chem. Soc.*, 2010, **132**, 3688–3690.
- 110 P. V. Changa, J. A. Preschera, E. M. Sletten, J. M. Baskin, I. A. Miller, N. J. Agard, A. Lo and C. R. Bertozzi, *Proc. Natl. Acad. Sci. U. S. A.*, 2010, **107**, 1821–1826.
- 111 J. Dommerholt, S. Schmidt, R. Temming, L. J. A. Hendriks, F. P. J. T. Rutjes, J. C. M. Van Hest, D. J. Lefeber, P. Friedl and F. L. Van Delft, *Angew. Chemie Int. Ed.*, 2010, **49**, 9422–9425.
- 112 D. L. Davis, E. K. Price, S. O. Aderibigbe, M. X. H. Larkin, E. D. Barlow, R. Chen, L. C. Ford, Z. T. Gray, S. H. Gren, Y. Jin, K. S. Keddington, A. D. Kent, D. Kim, A. Lewis, R. S. Marrouche, M. K. O'Dair, D. R. Powell, M. H. C. Scadden, C. B. Session, J. Tao, J. Trieu, K. N. Whiteford, Z. Yuan, G. Yun, J. Zhu and J. M. Heemstra, *J. Org. Chem.*, 2016, **81**, 6816–6819.
- 113 R. N. Butler and A. G. Coyne, *J. Org. Chem.*, 2015, **80**, 1809–1817.
- 114 R. N. Butler, W. J. Cunningham, A. G. Coyne and L. A. Burke, *J. Am. Chem. Soc.*, 2004, **126**, 11923–11929.
- 115 S. Narayan, J. Muldoon, M. G. Finn, V. V. Fokin, H. C. Kolb and K. B. Sharpless, *Angew. Chemie Int. Ed.*, 2005, **44**, 3275–3279.
- 116 G. La Sorella, G. Strukul and A. Scarso, *Green Chem.*, 2015, **17**, 644–683.
- 117 G. I. Anderton, A. S. Bangerter, T. C. Davis, Z. Feng, A. J. Furtak, J. O. Larsen, T. L. Scroggin and J. M. Heemstra, *Bioconjug. Chem.*, 2015, **26**, 1687–1691.
- 118 M. L. Blackman, M. Royzen and J. M. Fox, *J. Am. Chem. Soc.*, 2008, **130**, 13518–13519.
- 119 F. Thalhammer, U. Wallfahner and J. Sauer, *Tetrahedron Lett.*, 1990, **31**, 6851–6854.
- 120 N. K. Devaraj, R. Weissleder and S. A. Hilderbrand, *Bioconjug. Chem.*, 2008, **19**,

- 2297–2299.
- 121 D. M. Patterson, L. A. Nazarova, B. Xie, D. N. Kamber and J. A. Prescher, *J. Am. Chem. Soc.*, 2012, **134**, 18638–18643.
- 122 J. Yang, J. Šečkute, C. M. Cole and N. K. Devaraj, *Angew. Chemie Int. Ed.*, 2012, **51**, 7476–7479.
- 123 T. Deb, J. Tu and R. M. Franzini, *Chem. Rev.*, 2021, **121**, 6850–6914.
- 124 J. Sauer, D. K. Heldmann, J. Hetzenegger, J. Krauthan, H. Sichert and J. Schuster, *European J. Org. Chem.*, 1998, **1998**, 2885–2896.
- 125 M. R. Karver, R. Weissleder and S. A. Hilderbrand, *Bioconjug. Chem.*, 2011, **22**, 2263–2270.
- 126 R. J. Blizzard, D. R. Backus, W. Brown, C. G. Bazewicz, Y. Li and R. A. Mehl, *J. Am. Chem. Soc.*, 2015, **137**, 10044–10047.
- 127 R. M. Versteegen, R. Rossin, W. Ten Hoeve, H. M. Janssen and M. S. Robillard, *Angew. Chemie Int. Ed.*, 2013, **52**, 14112–14116.
- 128 J. Li, S. Jia and P. R. Chen, *Nat. Chem. Biol.*, 2014, **10**, 1003–1005.
- 129 X. Fan, Y. Ge, F. Lin, Y. Yang, G. Zhang, W. S. C. Ngai, Z. Lin, S. Zheng, J. Wang, J. Zhao, J. Li and P. R. Chen, *Angew. Chemie Int. Ed.*, 2016, **55**, 14046–14050.
- 130 J. C. T. Carlson, H. Mikula and R. Weissleder, *J. Am. Chem. Soc.*, 2018, **140**, 3603–3612.
- 131 M. T. Taylor, M. L. Blackman, O. Dmitrenko and J. M. Fox, *J. Am. Chem. Soc.*, 2011, **133**, 9646–9649.
- 132 F. H. Crick, in *Symposia of the Society for Experimental Biology*, 1957, pp. 138–63.
- 133 D. Van Vranken and G. A. Weiss, *Introduction to Bioorganic Chemistry and Chemical Biology*, Garland Science, New York, 1st edn., 2012.
- 134 J. C. M. van Hest, K. L. Kiick and D. A. Tirrell, *J. Am. Chem. Soc.*, 2000, **122**, 1282–1288.
- 135 K. L. Kiick, E. Saxon, D. A. Tirrell and C. R. Bertozzi, *Proc. Natl. Acad. Sci.*, 2002, **99**, 19–24.
- 136 D. de la Torre and J. W. Chin, *Nat. Rev. Genet.*, 2021, **22**, 169–184.
- 137 D. R. Liu, T. J. Magliery, M. Pasternak and P. G. Schultz, *Proc. Natl. Acad. Sci.*, 1997, **94**, 10092–10097.
- 138 L. Wang, A. Brock, B. Herberich and P. G. Schultz, *Science*, 2001, **292**, 498–500.
- 139 L. Wang, J. Xie and P. G. Schultz, *Annu. Rev. Biophys. Biomol. Struct.*, 2006, **35**, 225–249.

- 140 A. Dumas, L. Lercher, C. D. Spicer and B. G. Davis, *Chem. Sci.*, 2015, **6**, 50–69.
- 141 K. J. Lee, D. Kang and H. S. Park, *Mol. Cells*, 2019, **42**, 386–396.
- 142 V. Beránek, J. C. W. Willis and J. W. Chin, *Biochemistry*, 2019, **58**, 387–390.
- 143 W. Brown, J. Liu and A. Deiters, *ACS Chem. Biol.*, 2018, **13**, 2375–2386.
- 144 D. L. Dunkelmann, J. C. W. Willis, A. T. Beattie and J. W. Chin, *Nat. Chem.*, 2020, **12**, 535–544.
- 145 J. S. Italia, P. S. Addy, S. B. Erickson, J. C. Peeler, E. Weerapana and A. Chatterjee, *J. Am. Chem. Soc.*, 2019, **141**, 6204–6212.
- 146 W. E. Robertson, L. F. H. Funke, D. de la Torre, J. Fredens, T. S. Elliott, M. Spinck, Y. Christova, D. Cervettini, F. L. Böge, K. C. Liu, S. Buse, S. Maslen, G. P. C. Salmond and J. W. Chin, *Science*, 2021, **372**, 1057–1062.
- 147 J. Fredens, K. Wang, D. de la Torre, L. F. H. Funke, W. E. Robertson, Y. Christova, T. Chia, W. H. Schmied, D. L. Dunkelmann, V. Beránek, C. Uttamapinant, A. G. Llamazares, T. S. Elliott and J. W. Chin, *Nature*, 2019, **569**, 514–518.
- 148 P. Arranz-Gibert, K. Vanderschuren and F. J. Isaacs, *Curr. Opin. Chem. Biol.*, 2018, **46**, 203–211.
- 149 J. Ficini and A. Krief, *Tetrahedron Lett.*, 1970, **11**, 1397–1400.
- 150 G. A. Burley, Y. Boutadla, D. L. Davies and K. Singh, *Organometallics*, 2012, **31**, 1112–1117.
- 151 M. Z. C. Hatit, J. C. Sadler, L. A. McLean, B. C. Whitehurst, C. P. Seath, L. D. Humphreys, R. J. Young, A. J. B. Watson and G. A. Burley, *Org. Lett.*, 2016, **18**, 1694–1697.
- 152 M. Z. C. Hatit, C. P. Seath, A. J. B. Watson and G. A. Burley, *J. Org. Chem.*, 2017, **82**, 5461–5468.
- 153 C. P. Seath, G. A. Burley and A. J. B. Watson, *Angew. Chemie Int. Ed.*, 2017, **56**, 3314–3318.
- 154 V. O. Rodionov, V. V. Fokin and M. G. Finn, *Angew. Chemie Int. Ed.*, 2005, **44**, 2210–2215.
- 155 D. Giustarini, D. Tsikas, G. Colombo, A. Milzani, I. Dalle-Donne, P. Fanti and R. Rossi, *J. Chromatogr. B Anal. Technol. Biomed. Life Sci.*, 2016, **1019**, 21–28.
- 156 H. Sies, *Free Radic. Biol. Med.*, 1999, **27**, 916–921.
- 157 D. A. Dickinson and H. J. Forman, *Biochem. Pharmacol.*, 2002, **64**, 1019–1026.
- 158 H. J. Forman, *Arch. Biochem. Biophys.*, 2016, **595**, 64–67.
- 159 J. H. Freedman, M. R. Ciriolo and J. Peisach, *J. Biol. Chem.*, 1989, **264**, 5598–5605.

- 160 H. Speisky, M. Gómez, C. Carrasco-Pozo, E. Pastene, C. Lopez-Alarcón and C. Olea-Azar, *Bioorg. Med. Chem.*, 2008, **16**, 6568–6574.
- 161 M. T. Morgan, L. A. H. Nguyen, H. L. Hancock and C. J. Fahrni, *J. Biol. Chem.*, 2017, **292**, 21558–21567.
- 162 R. Ciriolo, Maria, Desideri, Alessandro, Paci, Maurizio, Guiseppe, *J. Biol. Chem.*, 1990, **265**, 11030–11034.
- 163 C. J. Reed and K. T. Douglas, *Biochem J*, 1991, **275**, 601–608.
- 164 N. Spear and S. D. Aust, *Arch. Biochem. Biophys.*, 1995, **317**, 142–148.
- 165 H. Speisky, C. López-Alarcón, C. Olea-Azar, C. Sandoval-Acuña and M. E. Aliaga, *Bioinorg. Chem. Appl.*, 2011, **2011**, 1–8.
- 166 M. E. Aliaga, C. López-Alarcón, L. García-Río, M. Martín-Pastor and H. Speisky, *Bioorganic Med. Chem.*, 2012, **20**, 2869–2876.
- 167 A. V. Kachur, C. J. Koch and J. E. Biaglow, *Free Radic. Res.*, 1998, **28**, 259–269.
- 168 L. Banci, I. Bertini, S. Ciofi-Baffoni, T. Kozyreva, K. Zovo and P. Palumaa, *Nature*, 2010, **465**, 645–648.
- 169 D. K. Johnson, M. J. Stevenson, Z. A. Almadidy, S. E. Jenkins, D. E. Wilcox and N. E. Grosseohme, *Dalt. Trans.*, 2015, **44**, 16494–16505.
- 170 A. Corazza, I. Harvey and P. J. Sadler, *Eur. J. Biochem.*, 1996, **236**, 697–705.
- 171 M. E. Aliaga, C. Carrasco-Pozo, C. López-Alarcón and H. Speisky, *Transit. Met. Chem.*, 2010, **35**, 321–329.
- 172 B. K. Maiti, K. Pal and S. Sarkar, *Eur. J. Inorg. Chem.*, 2007, **4**, 5548–5555.
- 173 D. Coucouvanis, C. N. Murphy and S. K. Kanodia, *Inorg. Chem.*, 1980, **19**, 2993–2998.
- 174 R. A. Ward, M. J. Anderton, S. Ashton, P. A. Bethel, M. Box, S. Butterworth, N. Colclough, C. G. Chorley, C. Chuaqui, D. A. E. Cross, L. A. Dakin, J. É. Debreczeni, C. Eberlein, M. R. V. Finlay, G. B. Hill, M. Grist, T. C. M. Klinowska, C. Lane, S. Martin, J. P. Orme, P. Smith, F. Wang and M. J. Waring, *J. Med. Chem.*, 2013, **56**, 7025–7048.
- 175 R. Lonsdale, J. Burgess, N. Colclough, N. L. Davies, E. M. Lenz, A. L. Orton and R. A. Ward, *J. Chem. Inf. Model.*, 2017, **57**, 3124–3137.
- 176 R. van Geel, G. J. M. Pruijn, F. L. van Delft and W. C. Boelens, *Bioconjug. Chem.*, 2012, **23**, 392–398.
- 177 C. Zhang, P. Dai, A. A. Vinogradov, Z. P. Gates and B. L. Pentelute, *Angew. Chemie Int. Ed.*, 2018, **57**, 6459–6463.

- 178 G. J. Wørmer, B. K. Hansen, J. Palmfeldt and T. B. Poulsen, *Angew. Chemie Int. Ed.*, 2019, **58**, 11918–11922.
- 179 V. Hong, S. I. Presolski, C. Ma and M. â. G. Finn, *Angew. Chemie Int. Ed.*, 2009, **48**, 9879–9883.
- 180 C. Gaulier, A. Hospital, B. Legeret, A. F. Delmas, V. Aucagne, F. Cisnetti and A. Gautier, *Chem. Commun.*, 2012, **48**, 4005–4007.
- 181 T. V. Tran, G. Couture and L. H. Do, *Dalt. Trans.*, 2019, **48**, 9751–9758.
- 182 Y. Tian and Q. Lin, *ACS Chem. Biol.*, 2019, **14**, 2489–2496.
- 183 R. D. Row and J. A. Prescher, *Acc. Chem. Res.*, 2018, **51**, 1073–1081.
- 184 J. C. Jewett and C. R. Bertozzi, *Chem. Soc. Rev.*, 2010, **39**, 1272–1279.
- 185 P. V. Chang, J. A. Prescher, E. M. Sletten, J. M. Baskin, I. A. Miller, N. J. Agard, A. Lo and C. R. Bertozzi, *Proc. Natl. Acad. Sci.*, 2010, **107**, 1821–1826.
- 186 N. K. Devaraj, *ACS Cent. Sci.*, 2018, **4**, 952–959.
- 187 F. Friscourt, P. A. Ledin, N. E. Mbua, H. R. Flanagan-Steet, M. A. Wolfert, R. Steet and G. J. Boons, *J. Am. Chem. Soc.*, 2012, **134**, 5381–5389.
- 188 J. Tu, D. Svatunek, S. Parvez, A. C. Liu, B. J. Levandowski, H. J. Eckvahl, R. T. Peterson, K. N. Houk and R. M. Franzini, *Angew. Chemie Int. Ed.*, 2019, **58**, 9043–9048.
- 189 A. Darko, S. Wallace, O. Dmitrenko, M. M. Machovina, R. A. Mehl, J. W. Chin and J. M. Fox, *Chem. Sci.*, 2014, **5**, 3770–3776.
- 190 E. G. Burke, B. Gold, T. T. Hoang, R. T. Raines and J. M. Schomaker, *J. Am. Chem. Soc.*, 2017, **139**, 8029–8037.
- 191 G. Qiu, P. Nava, A. Martinez and C. Colomban, *Chem. Commun.*, 2021, **57**, 2281–2284.
- 192 T. V. Tran, G. Couture and L. H. Do, *Dalt. Trans.*, 2019, **48**, 9751–9758.
- 193 J. Dommerholt, S. Schmidt, R. Temming, L. J. A. Hendriks, F. P. J. T. Rutjes, J. C. M. Van Hest, D. J. Lefeber, P. Friedl and F. L. Van Delft, *Angew. Chemie Int. Ed.*, 2010, **49**, 9422–9425.
- 194 J. Yang, J. Šečutè, C. M. Cole and N. K. Devaraj, *Angew. Chemie Int. Ed.*, 2012, **51**, 7476–7479.
- 195 N. Z. M. Homer, J. Reglinski, R. Sowden, C. M. Spickett, R. Wilson and J. J. Walker, *Cryobiology*, 2005, **50**, 317–324.
- 196 D. Listunov, N. Saffon-Merceron, E. Joly, I. Fabing, Y. Génisson, V. Maraval and R. Chauvin, *Tetrahedron*, 2016, **72**, 6697–6704.

- 197 G. A. Burley, D. L. Davies, G. A. Griffith, M. Lee and K. Singh, *J. Org. Chem.*, 2010, **75**, 980–983.
- 198 A. A. Kislukhin, V. P. Hong, K. E. Breitenkamp and M. G. Finn, *Bioconjug. Chem.*, 2013, **24**, 684–689.
- 199 R. Huisgen, *Angew. Chemie Int. Ed.*, 1963, **2**, 633–645.
- 200 J. Dommerholt, F. P. J. T. Rutjes and F. L. van Delft, *Top. Curr. Chem.*, 2016, **374**, 16.
- 201 M. R. Karver, R. Weissleder and S. A. Hilderbrand, *Bioconjug. Chem.*, 2011, **22**, 2263–2270.
- 202 M. Burk, S. Rothstein and P. Dubé, *Org. Process Res. Dev.*, 2018, **22**, 108–110.
- 203 Y. Qu, F. X. Sauvage, G. Clavier, F. Miomandre and P. Audebert, *Angew. Chemie Int. Ed.*, 2018, **57**, 12057–12061.
- 204 D. M. Patterson, L. A. Nazarova, B. Xie, D. N. Kamber and J. A. Prescher, *J. Am. Chem. Soc.*, 2012, **134**, 18638–18643.
- 205 S. N. Semenov, L. Belding, B. J. Cafferty, M. P. S. Mousavi, A. M. Finogenova, R. S. Cruz, E. V. Skorb and G. M. Whitesides, *J. Am. Chem. Soc.*, 2018, **140**, 10221–10232.
- 206 E. D. Clarke, D. T. Greenhow and D. Adams, *Pestic. Sci.*, 1998, **54**, 385–393.
- 207 J. W. Dolan, *LCGC North Am.*, 2012, **30**, 474–480.
- 208 B. Amgarten, R. Rajan, N. Martínez-Sáez, B. L. Oliveira, I. S. Albuquerque, R. A. Brooks, D. G. Reid, M. J. Duer and G. J. L. Bernardes, *Chem. Commun.*, 2015, **51**, 5250–5252.
- 209 Y. Park, A. L. Baumann, H. Moon, S. Byrne, M.-A. Kasper, S. Hwang, H. Sun, M.-H. Baik and C. P. R. Hackenberger, *Chem. Sci.*, 2021, **12**, 8141–8148.
- 210 A. Mirzahassemi, M. Somlyay and B. Noszál, *Chem. Phys. Lett.*, 2015, **622**, 50–56.
- 211 R. J. Mayer and A. R. Ofial, *Angew. Chemie Int. Ed.*, 2019, **58**, 17704–17708.
- 212 P. W. Szafranski, P. Kasza and M. T. Cegła, *Tetrahedron Lett.*, 2015, **56**, 6244–6247.
- 213 R. Breslow, *Acc. Chem. Res.*, 1991, **24**, 159–164.
- 214 J. J. Gajewski, *Acc. Chem. Res.*, 1997, **30**, 219–225.
- 215 S. Otto and J. B. F. N. Engberts, *Org. Biomol. Chem.*, 2003, **1**, 2809.
- 216 S. Narayan, J. Muldoon, M. G. Finn, V. V. Fokin, H. C. Kolb and K. B. Sharpless, *Angew. Chemie Int. Ed.*, 2005, **44**, 3275–3279.
- 217 M. Cortes-Clerget, J. Yu, J. R. A. Kincaid, P. Walde, F. Gallou and B. H. Lipshutz, *Chem. Sci.*, 2021, **12**, 4237–4266.
- 218 Y. Hu and J. M. Schomaker, *ChemBioChem*, 2021, **53706**, cbic.202100164.
- 219 M. L. Blackman, M. Royzen and J. M. Fox, *J. Am. Chem. Soc.*, 2008, **130**, 13518–

- 13519.
- 220 M. X. W. Jiang, M. Rawat and W. D. Wulff, *J. Am. Chem. Soc.*, 2004, **126**, 5970–5971.
- 221 P. Conti, L. Tamborini, A. Pinto, L. Sola, R. Ettari, C. Mercurio and C. De Micheli, *Eur. J. Med. Chem.*, 2010, **45**, 4331–4338.
- 222 P. Kleiner, W. Heydenreuter, M. Stahl, V. S. Korotkov and S. A. Sieber, *Angew. Chemie Int. Ed.*, 2017, **56**, 1396–1401.
- 223 A. H. Banday, S. A. Shameem, B. D. Gupta and H. M. S. Kumar, *Steroids*, 2010, **75**, 801–804.
- 224 A. Nocentini, M. Ferraroni, F. Carta, M. Ceruso, P. Gratterer, C. Lanzi, E. Masini and C. T. Supuran, *J. Med. Chem.*, 2016, **59**, 10692–10704.
- 225 A. Haslop, A. Gee, C. Plisson and N. Long, *J. Label. Compd. Radiopharm.*, 2013, **56**, 313–316.
- 226 L. J. Stewart, C. L. Y. Ong, M. M. Zhang, S. Brouwer, L. McIntyre, M. R. Davies, M. J. Walker, A. G. McEwan, K. J. Waldron and K. Y. Djoko, *MBio*, 2020, **11**, 1–19.
- 227 L. Milne, P. Nicotera, S. Orrenius and M. J. Burkitt, *Arch. Biochem. Biophys.*, 1993, **304**, 102–109.
- 228 M. E. Aliaga, C. López-Alarcón, R. Bridi and H. Speisky, *J. Inorg. Biochem.*, 2016, **154**, 78–88.
- 229 G. C. Kuang, P. M. Guha, W. S. Brotherton, J. T. Simmons, L. A. Stankee, B. T. Nguyen, R. J. Clark and L. Zhu, *J. Am. Chem. Soc.*, 2011, **133**, 13984–14001.
- 230 M. E. Aliaga, C. López-Alarcón, R. Bridi and H. Speisky, *J. Inorg. Biochem.*, 2016, **154**, 78–88.
- 231 D. Dipankar, *Indian J. Chem.*, 1987, **26A**, 605–606.
- 232 C. L. Merrill, L. J. Wilson, T. J. Thamann, T. M. Loehr, N. S. Ferris and W. H. Woodruff, *J. Chem. Soc. Dalt. Trans.*, 1984, 2207–2221.
- 233 P. M. Murray, F. Bellany, L. Benhamou, D.-K. Bučar, A. B. Tabor and T. D. Sheppard, *Org. Biomol. Chem.*, 2016, **14**, 2373–2384.
- 234 R. Leardi, *Anal. Chim. Acta*, 2009, **652**, 161–172.
- 235 J. Burés, *Angew. Chemie Int. Ed.*, 2016, **55**, 2028–2031.
- 236 J. Burés, *Angew. Chemie Int. Ed.*, 2016, **55**, 16084–16087.
- 237 C. D. T. Nielsen and J. Burés, *Chem. Sci.*, 2019, **10**, 348–353.
- 238 D. M. Kaphan, K. R. Brereton, R. C. Klet, R. J. Witzke, A. J. M. Miller, K. L. Mulfort, M. Delferro and D. M. Tiede, *Organometallics*, 2021, **40**, 1482–1491.
- 239 C. Catiuela, J. I. García, J. A. Mayoral and L. Salvatella, *Can. J. Chem.*, 1994, **72**,

- 308–311.
- 240 J. Liu, L. Wang, X. Wang, L. Xu, Z. Hao and J. Xiao, *Org. Biomol. Chem.*, 2016, **14**, 11510–11517.
- 241 J. P. Bégué, D. Bonnet-Delpon and B. Crousse, *Synlett*, 2004, 18–29.
- 242 A. Berkessel, J. A. Adrio, D. Hüttenhain and J. M. Neudörfl, *J. Am. Chem. Soc.*, 2006, **128**, 8421–8426.
- 243 N. Hirota-Nakaoka and Y. Goto, *Bioorg. Med. Chem.*, 1999, **7**, 67–73.
- 244 N. Hirota, K. Mizuno and Y. Goto, *J. Mol. Biol.*, 1998, **275**, 365–378.
- 245 B. Czarnik-Matusiewicz, S. Pilorz, L. P. Zhang and Y. Wu, *J. Mol. Struct.*, 2008, **883–884**, 195–202.
- 246 T. Yamaguchi, S. Imura, T. Kai and K. Yoshida, *Z Naturforsch.*, 2013, **68**, 145–151.
- 247 K. Yoshida, T. Yamaguchi, T. Adachi, T. Otomo, D. Matsuo, T. Takamuku and N. Nishi, *J. Chem. Phys.*, 2003, **119**, 6132–6142.
- 248 O. Hollóczki, A. Berkessel, J. Mars, M. Mezger, A. Wiebe, S. R. Waldvogel and B. Kirchner, *ACS Catal.*, 2017, **7**, 1846–1852.
- 249 Y. Ma and J. R. Yates, *Expert Rev. Proteomics*, 2018, **15**, 545–554.
- 250 A. Ali Khan, J. Hansson, P. Weber, S. Foehr, J. Krijgsveld, S. Herzig and M. Scheideler, *Mol. Cell. Proteomics*, 2018, **17**, 2358–2370.
- 251 N. Sun, Y. Wang, J. Wang, W. Sun, J. Yang and N. Liu, *Anal. Chem.*, 2020, **92**, 8292–8297.
- 252 K. Astakhova, R. Ray, M. Taskova, J. Uhd, A. Carstens and K. Morris, *Mol. Pharm.*, 2018, **15**, 2892–2899.
- 253 R. S. Geary, *Expert Opin. Drug Metab. Toxicol.*, 2009, **5**, 381–391.
- 254 H. Liu, F. Zeng, M. Zhang, F. Huang, J. Wang, J. Guo, C. Liu and H. Wang, *J. Control. Release*, 2016, **226**, 124–137.
- 255 M. Taskova, C. S. Madsen, K. J. Jensen, L. H. Hansen, B. Vester and K. Astakhova, *Bioconjug. Chem.*, 2017, **28**, 768–774.
- 256 A. A. H. Ahmad Fuaad, F. Azmi, M. Skwarczynski and I. Toth, *Molecules*, 2013, **18**, 13148–13174.
- 257 N. Z. Fantoni, A. H. El-Sagheer and T. Brown, *Chem. Rev.*, 2021, **121**, 7122–7154.
- 258 Z. Zhu, H. Chen, S. Li, X. Yang, E. Bittner and C. Cai, *Catal. Sci. Technol.*, 2017, **7**, 2474–2485.
- 259 E. C. Vatansever, J. Kang, A. Tuley, E. S. Ward and W. R. Liu, *Bioorganic Med. Chem.*, 2020, **28**, 115808.

- 260 J. Xiao and T. J. Tolbert, *Org. Lett.*, 2009, **11**, 4144–4147.
- 261 M. Pretze, M. Kuchar, R. Bergmann, J. Steinbach, J. Pietzsch and C. Mamat, *ChemMedChem*, 2013, **8**, 935–945.
- 262 D. N. Kamber, L. A. Nazarova, Y. Liang, S. A. Lopez, D. M. Patterson, H.-W. Shih, K. N. Houk and J. A. Prescher, *J. Am. Chem. Soc.*, 2013, **135**, 13680–13683.
- 263 R. R. Ramsubhag and G. B. Dudley, *Org. Biomol. Chem.*, 2016, **14**, 5028–5031.
- 264 V. F. Schart, J. Hassenrück, A.-K. Späte, J. E. G. A. Dold, R. Fahrner and V. Wittmann, *ChemBioChem*, 2019, **20**, 166–171.
- 265 Y. Hu, J. M. Roberts, H. R. Kilgore, A. S. Mat Lani, R. T. Raines and J. M. Schomaker, *J. Am. Chem. Soc.*, 2020, **142**, 18826–18835.
- 266 S. Yoshida, Y. Hatakeyama, K. Johmoto, H. Uekusa and T. Hosoya, *J. Am. Chem. Soc.*, 2014, **136**, 13590–13593.
- 267 S. Yoshida, T. Kuribara, H. Ito, T. Meguro, Y. Nishiyama, F. Karaki, Y. Hatakeyama, Y. Koike, I. Kii and T. Hosoya, *Chem. Commun.*, 2019, **55**, 3556–3559.
- 268 E. R. Strieter, D. G. Blackmond and S. L. Buchwald, *J. Am. Chem. Soc.*, 2005, **127**, 4120–4121.
- 269 T. Sano, S. Vajda and C. R. Cantor, *J. Chromatogr. B Biomed. Appl.*, 1998, **715**, 85–91.
- 270 J. D. Hirsch, L. Eslamizar, B. J. Filanoski, N. Malekzadeh, R. P. Haugland, J. M. Beechem and R. P. Haugland, *Anal. Biochem.*, 2002, **308**, 343–357.
- 271 D. Derossi, G. Chassaing and A. Prochiantz, *Trends Cell Biol.*, 1998, **8**, 84–87.
- 272 P. E. G. Thorén, D. Persson, M. Karlsson and B. Nordén, *FEBS Lett.*, 2000, **482**, 265–268.
- 273 P. E. Schneggenburger, B. Worbs and U. Diederichsen, *J. Pept. Sci.*, 2010, **16**, 10–14.
- 274 T. Fuselier and W. C. Wimley, *Biophys. J.*, 2017, **113**, 835–846.
- 275 M. Kollaschinski, J. Sobotta, A. Schalk, T. Frischmuth, B. Graf and S. Serdjukow, *Bioconjug. Chem.*, 2020, **31**, 507–512.
- 276 L. A. Finney, *Science*, 2003, **300**, 931–936.
- 277 J. L. Burkhead, K. A. Gogolin Reynolds, S. E. Abdel-Ghany, C. M. Cohu and M. Pilon, *New Phytol.*, 2009, **182**, 799–816.
- 278 J. Miguel-Ávila, M. Tomás-Gamasa, A. Olmos, P. J. Pérez and J. L. Mascareñas, *Chem. Sci.*, 2018, **9**, 1947–1952.
- 279 J. Clavadetscher, S. Hoffmann, A. Lilienkamp, L. Mackay, R. M. Yusop, S. A. Rider, J. J. Mullins and M. Bradley, *Angew. Chemie Int. Ed.*, 2016, **55**, 15662–15666.

- 280 K. Sivakumar, F. Xie, B. M. Cash, S. Long, H. N. Barnhill and Q. Wang, *Org. Lett.*, 2004, **6**, 4603–4606.
- 281 M. Mettry, M. P. Moehlig, A. D. Gill and R. J. Hooley, *Supramol. Chem.*, 2017, **29**, 120–128.
- 282 R. H. Nagaraj, D. R. Sell, M. Prabhakaram, B. J. Ortwerth and V. M. Monnier, *Proc. Natl. Acad. Sci.*, 1991, **88**, 10257–10261.
- 283 M. R. Levengood, C. C. Kerwood, C. Chatterjee and W. A. van der Donk, *ChemBioChem*, 2009, **10**, 911–919.
- 284 F. Wang, Y. Zhang, Z. Liu, Z. Du, L. Zhang, J. Ren and X. Qu, *Angew. Chemie Int. Ed.*, 2019, **58**, 6987–6992.
- 285 Y. Bai, X. Feng, H. Xing, Y. Xu, B. K. Kim, N. Baig, T. Zhou, A. A. Gewirth, Y. Lu, E. Oldfield and S. C. Zimmerman, *J. Am. Chem. Soc.*, 2016, **138**, 11077–11080.
- 286 D. Sun, X. Fan, Y. Shi, H. Zhang, Z. Huang, B. Cheng, Q. Tang, W. Li, Y. Zhu, J. Bai, W. Liu, Y. Li, X. Wang, X. Lei and X. Chen, *Nat. Methods*, 2021, **18**, 107–113.
- 287 C. Y. Jao, M. Roth, R. Welti and A. Salic, *ChemBioChem*, 2015, **16**, 472–476.
- 288 M. Tera, Z. Harati Taji and N. W. Luedtke, *Angew. Chemie Int. Ed.*, 2018, **57**, 15405–15409.
- 289 K. C. Chang, I. H. Su, A. Senthilvelan and W. S. Chung, *Org. Lett.*, 2007, **9**, 3363–3366.
- 290 A. N. Fakhrutdinov, B. Y. Karlinskii, M. E. Minyaev and V. P. Ananikov, *J. Org. Chem.*, 2021, **86**, 11456–11463.
- 291 Y. C. Hsieh, J. L. Chir, H. H. Wu, P. S. Chang and A. T. Wu, *Carbohydr. Res.*, 2009, **344**, 2236–2239.

Appendix

Available at:

<https://strath->

[my.sharepoint.com/:f:/g/personal/frederik_peschke_strath_ac_uk/ElFpAlyMbf1Mr6yiGKq7](https://strath-my.sharepoint.com/:f:/g/personal/frederik_peschke_strath_ac_uk/ElFpAlyMbf1Mr6yiGKq7)

[LNYBL08STZpd9x9TjcFw-Bk1MQ?e=vHa3mQ](https://strath-my.sharepoint.com/:f:/g/personal/frederik_peschke_strath_ac_uk/ElFpAlyMbf1Mr6yiGKq7)

or as a .zip file